Palaeotsunami Deposits On The Southern Hikurangi Margin; Contributions From Lake Grassmere, Marlborough

PIZER, CHARLOTTE,OLIVIA

MATERIAL ABSTRACT

Palaeotsunami Deposits On The Southern Hikurangi Margin; Contributions From Lake Grassmere, Marlborough

Charlotte Pizer

The Hikurangi subduction margin poses the most significant hazard for New Zealand, with particular threat for populated regions on the east coast. Strain accumulation on the margin suggests likely future scenarios of ruptures of > M_w 9, with great potential for large tsunamis. The southern section of the Hikurangi subduction margin is particularly poorly constrained, due to the lack of historic earthquakes and limited evidence of palaeotsunami and palaeoearthquake. Furthermore, the unknown rupture extent into the Cook Strait has major implications for tsunami height.

The shallow coastal embayment of Lake Grassmere in Marlborough is located at the southern end of the Hikurangi margin and has potential for preserving a record of prehistoric subduction earthquakes. In this thesis, I conduct a multiproxy study of sediment cores from the lake edges that includes; grain size analysis, microfossil analysis and radiocarbon dating. From these results, I delineate the palaeoenvironmental evolution of Lake Grassmere through the late Holocene. Two anomalous deposits are identified and characterised by a densely packed shell hash of articulated and disarticulated bivalves in sand, with sharp, erosive contacts that are laterally extensive over 1.7 km inland. The deposits display many affinities with globally derived characteristics of palaeotsunami deposits and therefore I attribute a tsunami source to both units. Consideration is given to the possible evidence of coseismic vertical uplift within the cores and the beach ridge sequence. Radiocarbon dates place Tsunami 1 at 2089 -1875 cal BP and Tsunami 2 at 1509-1314 cal BP. Regional palaeoseismology presents no suitable synchronous upper plate ruptures and therefore I suggest that the simplest explanation is a subduction earthquake on the southern Hikurangi margin. Attributing this fault source has major implications for developing understanding of the southern section of the margin and I recommend next steps that should be taken to further this study.

Palaeotsunami Deposits On The Southern Hikurangi Margin: Contributions From Lake Grassmere, Marlborough

Miss Charlotte Olivia Pizer

Masters of Science by Research

Department of Geography, Durham University

2019

(Lake Grassmere, New Zealand)

TABLE OF CONTENTS

Preliminary pages

Material Abstract ……..……..……..……i
Title Page ……..……..……..……..……ii
Table Of Contents ..……..……..……..……iii
List Of Table ……..……..……..……..……vii
List Of Figures ……..……..……..……vii
Declaration and Statement of Copyright……..……..……..…ix
Acknowledgements.……..……..……..……..……..……..……x

Thesis

1. Introduction ……..……..……1
2. Context Of Research ……..……..……..……2
   2.1. Subduction Zones ……..……..……..……2
   2.2. Tsunamis ……..……..……3
   2.3. Geologic Evidence Of Palaeotsunami And Palaeoearthquakes ……..……4
      2.3.1. Sedimentological Evidence……..……..……..…6
      2.3.2. Biostratigraphic Evidence……..……..……..…7
      2.3.3. Attributing Seismically-Induced Changes Within Sediment Sequence..…9
   2.4. Dating Palaeoearthquakes And Palaeotsunami Deposits ……..……..……..10
      2.4.1. Calibration And The Marine Reservoir Effect ……..……..……...11
   2.5. Chapter Summary……..……..……..……11
3. Study Area ……..……..……..……..……12
   3.1. Tectonic Setting Of New Zealand ……..……..……..……12
      3.1.1. The Hikurangi Subduction Margin ……..……..……12
      3.1.2. The Marlborough Fault System……..……..……..……13
   3.2. Historic Earthquakes And Tsunami On The Hikurangi Subduction Margin And The Marlborough Fault System……...15
      3.2.1. Subduction Earthquakes And Tsunami ……..……16
      3.2.2. Upper Plate Earthquakes……..……...17
      3.2.3. Distant Source Tsunamis……..……17
      3.2.4. Alternative Sources……..……..18
      3.2.5. Pūrākau……18
   3.3. Prehistoric Earthquakes And Tsunami On The Southern Hikurangi Margin……19
   3.4. Lake Grassmere……..22
      3.4.1. Geology And Geomorphology……..……...23
      3.4.2. Holocene Sea Level……..……..24

3.4.3. Previous Geological Studies……..……..25
3.5. Chapter Summary And Research Questions ……...26
4. Methods…….……..……..……..…….28
4.1. Field Methodology ……28
4.1.1. Sediment Cores ……..…….……..28
4.1.2. Modern Samples……..……30
4.1.3. Surface And Stratigraphic Models ……..……...31
4.2. Sedimentology ……...31
4.2.1. Computed Tomography And Itrax……..….31
4.2.2. Grain Size……..……32
4.3. Biostratigraphy ..……..……..33
4.3.1. Foraminifera ……...33
4.3.2. Diatoms ……...34
4.3.3. Mollusc Shells ……..……35
4.4. Radiocarbon Dating ……..……..……..35
4.4.1. Terrestrial Samples ……..……35
4.4.2. Carbonate Samples……..……35
5. Results ……37
5.1. Stratigraphy And Sedimentology ……..……37
5.1.1. Descriptions Of Sedimentary Units ……..……..40
5.1.2. Landward And Barrier-Normal Trends ……..…… 42
5.1.3. Supporting Grain Size Samples ……..……44
5.1.4. Modern Grain Size Comparison ……..……45
5.2. Biostratigraphy ……..……..46
5.2.1. Foraminiferal Species Assemblages ……..46
5.2.2. Foraminiferal Abundance And Test Size Variations ……..…...50
5.2.3. Mollusc Assemblages ……...51
5.2.4. Modern Shell Assemblages ……..……..53
5.3. Radiocarbon ……..……..56
5.4. Surface Topography ……..……..61
6. Discussion Of Research Question 1: How Did The Morphology Of Lake Grassmere Evolve During The Late Holocene?.....63
6.1. Palaeoenvironmental Interpretations Of Units ……....65
6.2. Chronology And Sea Level ……..……69
6.3. Evolution Summary……74
7. Discussion Of Research Question 2: Is There Any Evidence Of Palaeotsunami Inundation Or Sudden Coseismic Vertical Deformation?.....75
7.1. Anomalous Deposits And Palaeotsunami Characteristics ……..…..75

7.1.1. Sedimentology ……...75
7.1.2. Shell Hash Material ……..……77
7.1.3. Microfossils ……78
7.1.4. Palaeogeography ……..78
7.1.5. Incongruous Characteristics …….....…….79
7.2. Alternative Mechanisms For The Deposition Of Anomalous Units At Lake Grassmere…….…..80
7.2.1. Sea-Level Change ……..……...80
7.2.2. Barrier Change ……...……...81
7.2.3. Relict Beach Deposit …….....…….81
7.2.4. Floods ……..……82
7.2.5. Hiatus In Clastic Sedimentation ……..……...82
7.2.6. Storms ……83
7.2.7. Summary …….....86
7.3. Assessing Evidence For Coseismic Vertical Deformation……..86
7.3.1. Beach Ridges As Palaeoseismic Indicators……..…..…..87
7.3.2. Summary……89
8. Discussion Of Research Question 3: How Does The Timing Of Palaeotsunami Events At Lake Grassmere Fit Within The Regional Palaeoseismic Record And What Are The Implications For Possible Fault Sources? ……..……91
8.1. Age Modelling ……91
8.2. Regional Palaeoseismology ……94
8.3. Possible Fault Sources ……..……..98
8.3.1. Distant Source ……..……98
8.3.2. Submarine Landslides ……..……...98
8.3.3. Cook Strait Faults ……..……...99
8.3.4. Awatere Fault……..……..100
8.3.5. Wairau Fault ……...……100
8.3.6. Wairarapa Fault ……..……100
8.3.7. The Hikurangi Subduction Margin ……....102
8.4. Summary ……104
9. Conclusions ……106
9.1. Summary And Implications ……106
9.2. Future Work ……..…..107
9.2.1. Reanalysis Of Cores Taken By King Et Al (2017) At Mataora-Wairau Lagoon…….....108
9.2.2. Constraining The Tsunami Model Parameters To Satisfy The Deposit Characteristic……108

Appendices

Appendix 1: Gouge core descriptions ……..……111
Appendix 2: Stratigraphic logs of piston cores…….……..……..122
Appendix 3: Coordinates and elevation of gouge and piston cores……..137
Appendix 4: Grain size data ……139
Appendix 5: Foraminifera data…….....143
Appendix 6: Oxcal model codes……..145

References

References ……147

LIST OF TABLES

Table 1 – Fault Of The Marlborough Fault System ……..15
Table 2 – Historic Earthquakes In New Zealand ……..….17
Table 3 – All Radiocarbon Results ……..57
Table 4 – Recalibrated Dates From Ota Et Al (1995)……60
Table 5 – Summary Of Alternative Mechanisms ……..…..86
Table 6 - Features To Inform Tsunami Models ……..…..109

LIST OF FIGURES

Figure 1 – Earthquake Deformation Cycle ……..……3
Figure 2 – Coastal Preservation Of Coseismic Vertical Deformation And Tsunami…...…5
Figure 3 – Vertical Zonation Of Microfossils ……..……..8
Figure 4 – Tectonic Setting Of New Zealand ……13
Figure 5 – Faults Of The Marlborough Fault System…….……14
Figure 6 – Locations Of Historic Earthquakes ……..16
Figure 7 – Tsunami Heights For Four Different Southern Hikurangi Rupture Patches……..20
Figure 8 – Tsunami Model Of Mw 8.8 Subduction Earthquake And The 1855 Wairarapa Earthquake……...…….21
Figure 9 – Lake Grassmere Setting ……...……..22
Figure 10 – Historic Vs Modern Lake Grassmere……..……23
Figure 11 – Sea Level Curve …….……...24
Figure 12 – 2016 Reconnaissance Study …….……..26
Figure 13 – Map Of Sampling Strategy…….……...29
Figure 14 – Sampling Strategy Within Cores……..…….33
Figure 15 - Fence Diagram Of Piston Cores …….…….38
Figure 16 – Grain Size Statistics And Densitometry Of Core 22P……...39
Figure 17 – Particle Size Distributions Of Core 22P, Core P1, Core P3 And The Modern Samples……...……..40
Figure 18 – Box Model Of Lake Grassmere Stratigraphy……..……42
Figure 19 – Core 40P……..43
Figure 20 – Thickness of Unit 2 And Unit 4 ……..……..…..44
Figure 21 - Foraminifera Assemblage Of Core 22P……..……..…...48
Figure 22 – Foraminifera Assemblage Of Additional Cores…….……49
Figure 23 – Test Size Of Foraminifera ……51
Figure 24 – Shell Assemblage Of Unit 2 And Unit 4……..……..……..52

Figure 25 – Preservation Of Shells ……..…..……..53
Figure 26 – Shell Assemblages Of Modern Samples……..55
Figure 27 – Multiplot Of All Radiocarbon Dates……..……56
Figure 28 – Multiplot Of Recalibrated Dates From Ota Et Al (1995) ……..…60
Figure 29 – Map Of Elevation Profile Locations ……..……..…61
Figure 30 – Elevation Profiles Of The Northern Beach Ridge Sequence ……..…62
Figure 31 – Elevation Profile Of The Northern Beach Ridges, From The Barrier Polygon……..62
Figure 32 – Elevation Profiles Of The Beach Barrier ……..……..62
Figure 33 – Schematic Of The Holocene Evolution Of Lake Grassmere ……..63
Figure 34 – Images Of The Sharp Lower Contacts Of Anomalous Units ……..67
Figure 35 – Map Of Radiocarbon Dates At Lake Grassmere……...71
Figure 36 – Schematic Of Tsunami Wave Inundation ……..…….……79
Figure 37 – Evidence Of Storm Debris ……..……..……85
Figure 38 – Beach Ridge Uplift ……..……..……88
Figure 39 – Schematic Of Beach Ridge Formation ……..……..…89
Figure 40 – Sequence Model ……..…….……92
Figure 41 – Combine Model For Tsunami 1……..……93
Figure 42 – Combine Model For Tsunami 2……..……93
Figure 43 – Comparison Of Age Results ……..……..94
Figure 44 – Regional Palaeoseismology ……..……95
Figure 45 – Model Of Mw 8.9 Southern Hikurangi Earthquake ……..…..……..104
Figure 46 – Upper Plate Deformation Model ……..…..……..…104

DECLARATION

This thesis is the result of my own work and has not been submitted for consideration in any other examination. Material from the published or unpublished work of others, which is referred to in the dissertation, is credited to the author(s) in questions in the text.

STATEMENT OF COPYRIGHT

ACKNOWLEDGEMENTS

I would like to acknowledge the following people for their assistance that has made this thesis possible. The landowners, for granting access to the site for multiple visits. Jenny Dahl and the staff at the Rafter Radiocarbon laboratory, for their training in the preparation of radiocarbon samples and dating methods. Bruce Hayward, for his help identifying foraminifera species. Alan Beu, for his help identifying mollusc species. Daphne Lee and Wendy Nelson, for their knowledge of coralline algae fossils. Peter Meihana for his guidance on the Māori oral histories of Lake Grassmere. Everyone at GNS Science for making me feel so welcome. Andrew Howell for his superb fieldwork assistance and drone flying skills. Jamie Howarth for his continued support and valuable discussions. Ed Garrett and Sarah Woodroffe for their comments and reviews of endless versions of this thesis. And Kate Clark, for being the most wonderful role model and mentor.

1.0 INTRODUCTION

Globally, human populations are concentrated in coastal zones that are vulnerable to extreme wave events such as tsunami and storm surges. As these densely populated areas continue to grow, alongside sea-level rise, the hazard posed by extreme wave events becomes more prominent for coastal communities (McGranahan et al., 2007; Neumann et al., 2015). While there are many causes for these incidents, the largest wave magnitudes are generated by tsunamigenic earthquakes at subduction zones (Wallace et al., 2012). Such scenarios have been evidenced by the 2004 Sumatra-Andaman earthquake and Indian Ocean tsunami (Fujii and Satake, 2007), and the 2011 Tohoku earthquake and tsunami (Mori et al., 2011). Investigating the complex combination of earthquake and tsunami hazards in coastal zones adjacent to plate boundaries presents an extremely important topic of geological research for the protection of global coastal populations.

Tsunamigenic subduction earthquakes present the most significant natural hazard for New Zealand, with particular importance for the populated regions on the east coast (Power et al, 2016 b). There have been no significant subduction earthquakes on the Hikurangi margin in written history and therefore the geologic record must be investigated to decipher parameters such as return period, magnitude and frequency and rupture patterns (Wallace et al, 2009). While evidences of prehistoric subduction earthquakes have been located on the central and northern sections of the Hikurangi subduction margin, the southern section is poorly understood (Clark et al., 2019). The southern section is highlighted as a region of particular interest due to its limited geological record of past ruptures, which means that the magnitude and frequency of large to great earthquakes is poorly constrained, despite the potential for M_w >8 earthquakes and generation of major tsunamis (Power et al., 2018). Tsunami wave height for modelled subduction earthquakes on the southern Hikurangi margin is highly sensitive to the termination of rupture into the Cook Strait (Power et al., 2016 b). As a result, it is necessary to develop understanding of the rupture dynamics of prehistoric subduction earthquakes. Lake Grassmere is located adjacent to the Cook Strait in Marlborough, New Zealand and represents an environment with potential to contain a well-preserved record of prehistoric earthquakes and tsunamis that has not yet been investigated. This thesis explores the above themes and Holocene palaeoenvironmental changes at Lake Grassmere in order to discuss the following research questions:

1) How did the morphology of Lake Grassmere evolve during the late Holocene?
2) Is there any evidence of palaeotsunami or sudden coseismic vertical deformation?

3) How does the timing of palaeotsunami events at Lake Grassmere fit within the regional palaeoseismic record, and what are the implications for possible fault sources?

I aim to uncover a catalogue of evidence using a multiproxy approach to palaeoenvironmental reconstruction including micropalaeontology, sedimentology and radiocarbon dating, in order to answer the research question stated. I begin by providing a background on the techniques applied in the study, and then set these themes within the context of New Zealand. Detailed methodology is included, followed by a comprehensive range of results. Discussion of the results is guided by the research questions in sections 6.0 to 8.0. I summarise my findings in section 9.0, and consider the implications and recommendations for future work.

2.0 CONTEXT OF RESEARCH

In this chapter I provide a foundation of knowledge for topics including subduction zones, tsunami generation and palaeoenvironmental reconstruction, as well as the methods that have been developed to facilitate research. This is necessary for understanding the importance of the work within a global context of palaeoseismology and to support the approaches that have been taken within this thesis. Where necessary, more detail is given on topics (such as tsunamigenic submarine landslides) that hold particular relevance for the study site at Lake Grassmere, New Zealand.

2.1 Subduction Zones

Subduction zones can produce the largest and most devastating earthquakes and tsunamis. Examples include the 1960 magnitude (M_w) 9.5 in Chile and the 2004 M_w 9.3 event in Sumatra (Kanamori, 1977; Reyners, 1998; Cisternas et al*.,* 2005; Wang and Liu, 2006). In general, relatively few events have occurred within the instrumental and written historic record, increasing the importance of prehistoric studies in assessing the hazards posed by subduction zones.

Subduction zones are located where two tectonic plates converge and subduction of one plate beneath the other occurs. The force of the plates moving against each other creates a cycle of strain accumulation and sudden release in large megathrust earthquakes, namely the earthquake deformation cycle (Figure 1) (Thatcher, 1984). During the interseismic phase, extended periods of strain accumulation normally manifest in deformation of the overlying plate through shortening and extension as the interface between the plates becomes locked in places (Yeats et al., 1997). The direction of horizontal as well as vertical deformation (subsidence or uplift) at a location is a function

of proximity to the underlying plate interface and the zone of interseismic locking (Schellart, 2008). Sudden coseismic strain release during an earthquake frequently results in rapid vertical deformation in the opposite direction to the interseismic movement. Due to the large area of potential fault slip (potentially exceeding several hundreds of kilometres), subduction earthquakes can be of large magnitude (>M_w 9), with metre-scale associated vertical displacements possible on all subduction interfaces globally (McCaffrey, 2008; Schellart and Rawlinson, 2013; Senatorski, 2017). In many subduction zones, much of the locked portion of the subduction interface is offshore, and therefore when seafloor displacement occurs during large earthquakes, a tsunami may be triggered with far-reaching effects (Titov et al., 2005). This was the case for the aforementioned earthquakes of 1960 and 2004, as well as the M_w 9.2 Alaska earthquake in 1964, which generated a tsunami causing fatalities as far south as California (Shennan et al., 2009).

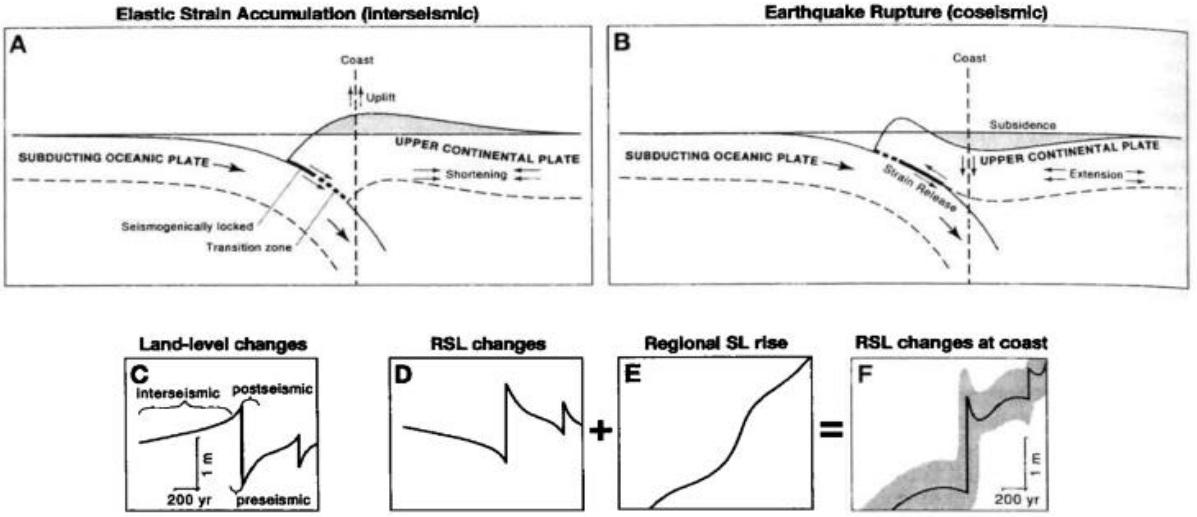

Figure 1 - Schematic diagram showing the pattern of a) gradual vertical displacement during the interseismic phase as the plates become locked and b) coseismic deformation at subduction thrust faults, c) land-level changes at the coast during two earthquakes with coseismic deformation of different amplitudes, d) relative sea level changes as a result of these cycles during a period of static sea level, e) a gradual rise in sea level over the cycles that does not account for small-scale or local variations, and f) relative sea level changes at the coast as a result of d and e. shading represents uncertainty. Figure from Nelson et al 1996.

2.2 Tsunamis

Tsunamis are defined as waves with long wavelengths and periods, caused by the sudden displacement of water by earthquakes (among other mechanisms), as energy from the rupture is transferred to the water column (Shanmugan, 2012). Tsunamigenic submarine displacement is most common on reverse (or thrust) faults in which the coseismic movement is vertical, as opposed to strike-slip faults on which coseismic movement is commonly horizontal. Consequently, large-magnitude offshore ruptures do not always generate a tsunami evidenced by the 2012 M_w 8.6 and 2016 M_w 7.9 strike-slip

earthquakes in Wharton Basin (Hill et al., 2015; Gusman et al., 2017). The longer wavelength (kilometres) of tsunamis means that they have greater potential to scour deeper and travel further inland than storm waves, which have variable energy dominated by wind-generated waves (wavelengths of metres) (Donato et al., 2008). While tsunamis generated by subduction earthquakes may generate the largest tsunamis, upper plate faults that extend offshore also pose a significant tsunami hazard.

Other causal mechanisms of tsunamis include volcanic eruptions, cosmic-body impact, and submarine landslides. Submarine landslides are particularly relevant for this study due to the identification of active land sliding in the canyons of Cook Strait, 60 km east and northeast of Lake Grassmere (Mountjoy et al., 2014; Mueller et al., 2016). While tsunami generation by submarine landslides has received little attention overall, it is thought to be associated with 7% of tsunamis worldwide (Harbitz et al., 2014). Lane et al (2016) recognise submarine landslides as an important hazard following several historic events, including the fatal Grand Banks submarine failure in 1929 (Fine et al., 2005), and the 1997 tsunami in Papua New Guinea that saw water levels rise up to 12 m and killed over 2000 people (Tappin et al., 2008). Most large failures are expected to occur during earthquake shaking but the process of scouring the base of the canyon slopes by strong tidal currents is also believed to be an important process in instigating slope failure (Power et al., 2016 a).

Tsunamis can also be discussed relative to the location where they are received. For example, a tsunami generated at the Hikurangi subduction zone would be classed as: a local source tsunami for east coast of New Zealand, a regional source tsunami for Tonga and a distant (also known as far-field or transoceanic) source tsunami for South America. This is important to consider when investigating the source of tsunami deposits as they can display similar characteristics, yet have extremely different implications in terms of their contribution to the palaeoseismology and seismic hazard assessments of a region.

2.3 Geologic evidence of palaeotsunami and palaeoearthquakes

The geologic record of events such as earthquakes and tsunamis that is preserved in sediment stratigraphy is extremely valuable for estimating various fault properties such as; the calculation of recurrence intervals, magnitudes, rupture locations and variability in fault behaviour. This is essential in locations where few large earthquakes have occurred within recorded history, such as New Zealand. Globally, the number of studies regarding subduction zone palaeoearthquakes and palaeotsunami has increased since the seminal publication of Atwater's (1987) paper describing the evidence of great Holocene earthquakes on the Cascadia subduction zone. A suite of methods to identify events

through stratigraphic and palaeoenvironmental reconstruction has now been applied in locations across the world (Nelson et al*.,* 1996; Shennan and Hamilton, 2006).

Low energy, coastal settings such as saltmarshes or coastal lagoons provide ideal locations for palaeoenvironmental reconstructions to decipher vertical land displacements, as the sea level can be used as a benchmark. This is the case at Lake Grassmere, the focus of this study. Rapid vertical deformation that is associated with sudden coseismic strain release, results in a change in environment at the coast. Over time, these land motions are recorded within the coastal sediment stratigraphy, as the depositional environments respond to alterations in marine influence (Figure 2) (Dura et al., 2016a). If conditions for preservation are conducive, records of prehistoric earthquakes and tsunamis can be extended on millennial timescales, revealing information regarding the timing, location, magnitude and recurrence intervals of major events (Witter et al., 2003; Sieh et al., 2008; Clark et al., 2015; Garrett et al., 2015). Optimal conditions for preservation are largely dependent on sea level providing sufficient accommodation space for sediment accumulation (Reed, 1995; Kelsey et al., 2015; Dura et al., 2016a). In order for tectonic vertical land motions to be deciphered, baseline understanding of the sea-level history at the study site is required (e.g. Barlow et al., 2013) (see section 3.4.2 for study-site-specific reconstruction). Techniques for the study of sea-level histories are well developed and can now facilitate the detection of coseismic land-level changes and tsunami using a range of proxies, some of which are outlined below (Atwater, 1987; Nelson et al., 1996).

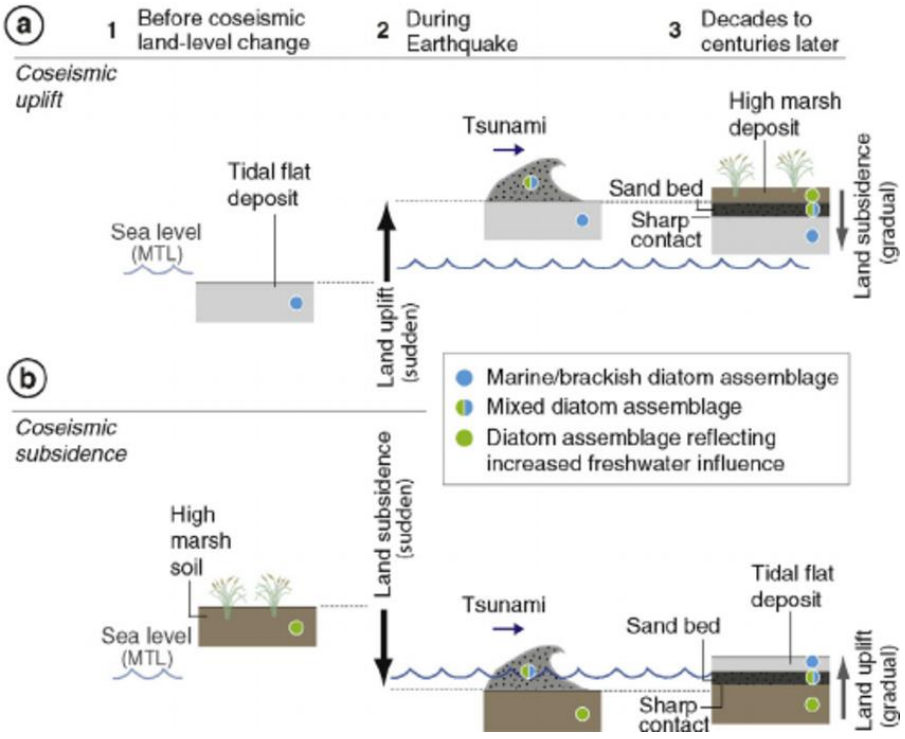

Figure 2 - Simplified schematic of coseismic uplift (a) and subsidence (b) with accompanying tsunami inundation. Figure from Dura et al 2016 b.

2.3.1 *Sedimentological evidence*

Analysis of sedimentology can reveal pattern of coseismic deformation and tsunami even by visual inspection (Atwater, 1987; Nelson et al., 1996). Shennan et al (2016) discusses sediment features of great earthquakes at subduction margins, summarised by the assessment of the following key criteria:

(a) Lateral extent of peat-mud or mud-peat couplets with sharp contacts
(b) Suddenness of submergence or emergence, replicated at multiple locations within a site
(c) Amount of vertical motion, quantified with 95% error terms, replicated at multiple locations within a site
(d) Synchronicity of submergence and emergence based on statistical age modelling
(e) Spatial pattern of submergence and emergence
(f) Possible additional evidence of coseismic motions, including tsunami or liquefaction concurrent with submergence or emergence.

Often, this is investigated through particle size analysis that can detect rapid changes in grain size associated with variations in depositional energy and environments (Plater and Shennan, 1992; Chague-Goff et al., 2011). Similarly, sediment characteristics commonly associated with tsunami deposition derived from global palaeoseismology studies have been collated by many, including Shanmugam (2012) summarised here:

(a) Sharp or erosional basal contact
(b) Upward-fining and upward-coarsening sequences
(c) Landward fining and landward thinning sand sheets
(d) Rapid increase in grain size with rip-up clasts and coarse material up to boulders
(e) Allochthonous mixing of articulated bivalve species out of life position and high amount of fragmented valves, with angular breaks and stress fractures
(f) Allochthonous microfossils indicating marine inundation (diatoms and foraminifera)

Statistical parameters such as skewness can reveal abrupt deviations in grain size that allow individual waves to be inferred (Donato et al., 2008; Higman and Bourgeois, 2008). Grain size composition can also indicate the provenance of sediment, particularly when analysed alongside modern samples of coastal environments (Chague-Goff et al., 2011).

The use of X-ray computed tomography (CT) can support grain size information or act as a proxy for grain size and density to further demonstrate variations in profiles through cores (Renter, 1989; Orsi et al., 1994). The technique was first described by Stanley and Blanchard (1967) for the interpretation of sediment cores and locating structures such as shells and pebbles. Schallenberg et al (2012), demonstrate how densitometry is used to identify abrupt changes in sediment characteristics based on the density of material. Data are extracted from a slice down the centre of the core and reported in Hounsfield Units, with -1024 reflecting air, 0 reflecting water and +2500 reflecting calcites (Fortin et al., 2013). The use of CT data for this purpose is particularly useful as the method is non-destructive and much more rapid than extensive preparation methods necessary for traditional grain size analysis, allowing comprehensive core-to-core correlation (Axelsson, 2001).

2.3.2 Biostratigraphic evidence

Techniques designed for high-resolution sea-level reconstructions identify vertical land motions within the sediment record using microfossils (Shennan et al., 1999; Cochran et al., 2007). A schematic of how this works is shown in Figure 3 (Pilarczyk et al., 2014). Microfossil assemblages can be sensitive to changes in coastal environments associated with vertical land deformation and marine inundation (Scott and Medioli, 1980; Shennan et al., 1999). The taphonomy of microfossil and macrofossil assemblages can be used to infer the provenance and transport history of sediments, through the analysis of features such as fragmentation, preservation and bio-encrustation (Hemphill-Haley, 1996; Pilarczyk and Reinhardt, 2012). Nevertheless, conditions are not always conducive for preservation, and other issues such as reworking can complicate interpretation and should be kept in mind when considering microfossils. Statistical analysis is often performed on fossil assemblages, using modern analogues to reconstruct palaeoenvironments within sediment cores (Scott and Medioli, 1986; Guibault et al., 1995; Shennan et al., 1996). The resolution of microfossil data in this study is not suited to further statistical manipulation and therefore discussion of techniques is not included.

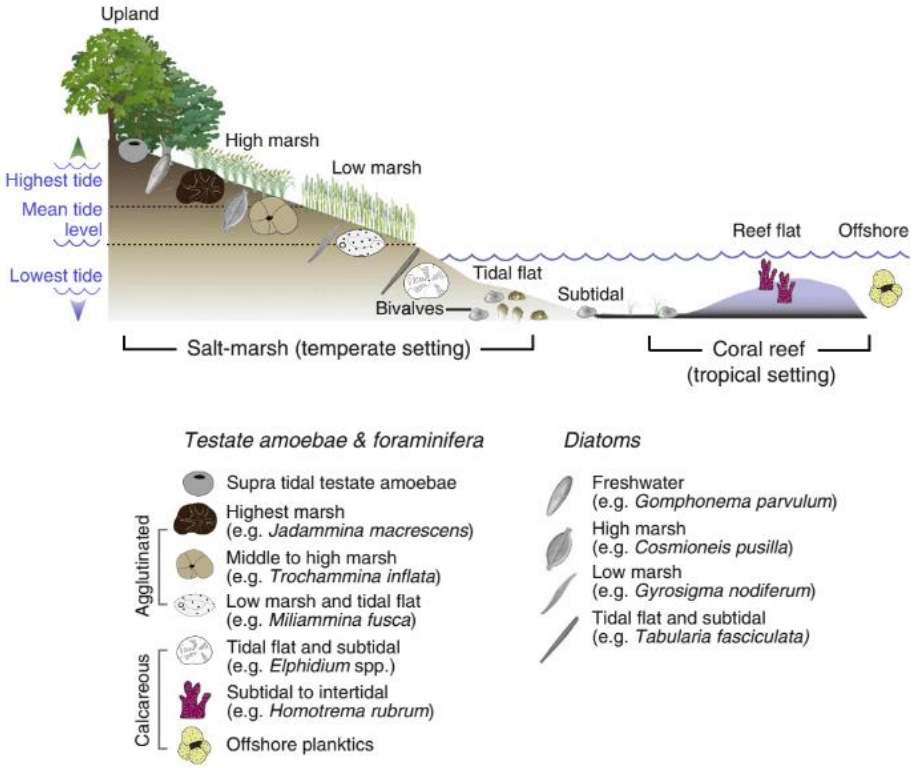

Figure 3 - Schematic showing the generalized varied ecological tolerances and optima of microfossils demonstrating a vertical zonation of assemblages in accordance with the tidal frame at a location. Figure from Pilarczyk et al 2014.

Foraminifera: Foraminifera are single-celled protozoans with secreted or agglutinated tests that inhabit brackish to marine environments (Murray, 2011). Agglutinated species are particularly useful as they are restricted to upper-intertidal settings (Horton, 1999). Multiple studies have utilised foraminifera to reconstruct coseismic land-level changes near subduction zones, such as in Cascadia (Hawkes et al., 2010) and in New Zealand (Hayward et al., 2015 b). Investigation into the variation in test sizes of foraminifera has been used to distinguish high-energy deposits within sediment cores. Scott (1961) used one common species of benthic foraminifera to identify Miocene turbidites by recognising a minor modification of the faunal test sizes from original distributions. Hayward et al (2019) show that test size profiles of foraminifera can be a useful tool to distinguish between unmodified and taphonomically-modified foraminiferal faunas.

Diatoms: Diatoms are single-celled photosynthetic algae with siliceous shells, that live in a range of environments from fully marine to freshwater - an advantage over foraminifera that do not inhabit locations above local highest astronomical tide level (Murray, 2011; Pilarczyk et al., 2014). Examples of the application of diatom analysis within palaeoseismology include Shennan and Hamilton (2006) and Zong et al (2003), who identify six episodes of the earthquake deformation cycle in south Alaska, showing preseismic as well as coseismic signals. A study by Hemphill-Haley (1995) demonstrates how diatom analysis can define the landward limit of tsunami inundation, showing that

microfossils can trace a signal inland more accurately than the extent of the sediment deposit.

Molluscs: Mollusc shells have been utilised in studies of palaeotsunamis (Morales et al., 2008; Engel et al., 2016; Ando et al., 2018; Mannen et al., 2018) in locations including Oman (Donato et al., 2008) and the British Virgin Islands (Reinhardt et al., 2012). Some research suggests that bivalves are more suitable for the identification of tsunami deposits than microfossils due to their ability to infer live transport (Donato et al., 2008). Kitamura et al (2018 b) demonstrate how allochthonous, articulated bivalves within an anomalous sediment deposit can indicate mass live transport of individuals over substantial distances. The landward extent of deposits containing such shell characteristics infer a tsunami origin, as other mechanisms such as storm waves would be unable to entrain and transport such dense collections of fragile molluscs over long distances. The taphonomy of shells can also be indicative of depositional mechanisms, as the degree of fragmentation and abrasion can suggest whether individuals were reworked post-death, or whether they are well-preserved due to the rapid infilling of sediment (Reinhardt et al., 2006).

2.3.3 Attributing seismically-induced changes within sediment sequences

As outlined, a substantial catalogue of sedimentary and biostratigraphic characteristics have been compiled for the purpose of identifying coseismic deformation within sediment sequences (Nelson et al., 1996; Shennan et al., 2016). Nevertheless, it is often difficult to differentiate sedimentary couplets caused by coseismic deformation from those generated by other mechanisms, as processes such as rapid compaction (Plafker, 1969) and sudden breaching of coastal barriers may produce comparable deposits. In such cases, the lateral extent of synchronous deposits and possibility of accompanying tsunami sediment becomes important (Nelson, 1992).

While the presence of an overlying tsunami deposit is often the most useful indicator of coseismic deformation it is possible to encounter a palaeotsunami deposit that is not concurrent with a signature vertical deformation. In this case it is extremely difficult to isolate tsunami deposits from other high-energy overwash sources such as fluvial floods, storm surges and hurricanes (Pilarczyk et al., 2014). It is here that detailed microfossil studies are of high priority for distinguishing the environmental origin of species within displaced sediment e.g. offshore marine or freshwater. Shanmugam (2012) gives an example, with a compelling argument for the likeness between prehistoric cyclone and tsunami deposits, claiming that there are “no reliable sedimentological criteria for distinguishing palaeotsunami deposits in various environments”. To date, no single

diagnostic characteristic of palaeotsunami deposits has been identified therefore; a multi-proxy approach that gives attention to the local geomorphic and stratigraphic context of the deposit is favoured (Chagué-Goff et al., 2011).

2.4 Dating Palaeoearthquakes and Palaeotsunami Deposits

The most commonly applied technique used to date coseismic deformation and palaeotsunami deposits is radiocarbon dating (Engel et al., 2016). This involves accelerator mass spectrometry (AMS) to determine the decay of the carbon-14 isotope in organic and carbonate material. AMS is a destructive method but is advantageous as in most cases it only requires a small sample size to obtain a radiocarbon date, which is useful when the size of sediment cores limits how much material is captured (Linick et al., 1989).

While methods for dating palaeotsunami and coseismic deformation can vary slightly, it is common practice to target dating resources at horizons that bound the event in order to give the best age estimate for the timing of the event by avoiding reworked material, for example above and below the allochthonous tsunami sediment, or just below and above the deformation layer (Clark et al., 2015; Engel et al., 2016). It is important to be specific in selecting material for dating; short-lived fragile organic fractions (e.g. fine reed segments, juvenile shells and seeds) are often preferred, due to a lesser chance of selecting material that has been reworked into the targeted unit and carries a high inbuilt from older sediments (McFadgen, 1982). Sometimes this is not possible for palaeotsunamis if there is insufficient dateable material in bounding units, as in this study, in which case dating is focused within the tsunami deposit itself (Fujino et al., 2014; King et al., 2017; Ando et al., 2018; Ishizawa et al., 2018. The nature of tsunami deposits means that the sediment is reworked and therefore dateable material, such as shells, is likely to reflect a range of environments and ages that do not represent the timing of the event (Ando et al., 2018; Kitamura et al., 2018 b; Mannen et al., 2018). This means that only a maximum possible age for the event can be obtained, under the assumption that the dated specimen died as a direct result of the tsunami. For this reason the selection of specimens is important and often targets the outer growth rings of fragile, juvenile, articulated bivalves, as they are most likely to have been transported alive and subsequently died as a result of the tsunami deposition, rather than dying prior to the event and being subject to reworking. Additionally, dating a common species can useful as it allows comparisons between other studies. The intertidal bivalve *Austrovenus stutchburyi* (common cockle) is commonly dated in New Zealand (Higham and Hogg, 1995; Hogg et al., 1997), and information regarding the lifecycle of this species is well known. This infaunal suspension feeding clam can grow to between 15-65 mm in length

and live for ~10 years in the top 5 cm of sediment intertidal mud and sand flats (Purchase and Fergusson, 1986; Hewitt et al., 1996).

Foraminifera can also be used for radiocarbon dating palaeotsunamis and are often useful in tsunami sediments that do not contain molluscs or terrestrial material (Wacker et al., 2013). Issues with using benthic foraminifera include the difficulty in obtaining sufficient mass to produce a large enough target for dating. Furthermore, there is no method for the preparation of foraminifera samples as they are too fragile for the commonly used acid etching process and removal of infilling sediments (Beta Analytic, 2019).

2.4.1 Calibration and the marine reservoir effect

Terrestrial and marine radiocarbon dates require different calibrations to convert results from conventional radiocarbon ages to calendar ages. Calibration is necessary as elemental ratios have not been constant through time. In this study, the southern hemisphere calibration SHCal13 is used for terrestrial samples (Hogg et al., 2013). The ocean is a large reservoir for carbon and therefore specimens that acquire carbon from the ocean (marine carbonates) require a correction (ΔR) when calculating radiocarbon ages to allow comparison of marine dates with terrestrial dates. The global average reservoir (R) offset is ~400 radiocarbon years; however this value varies regionally as a function of climate and oceanic circulation (Ascough et al., 2005). The Marine13 calibration curve (Reimer et al*.,* 2013) is used for carbonate samples in this study, with the most suitable regional ΔR correction of 4 ± 25 years. This value was derived from dating 10 rocky shoreline molluscs that died due to coastal uplift in the AD 1855 Wairarapa earthquake at Turakirae Head, 70 km north east of Lake Grassmere (McSaveney et al., 2006; J Turnbull 2018, personal communication, 10 December).

2.5 Chapter Summary

This chapter has given a broad overview of the cornerstone topics within this thesis, giving background to research techniques that will be applied. As a result, it is now possible to set the research themes within the geographic context of New Zealand, giving more specific details regarding the state of research in this location, in order to highlight gaps in knowledge that substantiate the importance of this study.

3.0 STUDY SITE

3.1 Tectonic Setting of New Zealand

This section considers the tectonic setting, historic and prehistoric seismicity, sea-level change and previous studies relevant to the Lake Grassmere study site. Attention is given to the southern Hikurangi subduction margin and the north-eastern Marlborough fault system, as Lake Grassmere straddles these two tectonic regimes.

3.1.1 The Hikurangi Subduction margin

The Hikurangi subduction zone is located offshore of the east coast of the North Island, where the Australian and Pacific plates converge obliquely at rates ranging from 27 mm/yr in the south to 57 mm/yr in the north (Figure 4a) (Wallace et al, 2004). The plate interface dips westward beneath the southern North Island and northeastern South Island and lies approximately 25 km beneath Wellington and Blenheim (Williams et al., 2013). Interseismic coupling patterns are variable along the margin, shown in Figure 4b (Wallace et al., 2014). There is no formal method of partitioning the margin, however for the purpose of this study it has been split into the northern, central and southern sections based on Clark et al (2019) (Figure 4b). The northern and central sections of the offshore of Hawke's Bay and the Raukumara Peninsula are weakly coupled, however have been the focus of 'tsunami earthquakes' (section 3.2.1) (Power et al*.,* 2008). The southern section of the interface, offshore of the east coast and underlying the southern region of the North Island is strongly coupled and is storing elastic energy that is capable of release in large earthquakes (Power et al*.,* 2008). Wallace et al. (2009) suggest that the particularly strongly coupled patch from Cook Strait to Cape Turnagain is a likely rupture area for a M_w >8 plate interface earthquake.

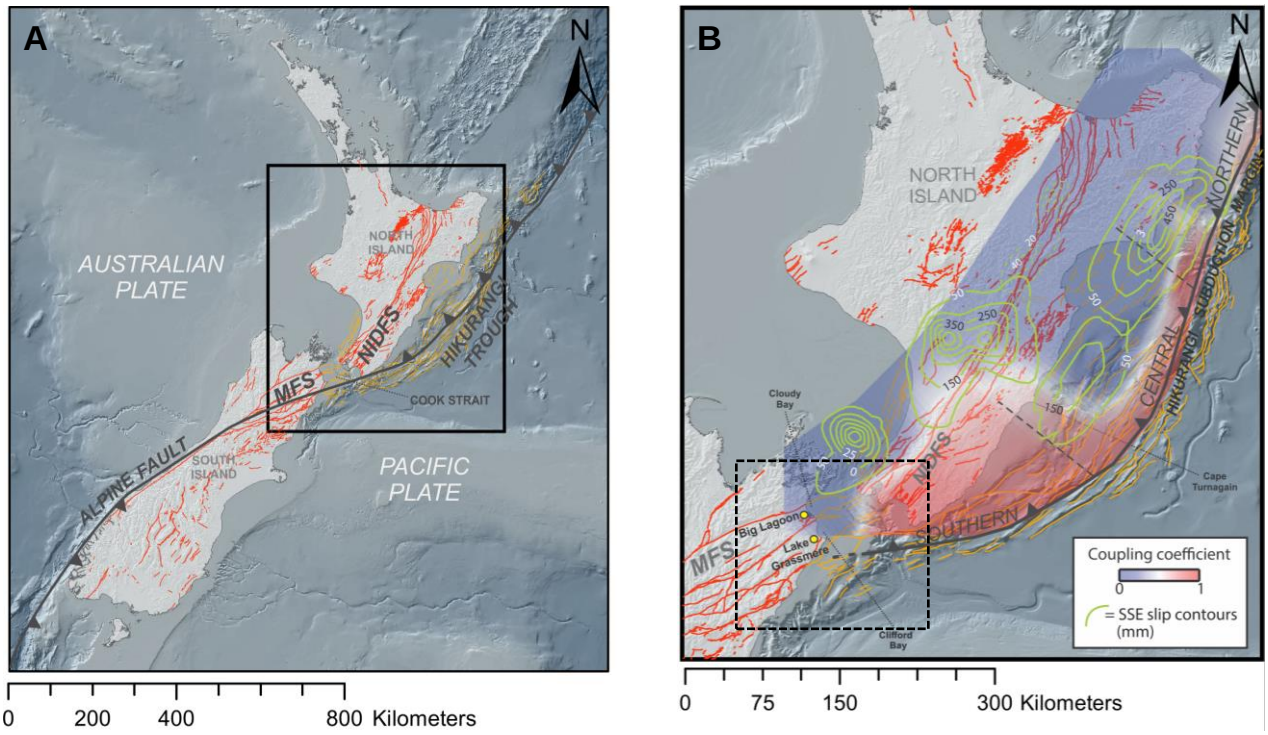

Figure 4 – A) Tectonic setting of New Zealand including plate boundaries and active onshore (red) and offshore (yellow) faults. B) Hikurangi subduction margin is shown, with displayed subdivisions of southern, central and northern sections used in this study). NIDFS = North Island Dextral Fault System, MFS = Marlborough Fault System. Interseismic coupling coefficients (red to blue scale) measured by campaign GPS, and cumulative slip in slow slip events between 2002 and 2012 (SSEs) (green contours, in mm). Yellow dots highlight the location of Lake Grassmere and Mataora-Wairau Lagoon. Dashed line indicates extent of Figure 5.

3.1.2 The Marlborough Fault System

Transpressional northeast-striking dextral strike-slip faults, known as the North Island dextral fault system (NIDFS), in the forearc of the Hikurangi margin, accommodate most of the margin-parallel plate motion (Nicol and Beavan, 2003; Litchfield et al., 2013). Around 70% of dextral slip is taken up on the Wairarapa and Wellington (Figure 5) (Little et al., 2009). At the southern end of the margin, plate motion is transferred onto the upper plate faults of the Marlborough fault system (MFS) (Figure 5). A complex network of submarine stepovers across the Cook Strait links these two systems (Pondard and Barnes, 2010).

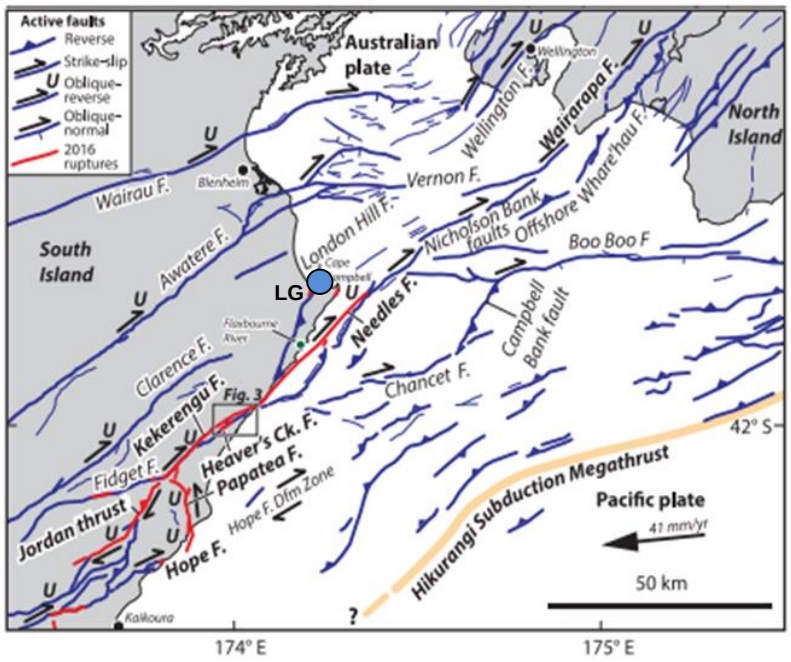

Figure 5 - Tectonic map of the Cook Strait and major faults within the Marlborough Fault System (MFS), including the northern ruptures of the 2016 Mw 7.8 Kaikoura earthquake (red). Note LG = Lake Grassmere, indicated by the blue circle. Extent is shown in Figure 4b. Adapted from Little et al., 2018.

The MFS comprises active strike-slip upper plate faults such as the Wairau, Awatere, Clarence, and Kekerengu faults. These faults facilitate the transition from oblique subduction at the Hikurangi trough to continental transpression at the Alpine fault transform plate boundary in the south (Bourne et al., 1998; Van Dissen and Yeats, 1991; Wallace et al*.,* 2012 a). Late Quaternary slip rates and geodetic strain measurements suggest that the MFS accommodates most (~80%) of the relative motions between the Pacific and Australian plates (Benson et al*.,* 2001). Recent discussion surrounds the degree to which the subduction interface actively accommodates plate motion in the region beneath the northern and eastern parts of the MFS (e.g. Holden et al., 2017; Wang et al., 2018), after studies of the 2016 Kaikoura earthquake suggested there may have been slip on the subduction interface during and after the 2016 earthquake (Wallace et al., 2018).

Within the MFS, active faults closest to Lake Grassmere include: London Hills, Needles, Kekerengu, Awatere, Clarence and Wairau. Knowledge of regional palaeoseismology is important when investigating potential palaeoearthquake and palaeotsunami deposits, as the correlation of event ages can aid the attribution of rupture sources. Table 1 outlines recurrence intervals and slip rates of relevant faults within an 80 km radius of the study site.

*Table 1 – Information on faults within the NFS and NIDFS, relevant for the study of Lake Grassmere. Recurrence intervals and slip rates have been collated from papers indicated in the references column, where more information on the faults can be found. Fault type: SS = Strike-slip, R = Reverse, T = thrust, N = Normal. * Slip rates from models of faults that have no current palaeoearthquake record, from Pondard and Barnes, 2010.*

Fault	Proximity to Lake Grassmere	Slip rate / mm/yr	Recurrence interval / yrs	Fault type	References
Awatere	15 km north	6	1400	SS	DeMets et al., 1994; Little et al., 1998; Benson et al., 2001; Mason and Little, 2006
Boo Boo	63 km east	11*	-	SS	Pondard and Barnes, 2010
Clarence	25 km south-west	4.5	1700	SS	van Dissen and Nicol, 2009; Pondard and Barnes, 2010
Cloudy	30 km north-east	2.5	3000	N	Pondard and Barnes, 2010
Hope	45 km south	11	130	SS	Cowan and McGlone, 1991; Nicol et al., 2012
Kekerengu	30 km south	24 ± 12	376 ± 32	SS	Little et al., 2018
London Hills	5 km east			R	Townsend and Little, 1998
Needles	15 km east	11*		SS	Kearse et al., 2018
Nicholson Bank	30 km north east	-	-	SS	-
Ohariu	60 km north east	1.5	1180	SS	Litchfield et al., 2010
Vernon	20 km north	3.1	3140	SS	Pondard and Barnes, 2010; Nicol et al., 2012
Wairarapa	80 km north-east	11.3 ± 3	1230 ± 190	SS / R	Langridge et al., 2005; McSaveney et al., 2006; Little et al., 2009
Wairau	35 km north	3-5	1000	SS	Zachariasen et al., 2006; Barnes and Pondard, 2010; Nicol and van Dissen, 2018
Wellington	60 km north-east	6.6	1910	SS	Pondard and Barnes, 2010
Wharekahau	40 km north-east	2.5*	-	T	Schermer et al., 2009; Pondard and Barnes, 2010

3.2 Historic Earthquakes and Tsunami on the Hikurangi Subduction Margin & MFS

The governing reason for the lack of knowledge surrounding past earthquakes in New Zealand is the short (~170 years) written historical record of events that only extends back to 1840 (Wallace et al., 2009). In order to compile existing data, a database of historic tsunami in New Zealand was constructed in 1986, dating 32 events back to 1840 AD (De Lange and Healy, 1986). The database was most recently updated by Downes et al (2017). There is no equivalent resource for earthquakes; however, all large historic events are listed online by GeoNet (2019). Despite the shortness of the historical record, a wealth of knowledge is held in the events that New Zealand has experienced, providing marked insights into rupture patterns and mechanisms (Figure 6).

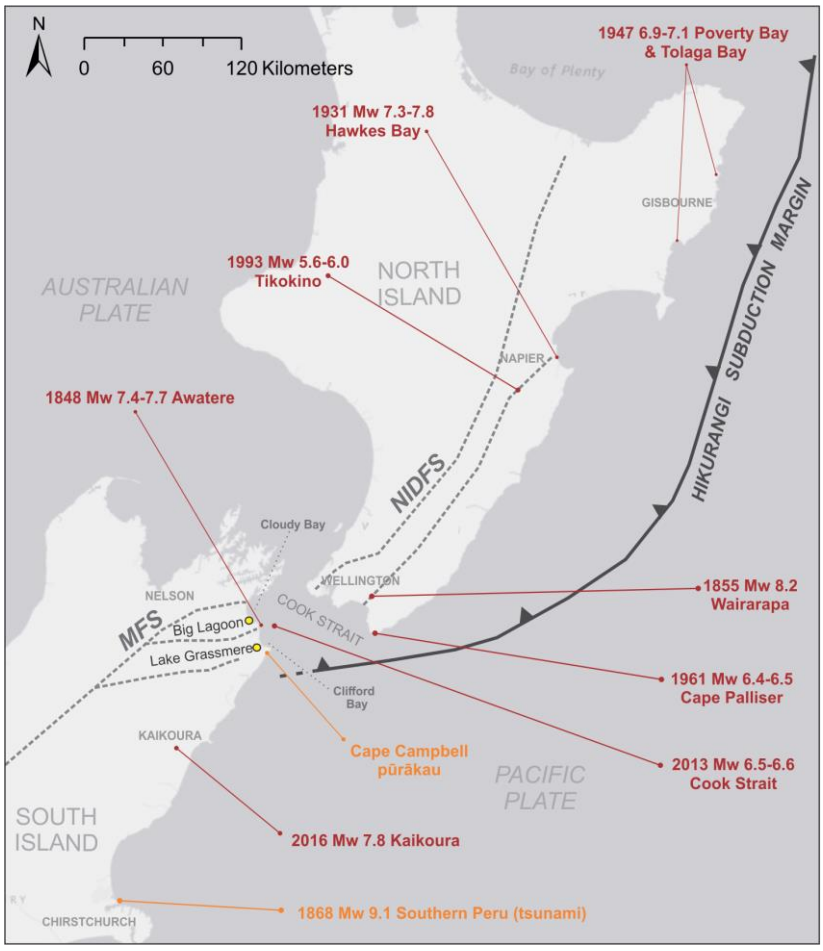

Figure 6 - Map of epicentres of notable historic earthquakes in New Zealand. Also included are references to the Cape Campbell pūrākau (section 3.2.5) and the location near Christchurch where the tsunami from the 1868 Mw 9.1 Southern Peru earthquake was recorded (section 3.2.3).

3.2.1 Subduction earthquakes and tsunami

There have been no significant (M_w >7.2) earthquakes that can be unequivocally located on the Hikurangi subduction interface since historic records began ~170 years ago (Doser and Webb, 2003; Wallace et al., 2009). The largest subduction earthquakes that have been recorded on the Hikurangi margin occurred in Poverty Bay (M_w 7.0–7.1) and Tolaga Bay (M_w 6.9–7.1) in 1947. These earthquakes, on the northern section of the margin, triggered a regional tsunami with a maximum run up of 10-11 m north of Gisborne (Bell et al*.,* 2014). This type of event is now referred to as a 'tsunami earthquake', in which the shallow, often prolonged shaking causes a larger than expected tsunami response (Polet and Kanamori, 2000), and is characteristic of seismic activity close to the shallow northern section of the margin (Bell et al., 2014). Other earthquakes that have occurred elsewhere on the subduction interface include the 1961 (M_w 6.4–6.5) offshore of Cape Palliser in the southern section, and the 1993 M_w 5.6–6.0 Tikokino earthquake in the central section around Hawke's Bay (Wallace et al*.,* 2009).

3.2.2 Upper plate earthquakes

While the Hikurangi margin has been seismically active in historic times, almost all significant earthquakes have been on upper plate faults (Clark et al*.,* 2015). Table 2 details five damaging, large magnitude earthquakes that have impacted New Zealand in recorded history, the locations of which are displayed in Figure 6.

Table 2 – Information on five large-magnitude earthquakes that have occurred in New Zealand since 1840's.

Fault	Location	Year	Magnitude / M_w	Coastal deformation	Tsunami	References
Awatere	Marlborough	1848	7.4-7.7	0.4-3.2 m	None reported	Grapes et al*.,* 1998; Grapes and Holdgate, 2014
Wairarapa	South North Island and Cook Strait	1855	8.2	6.4 m max. at Turakirae Head	Up to 10 m run up south of Wellington	Darby & Beanland 1992; Grapes and Downes, 1997; Beavan & Darby 2005; McSaveney et al., 2006; Little et al*.,* 2009; Grapes and Holdgate, 2014
Reverse-dextral blind upper plate fault near Napier	Hawkes Bay	1931	7.8	-0.7 to +2.7 m	Some inundation into river channels	De Lange and Healy, 1986; Hull, 1990
Unidentified northeast–southwest oriented upper plate structure	Southern Cook Strait	July & August 2013	6.6 & 6.5	None reported	None reported	Holden et al., 2013; van Dissen et al., 2014; Hamling et al., 2014; Kaneko *et al.*, 2015
Multiple inc. Kekerengu, Hope, Needles.	Kaikoura	2016	7.8	-2.5 to +6.5 m along 110 km	Max. run up 7 m	Clark et al*.,* 2017; Hamling et al*.,* 2017; Power et al*.,* 2017

3.2.3 Distant source tsunamis

Most documented historic tsunamis from the Pacific basin have impacted the east coast of New Zealand, partly highlighting its exposure to pan-Pacific events as well as the presence of a tsunamigenic seismic zone off the east coast of the North Island (De Lange and Healy, 1986). As a result, distant source tsunamis must be considered in this study as Lake Grassmere is situated on the east coast of the South Island. Of the nine documented historic distant source tsunami, South America is identified as the source that produces the highest waves reaching New Zealand; however, tsunami heights remain considerably higher from

regional sources (De Lange and Healy, 1986). Three of these South American tsunamis propagated towards New Zealand from locations in the vicinity of northern Chile in AD 1868, AD 1877 (M_w 9.0 Northern Chile), and AD 1960 (M_w 9.5 Southern Chile) (Power et a*l.,* 2007). The most extensively recorded tsunami experienced in New Zealand was a result of the 1868 M_w 9.1 earthquake in Southern Peru. The earthquake that occurred off the coast of the Peru-Chile border generated three waves that reached New Zealand 15 hours after the main earthquake (Berryman, 2005). Reports suggest waves of up to 10 m were experienced on Chatham Islands, decreasing to 7.6 m in Lyttleton Harbour on the east coast of the South Island (near Christchurch) (De Lange and Healy, 1986). Other locations recorded to have produced tsunamis that reached New Zealand include Alaska, Indonesia and Japan.

3.2.4 Alternative sources

Alternative sources of tsunami wave generation are mentioned in section 2.2 and triggers such as submarine landslides within the Cook Strait canyon are significant for central New Zealand and the study area (Mountjoy et al*.,* 2014; Mountjoy et al., 2018). Geological studies of the canyon system walls have mapped over 100 large landslide scars in the upper, shelf-incising canyons that are in shallower water closer to the land and therefore likely to pose a tsunami threat (Power et al., 2016 a). While radiocarbon dating has revealed that these landslides were all active during the Holocene, it remains challenging to assess their tsunamigenic potential on land (Power et al., 2016 a). While evidence for submarine landslides was recovered after the 2016 Kaikoura earthquake, the offshore fault rupture component satisfies the tsunami budget recorded by tide gauges (Gusman et al., 2018). It could be suggested that high-magnitude regional earthquakes do not activate submarine landslides capable of tsunami generation in Cook Strait, however more localised ruptures have the potential to generate tsunamigenic submarine landslides, and therefore should be considered within palaeotsunami studies.

3.2.5 Pūrākau

Traditional narratives of Maori (pūrākau) hold potential to record past seismic events and tsunamis in New Zealand and can be used to indicate areas of historic activity. Archaeological studies have located human remains from the Wairau bar (enclosing Mataora-Wairau Lagoon) dating back to the early 13th century, close to when humans are thought to have first arrived in New Zealand (Higham et al., 1999). The study area of Lake Grassmere (Kāpara Te Hau) and surrounding land is an example of an area in which pūrākau could be suggestive of palaeotsunami events. Traditions tell of a taniwha (monster) that lived in a cave at Cape Campbell, who took the form of a large tidal wave that would

wash several hundred people at a time into the Wairau Lagoon where they would drown (King and Goff, 2010). One particular oral history detailed by Elvy (1949), tells of how Kupe (of the Matahourua canoe) created Lake Grassmere and Wairau Lagoon 'in anger' when he caused the sea to rise up and wash over Haumia's land and gardens. Elvy (1949) and King and Goff (2010) suggest that this pūrākau and similar traditions in the area hold significant information regarding 'ancient seismic disturbance' and are likely referencing events that occurred within Maori settlement that caused significant migrations (King and Goff, 2010; King et al., 2017).

3.3 Prehistoric Earthquakes and Tsunami on the Southern Hikurangi Margin

Determining the seismogenic potential of the subduction interface is critical for estimating seismic and tsunami hazard in central New Zealand (Wallace et al., 2009). In the absence of a rich historic record of subduction earthquakes, the prehistoric record derived from geological studies is critical. Geomorphic and sedimentary evidence for coseismic events in coastal areas adjacent to the central section of the Hikurangi margin has been attributed to subduction earthquakes (Cochran et al., 2006; Hayward et al., 2016). Cochran et al (2006) discusses evidence for two instances of coseismic subsidence and tsunami in northern Hawke's Bay at ~5550 and ~7100 cal BP, characterised by abrupt interruptions of chaotic, coarse-grained units of marine origin with microfossil assemblages indicative of land level change. Hayward et al (2016) also locate these events at Ahuriri Lagoon and suggest four younger earthquake displacement events at 4200, 3000, 1600, and 600 cal B.P. While these findings are extremely important for Hawkes Bay, without any correlative evidence from elsewhere on the margin a recurrence interval from Hawkes Bay alone would not apply to the whole margin. Further to this, the national palaeotsunami database that collects information on inferred tsunami evidence of varying validity from disparate sources, only contains entrances of palaeotsunami evidence of excellent validity from 4 locations south of Hawke's Bay (Goff et al., 2009; Downes et al., 2017; New Zealand Palaeotsunami Database, 2017). These issues highlight the need to expand current understanding of the northern and southern Hikurangi margin, to correlate strong evidence of subduction earthquakes found in the central region.

The southern section of the Hikurangi subduction margin has been highlighted as an area that requires further research to expand current knowledge of its rupture behaviour and to forecast behaviour during future earthquakes (Clark et al., 2015; Power et al., 2016; Clark et al., 2019). There have been no historic earthquakes on the southern section of the Hikurangi

subduction margin and evidence of only two prehistoric subduction EQs has been identified (Clark et al., 2015). This means that it is particularly poorly constrained with regards to low frequency, large magnitude earthquakes that pose the largest seismic threat to central New Zealand, particularly for the capital city of Wellington (Power, 2013; King, 2015).

Understanding the southern portion of the subduction margin is of particular importance as locking models suggest that it is currently accumulating substantial elastic strain (Wallace et al., 2014). The slip rate deficit on the interface becomes lower beneath the Cook Strait and northern South Island, suggesting that a subduction earthquake rupture would be likely to terminate in this region (Wallace et al., 2004). Wallace et al (2009) calculate that if the scaling relationships between fault area and seismic moment of Abe (1975) are applied to the 230 km southern segment of the interface beneath the lower north Island and into Cook Strait, the outcome would be a rupture with a magnitude of ~ M_w 8.5-8.7.

The poorly understood southern limit of ruptures on the southern Hikurangi has implications for tsunami hazard in central New Zealand. Power et al (2016 b) provide modelled scenarios highlighting that the distance the interface rupture patch extends into the Cook Strait has significant implications for tsunami wave height within Wellington harbour. Figure 7 shows the predicted wave height for Wellington increases by a factor of 3 with a 33 km extension of the rupture patch southward into the Cook Strait.

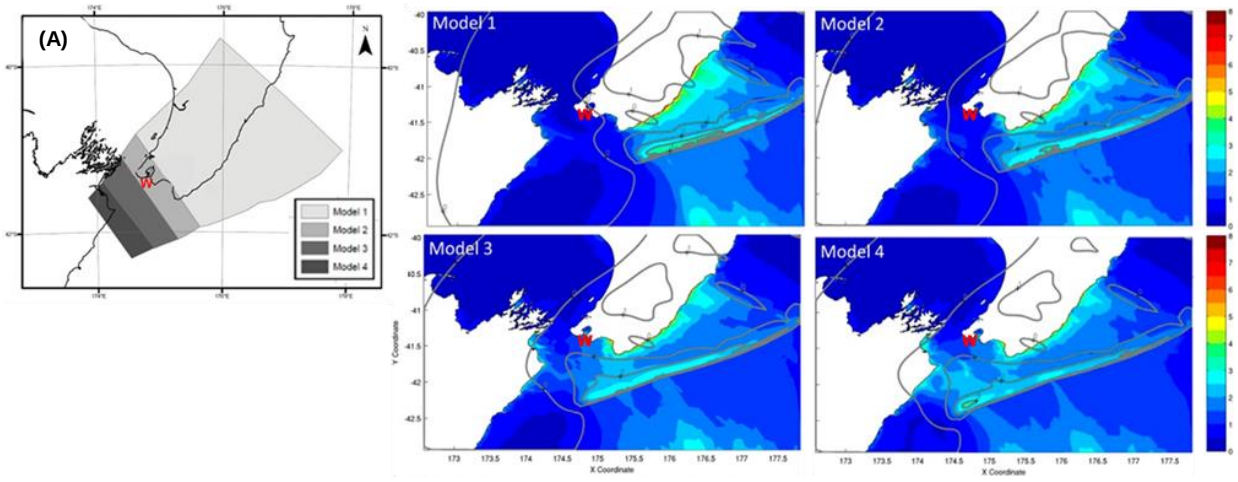

Figure 7 – A) Rupture blocks used for four models (1-4). Rupture areas build cumulatively e.g. model 4 includes extensions made in models 2 and 3. All models represent M_w 8.7 earthquakes but differ in extent of rupture into the Cook Strait. Models 1-4 show the tsunami maximum water surface elevations (m) for each rupture block. Adapted from Power et al., 2016 b.

Clark et al (2015) revealed evidence of two instances of coseismic subsidence in the last 1000 years in the north-eastern South Island at Mataora-Wairau Lagoon (also called Big Lagoon). Mataora-Wairau Lagoon is a low-lying series of lagoons adjacent to Cloudy Bay, just south of Cook Strait. The sequence studied by Clark et al (2015) consisted of subsided

paleosols overlain by marine silt and sand and in one case, evidence of tsunami inundation. Coseismic subsidence of ~0.5 m was dated to 880-800 cal BP, accompanied by a tsunami deposit, with another event of ~0.3 m subsidence at 520-470 cal BP. Consideration of regional palaeoseismicity and elastic dislocation modelling suggested that the most likely source for these events is rupture of the subduction interface.

A second study at the same location by King et al (2017), confirmed the two subsidence events as well as a possible tsunami accompanying the ~500 cal BP earthquake. In addition, King et al (2017) report a third possible tsunami dated to ~2000 cal BP, characterised by an anomalous fine-medium sand with embedded shell hash and charcoal. It is suggested that this older tsunami was also generated by slip on the subduction interface or the Wairarapa fault. Clark et al (2015) show tsunami models of a hypothetical rupture of the southern Hikurangi margin (Figure 8a) and the 1855 M_w 8.2 Wairarapa earthquake (Figure 8b), both of which show tsunami waves capable of inundating Cloudy Bay and Clifford bay.

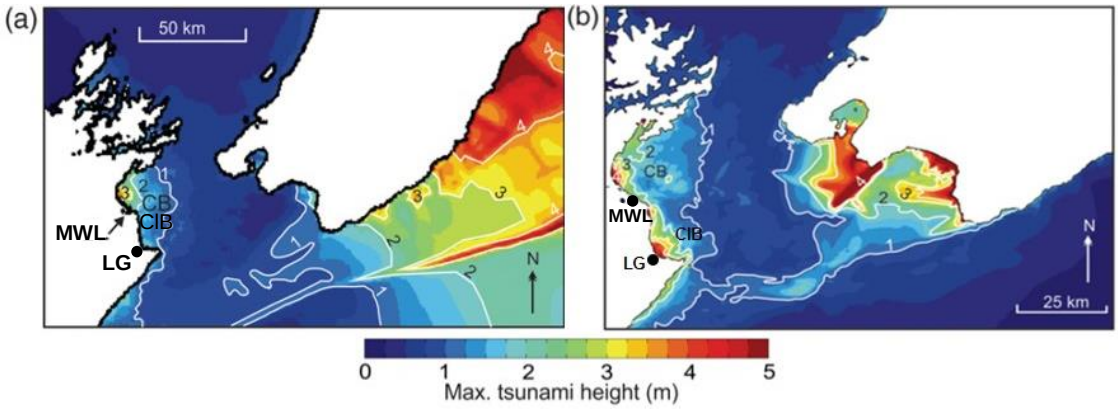

Figure 8 - (a) Model of a subduction earthquake generated tsunami (Mw 8.8) along the southern and central margin. The scale shows the maximum increase in water level above (0-5 m max). White contours show meter gradations in tsunami height. Note MWL = Mataora-Wairau Lagoon, CB = Cloudy Bay, ClB = Clifford Bay, LG = Lake Grassmere. (b) Model of the tsunami generated by the 1855 Mw 8.2 Wairarapa earthquake. Note inundation into Cloudy Bay and Clifford Bay. Adapted from Clark et al., 2015.

It is clear that the southern section of the Hikurangi margin represents an area of great potential hazard that is currently poorly constrained due to a lack of evidence of prehistoric events. While there is difficulty in isolating interface-induced vertical displacements and tsunami deposits from other upper plate events, such studies are of very high value as current knowledge is limited. Consequently, papers such as Power et al (2016 b) call for paleosiesmological studies to build on studies such as Clark et al*.,* (2015) to uncover more evidence of palaeoearthquakes and tsunamis occurring in the region of the southern section of the margin to identify more possible subduction events and extend the record to improve modelling. As a result, Lake Grassmere was carefully chosen as the study site for this thesis to fulfil this need.

3.4 Lake Grassmere

Lake Grassmere is a large coastal lake located ~40 km south east of Blenheim and 20 km south of Mataora-Wairau Lagoon (Figure 9). The former estuary embayment currently occupies approximately 17 km^2, separated from the adjacent Clifford Bay by a gravel barrier. The modern landscape at Lake Grassmere has been heavily modified for salt extraction since the 1940s (Figure 10) due to its optimal conditions of low-lying land with a warm and dry climate (Boffa Miskell, 2015). Connection to the ocean is artificially controlled by the saltworks to allow the correct amount of inflow for various stages in the salt extraction process (Dominion Salt Ltd, 2019). Previous to this modern land-use, historic accounts refer to Lake Grassmere existing as a 'dust bowl' in summer months and a 'muddy puddle' in winter, with other uses including a bombing range and aerodrome during the Second World War (Walrond, 2006).

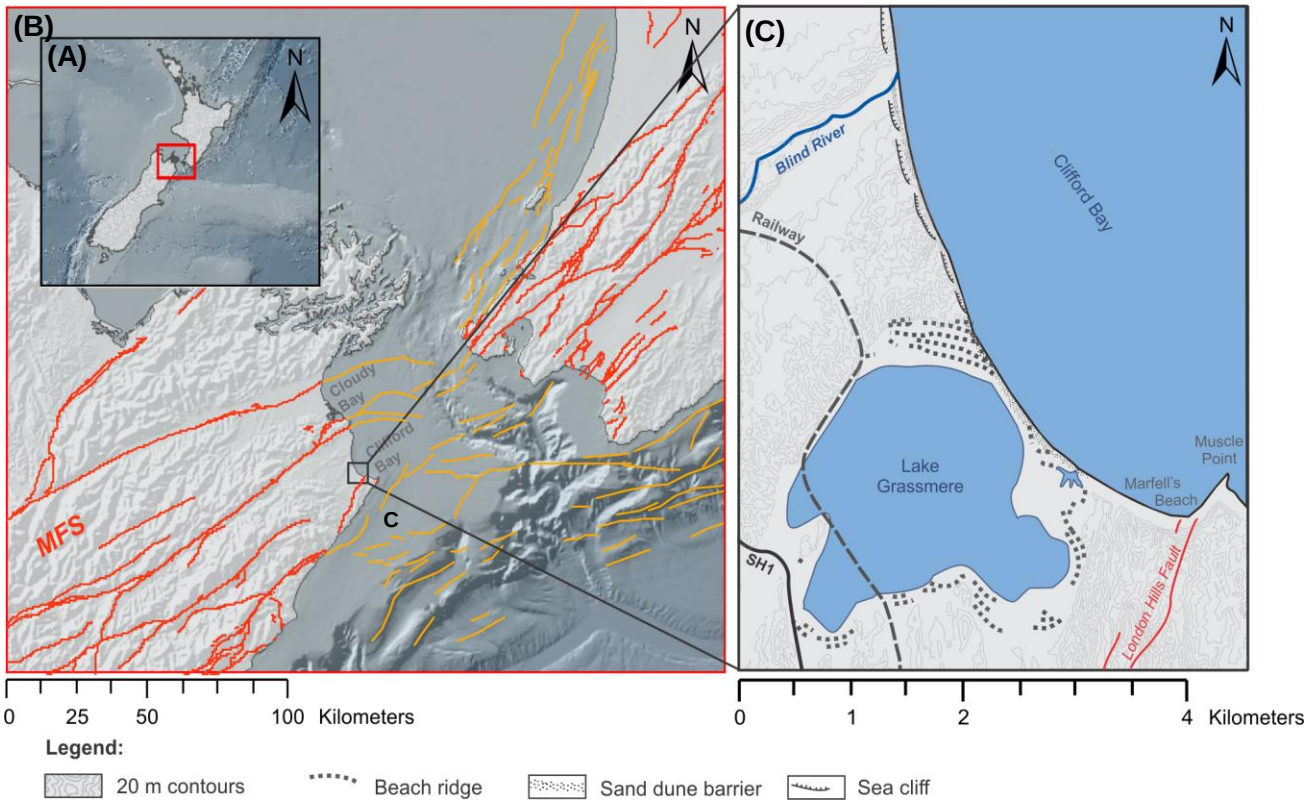

Figure 9 – Map showing the location of the study site (A) within New Zealand, and (B) within the MFS. Note onshore active faults are in red, and offshore active faults are in orange. (C) Geomorphic schematic of Lake Grassmere and the surrounding area, highlighting features such as beach ridges, the small lagoon to the east of the lake, Blind River and London Hills Fault.

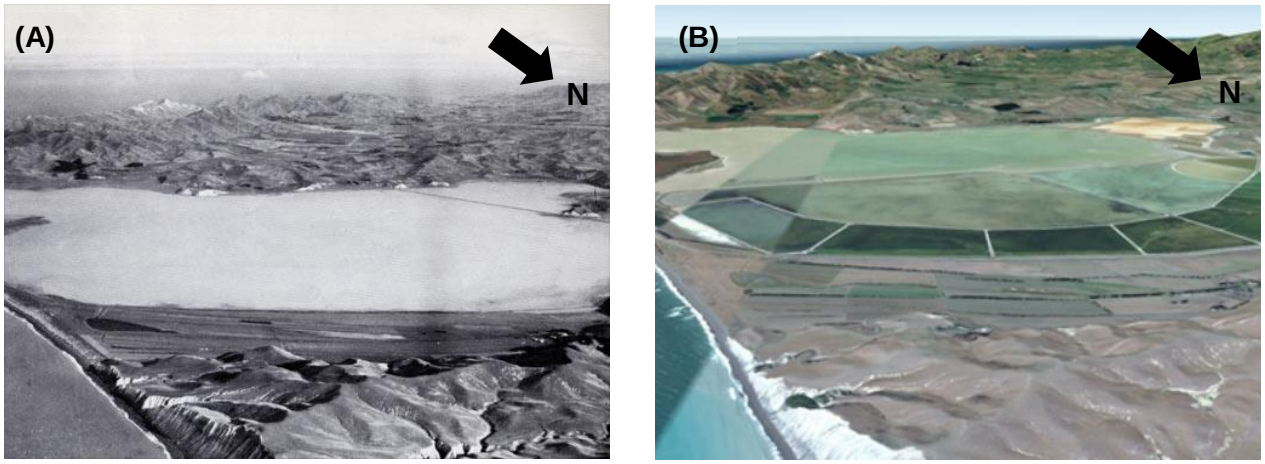

Figure 10 - (A) Historical image of Lake Grassmere pre-1940, prior to saltworks (Reid, 2019). (B) Modern aerial image of Lake Grassmere (Google Earth, 2018).

3.4.1 Geology and geomorphology

The lake is situated 8 km northwest of Cape Campbell and ~ 6 km south of the mouth of the Awatere River. The Blind River that drains into the ocean ~ 3 km north of Lake Grassmere is the closest significant fluvial system. There are no natural inflows of rivers or major streams into the modern lake basin. The geology of the surrounding hills is predominantly within the Starborough and Upton rock formations as part of the Upper Miocene-Pliocene Awatere group. Cotton (1914) attributes the initial formation of the deep embayment to warping or tilting of the weak Awatere group rocks by vertical coastal tectonics, however no further clarification of this has been made.

The modern barrier height sits at 4-5.5 m above mean sea-level (AMSL), however the degree to which it has been manipulated by the saltworks is unclear. Multiple series of beach ridges are identifiable in the study area, highlighted in Figure 9c. The beach ridges are more prominent towards the north and are mostly oriented parallel with the lake edge and extending northwards towards the hills, suggesting previous limits of the lake/embayment extent. To the east of the lake there is a small tidal lagoon (Figure 9c). The orientation of beach ridges and the small lagoon in the southern area allude to a possible position of the relict channel or estuary mouth providing an open connection to the ocean. A small area of dunes is active in the south-eastern corner of the embayment north of Marfells Beach.

The mean tidal range at Lake Grassmere is ~1.2 m (0.45-1.65 m) (LINZ, 2018). Located in the lee of Cape Campbell, the coastline is exposed to the north and sheltered from the southerly swells, and therefore north and northwesterly winds dominate. As a result, the beach enclosing the lake is exposed to short-period, steep, storm waves resulting in a steep and narrow beach of fine sand (Pickrill, 1977).

3.4.2 Holocene sea-level

Low energy coastal environments have been highly successful in a global context for recovering evidence for past subduction earthquakes and tsunamis. The accommodation space in settings such as saltmarsh and coastal lagoons provide a chronology of palaeoenvironmental changes including sea level and tectonics. Using sea-level as a benchmark onto which uplift and subsidence can be inferred requires understanding the non-tectonic sea-level history of a region. Unfortunately, regional sea-level reconstructions in New Zealand are fragmented, and for many years the only the sea-level curve available was Gibb (1986). Gibb (1986) suggested current mean sea-level (MSL) was reached at ~6500 BP for the whole of New Zealand and has remained relatively static since. A study by Clement et al (2016) highlighted many errors with this reconstruction, showing it not only overlooks a significant mid-Holocene highstand of 1.4 to 3.0 m above present sea-level, but also the fluctuation was spatially and temporally variable. Clement *et al* (2016) developed regional sea-level curves for New Zealand.

The most applicable regional sea-level reconstruction for Lake Grassmere is the Canterbury region sea-level record, shown in Figure 11. Clement et al (2016) suggest rising sea-level reached current MSL at around 8000-7000 cal BP, followed by a mid-Holocene highstand of ~2 m above MSL around 4000 cal BP, and a gradual fall to present MSL. An alternative compilation by Hayward et al (2016) uses index points from tectonically stable regions to create a generalised sea-level curve for all of New Zealand that includes a fall to a late Holocene lowstand of -0.6 m at around 600 cal BP, followed by a rapid rise at the onset of the 20th century to bring MSL to present. Both interpretations are depicted in Figure 11 and will be used in conjunction for further discussion of sea-level in this study.

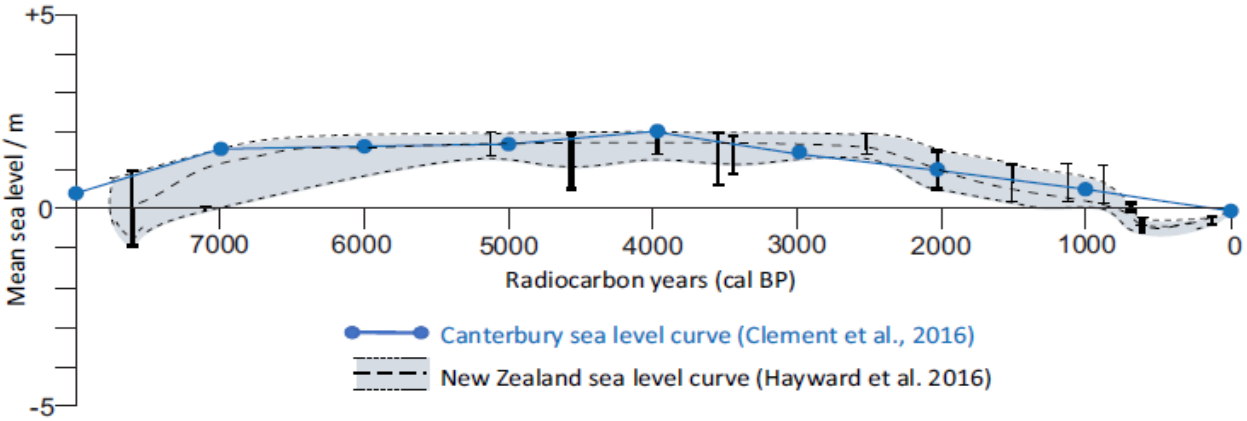

Figure 11 – A compilation of Holocene sea-level curves for New Zealand based on index points from Hayward et al (2016) and regional sea-level index points for northeast South Island from Clement et al (2016). Adapted from Clark et al., 2019.

3.4.3 Previous geological studies at Lake Grassmere

Ota et al (1995) is currently the only in-depth study that has been conducted at Lake Grassmere. Holocene transgressive deposits from locations between the lower Wairau Plain and Lake Grassmere were obtained by subsurface sampling for analysis of macrofossils and diatoms, as well as radiocarbon dating. Cores from the northern and southern fringes of Lake Grassmere were described and geomorphology such as beach ridges, were mapped. Ota et al. (1986) propose the maximum inland extent of sea level at Lake Grassmere was reached at c. 7 ka, however this estimation is based on the sea-level reconstruction of Gibb (1986), which is now thought to be erroneous. Ota et al (1995) suggest an estuarine environment persisted during the early-mid Holocene until 5200 cal BP when RSL fall facilitated beach ridge formation and enclosure of Lake Grassmere from the ocean. The timing of the isolation of the lake is attributed to the formation of a gravel barrier ~1800 years ago. Ota et al (1995) calculated ~1 m of tectonic uplift over 6500 years from the modern elevation of Holocene molluscs, in addition to providing age estimates for the beach ridges of 1731-990 cal BP and 2162-1920 cal BP.

The series of sand dunes at the southeastern corner of the embayment have been the subject of significant archaeological study due to the deposition of large amounts of avifauna fossils, midden and human remains in the last 1800 years (Worthy, 1998). While the archaeological findings yielded no information regarding tectonic or tsunami history at Lake Grassmere, they confirm Maori inhabitation.

Within the online palaeotsunami database, there are two records for Lake Grassmere and Clifford Bay (New Zealand Palaeotsunami Database, 2017). One record is made for a possible palaeotsunami deposit overlying a midden on the eastern edge of Lake Grassmere, proposed in an archaeological study by McFadgen et al (1996), however evidence in the original report does not confirm a tsunami source. The second entrance is a pūrākau of cultural significance, referencing “Kupe in anger caused sea to wash over the land”, noted by King and Goff (2010) (as discussed in section 3.2 5).

In October 2016, a group of scientists from GNS Science lead by Kate Clark visited Lake Grassmere to undertake reconnaissance work on behalf of the “It’s Our Fault” Wellington regional seismic hazard and resilience project. Exploratory gouge cores were taken around the north and south of the lake and 6 piston cores were collected (Figure 12a, b). The sediment cores revealed stratigraphy indicative of abrupt environmental changes characterised by sharp contacts and visually distinguishable changes in particle size of sediments, including units of shell hash (Figure 12c). Preliminary inspection of the cores

suggested the Lake Grassmere site potentially held a record of coseismic land-level changes and tsunami. Several radiocarbon dates were obtained from the piston cores but no other analysis or interpretation was done. The cores were stored at GNS Science, Lower Hutt and were reanalysed as part of this study that commenced in 2018, informing initial exploration at the study site. I hypothesized that the stratigraphy within the 2016 cores from the southern site may be complicated by close proximity to the intertidal channel that once connected the lake to the ocean. The one core taken from the northern side of the lake (LG6 or 6P from here onwards) had contrasting stratigraphy, including laminated silts and clays suggesting that deposition at this location was less disturbed and that stratigraphic units were intact. As a result, this thesis focuses on the area on northern side of the lake, in order to increase the possibility of uncovering an undisturbed record of prehistoric earthquakes and tsunami.

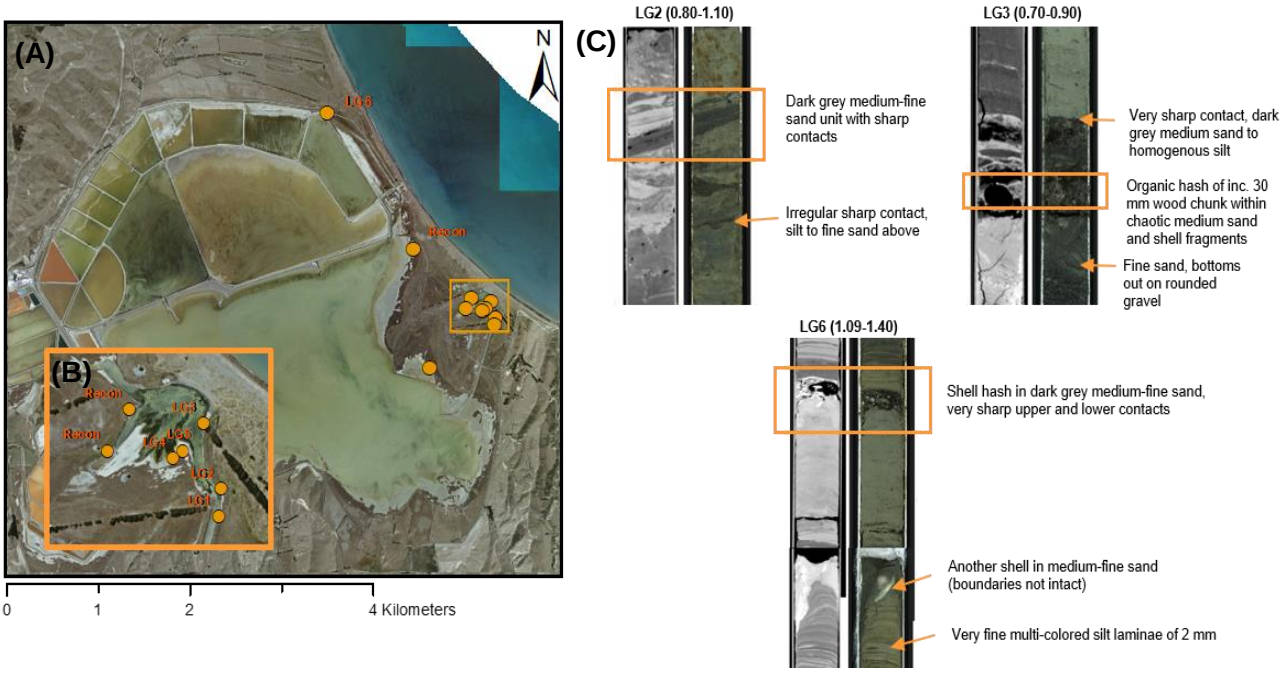

Figure 12 – (A) Map of the reconnaissance for undertaken in 2016, showing the locations of reconnaissance gouge cores ('Recon') and piston cores (e.g. LG6). (B) Close-up of core locations at the south of Lake Grassmere. (C) High-resolution images and computed tomography (CT) images of of three cores extracted, highlighting anomalous stratigraphic features encountered.

3.5 Chapter Summary and Research Questions

This chapter has discussed the tectonic setting of New Zealand, and more specifically the Hikurangi subduction margin and the MFS. Historic and prehistoric record of earthquakes on upper plate faults and tsunami within the region have been outlined, also acknowledging the evidences for ruptures of the central part of the interface. The southern section of the

Hikurangi margin has been identified as a region that is in need of further research due to a limited geological record of past ruptures, meaning that the magnitude and frequency of large to great earthquakes is poorly constrained, despite the potential for M_w >8 earthquakes capable of generating major tsunamis. Lake Grassmere has been chosen as a location for the development of this research for many reasons including its environmental similarities to the nearby Mataora-Wairau Lagoon, suggesting that any instances of Holocene coseismic land-level changes and tsunami are likely to be preserved within the sediment record.

In order to investigate these themes, I have designed three research questions that will guide this study:

1) How did the morphology of Lake Grassmere evolve during the late Holocene?
2) Is there any evidence of palaeotsunami or sudden coseismic vertical deformation?
3) How does the timing of palaeotsunami events at Lake Grassmere fit within the regional palaeoseismic record, and what are the implications for possible fault sources?

4.0 METHODOLOGY

This section outlines the methods used to extract data in order to answer the research questions of this project. I used a combination of field, laboratory and analytical methods to build a comprehensive set of results. I visited Lake Grassmere to collect field data in May, July and August 2018 and processed this data using the methods below between August and December 2018.

4.1 Field methodology

4.1.1 Sediment cores

I targeted areas undisturbed by the operations of the saltworks and sediment soft enough to be suitable for coring (e.g. not gravel). The placement of study sites was also guided by the results of field surveys undertaken in 2016 by Kate Clark (section 3.4.3). I undertook preliminary surveys using a gouge corer to identify locations suitable for further coring, taking detailed notes. On the northern lake edge, I constructed a transect along the periphery of the lake from the most seaward point at which barrier gravels were not encountered, towards the hillside in the northwest (Core Transect 1) (Figure 13). This transect followed a ditch excavated to build levees around the lake, meaning that the surface of the gouge cores was lower than the surrounding paddocks and therefore modern reworked topsoil units of up to 2 m did not have to be cored through for this procedure. I aligned five additional transects perpendicular to Transect 1, extending northwards into the paddocks and northern beach ridge series. Lithostratigraphic information was collected from sediment extracted from a total of 30 gouge cores using a 20 mm diameter, 0.5 m long gouge barrel. Depths and descriptions were completed in the field using a method adapted from Troels-Smith (1995). I conducted all of the sediment descriptions myself to maintain consistency throughout. Full descriptions of the gouge cores are included in Appendix 1. Locations were recorded using a handheld Global Positioning System (GPS).

I explored a few additional locations for coring including a site with natural saltmarsh vegetation close to the barrier, north of Transect A and saltmarsh areas around the south of the lake where piston cores were taken during the 2016 reconnaissance work. I followed the same procedure as above and descriptions are included in Appendix 1, however no further work was done at these sites.

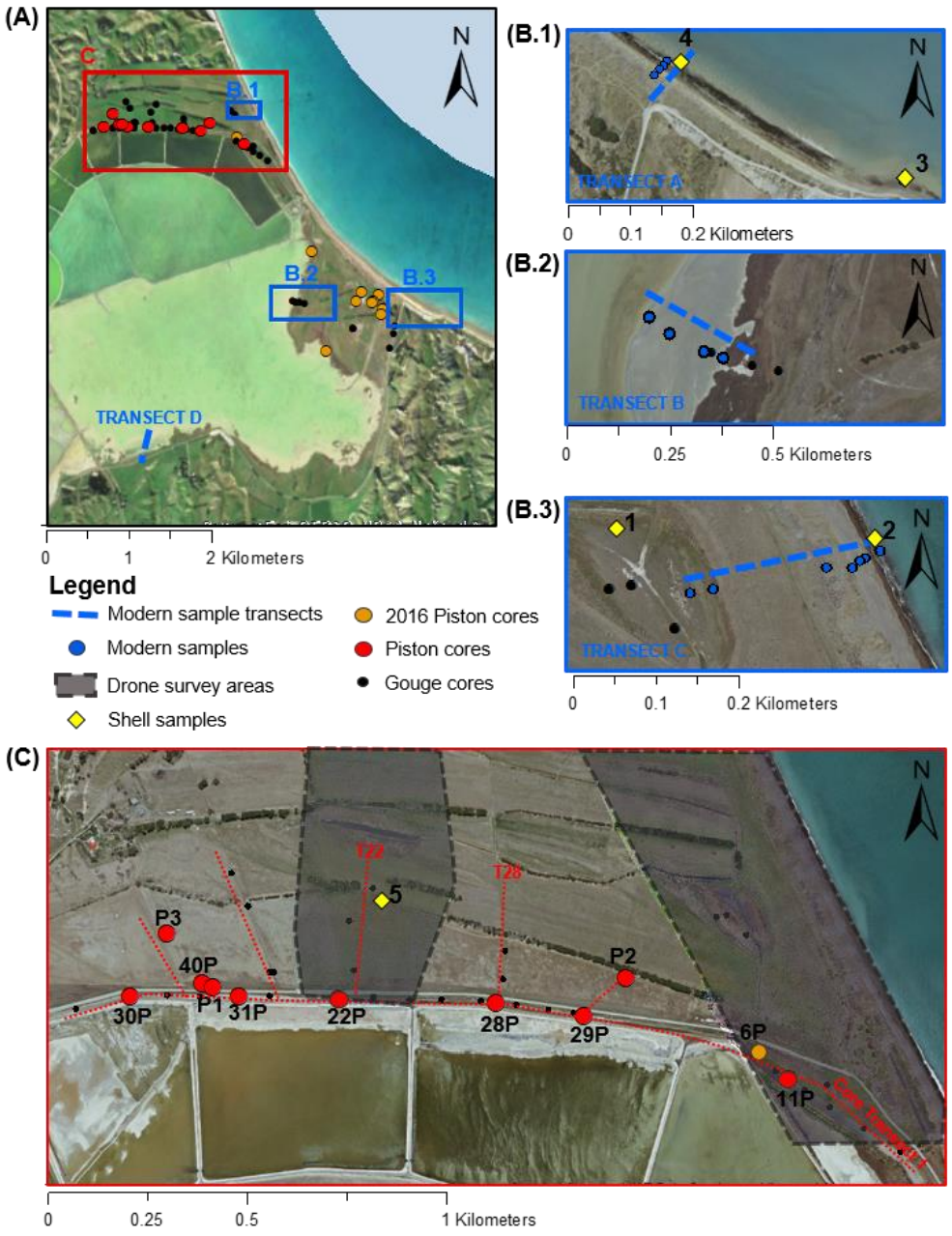

Figure 13 – (A) Map of the study site at Lake Grassmere and the locations of sampling points, including; piston cores, gouge cores and reconnaissance cores taken in 2016. (B) The location of modern sediment sampling transects for grain size analysis; across the beach barrier at the south of the lake (B.1), across natural saltmarsh at the east edge of the lake (B.2), and across the beach barrier and into saltmarsh at the north of the lake (B.3). (C) The location of gouge cores and piston cores extracted in this study, and two areas covered by drone surveys (beach barrier and beach ridges). The main core transect 'Core Transect 1' is shown on the map, with the perpendicular transects extending from this line to the north. Two secondary core transects are labelled; Transect 22 (T22) and Transect 28 (T28). Locations of the shell samples are also indicated by yellow diamonds and are numbered for reference in section 5.2.4.

Visual results from the gouge surveys informed optimal locations for the distribution of ten piston cores in the study area to capture the overall stratigraphy of the site. I recorded locations and surface height using a Real Time Kinematic (RTK) GPS with a base station

positioned on the barrier. In most cases I removed the reworked top unit of sediment with an auger, as this was described within the exploratory gouge logs and not necessary to capture within the piston core. I used a 50 mm by 1 m manual piston corer and extruded sediments at the site, then wrapped, labelled and transported them back to GNS Science. Care was taken to wash equipment between drives and between cores to avoid contamination. Sediment cores were stored in a fridge at 5°C for the duration of the project. Detailed descriptions were completed at GNS Science, using the same adapted Troels-Smith (1995) approach (Appendix 2). Compression due to deformation while coring was identified and consistently accounted for by altering the top depth of the core. For example, a 1 m length of core taken from 0.5 to 1.5 m below the surface, with 0.2 m of compression would be recorded as 0.7 to 1.5 m in descriptions. Where possible, one half of the split cores were archived, the other half being sampled for analyses outlined in the following sections.

Descriptions of gouge and piston cores were used to create visual logs of sediment stratigraphy in CorelDraw Graphics Suite 2018. All depths within the cores have been converted to the New Zealand Vertical Datum (2016) using the online conversion tool, taking the data obtained from the RTK-GPS relative to the base station, and projecting onto the vertical datum grid. Elevation relative to mean sea level is given for some points where necessary, however the tide gauges in New Zealand are sparse and poorly constrained due to tectonic activity. Where elevations above mean sea level (AMSL) are included, I have calculated them using the datum of Nelson 1955 that gives an offset of +0.34 m from the NZVD, which agrees with observations made with the RTK-GPS at mid-tide at the study site (LINZ, 2019).

4.1.2 Modern samples

Analysis of the characteristics of modern samples can be useful to compare to the characteristics of sediment from cores. If grain sizes are comparable, it is possible to infer the palaeoenvironment of lithofacies. To do this, we selected areas representative of the modern environment and constructed two transects including two beach transects (north and south, Transects A and C) extending from the intertidal zone to over the beach barrier/dune system, and a transect across natural saltmarsh around the southern lake edge (Transect B) (Figure 13). We collected samples of surface sediment using a spatula from the top 2 cm. We collected representative shell assemblages at the high tide line along the beach transects from a 0.5 x 0.5 m sample area to avoid bias. Additional shell samples were taken from location indicated in Figure 13. Locations were recorded using the RTK GPS and are shown in Figure 13. Sediment samples were submitted for particle size analysis to compare

modern and past environments within the cores. Shells were washed and identified at GNS (Beu et al., 1990).

4.1.3 Surface and stratigraphic models

To obtain accurate surface elevations I surveyed two additional transects with the RTK-GPS, one across the beach to the lake edge, and one from the lake edge into the paddocks and northern beach ridge series. In addition, to obtain high-resolution topographic information of the study area, drone surveys were flown by Andy Howell (Victoria University of Wellington). I selected two areas to represent the study area; one polygon from the lake edge north across the northern beach ridge series to the hillside (1), and one polygon that spans the beach barrier from the cliffs to the lake edge (2) for later construction of Digital Surface Models (DSM). Twenty ground control points were distributed and surveyed with the RTK-GPS, relative to the base station on the barrier. Image grids were processed using structure from motion (SfM) techniques in AgiSoft PhotoScan 1.4.5 (2016) and manually calibrated using the ground control points, to create a three-dimensional DSM of the two areas. DSMs were used to obtain elevation profile data and to support the 'geologic model' outlined below.

Troels-Smith descriptions of the units were adapted to input into the program Leapfrog Geo 4.0 (2018) in order to visualise the study site as a 3D geological model. The model allowed barrier-normal and barrier-perpendicular trends to be identified (section 5.1.2) across the whole study site with the interpolation of facies between core locations. The model output was not suitable for presentation within this thesis and was only used to inform discussion; therefore it is not included in the results section.

4.2 Sedimentology

4.2.1 Computed tomography and Itrax

Unsplit cores were scanned using medical X-ray computed tomography (CT) by Pacific Radiology at Boulcott Hospital, Lower Hutt. The three-dimensional high-resolution density distributions were viewed in ImageJ, allowing features that may be not be identifiable from the split core surface such as contacts, rip up clasts and articulated shells within the sediment to be examined and recorded without disturbance (Ashi, 1997; Peterson et al*.,* 2011). Density profile data was extracted from a randomly selected 1 mm slice through the centre of the cores, and aligned with top and bottom of core logs to display changes in density down-core. Split cores were imaged using an Itrax XRF scanner at the University of

Otago, Dunedin. This process provides a high-resolution colour image of the full core without distortion, allowing the lithofacies to be re-analysed visually without referring to the physical core that may have been disturbed for sampling.

4.2.2 Grain size

Core 22P was selected for high-resolution grain size analysis due to its representative lithostratigraphy and coordination with microfossil samples. Samples were taken every other 1 cm from the top of the core (0.735 m) down the core to 1.08 m, where particle size was described as visually unchanging within the Troels-Smith descriptions (Figure 13). Some targeted grain size analysis was later done on cores P1, P2 and P3, sampling mainly from the shell hash units to compare compositions. The variation in angularity of particles is not monitored and has potential to affect results however, care is taken to ensure conglomeration does not occur so that only single grains are measured to give the best representation.

Preparation: Sediment samples were digested in 30% H_2O_2 over a period of approximately 24-48 hours in order to chemically remove all organic matter. Samples were heated following this to react off any remaining reagent. Reaction products were then rinsed from the sample three times with deionized water and centrifuged for 15 minutes at 3000 rpm. These steps were repeated with the addition of 2.5-5 mL of 10% HCl to remove carbonate material. Samples were frozen and freeze dried (using a Martin Christ Alpha 1-4LD) in a vacuum for 24 hours to powderize the sediment. Dried samples were split down into appropriate weights to be inputted into the laser granulometer. Weights varied according to overall grain size, as more sediment of sand size particles is needed to satisfy an obscuration value of 8-12%. To prevent conglomeration, 80 mL of Sodium Hexametaphosphate (NaPO3) solution was added to samples that were placed onto mechanic stirrers in a water bath at 22 °C for at least 20 minutes prior to analysis, to ensure particles remained in suspension until measuring.

Samples were placed into a Beckman Coulter L13 320 laser granulometer to measure particle size distribution in the range of 0.04 to 2000 µm. Repeats were run for 10% of the samples to ensure reproducible results. GRADISTAT v8.0 (Blott and Pye, 2001) was used to produce statistical data including mean, median, standard deviation, skewness and kurtosis. Results using the geometric method of moments were used, and descriptions of textural group were after Folk (1966). Data was inputted into Jupyter Notebook programme (Kluyver et al., 2016) and code was adapted to display grain size distributions in the form of a heat-map. Modern surface samples were also analysed using the same methods aside from

fractions larger than 1400 µm were analysed using sieve stacks in half phi (ϕ) steps, and then converted back to weight percentages of the original sample.

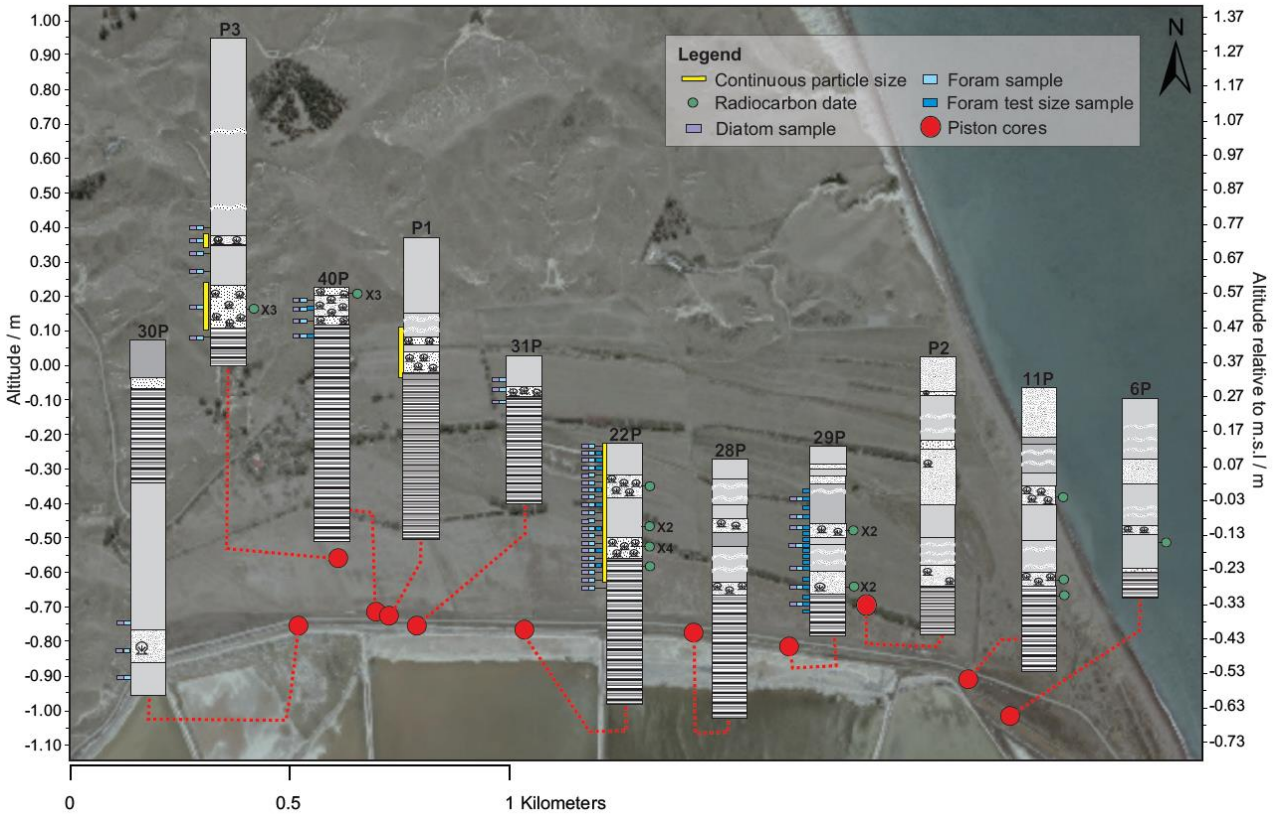

Figure 14 - Map displaying the location of piston cores extracted in this study, and the sampling strategy for each core. Radiocarbon samples are represented by green dots. Locations with multiple radiocarbon dates are indicated. Yellow bars indicate continuous grain size sampling locations. Microfossil sample locations are displayed on the left of each core, including locations used for the foraminifera test size analysis.

4.3 Biostratigraphy

Core 22P was chosen for high-resolution microfossil sampling, supported by samples from other cores where necessary. Samples were taken for diatom and foraminifera analysis to reconstruct past environments and indicate changes between and within lithofacies. The sampling strategy took into account likely contamination of the outer edges of the sediment cores and distortion of contacts from coring processes. Analysis takes into account the differing preservation of robust and fragile tests of foraminifera species and care will be taken to avoid preferential identification of well-preserved, robust specimens, in order to provide a representative assemblage.

4.3.1 Foraminifera

Preparation: Continuous 2 cm slices of the half-core were taken from the core up to 1.06 m where they were then taken every 6 cm (Figure 14). Supporting samples were also taken

from each lithofacies in cores P3, 6P, 29P, 30P, 31P and 40P as well as two surface samples from the mudstone hillsides. Samples were dried in a 50 °C oven and then weighed and passed through a 63 micron sieve, retaining the fraction greater than 63 microns. This removed fine material but retained the foraminifera. Samples were analysed under a Leica MZ 12 5 microscope at x40 magnification. A count of 100 individuals was obtained from each sample (limited due to low abundance), and specimens were placed on cardboard slides for identification. Identification was according to Hayward et al (1999), and assistance from Bruce Hayward (Geomarine Research) was sought for the identification of extinct Miocene species. Species were grouped according to environmental preference and inputted into C2 (Juggins, 2010) for representation.

Analysis of test sizes: A method for analysing the test size of foraminifera based on Hayward et al (2019) was trialled for samples in 22P, 29P and 40P. The number of samples was restricted by the cores and depths in which dried, unpicked sediment had been retained after picking for identification had taken place. As species assemblages were already known from the identification of picked samples, additional samples were taken to expand the dataset without needing to be identified. Dried sediment was weighed and sieved into three grain size fractions at 63-125, 125-250 and >250 µm. These sizes were then split down to an amount that contained approximately 300 tests. *Ammonia aotena* tests were counted in each size fraction in each sample and multiplied back up to the original dried sediment weight. All samples will be analysed using the raw number of tests within in size fraction per 1g of dried sediment, as well as the percentage distribution of tests within each size fraction per 1g of dried sediment to allow comparison.

4.3.2 Diatoms

Samples were dried in an oven at 40 °C and dry weights were recorded. To remove organic material, 20 ml of 20% Hydrogen Peroxide (H_2O_2) was added and left to soak overnight. To remove carbonate material, samples were heated to 80 °C on a hot plate and a pasteur pipette was used to add up to 20 ml of 10% Hydrochloric acid (HCl). Samples were then centrifuged at 3000 rpm for 5 minutes, decanted, filled with deionised water and shaken approximately 4 times to neutralise. The ‘shake and sit’ method was used to settle and remove sands. Six drops of Sodium Hexametaphosphate ($NaPO_3$) were added and then centrifuged at 1500 rpm for 3 minutes, decanting the supernatant to remove remaining clays, repeating 5-8 times until clear. Slides were prepared on a hot plate at 160 °C, using 20-40 uL of the sample (depending on concentration) and Naphrax to mount. Samples were analysed under a Zeiss Axioscop 2 microscope at x40 magnification initially and then at

x100 in more detail. A count of 100 individuals was aimed for in each sample initially however no diatoms were found and are therefore not discussed any further.

4.3.3 Mollusc shells

Shells extracted from the piston cores and from the modern transects were washed and identified (Beu *et al.,* 1990) with help from personal communications with Alan Beau. Care was taken to preserve and record articulated shells. I then listed and grouped according to environmental preference (Beu *et al.,* 1990) in C2 (Juggins, 2010). Species diversity was not calculated due to the limited sample sizes from the cores, and so discussion is based on comparing numbers of species listed in section 5.2.3.

4.4 Radiocarbon dating

Radiocarbon dating allows chronologies to be obtained for lithofacies of interest, particularly within and bounding disturbance units. GNS Science facilitated 23 (terrestrial and carbonate) radiocarbon dates processed at the Rafter Radiocarbon laboratory at National Isotope Centre in Lower Hutt, Wellington. I completed the preparation of the carbonate samples myself up to the graphization stage and have included details of this process below.

4.4.1 Terrestrial samples

In order to constrain the timing of disturbance events within the cores, dates that bound that deposit of interest are preferred over dates from within the unit that may contain reworked material (McFadgen, 1982; Goff et al., 2001). Terrestrial material is favoured here, as it does not carry a residual age that requires a marine reservoir correction (Clague et al., 2000; Goff *et al.,* 2001). Samples were taken from above and below the disturbance units in Cores 11, 22 and 29, and wet sieved to 63 µm. Identifiable organic material was picked and where possible identified under a microscope however, only three samples provided sufficient mass to obtain a reliable radiocarbon date. These samples were prepared and run by the technicians at the Rafter Radiocarbon Laboratory.

4.4.2 Carbonate samples

Due to the absence of abundant terrestrial material suitable for dating in the units bounding the deposits of interest, shells from within two disturbance units (shell hashes) were targeted. *Austrovenus Stutchburyi* (common cockle) (Beu et al., 1990) has been widely used for radiocarbon dating (Higham and Hogg, 1997; Hogg et al., 1997; Ota et al*.,* 1988) and is the dominant species in all cores. Preference was given to articulated, juvenile, well-

preserved individuals, in that order (Clague et al., 2000; Goff *et al.,* 2001). One articulated adult of *Nucula hartvigiana* was also submitted as this species was prevalent throughout the hashes, however it's suitability for radiocarbon dating is unknown. Two samples of *Ammonia aotena* foraminifera were processed later. Preparation of these small samples was not necessary and so they were weighed and introduced at the carbonate evolution stage.

Physical preparation: Preparation followed the standard operating procedure of the National Isotope Centre of New Zealand. Samples were cleaned and weighed, then photographed and described under a Leica MZ 12 5 microscope at x8 magnification. Samples were sonicated in deionised water for 2 minutes to remove attached material. An acid etch using 0.5 mol HCl was performed to remove any outer layers of crystallized carbon from the environment. The reaction was neutralised and then samples were dried in a 50 °C oven overnight. Dry weights were recorded and the where possible outer growth rings were clipped off, weighed (~20 mg) and ground into a powder. The samples then underwent carbonate evolution, using 2 ml of 85% Orthophosphoric acid (H3PO4) to generate carbon dioxide (CO2) that was purified from waste non-condensable gases and trapped using liquid nitrogen. International Atomic Energy Agency standards were run alongside sample (Rozanski et al*.,* 1992); C1 Marble as the background and C2 Travertine as the secondary for carbonate samples, and Kauri Renton Road wood blank (Hogg *et al.,* 2006) as a background with a FIRI I cellulose sample as a secondary for terrestrial samples. Technicians at the laboratory carried out procedures from this point. Graphitization was conducted by reduction with hydrogen over iron catalyst. Samples were measured by Accelerator Mass Spectrometry (AMS) following the methods of Baisden et al. (2013) and radiocarbon ages reported following the conventions of Stuiver and Polach (1977).

Calibration: Dates obtained were calibrated using the online software OxCal version 4.3.2 (Bronk Ramsey, 2017). The Marine13 calibration curve (Reimer *et al.,* 2013) was used for carbonate samples (shells and forams). The most suitable regional ΔR correction for the marine reservoir correction in this study is 4 ± 25 (McSaveney *et al.,* 2006; J Turnbull 2018, personal communication, 10 December). The SHCal13 curve (Hogg *et al.,* 2013) was used for terrestrial samples. Ages are reported in calendar years before present (Cal BP), where present is 1950. Radiocarbon dates were age modelled using two methods in OxCal, in order to constrain the chronology of the lithofacies. Sequence and combine functions were performed and their suitability is discussed in section 8.1.

5.0 RESULTS

In this section I outline the results from the multi-proxy analysis of sediment cores from Lake Grassmere. Firstly, the sedimentology of the piston cores is described which allows the correlation of common stratigraphic units across the study site. From here, I then use the defined sedimentary units to describe results from biostratigraphic analyses including foraminifera and molluscs. I outline calibrated results from the radiocarbon dating of bivalves to attach a chronology to the sediment stratigraphy. Lastly, I provide the elevation profiles constructed across the study site that were obtained from drone surveys and processed using structure from motion techniques to create a Digital Surface Model (DSM).

5.1 Stratigraphy and sedimentology

The palaeoenvironmental and tectonic history of Lake Grassmere is underpinned by the observations of sediment cores collected from the edges of the lake. In this section I describe the stratigraphy and sedimentology of the 11 sediment cores collected for this study. Full descriptive core logs including high resolution imagery and CT images of the piston cores included in Appendix 2. The locations of the cores are shown in Figure 13. Stratigraphic representations of the cores are compiled in Figure 15, with elevations aligned relative to the New Zealand Geodetic Datum (NZVD). Unless otherwise stated, positions in the cores are given as a depth relative to the surface and as elevation relative to NZVD (in brackets). In some figures I also provide conversions of elevation relative to NZDV into elevation relative to mean sea level (m AMSL).

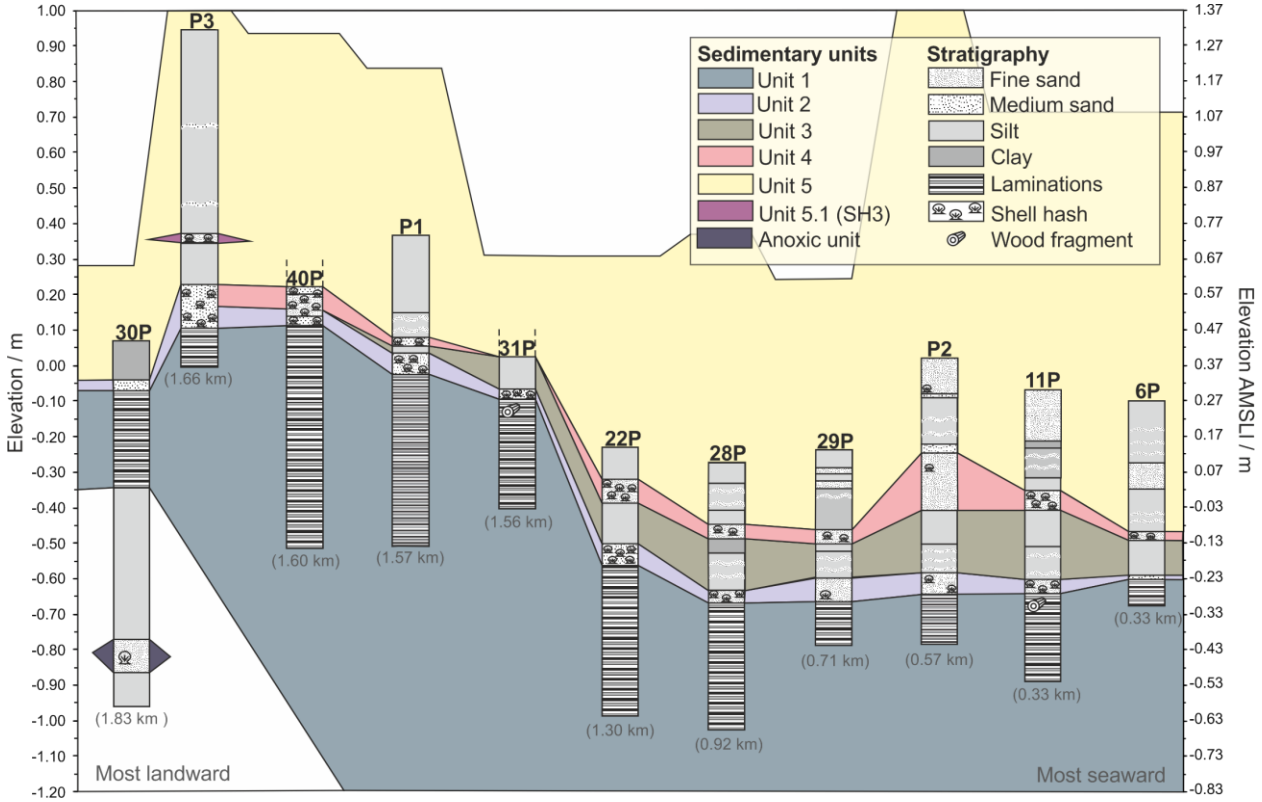

Figure 15 - Stratigraphy of all piston cores retrieved in this study, and well as 6P that was extruded in 2016. Cores are aligned by their elevation relative to the New Zealand Geodetic Datum (NZVD). Elevation relative to mean sea level (m AMSL) is also shown on the right axis. Cores are ordered by distance from the modern coastline, with distances given in grey beneath the core, increasing from right to left. Lateral continuity of units is suggested based on common stratigraphy within piston and supporting gouge cores. Units correspond to descriptions in section 5.1.1. The surface elevation at the core locations is indicated by the top limit of Unit 5. Note that cores P2 and P3 have a surface elevation of 1.5 m (extending beyond the scope of the figure), which is due to their location slightly further north than the main core transect. The base of Unit 1 was not located and therefore the unit is shown to extend below the base of the piston cores.

Common sedimentary units that can be traced across the study site are shown in Figure 15, with correlations in between the piston cores supported by information from gouge cores (Appendix 1 and Appendix 2). The cores are ordered by distance from the modern coastline. The stratigraphy can be subdivided into five sedimentary units, and each unit is particularly well represented in core 22P, so this forms my 'master core'. Consequently, I selected core 22P as the focus of high-resolution analysis. The most-landward core, 30P, shows the largest deviation from the typical stratigraphy of the site, it has an extra unit that is not seen in other cores and is missing some of the common units, but in general the stratigraphy is remarkably consistent across the study site.

The grain size descriptors based on the high-resolution results obtained from the master core (22P) and the values described are described for each lithostratigraphic unit are quoted are assumed to be representative for the to reflect the unit across all cores. Figure 16 shows the grain size results for the master core as mean particle size and statistical parameters such as skewness and kurtosis. Grain size distributions are visualized for the master core in Figure 17, along with additional measurements from cores P1 and P3, and modern samples that are discussed later. Densitometry results for

all cores are included in the stratigraphic logs in Appendix 2 and are aligned based on the top and bottom of the cores. The densitometry results for the master core have been included in Figure 16 to demonstrate the close correlation between densitometry and measured grain size. This correlation demonstrated the value of continuous densitometry measurements as a proxy for grain size. The cores are scanned whole to obtain the densitometry data and shells are not removed, the shells therefore produce sharp spikes of high HU (>2000) within the continuous densitometry.

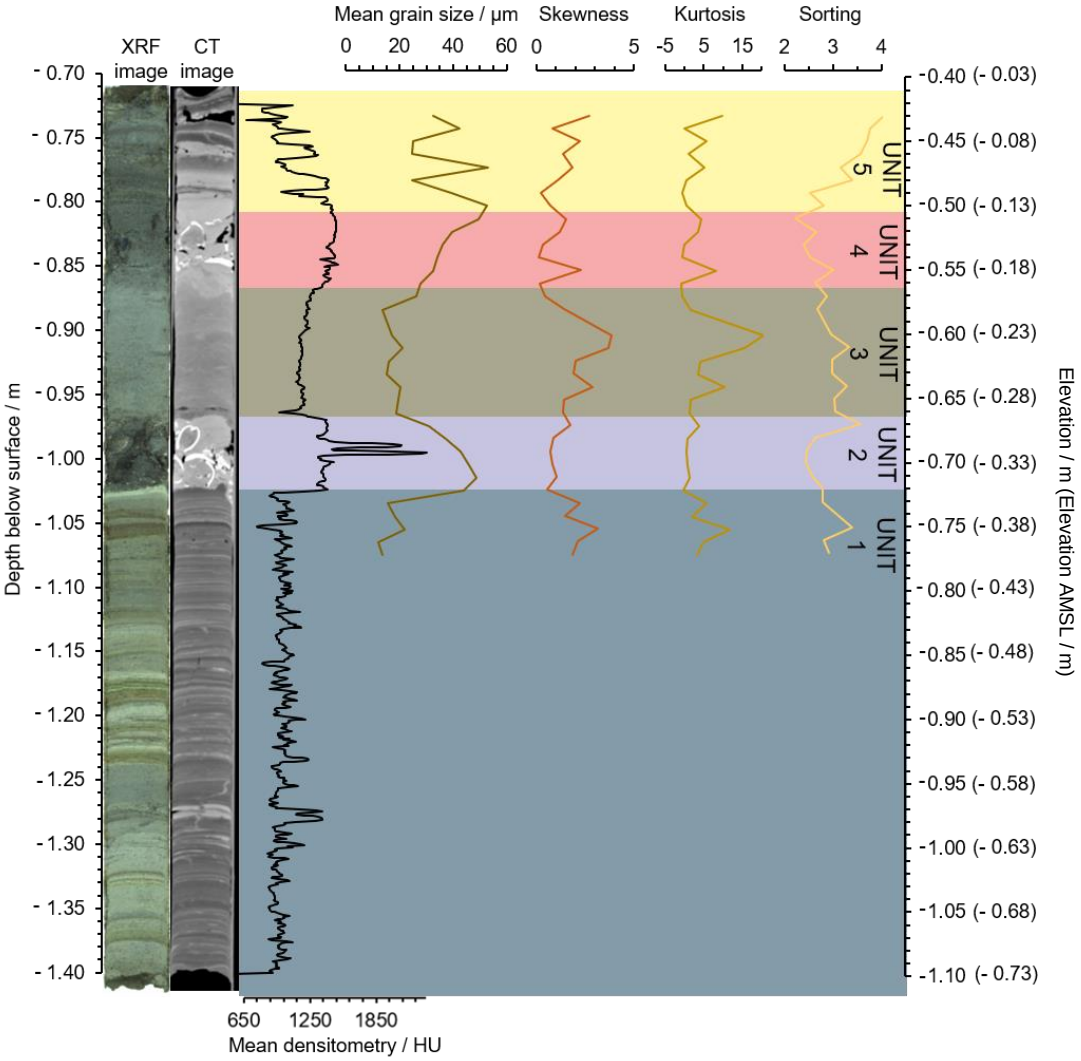

Figure 16 - Sediment composition of the master core (22P). Included are images derived from CT and XRF scanning. Densitometry results are given in Hounsfield Units (HU).

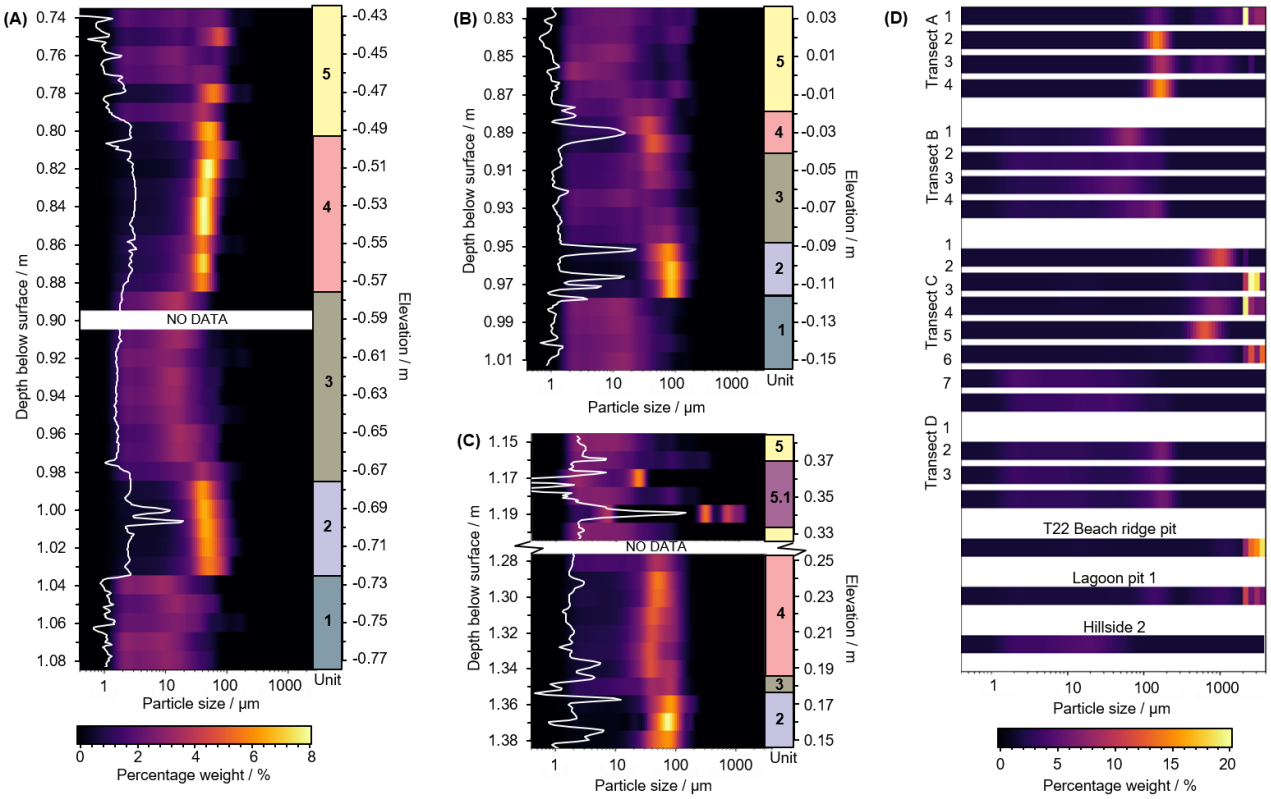

Figure 17 - Particle size distribution results for the master core 22P (A), core P1 (B), core P3 (C) and the modern sediment samples (D). Distributions are expressed as percentage weight of particle sizes (in μm) in each sample, on a logarithmic scale. Note that the percentage weight scale for (D) is different. Left-hand axis show depth below the surface in the cores. The right-hand axis shows the equivalent elevation relative to the datum (NZVD). Densitometry results (white lines) have been included to demonstrate its closeness of fit to grain size results, however units are not included in this figure. Representation of the sedimentary units is given so that variations within and between units can be observed. Colours correspond to Figure 15. The location of modern samples is shown in Figure 13. Transect A was sampled at 1) intertidal, 2) high tide, 3) storm beach and 4) dune top. Transect B was sampled at four points (1-4) from high marsh to the water's edge. Transect C was sampled at 1) intertidal, 2) high tide, 3) storm beach, 4) dune top, 5) dune swale and two points on the marsh (6 and 7). Transect D consists of three samples from high marsh to the water's edge.

5.1.1 Descriptions of sedimentary units

In this section I describe the typical sedimentary characteristics of each of the five lithostratigraphic units, and discuss how the unit varies between cores.

Unit 1: This is the basal unit identified across the piston cores at the study area (except for 30P) consists of finely laminated (2-3 mm-thick laminae), grey, light grey, brown and brown-grey clays and silts. The deepest Unit 1 reached was in core 11P where I recorded it to a depth of -2.96 m (-2.58 m AMSL), yet the true base of the unit was not reached and therefore the thickness of the unit is unknown. Seaward cores (6P, 11P, P2, 28P, 29P) include a few thin, fine sand laminations within Unit 1, these decrease in frequency with increasing distance landward and are entirely absent from the most landward cores such as P3. I did not encounter any macrofossils however, a 20 mm wood fragment was located 2.5 cm below the upper boundary in core 31P, and a 13 mm section of bark was retrieved from 5 cm below the upper boundary in core 11P. The mean grain size for Unit 1 is clay, with the cumulative clay to silt component (<63 μm)

varying slightly and occupying up to ~99% of the distribution. The overall grain size distribution is platykurtic and poorly sorted.

Unit 2: Unit 2 is a mixed shell hash within a fine to medium sand matrix. The shell hash is predominantly made up of well-preserved *Austrovenus stutchburyi* and *Nucula hartvigiana*. Whole and articulated bi-valves of a range of sizes including juveniles are present as well as fragments, however a component of fragmentation must be assumed to be due to the coring process. All mollusc species are noted in section 5.2.3. Unit 2 also occurs directly on top of Unit 1 in all piston and gouge cores. The maximum thickness of this unit is 6.5 cm in core 28P and the minimum thickness is 3.0 cm in core 11P. In core 22P, the mean grain size (excluding shells) fines upwards (48 µm to 18 µm) and at the upper contact it has a similar grain size distribution as Unit 1 (Figure 17). The overall grain size distribution is poorly sorted and very leptokurtic. The lower contact with Unit 1 is extremely sharp (<0.5 mm) and irregular, reflected by a sudden increase in mean grain size from 15 µm to 44 µm and overall rapid coarsening in the grain size distribution. These characteristics indicate an erosional lower contact and this sharp boundary is particularly prominent in cores P3, 40P, 31P and 22P.

Unit 3: Unit 3 is comprised of homogenous medium grey, clay to medium silt. Unit 3 thins landwards from a maximum thickness of 21 cm in core 11P, to a minimum thickness of 2 cm in core P1 where it is no longer present in further landward cores (Figure 15). Landward trends are discussed further in section 5.1.2. In some cores such as 11P, 28P and 29P the Unit 3 is interrupted by interbedded fine sands. There are no macrofossils or significant organic material in this unit. The lower contact with Unit 2 is sharp (~1 mm) and is reflected well in the grain size results as a decrease in the mean from 30 µm to 18 µm. The grain size distribution is poorly sorted and platykurtic.

Unit 4: Unit 4 is characterised by a fine sand matrix supporting a mixed shell hash. Mollusc species are similar to Unit 2 with *Austrovenus stutchburyi* dominating however, the composition is less densely packed and only contains a few shells in some cores (6P, P2, 28P). The maximum thickness is 6 cm in core 22P and the minimum thickness is 2 cm in cores 6P and P1. The basal contact with Unit 3 is sharp (e.g. in 22P), however the difference in grain size between Unit 3 and 4 is less significant and sometimes the lower contact is not very pronounced. The particle size distribution (excluding shells) coarsens upwards (27 µm to 52 µm), with dominant grain sizes of coarse silt and very fine sand (Figure 17). The general composition is poorly sorted and very leptokurtic.

Unit 5: All sediment above Unit 4 is encompassed by Unit 5, which is dominated by interbedded brown-grey silts and fine sands. The unit becomes more mottled and orange in colour as it is increasingly oxidised and reworked closer to the surface. The

unit is of variable thickness based on the surface elevation and compaction, and in most places the top 30 cm was removed with a gouge core to ensure the maximum number of units was captured within the piston cores. I did not encounter any macrofossils or significant organic material in this unit. The basal contact with Unit 4 is gradational over 0.5 cm. Variability in the grain size results reflect the sand layers that are non-uniform in distribution and thickness.

5.1.2 *Landward and barrier-normal trends*

The stratigraphic units described in section 5.1.1 can be traced laterally both normal and perpendicular to the coastal barrier. Figure 18 shows a schematic representation of the study site to emphasize variations and trends along two cross-sections, based on information gathered from piston and gouge cores.

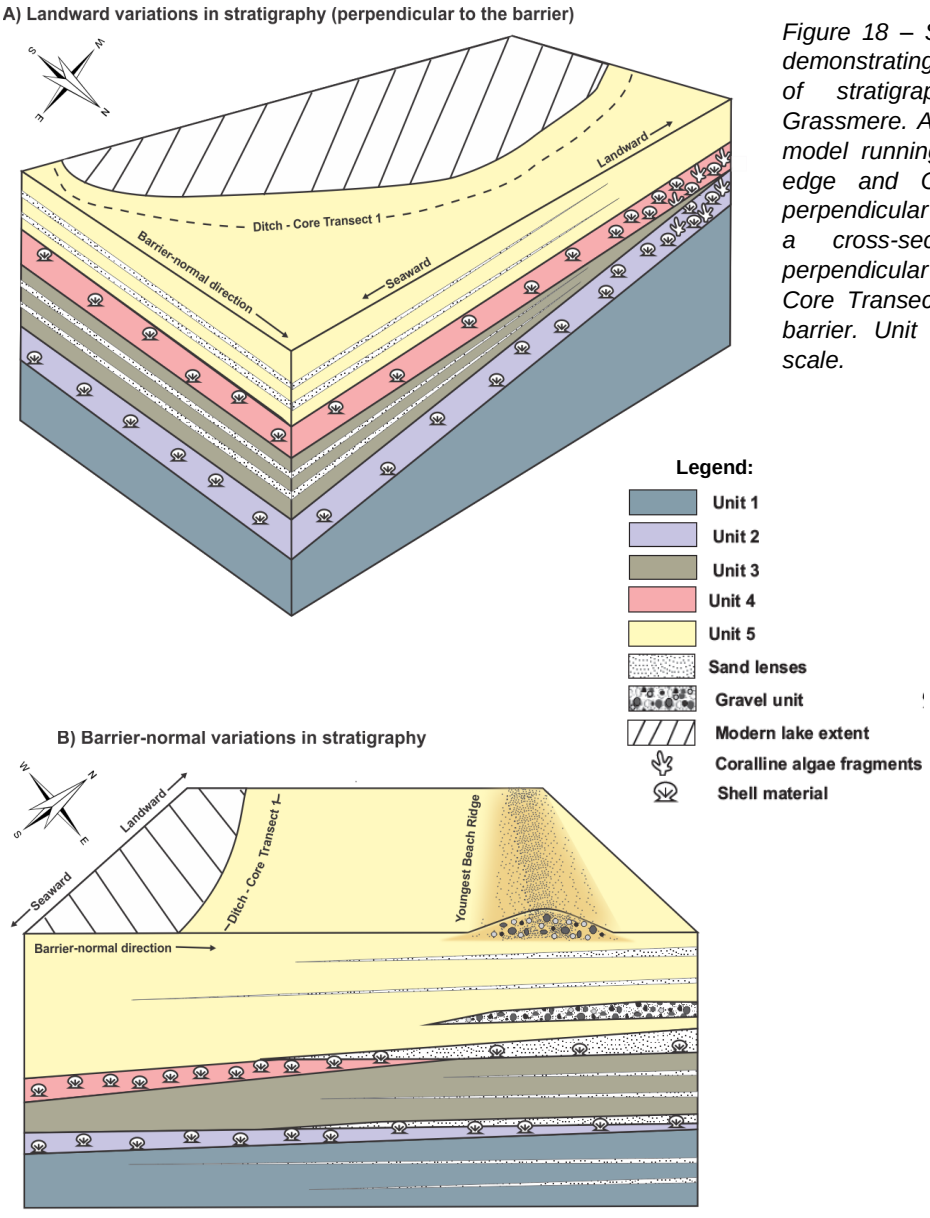

Figure 18 – Schematics showing the demonstrating trends lateral continuity of stratigraphic units at Lake Grassmere. A) shows a cross-section model running parallel with the lake edge and Core Transect 1, and perpendicular to the barrier. B) Shows a cross-section model running perpendicular to the lake edge and Core Transect 1, and parallel to the barrier. Unit thicknesses are not to scale.

Landward (perpendicular to the barrier) trends: Cores closer to the coast (e.g. 11P, 28P, 29P) exhibit some different characteristics to cores further inland (e.g. P3, 40P) (Figure 18a). Coastal cores have thin (3-15 mm) fine sand lenses within Units 3 and 5 that thin with distance from the barrier until they are no longer present in inland cores. The composition of the shell hash units (Unit 2 and 4) is much more densely packed in further inland cores, compared to cores closer to the coast. In addition, the mollusc species composition of the Unit 2 and Unit 4 becomes more diverse further inland (section 5.2.3), accompanied by an increased abundance of coralline algae fragments and clastic material. This is best evidenced in core 40P where a large (5 x 3 cm) greywacke clast is lodged at the boundary between Unit 2 and 4 (Figure 19). Although the thickness of Unit 2 and Unit 4 is variable (Figure 15), there are no trends with distance perpendicular or parallel to with the barrier (Figure 20). The thickness of the intervening Unit 3 thins landward so that in cores such as P1 and 40P it is very thin or not present, meaning that shell hash Units 2 and 4 sit directly on top of one another (Figure 15). It is assumed that this is also the case for P3, and that the shell hash identifiable at 0.35-0.37 m (0.73-0.75 m AMSL) represents an additional shell hash (SH3) within Unit 5 (labelled 5.1 in Figure 15). This is discussed further in section 5.1.3.

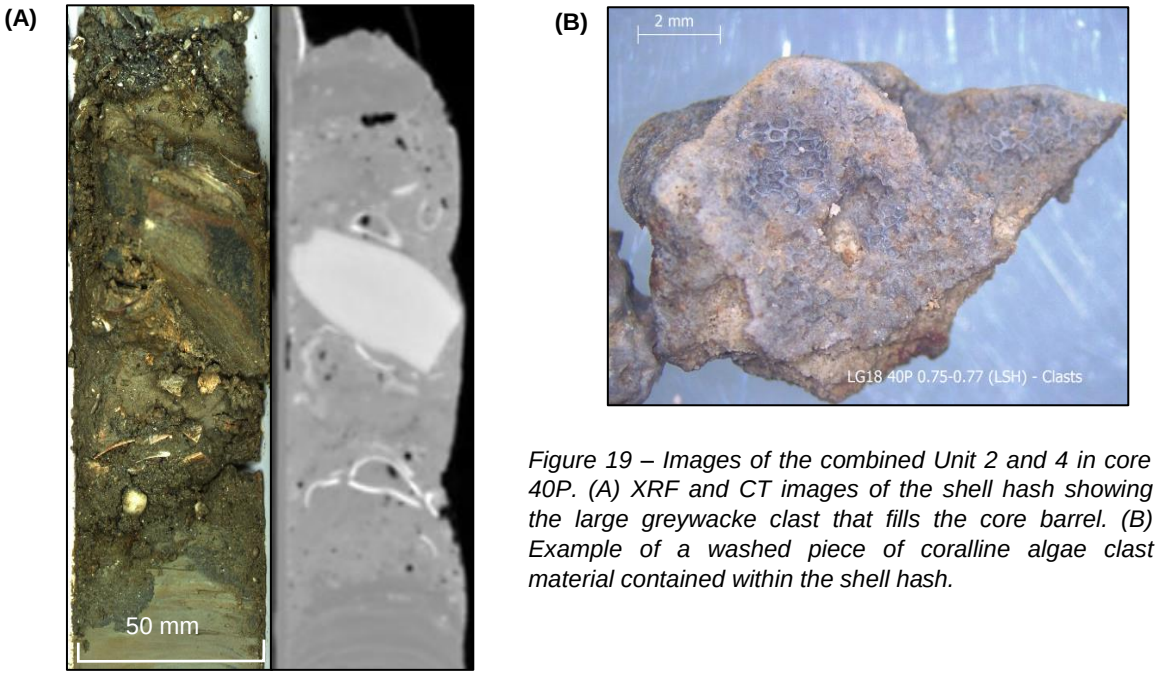

Figure 19 – Images of the combined Unit 2 and 4 in core 40P. (A) XRF and CT images of the shell hash showing the large greywacke clast that fills the core barrel. (B) Example of a washed piece of coralline algae clast material contained within the shell hash.

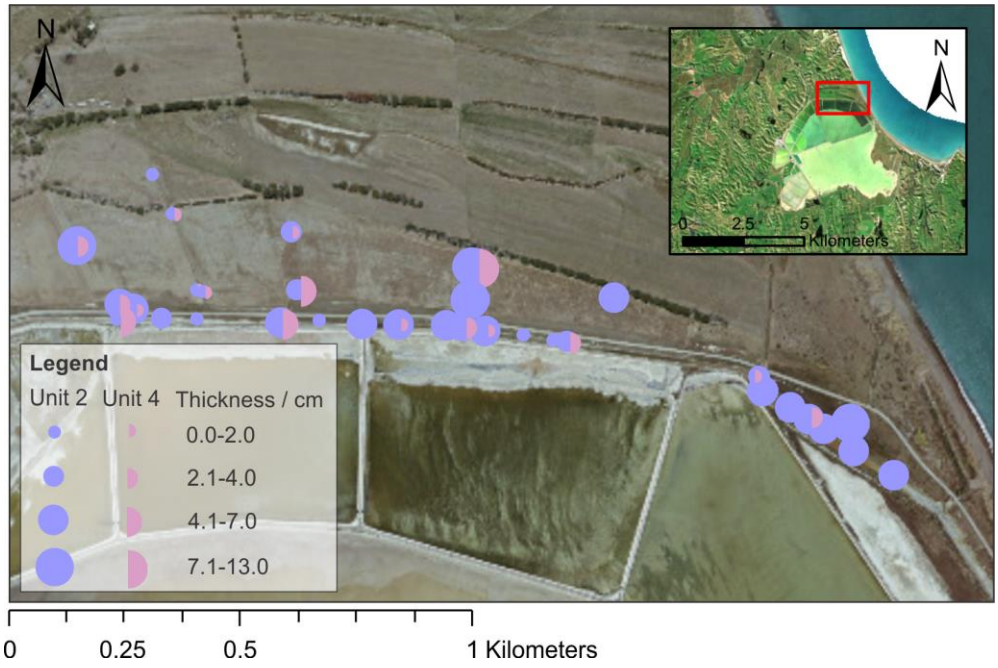

Figure 20 - Map displaying the presence/absence of shell hash units (Unit 2 and Unit 4) within piston and gouge cores, across the study site. Symbology is proportionate to shell hash thickness as shown in the legend.

Barrier-normal trends: While the density of piston cores is not as high for transects parallel to the barrier, comprehensive information was gathered during reconnaissance gouge coring (Appendix 1). The cross-section displayed in Figure 18b runs from the lake edge to the far side of the youngest beach ridge. Overall, unit slopes upwards with the topography of the lake, and shell hash units (Unit 2 and Unit 4) thin with distance from the lake edge. As these units thin, they are interpreted to transition into massive sand units rather than shell hashes, although shell material is still encountered in some gouge cores. Unit 3 thickens with distance from the lake edge. Sand lenses are prominent in Units 1, 3 and 5 in cores further from the lake edge. In the most landward gouge cores, a gravel unit was encountered within Unit 5. This unit was comprised of similar material to the youngest beach ridge (rounded gravels 5-30 mm and abraded shell material).

5.1.3 Supporting grain size samples

Cores P1 and P3 were sampled and processed by students from Victoria University of Wellington. The raw results have been incorporated in this study to support the grain size data from 22P, cross check grain size distributions and expand the data set for Unit 2 and Unit 4. The results are shown alongside the master core in Figure 17. Core P1 was sampled from 0.83 to 1.01 m (0.03 to -0.15 m), which spans all 5 units. Samples were also taken from P3, however only from within the shell hash units. A section of 1.29-1.40 m was sampled continuously and is interpreted as reflecting both Unit 2 and Unit 4 very close together with one sample between at 1.35 m (0.18 m) possibly reflecting a thin Unit

3. Particle size distributions in cores P1 and P3 support the general trends seen in 22P; Units 1 and 3 are fine and platykurtic, Units 2 and 4 are coarser and leptokurtic. Core P1 also shows the fining upwards trend of Unit 2.

A section of P3 was also sampled from 1.15-1.20 m (0.33-0.38 m) to encompass the shell hash unit (SH3, Unit 5.1) that punctures Unit 5, shown in Figure 15. The results in Figure 17c show that the particle size distribution of Unit 5.1 is distinctly different to Units 2 and 4 in all cores, as it is platykurtic with a predominantly clay matrix despite one coarse sample at 0.19 m (0.34 m). Consequently, Unit 5.1 (or SH3) is confirmed as a distinct third shell hash that cannot be corelated to other piston cores.

5.1.4 Modern grain size comparison

Modern samples were collected to compare the grain size distribution of the modern coastal and lake environments to sediments within the core. Modern sample results are shown in Figure 17. Transect A (Figure 13 B.1) was sampled from the intertidal zone, high tide line, storm beach line and dune top. Results in Figure 17d show the variability in grain sizes from these locations. The intertidal sample had the overall coarsest grain size distribution with a maximum of pebble size gravel. The dune top sample has the finest grain size distribution with a maximum of medium sand and dominant grain size of fine sand.

Transect C was sampled in the following locations; swash zone, high tide line, storm beach line, dune top, dune swale, high marsh and low marsh. There are some similarities and differences between the grain size profiles across Transect A and Transect C (Figure 17). The coarsest sample is at the high tide line and the dominant grain size on the dune top is coarse sand. The grain size of the dune swale shows the dominant grains of pebble sized gravel that comprises the barrier. The marsh samples show a highly contrasting finer grain size. Transect B and Transect D show comparable results for the grain size distribution of modern saltmarsh sediment, with a maximum of very fine to fine sand as the dominant grain size.

Figure 17d shows the grain size of a sample taken from the pit excavated on the youngest lake-parallel beach ridge on the north side of the lake (Figure 13). The dominant grain size of the ridge is pebble sized gravel (>50%). The grain size distribution is most similar to the high tide and dune swale samples in Transect C, close to the coastal barrier. A sample was also submitted from a pit excavated on Transect B (Figure 13), which consists of a varied grain size with abroad distribution across all ranges. The grain size of the hillside sample from the Miocene mudstone at the south of the embayment consists of a fine grain size distribution of predominantly silt.

The purpose of collecting sediment samples from modern lake and coastal environments proximal to the core sites was to compare between the modern grain size distributions and samples within the cores. None of the core samples contain distributions similar to the beach (swash, high tide, storm beach or dune) samples. Samples from marsh locations are more similar to general grain size distributions within the cores however the modern samples contain a higher sand percentage.

5.2 Biostratigraphy

In this section I outline the results from biostratigraphic analysis of the piston cores (and modern surface samples) including two forms of foraminiferal analysis and the results of mollusc species identification. The purpose of biostratigraphic investigation is to interpret assemblages so that inferences can be made regarding palaeoenvironments reflected within each stratigraphic unit of the cores. Figures and results are discussed both in terms of the corresponding stratigraphic units, as well as shell hash versus non-shell hash samples for comparison.

5.2.1 Foraminiferal species assemblages

Foraminifera from the master core 22P as well as P3, 6P, 29P, 30P, 31P and 40P were picked, counted and identified. The results for the master core have been collated in Figure 21, with samples from other cores presented in Figure 22. Species have been grouped into common environmental preferences based on Hayward et al (1999), in order to infer variations in palaeoenvironment. Descriptions here focus on the master core and are supported by the other cores sampled. The abundance of foraminifera is much lower in Unit 1, 3 and 5 than in Unit 2 and 4. This should be considered when observing percentage abundances, for example only 7 foraminfera in total were counted within the sample at 1.18 m in core 22P, causing the 16% abundance of *Globocassidulina* spp. to be misleading. No foraminifera were found in the 3 lowest samples in Unit 1 in the master core.

The dominant species in all samples is *Ammonia aoteana.* The predominantly monospecific assemblage occurs at 70-100% in all units. Both globally and within New Zealand, *A. aoteana* is recognised as having a particularly broad environmental niche. In New Zealand, *A. aoteana* can occur in monospecific faunas within sheltered intertidal and shallow subtidal environments, with salinity tolerances of up to 50‰, temperature range of 0-35 °C and water depth range of 0-50 m (Murray, 1991; Murray, 2006). Consequently, *A. aoteana* cannot distinguish intertidal from shallow subtidal to ~3m,

meaning that their abundance is not a sensitive indicator of environmental changes (Hayward et al., 2014).

Haynesina depressula is the second most common species in the cores and occurs at ~6% in Units 3, 4 and 5 in core 22P. *H. depressula* is generally found in low tidal and shallow subtidal water depths (Hayward et al., 1999). The presence *H. depressula* when occurring at 5-10% within a dominant *A. aoteana* assemblage, indicates environments restricted to below low tide. *Notorotalia* spp. is a fully marine, inner shelf (20-30 m) species, that occurs at 21% in Unit 4, and then at 5% in Unit 5. Although the fully marine, inner shelf (20-40 m) fauna *Quinqueloculina* spp. occurs in Units 2, 3 and 4, percentages are <5%. While the 'subtidal marine' species group contains the most species, all percentage abundances are very low and therefore are not likely to indicate a marine environment in general. The percentage abundances of other species in the master core and supporting cores are also very low (<5%) and there are no other obvious trends.

The foraminifera results within core 30P, align with its anomalous sediment characteristics compared to the other cores than display common units. While *A. aoteana* still dominates at ~60%, *H. depressula* and *Elphidium advenum* are both present at 20%.

In order to infer whether reworking of foraminifera from the surrounding hills occurs within the foraminiferal assemblages in the Lake Grassmere cores, samples were taken from the mudstone hillsides in the north and south of the lake. Both sides consist of the same bedrock lithology of the Upper Miocene-Pliocene Awatere group (Rattenbury et al., 2006) and the results are included in Figure 22. Both samples have very different assemblages to samples within the cores. The most abundant species are *Haynesina despressula, Bolivinita pliozea* and *Bulimina* spp. Species in common between the hillside samples and the core samples include *Notorotalia* spp., *Uvigerina bradyi and Elphidium charlottense.* The species grouping based on Hayward *et al* (1999) suggests that the hillside samples do not contain any species in the intertidal categories, inferring that the hillside samples are representative of a distinctly different palaeoenvironment. Despite low abundances, the subtidal to subtidal-marine species group dominates, which is consistent with the depositional environment of the Miocene-Pliocene mudstone.

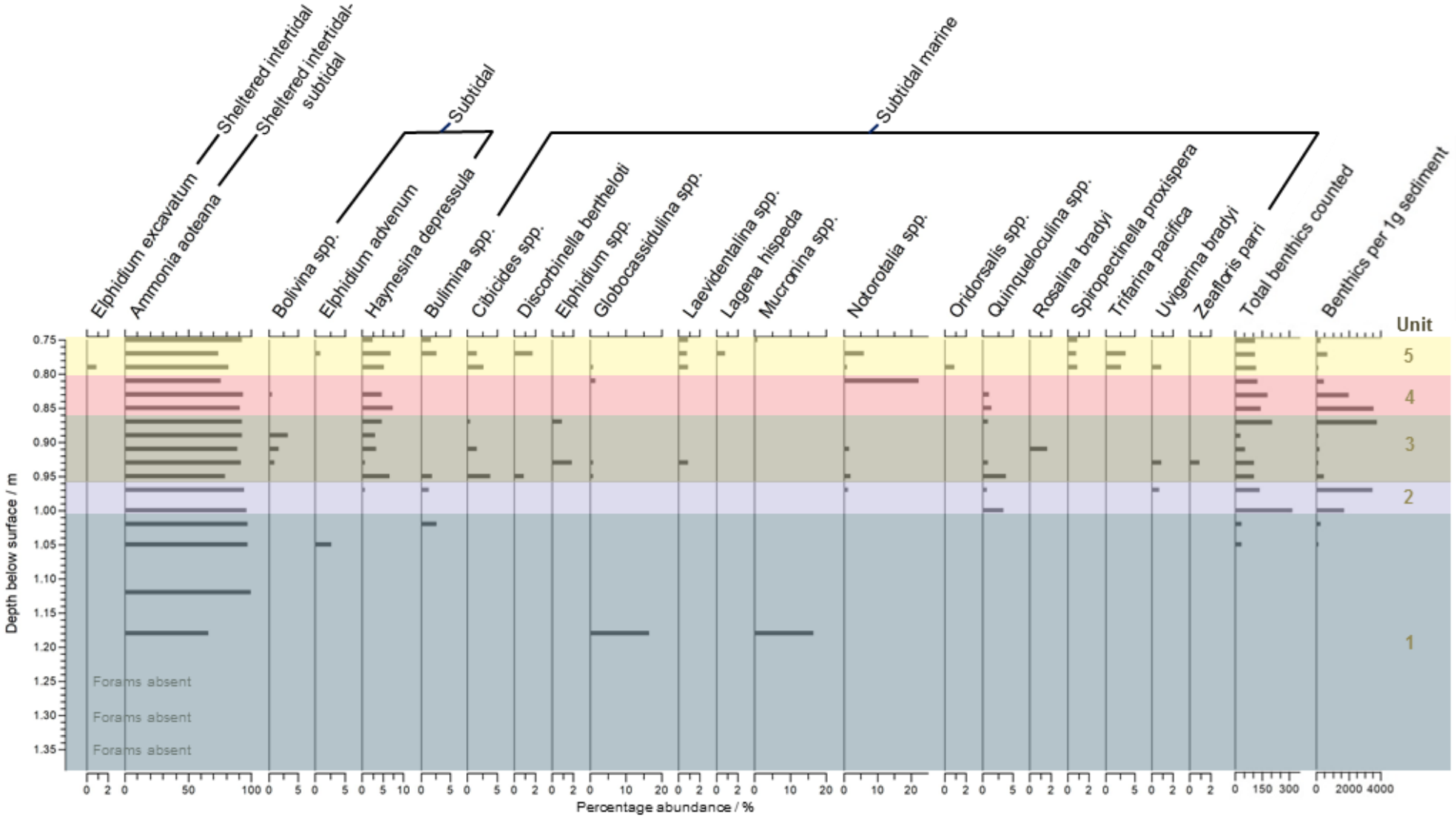

Figure 21 - Percentage abundance of foraminifera species in core 22P. Species have been grouped into environmental preference based on Hayward et al (1999). Colours correspond to sedimentary units outlined in section 5.1.1 and Figure 15.

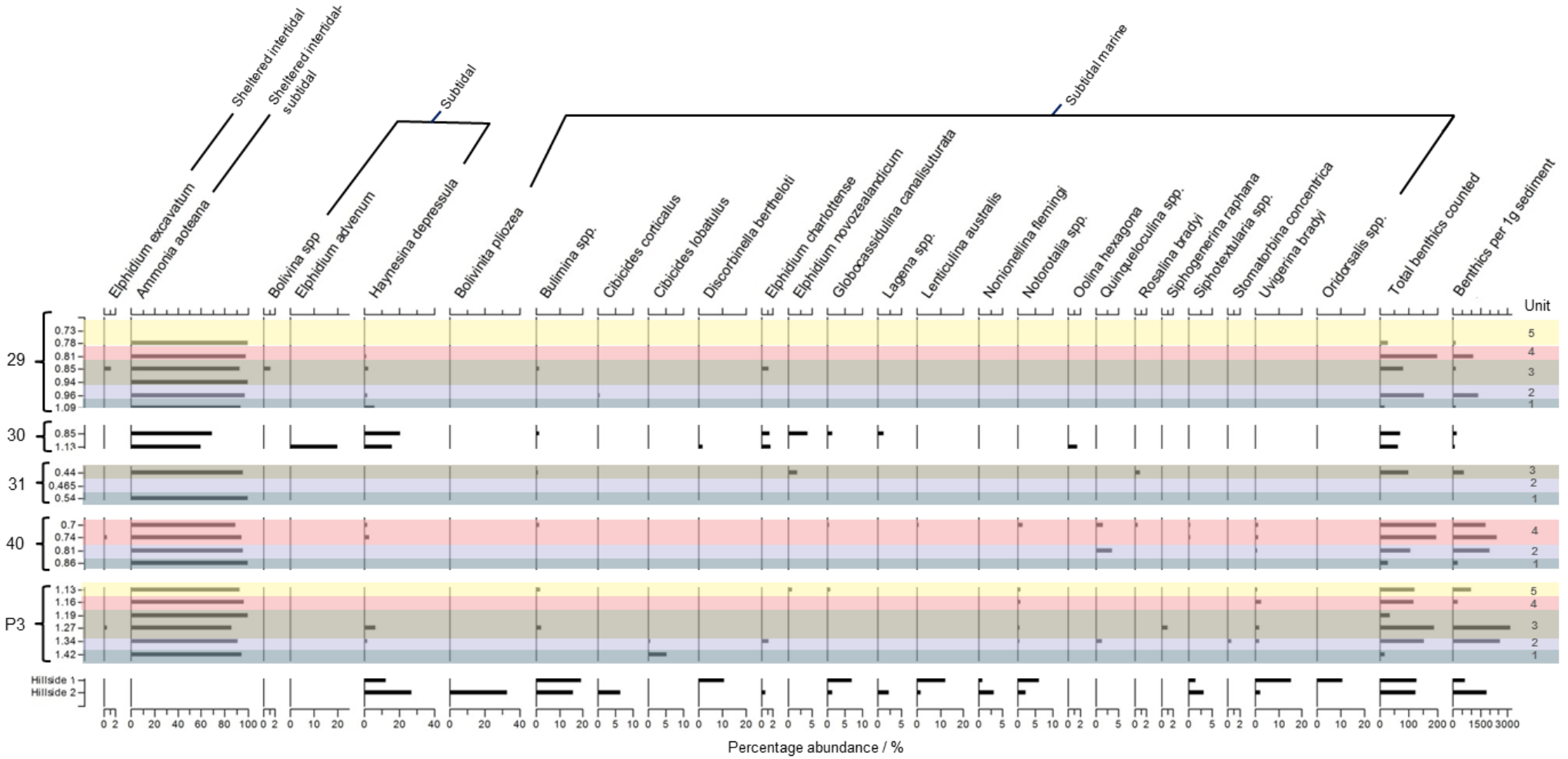

Figure 22 - Percentage abundance of foraminifera species in core 22P. Species have been grouped into environmental preference based on Hayward et al (1999).

5.2.2 Foraminiferal abundance and test size variations

In light of the inadequacy of *Ammonia* as an indicative species for palaeoenvironmental reconstruction, alternative methods of using foraminifera to distinguish differences between units were explored. The method designed by Hayward et al (2019) to distinguish between unmodified and taphonomically–modified foraminifera by assessment of test size profiles was applied to the dried foraminifera samples used for identification. As stated in section 4.3.1, additional samples were used to expand the dataset. These samples were not picked as it was already established that the assemblage was dominated by *A. aoteana*, and therefore only *A. aoteana* was counted. The results are described in terms of shell hash and non-shell hash samples rather than by depth in core or lithofacies as the main purpose of studying the test size was to look at how the shell hash sediment differed from surrounding sediment. The results displayed in Figure 23 show that the concentration of foraminifera increases greatly within the shell hashes in cores 22P, 29P and 40P, compared to the units above and below. In total, 7 shell hash samples and 22 non-shell hash samples were processed, however 4 did not contain any foraminifera. Increased concentration in shell hashes is prevalent in all the cores tested, with non-shell hash samples consisting of a maximum 24 individuals per 1 g sediment and shell hash samples containing up to 242 individuals per 1 g sediment.

Differences between the size groups are expressed as percentage distributions of each test size group in Figure 23b. Both Figure 23a and Figure 23b are considered when drawing conclusions from this data as the number of individuals differs greatly between samples and may be misleading. An example of this is 0.935-0.945 m in 29P, where only 5 individuals were counted, all within the 250 µm group, however calculations to represent data as per 1 g of sediment results in 19 individuals and 100% dominance of the 250 µm group. This is unlikely to be a strong representation of the actual foraminiferal size composition and therefore is not given much weight in interpreting trends in the data.

The foraminifera test sizes were categorised into three groups: 63-125, 125-250 and >250 µm. Tests in the 63-125 µm size range are present in all the shell hash samples, with a maximum of 2.7% (6 individuals) in the lower shell hash in 29P. The 63-125 µm size range is only present in 2 (out of 20) non-shell hash deposits with a maximum of 5.4%. The 125-250 µm size range is the most abundant size range in both shell hash and non-shell hash samples. Tests in the >250 µm size range are present in all shell hash samples, with a maximum of 58.6% in the lower shell hash in 40P. The >250 µm size group occurs more frequently than the 63-125 µm size group within non-shell hash samples, and occupying up to 52.4% in 14 of the 16 non-shell hash samples that contained foraminifera. Overall, trends in the test size ranges of foraminifera are:

- 125-250 µm size range is dominant across the majority of non-shell hash and shell hash samples
- The shell hash units have foraminifera within the 63-125 µm size range and an increased abundance of >250 µm size range foraminifera
- There does not appear to be any significant difference in the test size distribution between the upper and lower shell hash deposits across the cores tested.
- The sample size does not allow inferences to be made regarding how these relationships may vary with distance inland or north into the beach ridge series.

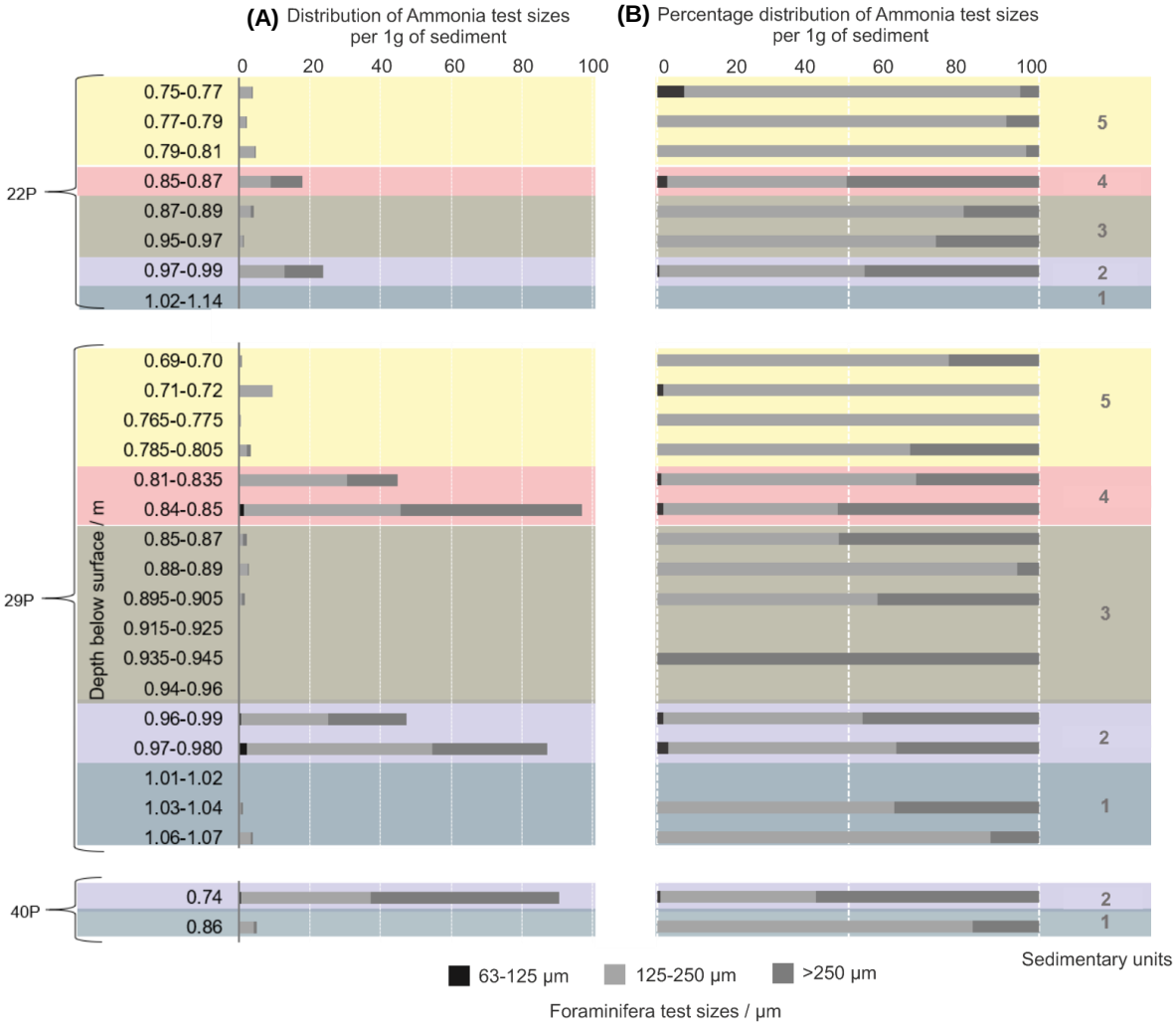

Figure 23 - (A) Shows the raw counts of Ammonia individuals in each test size group for each sample from cores 22P, 29P and 40P. (B) Shows the same data converted to the percentage distribution of test sizes for each sample in all the cores.

5.2.3 Mollusc assemblages

Mollusc shells were located within the piston cores, in other fossil assemblages at locations around Lake Grassmere and in the modern samples. Shell species were identified and grouped based on Beu et al (1990) in order to infer palaeoenvironments from the known environmental preferences of modern analogues. The results of shell identification will be discussed in terms of Unit 2 and Unit 4 for the piston cores, and then

for the modern assemblages for comparison. Shells were not analysed in 28P, or P2 as distinct shell hashes were not as recognisable.

Shell hash Units 2 and 4: The shell species identified in the shell hashes in core 11P, 22P, 29P, 31P 40P, P1 and P2 are shown in Figure 24. As numbers were low, the data have been expressed as present or not present for all species identified. The data has been grouped into samples from Unit 2, Unit 4, combined Unit 2 and 4, and anomalous shell units (core P3 SH3 and the anoxic shell in core 30P). The most dominant species, found in all shell hashes are *Austrovenus stutchburyi* and *Nucula hartvigiana*. The species have been grouped into environmental preferences based on Beu et al (1990). Three main groups of environmental preferences were identified; high tidal mudflat, intertidal estuarine and rocky intertidal (Beu et al., 1990).

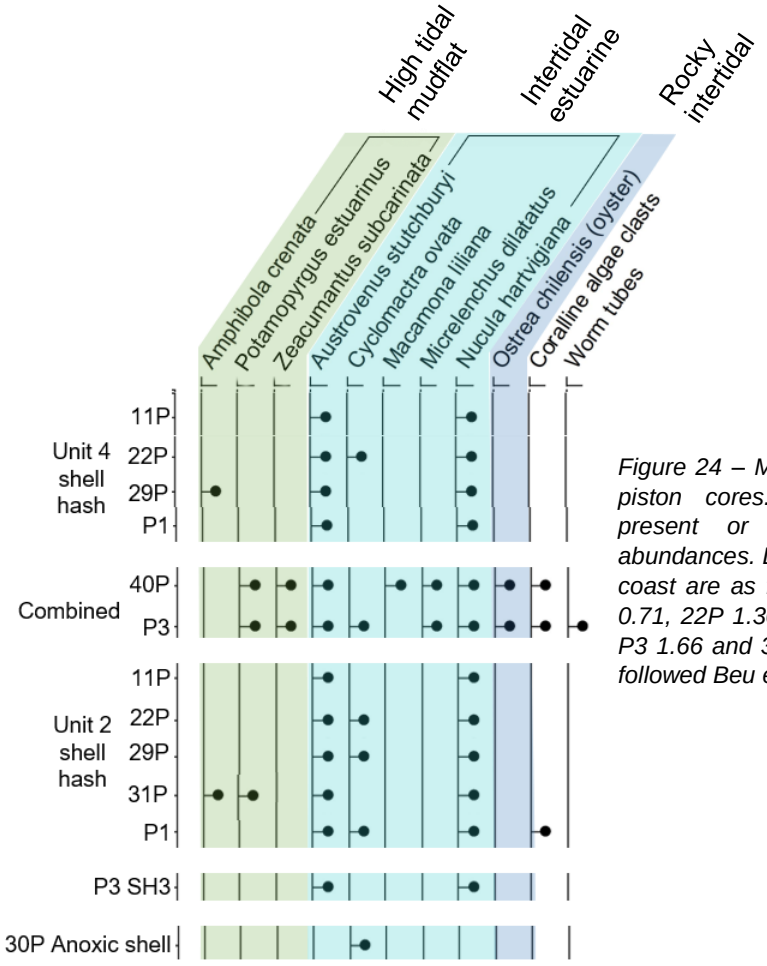

Figure 24 – Mollusc species identified in the piston cores. Data are represented as present or not present due to low abundances. Distances of each core from the coast are as follows (in km); 11P 0.33, 29P 0.71, 22P 1.30, 31P 1.56, P1 1.57, 40P 1.6, P3 1.66 and 30P 1.83. Species identification followed Beu et al (1990).

In general, Unit 2 has higher species diversity (maximum 9 species) compared to Unit 4 (maximum 3 species). Trends in species diversity and assemblages can also be observed with distance from the coast. Core distances are given in the caption of Figure 24. Figure 24 suggests that the species diversity of both shell hashes increases with distance landward over 1.33 km to core 40P. Cores closer to the coast (11P, 22P, 29P) mainly contain intertidal estuarine species, while further inland cores (40 and P3) contain

a more mixed assemblage including rocky intertidal species as well as high tidal mudflat species. The anomalous core 30P is the most landward core and is distinguishable by its single shell within an anoxic layer, identified as *Cyclomactra ovata*.

Overall the preservation of all shells including bivalves and gastropods is very good (Figure 25). There is little to no evidence of encrustation or abrasion on shells of all sizes in Unit 2 and Unit 4. A significant number of shell fragments make up the composition, and the fractures appear sharp and angular (Figure 25d). It is probable that a degree of fragmentation is attributable to the coring process. A number of whole and articulated bivalves are present in Unit 2 and Unit 4, identifiable during sediment description and within the CT scan imagery. Most articulated bivalves are firmly closed with the ligament attached, but filled with sediment that is generally finer than the sediment type of Unit 2 and Unit 4. Not enough sediment could be obtained from within the shells to perform grain size analysis. Similarly, the size of the piston cores limited the abundance of shells excavated from Unit 2 and Unit 4, meaning that no quantitative analysis of fragmented vs. whole/articulated bivalve ratios could be done.

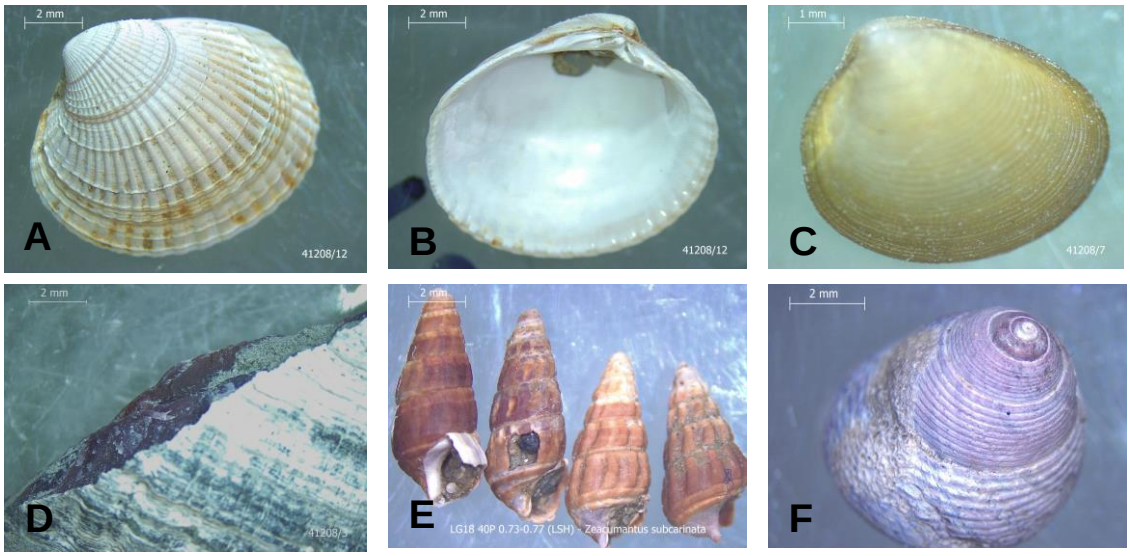

Figure 25 – Images of shells taken from Unit 2 and Unit 4. A) Whole Austrovenus stutchburyi shell outer and B) inner. C) Articulated Nucula hartvigiana. D) Angular fragment of a large A. stutchburyi shell. E) Zeacumantus subcarinata. F) Micrelenchus dialatatus.

5.2.4 Modern shell samples

Modern shell samples were collected to compare assemblages of known environments with shell assemblages found within the cores. Shells were collected from one location of saltmarsh (shell sample number 1) and the high tide line in 3 locations along the beach (shell sample numbers 2-4) (locations are displayed on Figure 13). Results of species identification are displayed in Figure 26. Once again, due to a small sample size, data is expressed as present or not present for the total assemblage in each sample. Species have been grouped by environmental preference according to Beu et al (1990). The

species identified at the saltmarsh include *Amphibola crenata* and *Zeacumantus subcarinata,* which agree well with the allocated environmental preference of high tidal mud flat. The species assemblages at all three beach locations are mixed, including species from rocky intertidal, low tidal, and subtidal environments. The most frequently encountered species were as *Barnea similis* and *Tawera spissa*. The assemblage from the 'cobble beach' in the south (shell sample number 3) contains the most species from subtidal exposed environments. The assemblage from the north beach (shell sample number 2) mainly includes species from low tidal to shallow subtidal environments. There are no common species identified in both beach and saltmarsh assemblages.

Figure 26 also includes the fossil shell assemblage (shell samples number 5) from a pit excavated on the beach ridge closest to the lake in the northern sequence, on Transect 22 (T22) (Figure 13). These shells were highly fragmented and abraded but were identified as *Barnea similis* and *Tawera spissa*.

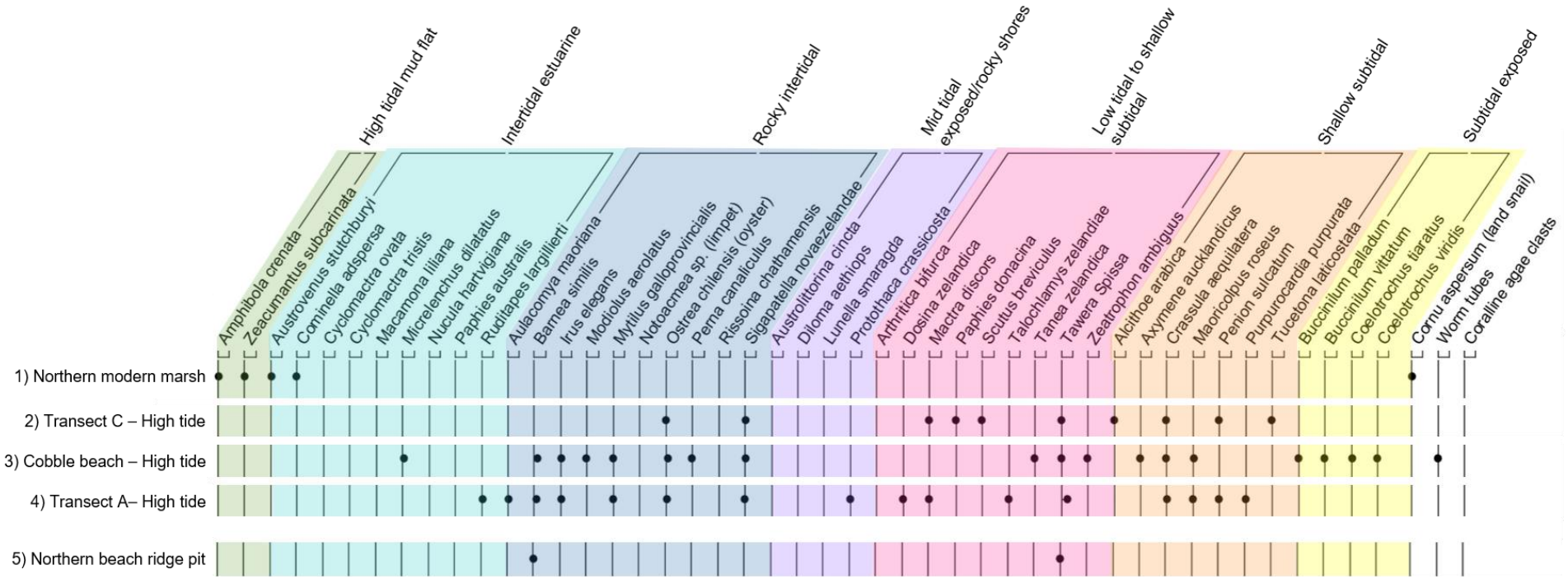

Figure 26 – Shell species identified in modern samples and other fossil locations around Lake Grassmere. Data is represented as present or not present due to low abundances. Species identification followed Beu et al (1990). Sample numbers correspond with locations shown in Figure 13.

5.3 Radiocarbon

In total, 25 radiocarbon dates were obtained from 6 cores. The majority of radiocarbon ages were obtained from bivalve shells, 18 of which were *Austrovenus stutchburyi*, and one of which was *Nucula hartvigiana.* Valves were selected from Unit 2 and Unit 4 in cores 11P, 22P, 29P, 40P and P3, based on the selection process outline in section 4.4.2 Seven dates were obtained from the upper shell hash, and 10 dates were obtained for the lower shell hash (Table 3). All dates were calibrated using OxCal v4 (Bronk Ramsey, 2017) using the methods outlined in section 4.4.2. Results are displayed in Table 3 and the probability density functions are plotted in Figure 27.

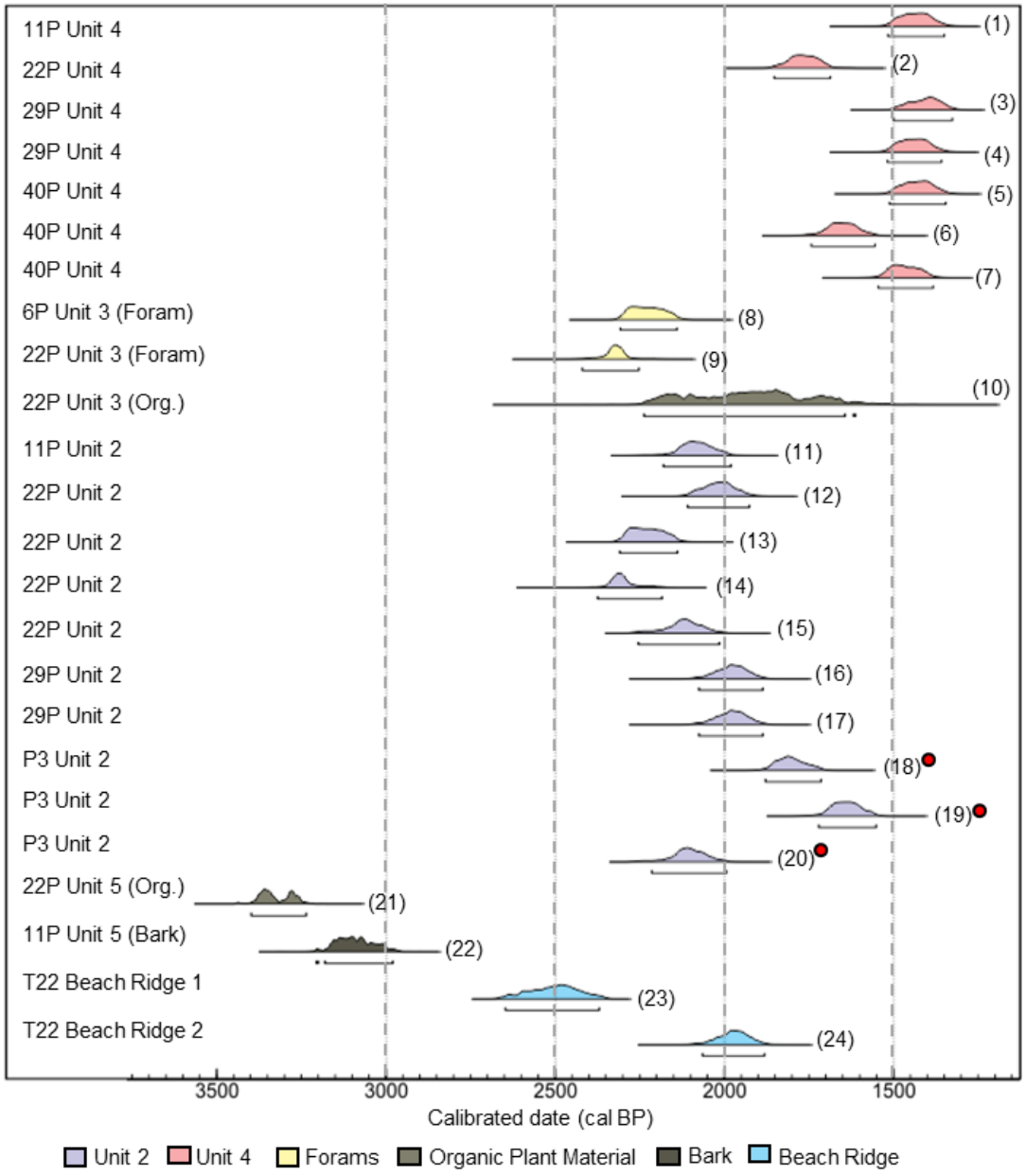

Figure 27 - Multiplot showing all calibrated radiocarbon age results. Results are organised stratigraphically and numbered to correspond with sample numbers in TABLE_RC. Shells from core P3 that are unreliable and therefore are excluded from further analyses are marked by red dots (●). Carbonate dates calibrated using Marine13 curve (Reimer et al., 2013), terrestrial dates calibrated using SHCal13 curve (Hogg et al., 2013), using OxCal v4.3.2 (Bronk Ramsey, 2017).

*Table 3 - Table showing all radiocarbon date results including the Conventional Radiocarbon Age (CRA) and calibrated age. Results are organised stratigraphically. Additional isotope information is included. Austrovenus stutchburyi (A. stutchburyi). NZA = Code signifying samples were processed at Rafter Radiocarbon Laboratory, New Zealand, using AMS. * Shells from core P3 that are unreliable and therefore are excluded from further analyses.*

Sample Number	NZA	Laboratory Code	NZ Fossil Number	Core	Sample Depth (m)	Elevation m NZVD (m AMSL)	Fraction Dated	Stratigraphic position	Radiocarbon Age	d13C (‰)	Modern Carbon (%)	Calibrated Age (cal BP)
1	65647	41208/1	P29/f0577	11	1.18-1.23	-0.44 – -0.49 (-0.06 – -0.11)	*A. stutchburyi* shell	Unit 4	1891 ± 27	0.6 ± 0.2	78.37 ± 0.26	1527-1337
2	65681	41208/3	P29/f0578	22	0.86	-0.55 (-0.18)	*A. stutchburyi* shell	Unit 4	2174 ± 26	-0.02 ± 0.2	73.16 ± 0.25	1869-1658
3	65686	41208/8	P29/f0580	29	0.82	-0.55 (-0.18)	*A. stutchburyi* shell	Unit 4	1865 ± 26	-0.1 ± 0.2	75.66 ± 0.25	1509-1314
4	65687	41208/9	P29/f0580	29	0.82	-0.55 (-0.18)	*A. stutchburyi* shell	Unit 4	1896 ± 26	0.41 ± 0.2	73.68 ± 0.24	1530-1341
5	65675	41208/12	P29/f0583	40	0.72-0.79	0.15 – 0.24 (0.53 – 0.60)	*A. stutchburyi* shell	Unit 4	1885 ± 26	0.91 ± 0.2	72.16 ± 0.24	1521-1334
6	65676	41208/13	P29/f0583	40	0.72-0.79	0.15 – 0.24 (0.53 – 0.60)	*A. stutchburyi* shell	Unit 4	2082 ± 26	0.3 ± 0.2	71.58 ± 0.24	1765-1545
7	65677	41208/14	P29/f0583	40	0.72-0.79	0.15 – 0.24 (0.53 – 0.60)	*A. stutchburyi* shell	Unit 4	1926 ± 26	2.28 ± 0.2	72.94 ± 0.24	1560-1365
8	66087	41225/6	P29/f0577	6	1.19-1.20	-0.45 – -0.46 (-0.07 – -0.08)	A. aoteana foraminfera	Unit 3, 6P	2553 ± 25	0.1 ± 0.2	78.32 ± 0.26	2315-2121
9	66088	41225/7	P29/f0578	22	0.97-0.99	-0.66 – -0.68 (-0.29 – -0.31)	A. aoteana foraminfera	Unit 3, 22P	2637 ± 25	-1.59 ± 0.2	73.95 ± 0.24	2429-2190
10	66233	41223/2	P29/f0578	22	0.97-0.98	-0.66 – -0.67 (-0.29 – -0.30)	Plant material	Unit 3, 22P	2395 ± 115	0.28 ± 0.2	78.63 ± 0.25	2741-2117
11	65648	41208/2	P29/f0577	11	1.42-1.45	-0.68 – -0.71 (-0.30 – -0.33)	*A. stutchburyi* shell	Unit 2	2444 ± 27	-1.78 ± 0.2	73.95 ± 0.24	2240-1958
12	65682	41208/4	P29/f0578	22	0.98-1.00	-0.67 – -0.69 (-0.30 – -0.32)	*A. stutchburyi* shell	Unit 2	2387 ± 26	1.06 ± 0.2	78.43 ± 0.25	2119-1905

13	65683	41208/5	P29/f0578	22	0.98-1.00	-0.67 – -0.69 (-0.30 – -0.32)	*A. stutchburyi* shell	Unit 2	2555 ± 26	0.31 ± 0.2	76.54 ± 0.25	2316-2124
14	65684	41208/6	P29/f0578	22	1.01	-0.70 (-0.33)	*A. stutchburyi* shell	Unit 2	2620 ± 27	1.4 ± 0.2	78.03 ± 0.25	2393-2159
15	65685	41208/7	P29/f0578	22	1.01	-0.70 (-0.33)	*Nucula hartvigiana* shell	Unit 2	2468 ± 27	-24.8 ± 0.2	-	2262-1996
16	65673	41208/10	P29/f0580	29	0.96-0.99	-0.69 – -0.72 (-0.32 – -0.35)	*A. stutchburyi* shell	Unit 2	2357 ± 26	-	-	2089-1874
17	65674	41208/11	P29/f0580	29	0.96-0.99	-0.69 – -0.72 (-0.32 – -0.35)	*A. stutchburyi* shell	Unit 2	2357 ± 26	-	-	2089-1875
18*	66084	41225/3	P29/f0584	P3	1.29-1.4	-0.43 – -0.54 (-0.06 – -0.17)	*A. stutchburyi* shell	Unit 2, P3	2206 ± 25	1.42 ± 0.2	-	1892-1697
19*	66085	41225/4	P29/f0584	P3	1.29-1.5	-0.43 – -0.64 (-0.06 – -0.27)	*A. stutchburyi* shell	Unit 2, P3	2071 ± 24	1.15 ± 0.2	-	1740-1535
20*	66086	41225/5	P29/f0584	P3	1.29-1.6	-0.43 – -0.74 (-0.06 – -0.37)	*A. stutchburyi* shell	Unit 2, P3	2459 ± 25	0.01 ± 0.2	-	2248-1987
21	66234	41223/3	P29/f0578	22	1.06-1.07	-0.75 – -0.76 (-0.38 – -0.39)	Plant material	Unit 1, 22P	3160 ± 22	1.68 ± 0.2	-	3398-3236
22	65849	41223/1	P29/f0577	11	1.51-1.52	-0.77 – -0.78 (-0.39 – -0.40)	Bark	Unit 1, 11P	2982 ± 23	-2.63 ± 0.2	-	3206-2980
23	66082	41225/1	P29/f0585	T22 Pit 1	0.5-0.7	2.49 – 2.69 (2.86 – 3.06)	*Tawera spissa* shell	Beach ridge pit	2769 ± 25	0.6 ± 0.2	72.18 ± 0.23	2650-2355
24	66083	41225/2	P29/f0585	T22 Pit 1	0.5-0.8	2.39 – 2.69 (2.76 – 3.06)	*Tawera spissa* shell	Beach ridge pit	2353 ± 25	0.33 ± 0.2	71.42 ± 0.23	2084-1870

The radiocarbon ages form two distinct clusters around 1500 and 2000 cal BP (Figure 26). The radiocarbon ages from core P3 do not fit. The depths of these shells were recorded by students at Victoria University of Wellington (VUW) and all three were labelled as 'lower shell hash', however the two dates (sample numbers 18 and 19) are significantly younger than dates obtained from the Unit 2 in other cores. One date (sample number 20) fits well with other dates for Unit 2. Upon further analysis of core P3, in particular the grain size data, I concluded that the shell hash in P3 is combination of Unit 2 and Unit 4 therefore the shells samples by the VUW students are probably from both units. Because there is uncertainty about exactly where the shell samples came from, I exclude them from further interpretation. *Nucula hartivigiana* was used as a test in this study as its suitability for radiocarbon dating was poorly known as it has rarely been dates in estuarine sediment core in New Zealand. The results show consistency between the date obtained for the *Nucula hartvigiana* sample (sample number 15) of 2262-1996 and the results obtained from *Austrovenus stutchburyi* in the same unit that have a range of 2393-1874 cal BP.

Two shell dates were obtained from the Transect 22 pit on the youngest lake-parallel beach ridge (sample numbers 23 and 24). The results of these samples give ages of 2650-2355 and 2084-1870 cal BP. This makes them similar to and slightly older than Unit 2, although it should be noted the shells were highly abraded so may carry an inherited age.

Two dates were obtained from samples of foraminifera (sample numbers 8 and 9). The radiocarbon results for these samples are older than expected and do not fit within the chronostratigraphic sequence as they are older than the shells within the unit directly below. Possible reasons for this are considered in the chronology of Unit 3 in section 6.2.

While all units were sieved at 2 cm intervals for the retrieval of organic material large enough to date, there were only two samples in Unit 3 that had enough mass to provide targets for dates to bound the Unit 2 (sample numbers 10 and 21). A single macrofossil could not be picked and therefore a mass of mixed plant fragments was submitted. It is recognised that this is not an ideal target for dating as it may contain fragments of aquatic plants that fix carbon from the water and therefore require corrections for the marine reservoir effect. The results are older than expected and do not fit the chronostratigraphic sequence as they predate Unit 2 directly below. However, both a bark sample (sample number 22) and a mixed organic sample (saple number 21) from Unit 1 pre-date Unit 2 by almost ~2000 years and therefore fit chronologically. The bark sample is slightly younger than the organic plant material sample.

Radiocarbon dates from Ota et al (1995) were re-calculated by Rafter Radiocarbon Laboratory (Lower Hutt, New Zealand) according to modern standards and recalibrated using the most up to date calibration curve for this study. Dates from the north side of the lake, within the beach ridge sequence were re-calibrated using the Marine13 curve (Reimer et al., 2013) and updated delta R (ΔR) of 4 ± 25, using OxCal v4.3.2 (Bronk Ramsey, 2017). The results are shown in Table 4 and in Figure 28, with the two beach ridge dates obtained in this study.

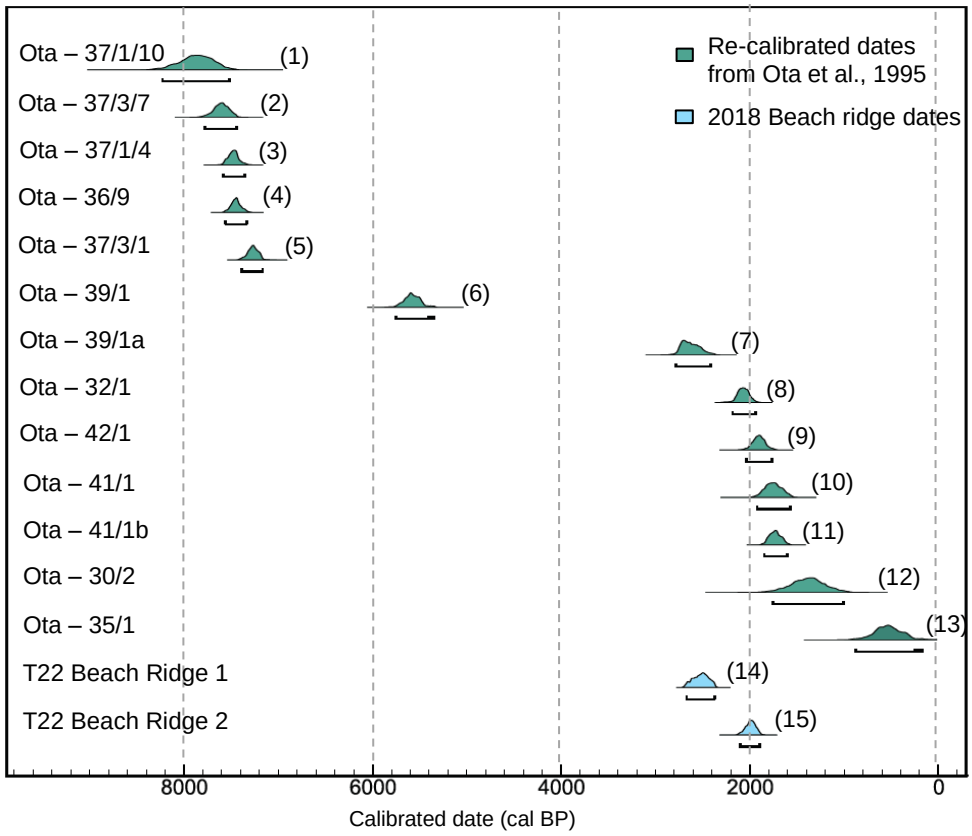

Figure 28 - Multiplot showing all re-calibrated radiocarbon ages from Lake Grassmere in Ota et al, 1995. Results are organised chronologically and numbered to correspond with sample numbers in Table 4. Carbonate dates were calibrated using Marine13 curve (Reimer et al., 2013), using OxCal v4.3.2 (Bronk Ramsey, 2017).

Table 4 - Table showing the re-calibrated radiocarbon dates from Ota et al (1995) and the two beach ridge dates obtained in this study (also included in Table 3).

NZ	NZ Fossil Number	Ota et al (1995) code	Elevation / m AMSL	Elevation / m (NZVD)	Radiocarbon Age	Calibrated Age
A1191	P29/f332	37/1/10	-1.3	-0.9	7377 ± 180	8207-7498
7792	P29/f322	37/3/7	-0.5	-0.1	7108 ± 87	7758-7421
7790	P29/f318	37/1/4	-0.8	-0.4	6953 ± 54	7563-7338
7789	P29/f317	36/9	0.2	0.6	6923 ± 47	7538-7318
7791	P29/f320	37/3/1	0.3	0.7	6721 ± 44	7369-7146
7793	P29/f324	39/1	3.3	3.7	5206 ± 75	5736-5333
5193	P29/083432	39/1a	-3.3	-2.9	2870 ± 64	2764-2399
7788	P29/f315	32/1	2.1	2.5	2418 ±32	2162-1920

7795	P29/f326	42/1	0.4	0.9	2278 ± 44	2020-1742
7794	P29/f325	41/1	1.7	2.1	2149 ± 69	1902-1547
5192	P29/079439	41/1b	1.0	1.4	2130 ± 34	1826-1585
A1185	P29/071444	30/2	1.1	1.5	1800 ± 166	1731-990
A1190	P29/071443	35/1	2.8	3.2	913 ± 168	855-149
A66082	P29/f0585	LG18 T22 BR 1	3.6	3.2	2769 ± 25	2650-2355
A66083	P29/f0585	LG18 T22 BR 2	3.6	3.2	2353 ± 25	2084-1870

5.4 Surface topography

The two DSMs created from drone imagery and structure from motion (SfM) techniques facilitate elevation profiles to be extracted along transects of interest (Figure 29). The profiles in Figures 30 to 32 demonstrate the variable topography across the study site and allow subtle geomorphic features such as beach ridges can be resolved and measured.

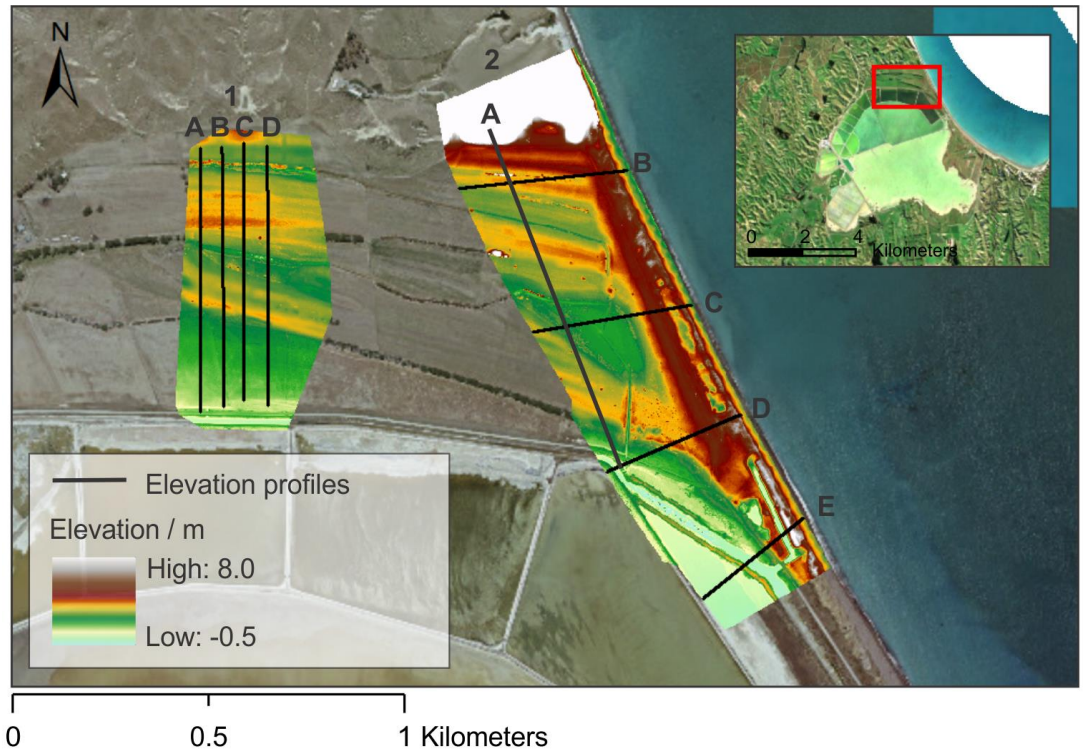

Figure 29 - Map detailing the location of DSM areas and elevation profiles.

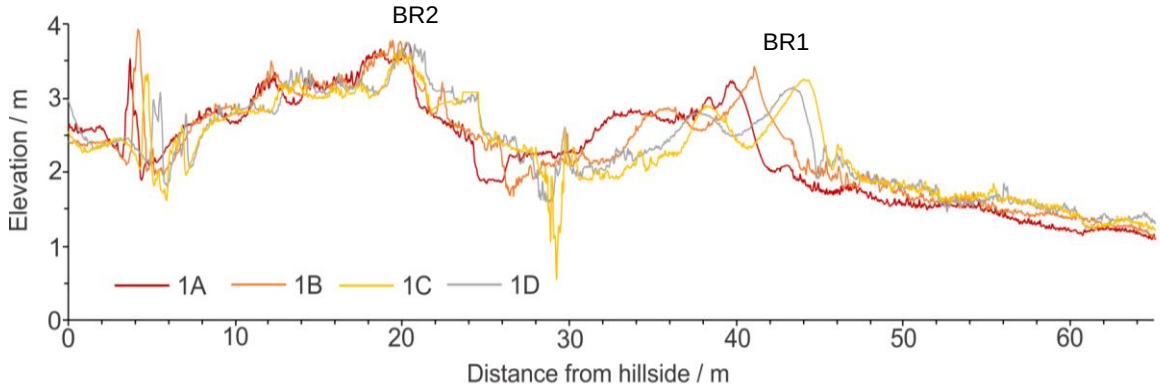

Figure 30 - This figure shows elevation profiles of the northern beach ridge series in transects from the hillside to the trench at the lake edge. Data was obtained from the DSM. Profile labels correspond to locations displayed in Figure 29.

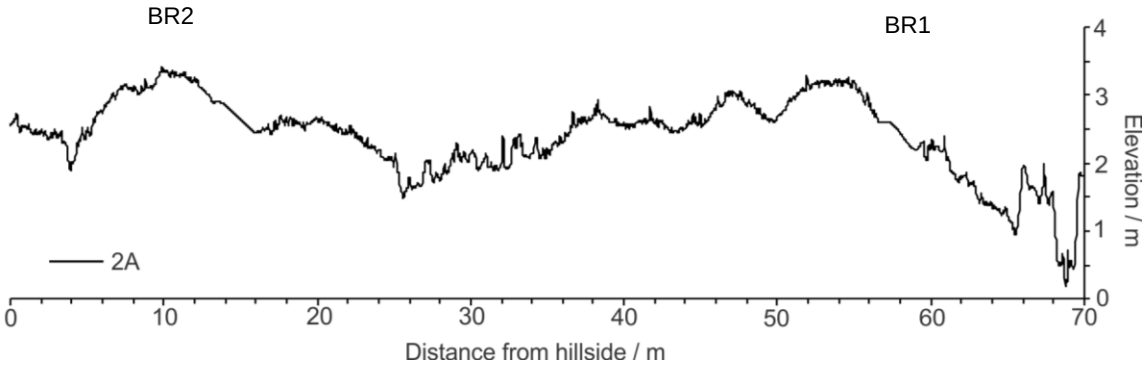

Figure 31 – Elevation profile of transect 2A across the northern beach ridge sequence, within the barrier DSM polygon.

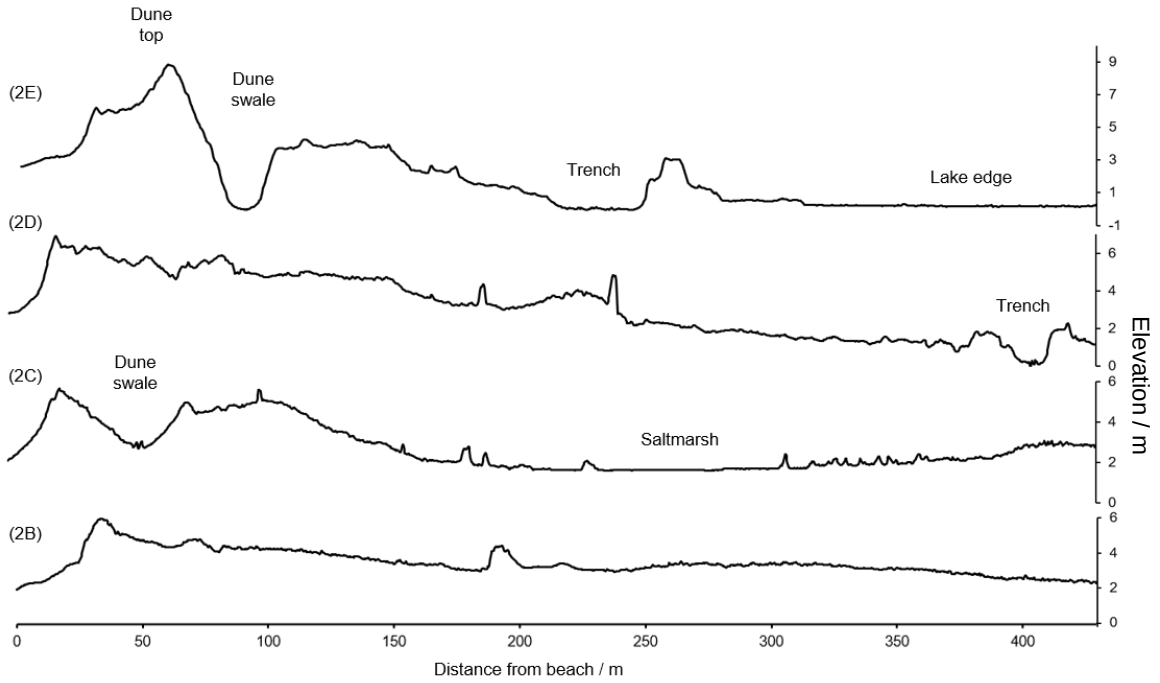

Figure 32 - This figure shows elevation profiles across the beach barrier in beach to saltmarsh transects. Data was obtained from the DSM. Profile labels correspond to locations displayed in Figure 29. Expressive features have been noted.

6.0 DISCUSSION OF RESEARCH QUESTION 1: HOW DID THE MORPHOLOGY OF LAKE GRASSMERE EVOLVE DURING THE LATE HOLOCENE?

In this section I discuss the palaeoenvironmental inferences that can be made from the sedimentary stratigraphy at Lake Grassmere. Multiproxy analysis of piston cores is used to document environmental changes that occur between and within defined sedimentary units. Where changes are identified, I consider them alongside the formation of geomorphic features such as the beach barrier and beach ridges. I use the radiocarbon dates obtained in this study, as well as from Ota et al (1995) to assign a chronology to the evolution of the lake. The discussion is summarised in a schematic representation of the evolution of Lake Grassmere during the late Holocene (Figure 33), included here as an aid.

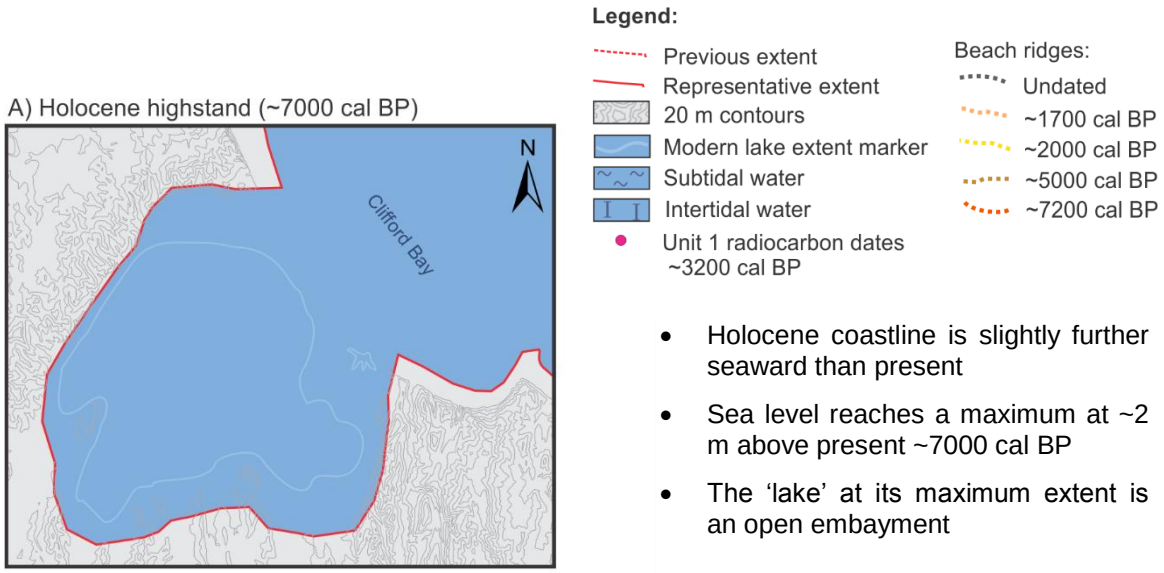

- Holocene coastline is slightly further seaward than present
- Sea level reaches a maximum at ~2 m above present ~7000 cal BP
- The ‘lake’ at its maximum extent is an open embayment

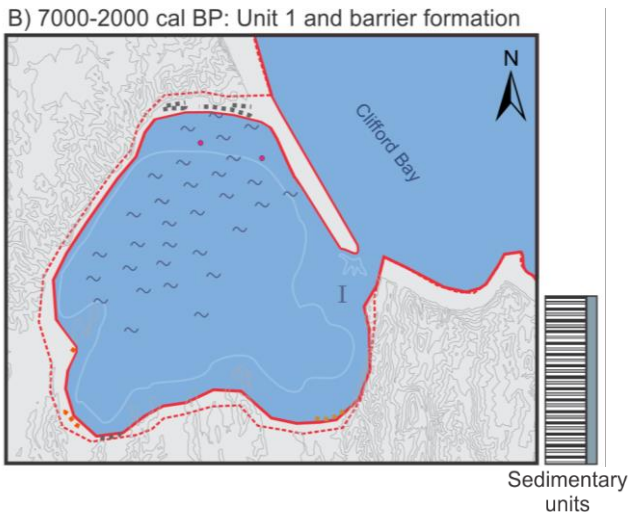

- Sea-level is stable is until ~4000 cal BP, then begins to fall gradually
- A barrier/spit is formed across the front of the ‘lake', welded to the north
- A small inlet remains in the southeast
- Subtidal sediment begins to accumulate prior to ~3200 cal BP, sheltered water allows fine laminations (Unit 1)
- The ‘lake’ extent begins to contract under sea-level fall
- Beach ridges form perpendicular to the coast in the north

C) ~2000 cal BP: Unit 2 deposited suddenly

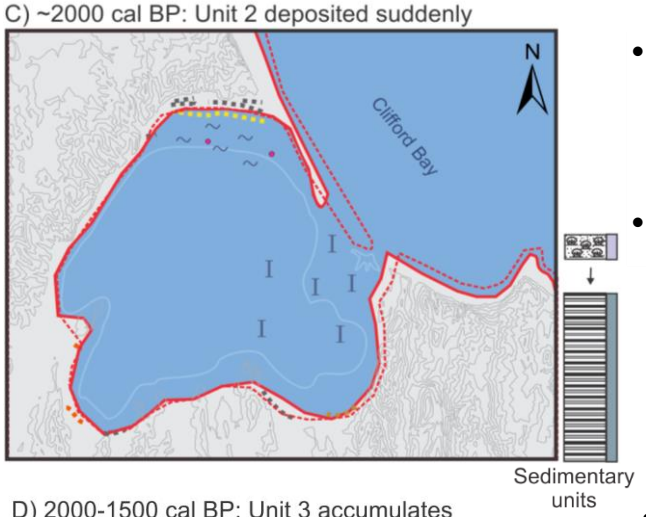

- A high energy event, possibly associated with sudden subsidence, breaches the barrier and opens the lake/lagoon to increased tidal and wave influence
- A dense shell hash consisting of intertidal bivalves is deposited (Unit 2)

D) 2000-1500 cal BP: Unit 3 accumulates

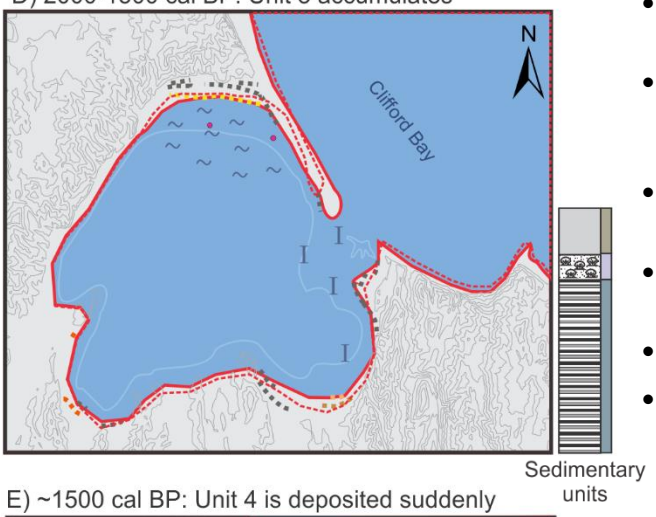

- The barrier is still in place and continues to build
- Increased exposure to tidal currents and waves from the wider inlet alters sediment deposition
- Unit 3 is deposited subtidally, as homogenous silt (no laminations)
- Intertidal conditions are present close to the inlet
- Sea level continues to fall gradually
- Beach ridges continue to form with contracting ‘lake’ extent

E) ~1500 cal BP: Unit 4 is deposited suddenly

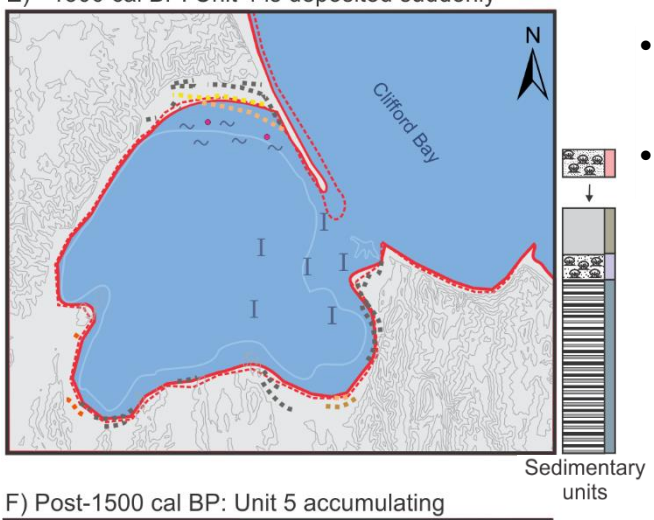

- A high energy event breaches the barrier and opens the lake/lagoon further
- A dense shell hash consisting of intertidal bivalves is deposited (Unit 4)

F) Post-1500 cal BP: Unit 5 accumulating

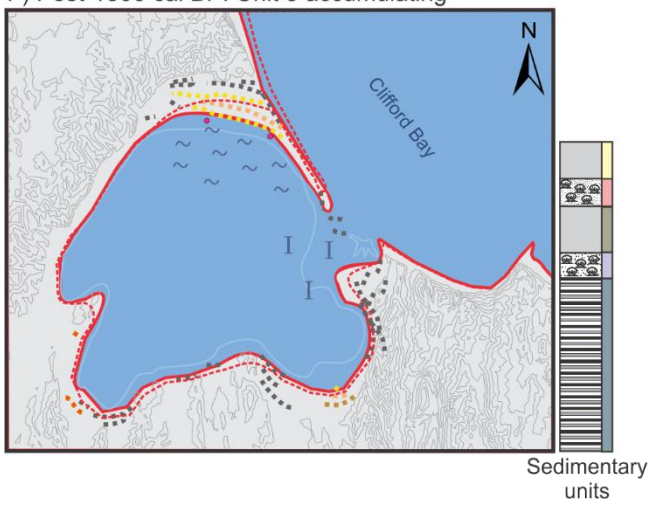

- The barrier re-grows southwards across the front of the lake
- Unit 5 accumulates subtidally
- Interbedded sand lenses indicate barrier fluctuations
- Sea level continues to fall gradually
- Beach ridges continue to form with the contracting ‘lake’ extent

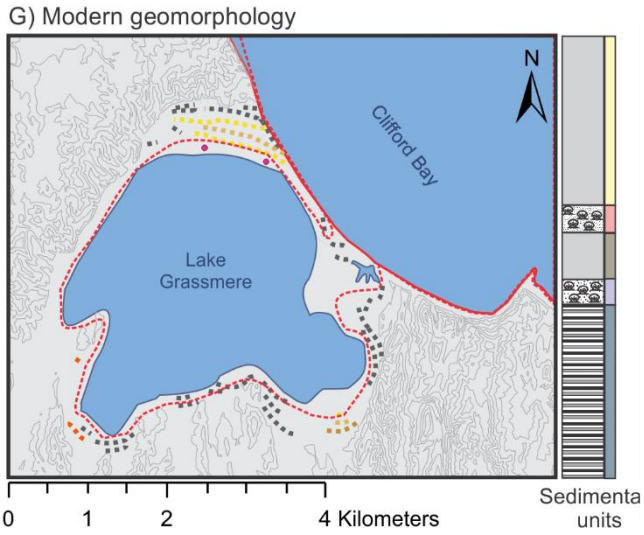

- Sea level has fallen to present
- The barrier has enclosed the ‘lake’, isolating it from Clifford Bay
- The small lagoon and beach ridges indicate the location of the former inlet
- Relict beach ridges mark previous lake extents
- Coastline is eroding under recent sea-level rise
- The lake is heavily modified for salt extraction

Figure 33 – Schematic representations of the evolution of Lake Grassmere during the late Holocene.

6.1 Palaeoenviromental interpretations of units

Preceding discussion of the palaeoenvironment at Lake Grassmere it is useful to consider the modern environment as a comparison. Our knowledge of the lake pre-saltworks is limited to the description in section 3.4, which does not detail whether water moved freely through the barrier before it became artificially controlled for salt extraction. Ideally, samples would be taken from the modern lake for analysis of sediments and microfossils, however access to the lake itself is restricted by the saltworks construction and therefore no direct samples from the lake were obtainable. Consequently, it is unknown whether the hypersaline lake supports any microfossil populations at present. In summary, the entire lake is heavily modified making comparative analyses of modern and prehistoric characteristics unreliable, as it is unlikely that the current conditions are representative of the environment at Lake Grassmere before human manipulation. Here, I interpret the results from piston cores in order to understand the palaeoenvironments during the deposition of each sedimentary unit. Observations from the sedimentary descriptions, grain size and biostratigraphy are considered together.

Unit 1 is present in 10 out of 11 piston cores at the study site at the north of the lake. The finely laminated unit of predominantly silt is indicative of deposition in subtidal water. The depositional environment must have been below the range in which wave and tidal mechanisms rework surface sediments, to facilitate such fine lamination of sediment. In order for subtidal conditions to be present at piston core locations such as 11P that are so close to the coast, I infer that a barrier must have been in place across the front of the lake/lagoon (welded to the north). The barrier is necessary to shelter the northern site of piston cores from wave and tidal influence, reducing the depth to which sediment

deposited on the lake/lagoon floor is disturbed, and allowing deeper subtidal water depth to build behind it.

The foraminifera results support this scenario, as the dominant species *Ammonia aoteana,* has a broad environmental range, which when present in a monospecific assemblage of up to 100% indicates intertidal to subtidal conditions down to 3 m (Hayward et al., 2014 a). The abundance of foraminifera throughout Unit 1 is very low. This may mean that the palaeoenvironment within the lake during the deposition of Unit 1 was not saline enough to support large populations of foraminifera. It is possible that this is a result of the barrier that formed across the front of the lake during this time, restricting the inflow of brackish waters. Nevertheless, *A.aoteana* does not occur in freshwater environments and therefore suggests that the lake must have had a sizeable open connection to the ocean to allow some *A. aoteana* to be present in Unit 1. The dominance of *A. aoteana* does not change throughout the unit, inferring that there were no substantial environmental disturbances while Unit 1 was accumulating. It must be considered that *A. aoteana* may not be sensitive enough to reflect small deviations in environmental conditions due to their broad environmental preferences. The foraminiferal test size composition of Unit 1 is dominated by the 125-250 µm size range; however, again it is important to note that the concentration of foraminifera in Unit 1 is very low, with a maximum of 13 tests per 1g of sediment (Unit 1 in core 40P).

Unit 2 is substantially different to Unit 1 in its composition, suggesting a substantial change in depositional environment. The sand matrix and dense shell hash is not compatible with undisturbed accumulation in deep water, and the extremely sharp basal and upper contacts suggest rapid change. A sudden increase in grain size is often associated with an event that either changes the depositional process or interrupts it (Morton et al., 2007; Peters and Jaffe, 2010). Further to this, the sharpness and irregularity of the basal contact in cores such as 40P suggest the depositional mechanism for Unit 2 was erosional and scoured the surface of Unit 1 (Figure 34). The grain size distribution of samples in Unit 2 is finer than the modern samples taken from the beach environments and more similar to the coarser saltmarsh deposits in Transects B and D (Figure 17), however neither of the modern samples are similar enough to infer the source of the coarser sediment in Unit 2.

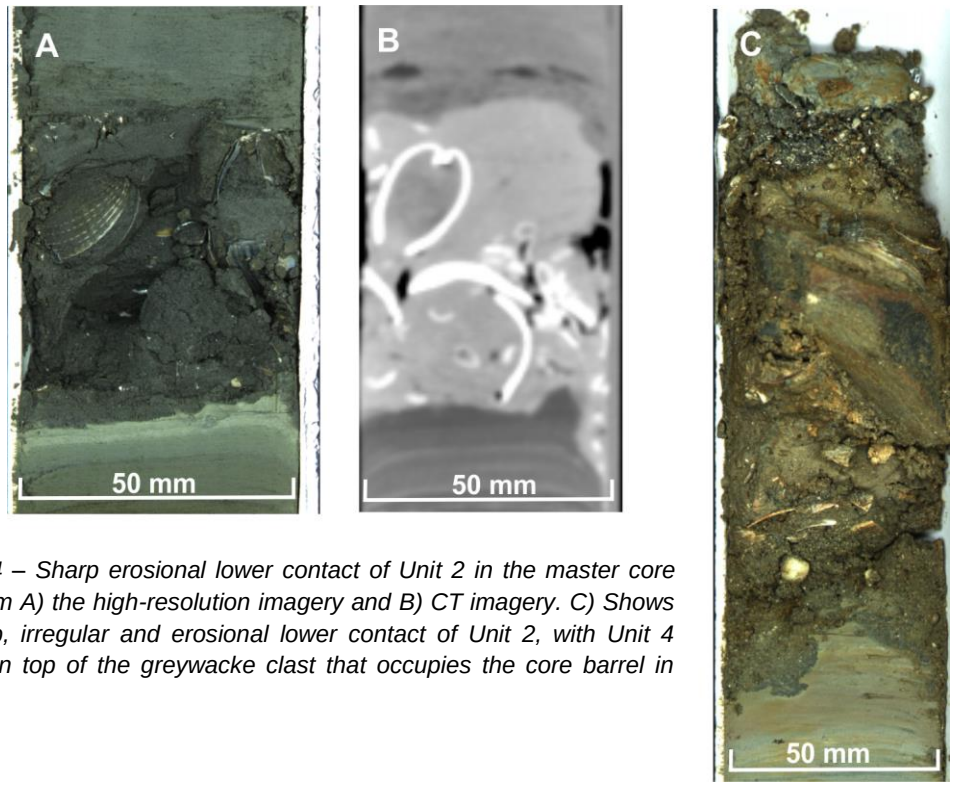

Figure 34 – Sharp erosional lower contact of Unit 2 in the master core (22P) from A) the high-resolution imagery and B) CT imagery. C) Shows the sharp, irregular and erosional lower contact of Unit 2, with Unit 4 directly on top of the greywacke clast that occupies the core barrel in core 40P.

Despite the change in grain size and shell content, the foraminiferal assemblage reflects Unit 1. The monospecific *A. aoteana* assemblage continues to indicate a broad (intertidal to subtidal) brackish water depth and therefore is unable to distinguish whether Unit 2 is an abruptly emplaced deposit or in situ unit. Nevertheless, a significant variation is seen in the increased abundance of foraminifera to a maximum of 226 tests per 1g of sediment in core 40P, as well as an increased percentage of tests in the >250 µm size range (up to 58% in core 40P). Increased concentration of foraminifera is not diagnostic of any specific depositional process or environment; however an increased abundance of foraminifera may be encouraged under increased salinity. It is possible that increased salinity could be facilitated by the opening of the barrier, increasing the inflow of brackish water into the lake. Overall, the foraminifera results alone do not indicate rapid environmental change or abrupt deposition, but do not discard it as an option.

The bivalve assemblage of the shell hash of Unit 2 is dominated in all cores by *Austrovenus stutchburyi* and *Nucula hartvigiana;* two infaunal bivalves that can be found together in intertidal estuaries and sandflats (Marsden, 2004). Other mollusc species found in Unit 2 include *Cyclomactra ovata, Potamopyrgus estuarinus* and *Amphibola crenata*, which represent a wider range of environments from estuarine to high saltmarsh. All shells are of mixed sizes including juveniles, and a high percentage of articulated *Austrovenus stutchburyi*, however they are not in life position suggesting that the assemblage is not in situ and that the shells have been transported. The excellent preservation and lack of abrasion of the shells (Figure 25) infers they were not exposed

for long before they were buried by the finer sediment, and that little reworking has occurred since (Reinhardt et al., 2006, Kitamura et al., 2018 b). In summary, Unit 2 probably represents a rapid, high energy event deposit as it displays an abrupt and stark contrast to the slow accumulation of sediment that occurs in Unit 1, with an increased grain size, dense shell hash of juvenile and articulated bivalves and altered foraminiferal test size composition. The origin of this unit is discussed in section 7.0.

The grey silt that comprises Unit 3 is massive in most cores, apart from where it is punctuated by fine sand lenses in coastal and northern cores (Figure 18). The overall grain size is similar to Unit 1 (silt), however Unit 3 is not laminated. The homogeneity of the sediment suggests that either the depth of the water in the lake changed or that the depositional environment became subject to tidal currents and/or wave action, resulting in the disturbance of the surface sediment. Once again, *A. aoteana* dominates the foraminiferal assemblage inferring a degree of open connection to the ocean, however *Haynesina depressula* is now present at ~6%. The presence of *H. depressula* within a the *A. aoteana* assemblage narrows the environmental range to below low tide, inferring that Unit 3 was also accumulating subtidally (Hayward et al., 2014 a). It is possible that the depth of the lake shallowed between Unit 1 and Unit 3 and that this change is undetectable within the *A. aoteana* assemblage. Reasons for changing water depth are discussed in section 7.1.1 and 7.3. On the other hand, the constant subtidal conditions indicate that the variation in sediment deposition is more likely to be a function of increased movement within the water column and consequent disturbance of surface sediments, which may have been instigated by the opening of the inlet during the deposition of Unit 2.

The foraminiferal test size results show a sharp decrease in the concentration of foraminifera compared to Unit 2, with some samples not containing any foraminifera. The test size distribution of samples in Unit 3 shows slightly variable results, however the 125-250 µm size group dominates, contrasting Unit 2. Overall, while the depositional characteristics are clearly different, the fine grain size distribution and foraminiferal composition of Unit 3 are similar to Unit 1, contrasting the coarse and concentrated Unit 2.

The composition of Unit 4 is similar to Unit 2, with a sandy matrix and dense shell hash of predominantly *A. stutchburyi* bivalves. Figure 24 suggests that the species diversity is higher in more landward cores where Unit 3 has pinched out and Unit 2 and 4 are directly on top of one another. The species assemblage of these cores is mixed, with mollusc species that inhabit high tidal mudflats, intertidal estuaries and rocky intertidal locations together. The species diversity, lack of burrowing across the contacts and out of life position of the bivalves suggests that Unit 4 does not reflect an in-situ assemblage and

that the shells were reworked from a range of sources into the deposit. Again, the excellent preservation of fragile bivalves and the lack of abrasion (Figure 25) infer minimal post-mortem exposure and reworking. Further to this, no shells were identified (visually and from the CT data) within units above or below the shell hashes (Unit 2 and Unit 4), implying that bivalves were not present in situ in bounding units. The increased abundance of coralline algae and other clastic material that is also associated with the Unit 4 and landward cores is interesting, especially as there are no greywacke outcrops around Lake Grassmere to explain the clast identified in core 40P.

The foraminiferal assemblage of Unit 4 is similar to the subtidal assemblage of Unit 3, with an assemblage of *A. aoteana* assemblage at ~94%, and *H. depressula* at ~6%. One sample in Unit 4 contains the fully marine, inner shelf species *Notorotalia* at 21% (Hayward et al, 1999). While this species is only present to this degree in one sample, it indicates marine inundation. The foraminiferal test size distribution in Unit 4 is extremely similar to Unit 2 with a significant increase in foraminifera abundance and increased frequency of foraminifera in the >250 µm size group. Additionally, as in Unit 2, the basal contact of Unit 4 is very sharp and there is a sudden change in grain size to a coarser (fine sand) and leptokurtic distribution (Figure 17). While the upper contact of Unit 4 is not as sharp as the upper contact of Unit 2, both shell hashes probably reflect anomalous units that can be interpreted as high-energy deposits based on the abruptness of grain size changes, sharpness of contacts and the dense shells hash that includes articulated bivalves. The origin of these deposits is discussed in section 7.0.

Unit 5 is a mixed unit of grey silt similar to Unit 3, with sand lenses of variable thickness that increase in abundance landwards and northwards (Figure 18). The basal contact with Unit 4 is gradational and difficult to distinguish due the sandier composition of the unit. The foraminferal results mostly mirror Units 3 and 4, with the near-monospecific *A. aoteana* and *H. depressula* association dominating. More subtidal species are identified in this unit however all are <5% of the assemblage, inferring that subtidal conditions are persistent from Unit 3 onwards. Thus, the barrier must also have been present throughout this period to provide the subtidal water depths landward of the coast, indicated by Unit 5. As there were no other microfossils or macrofossils identified within Unit 5 it is difficult to make any further interpretation of the palaeoenvironment, but I speculate that the periodic inter-fingering sand lenses may indicate fluctuating dynamics of the beach barrier which eventually lead to the isolation of the lake. The only other significant feature within Unit 5 (Figure 18) is the gravel layer located in gouge cores along core transect T22 (Figure 13) (see description of LG18 35 in Appendix 1). The rounded gravels and highly abraded shell material (*Tawera spissa* and *Barnea similis*) has strong affinities with the material extracted from the pit on top of the most-lakeward beach ridge along the same transect. I was not able to penetrate past this unit in cores

further north along the transect, suggesting that the thickness of the unit increased and so I infer that the gravel deposit within Unit 5 is the toe of an older beach ridge.

In summary, from the information collected in this study, I infer that a subtidal environment was present at the north of the lake throughout the stratigraphic sequence, facilitated by a beach barrier with an open connection to Clifford Bay to provide brackish conditions that support the foraminiferal assemblages. All core locations experienced two sudden interjections of coarse shell hash units (Unit 2 and Unit 4) that contrast the sediment composition of the units above and below, and display characteristics indicative of rapid deposition during a high-energy event. It is likely that these abrupt events transformed the morphology and extent of the coastal barrier, altering the exposure of the lake to the influence of tidal currents and waves. In the next section, I use radiocarbon dates to assign a chronology to these events.

6.2 Chronology and sea level

The radiocarbon dates in this study are used to place palaeoenvironmental changes at Lake Grassmere within the timeframe of the late Holocene (Table 3). I expand the northern study area to encompass the radiocarbon dates from beach ridge sequences at Lake Grassmere obtained by Ota et al (1995), as well as taking into account the sea-level trends of the time. Palaeoenvironmental events are discussed chronologically.

Sea-level overview: It is important to consider the behaviour of sea-level during the timespan of this study, as it is likely that many palaeoenvironmental changes may be in response to fluctuating sea-level trends. The sea-level curve that is most applicable to Lake Grassmere is displayed in Figure 11 in section 3.4.2, showing sea-level in Canterbury began steadily decreasing after the late Holocene highstand around 4000 cal BP (Clement et al., 2016; Hayward et al., 2016). Consequently, the record of sea-level fall at Lake Grassmere should show a gradual progression from subtidal to intertidal, shallower water microfossil species, as well as possible mobilisation of geomorphic features such as the beach barrier and beach ridges. Interestingly, no evidence of sea-level change is indicated in the foraminifera data, as the *A.aoteana* with *H. depressula* association assumes a subtidal environment throughout the cores. Nonetheless, the highstand was a maximum of only 2 m above present sea-level, and so the broad environmental range of *A. aoteana* (Hayward et al., 2014 a) may have been able to withstand this variability to remain dominant throughout the sequence observed in the piston cores.

With the falling sea-level trend in mind, we can consider the evolution of the lake under these conditions. Ota et al (1995) published radiocarbon dates obtained from shells in

beach ridges from the outskirts of Lake Grassmere, and the recalibrated age ranges are shown in section 5.3 (Table 4, Figure 27). All radiocarbon dates from Lake Grassmere have been compiled in Figure 35.

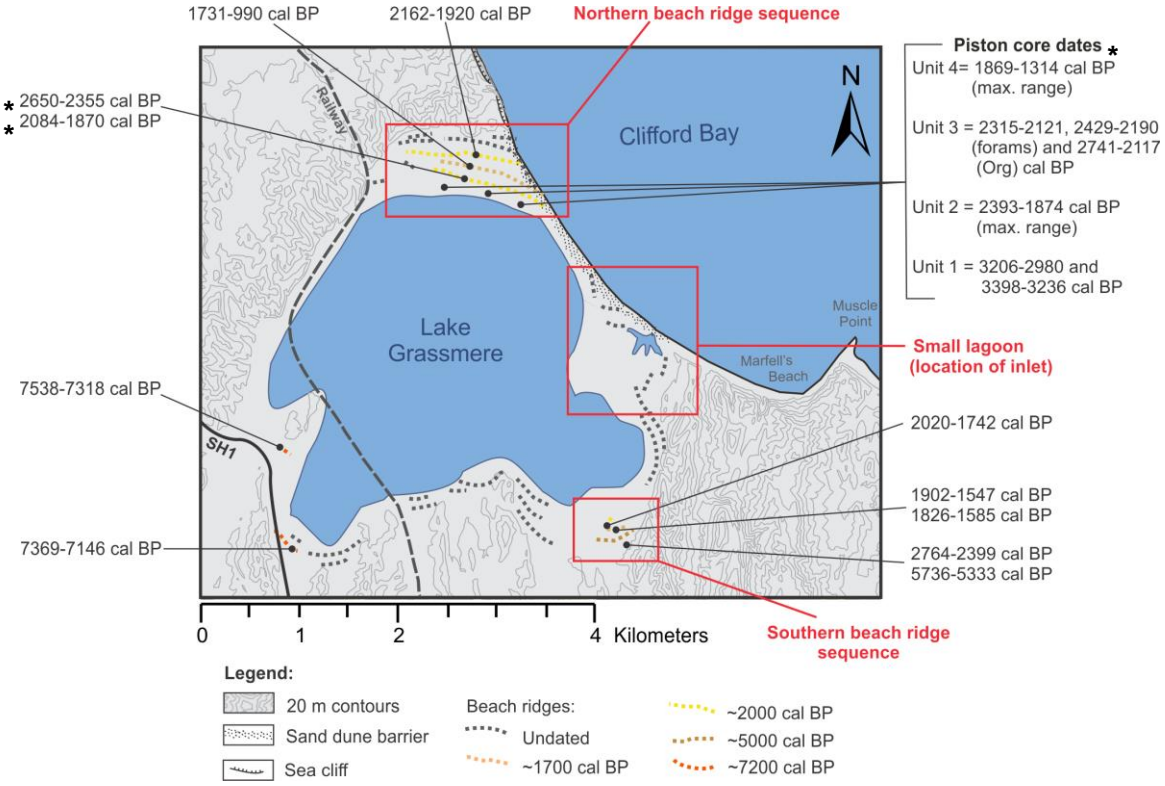

Figure 35 – Geomorphic map of Lake Grassmere including the location of dated and undated beach ridges and the modern lake extent. indicates dates obtained from this study (Table 3), all other dates are recalibrated ages obtained from Ota et al (1995), displayed in Table 4 in section 5.3.*

Holocene highstand: Figure 35 shows dates in Ota et al (1995) are taken from beach ridge sequences that are likely to represent previous lake extents (Thompson and Baedke, 1995). The dated beach ridges are younger as they progress towards the modern lake edge and their orientation mostly reflects the morphology of the basin. The oldest dates are ~7200 cal BP from the south west corner of the lake, which would place them at a similar time to the first sea-level highstand that occurred around 7000 cal BP around New Zealand (Clement et al., 2016). As a result, it is likely that these beach ridges mark the maximum extent of the lake at the highstand (Fraser et al., 2004; Brooke et al., 2019). The next beach ridge date is younger at 5736-5333 cal BP located in the dated southern beach ridge sequence (Figure 35), however another shell from the same beach ridge gives a date of 2764-2399 cal BP, suggesting that the older shell is reworked.

Barrier formation and Unit 1: Chronologically, the next date was obtained from organic fractions close to the upper contact of Unit 1, providing ages for this unit of 3206-2980 and 3398-3236 cal BP. While I could not obtain enough material to expand the dating of

Unit 1 in order to estimate the sedimentation rate, these dates are important for delineating the evolution of the beach barrier. As I established that Unit 1 was forming under sheltered subtidal conditions that would have required the beach barrier to be in place to allow the formation of laminations, we can infer that barrier formation and stabilization occurred prior to the oldest date in Unit 1 (3398-3236 cal BP). This is plausible within the sea-level context (Clement et al., 2016), as the formation of a spit or barrier may be facilitated by the onset of falling sea-level after the highstand at ~4000 cal BP (Tamura, 2012; Tamura et al., 2012; Brooke et al., 2019). Further to this, the northern beach ridge sequence is oriented perpendicular to the coast. In order for ridges to form at this angle the barrier must have been in place across the front of the semi-enclosed lagoon, welded to the north. Consequently, the beach ridges in the northern sequence must also postdate the formation the beach barrier that occurred prior to the deposition of Unit 5, earlier than ~3200 cal BP.

The positioning of the northern beach ridges infers that the barrier extended southwards across the front of the lake, however the foraminifera data requires there to be an open connection to the ocean to provide brackish conditions to support the subtidal *A. aoteana* association. The modern geomorphology of the irregular-shaped, small lagoon and surrounding beach ridges on the eastern side of the lake provides a possible candidate for the relict opening (Figure 35). In addition, the piston cores taken from the south side of the lake in 2016 were characterised by irregularly interbedded silts and sands that are more characteristic of intertidal estuarine settings (see Appendix __ for information on 2016 piston cores). Unit 1 was not encountered in these cores, supporting the suggestion that the south end of the lake was experiencing shallower, more intertidal conditions than the north side of the lake during the late Holocene.

Beach ridges: Ota et al (1995) dated 3 more beach ridges in the southern beach sequence (Figure 35) to 2764-2399, 1902-1547 (and 1826-1585) and 2020-1742 cal BP. In general, the beach ridges get progressively younger as they near the modern lake edge, agreeing with the theory that the beach ridges signify previous lake/lagoon extents that are likely to be in response to falling sea-level (Thompson and Baedke, 1995; Brooke et al., 2019). The beach ridge closest to the lake gives a slightly older date than the one behind it, however it is likely that this is a result of reworked material accrued into the beach ridge. This trend is also present for the northern beach ridge sequence that is less thoroughly dated. The beach ridges furthest from the lake are undated but assumed to post-date the barrier formation, the sequence getting progressively younger with increasing proximity to the modern lake. In summary, it is likely that the beach ridge sequences at Lake Grassmere represent the sheltered lagoon extent during the late Holocene, and that the older dates in more lakeward beach ridges are from reworked shells.

Unit 2: Chronologically, Unit 2 follows Unit 1 based on the radiocarbon ages within the units Radiocarbon dates in this study are focused on the shell hash units. The dates obtained from 7 bivalves in Unit 2 span from 2393 to 1874 cal BP (excluding the 3 shells from P3) (Table 3). As Unit 2 has been highlighted as an anomalous deposit, it is possible that the macrofossils dated within this unit are reworked, and therefore can only indicate the oldest age limit of the depositional event responsible.

Unit 3: Stratigraphically, Unit 3 follows Unit 2; however the radiocarbon dates are slightly older than expected. Three dates were obtained from Unit 3, two from calcareous foraminifera (2315-2121 and 2429-2190 cal BP) and one from mixed organic fragments (2741-2117 cal BP). These dates are older than all the dates obtained from Unit 2 directly below, which presents a few possible scenarios. Either the Unit 3 dates are reworked, or there was an error in the measurement of Unit 2 or Unit 3 dates. Firstly, the fragments used for the mixed organic date were too small to identify and many pieces were combined to provide a large enough mass for radiocarbon dating. There is a possibility that some fragments were from aquatic plants and therefore the atmospheric radiocarbon calibration that was applied would be inappropriate and give an older age, by not accounting for the inherited age of marine-derived carbon. Furthermore, dating a collection of small organic fragments is not ideal as they could be reworked from significantly older material.

The issue of radiocarbon ages of foraminifera samples appearing older has been encountered elsewhere (Heier-Neilson et al., 1995; Forman and Polyak, 1997; Callard et al., 2013; Hayward et al., 2015), and several explanations have been put forward. There is no formalised method for cleaning foraminifera before radiocarbon is measured. Unlike other carbonate samples such as mollusc shells, foraminifera samples are too small to perform an acid etch to remove any carbonates they may have formed/attached to the outer test (Beta Analytic, 2019). It is also not possible to remove sediment from foraminifera that are infilled. As a result, it is common practice to avoid infilled individuals however some may have been included in error. Additionally, *A. aotena* foraminifera are bottom-feeders and therefore take their carbon from other organisms in the ocean. Thus, it is a possibility that benthic foraminiferal samples have an inherited radiocarbon age from the sediment. At present, no suggestions of adapted calibration methods have been defined within literature. Unfortunately, I did not encounter any molluscs to date in Unit 3, so cannot compare foraminifera and terrestrial samples with mollusc samples from the units above and below. These points suggest that it is more likely that the Unit 3 dates are incorrect, and that the Unit 2 dates are legitimate. Consequently, I summarise that the older dates from Unit 3 are not a reliable estimation of the age of the unit.

Unit 4 and Unit 5: The dates from 7 bivalves in Unit 4 are the youngest, and have a maximum range of 1869 to 1314 cal BP. Unit 2 and Unit 4 display multiple characteristics that suggest they may represent abrupt inundation event deposits, meaning that the shells within are not in situ and therefore do not represent the age of the units. Nevertheless, in the absence of reliable Unit 3 dates, the dates from Unit 4 confirm that it is significantly younger than Unit 2. No radiocarbon dates were obtained from Unit 5, but we know that sea-level continued to gradually fall (Clement et al., 2016); the lake responded by decreasing in size and at some point, the barrier enclosed the water body.

6.3 Evolution Summary

The palaeoenviromental indicators and geomorphology delineates a possible trajectory for the evolution of Lake Grassmere under relative sea-level fall during the late Holocene. The events supported by evidence discussed in this chapter so far have been worked into a schematic representation of developments (Figure 33) that encompass radiocarbon dates from this study and from Ota et al (1995). Section 6.2 highlights the importance of the barrier dynamics within the evolution of the lake environments, throughout the period captured within the piston cores Lake Grassmere. The value of beach ridges as palaeo-sea-level indicators is evident, and will be discussed further in section 7.3. Most importantly, Unit 2 and Unit 4 are distinguished as anomalous deposits within the stratigraphic sequence, based on their incongruous sediment and macrofossil characteristics. The next section draws on these features to delineate the origin of the deposits, now that the palaeoenvironmental history of the study site has been deliberated.

7.0 DISCUSSION OF RESEARCH QUESTION 2: IS THERE ANY EVIDENCE OF PALAEOTSUNAMI INUNDATION OR SUDDEN COSEISMIC VERTICAL DEFORMATION?

In section 2.3 I discuss methods of identifying signatures of coseismic vertical deformation and palaeotsunami inundation within sediment stratigraphy. In section 6.0 I have highlighted Unit 2 and Unit 4 as anomalous units that could signify high-energy event deposits at Lake Grassmere. This section discusses in more detail, the features of the shell hash units that show affinities with the globally-derived characteristics of palaeotsunami deposits. The possibility of coseismic uplift associated with the palaeotsunami deposits is assessed. I also consider alternative mechanisms for the deposition of anomalous Units 2 and 4 that are capable of displaying comparable characteristics. Depositional mechanisms such as storm surges and sea-level change are examined, taking into account the main features of the anomalous deposits, in order to build an argument for the most likely process responsible for Unit 2 and Unit 4.

7.1 Anomalous deposits and palaeotsunami characteristics

Unit 2 and Unit 4 exhibit characteristics that make them anomalous within the sedimentary sequence at Lake Grassmere. In this section, I discuss these features and how they are indicative of high-energy deposition, and in particular tsunami. I also consider the aspects of palaeotsunami deposits that are absent from Unit 2 and Unit 4, calling for the careful examination of alternative mechanisms.

7.1.1 Sedimentology

The composition of sediment within Unit 2 and Unit 4 contrasts with the bounding units, signifying anomalous deposition within the sequence. There are four sedimentary features of Units 2 and 4 that are consistent with tsunami deposition (section 2.3.1) (Goff et al., 2012; Shennan et al., 2016; Putra, 2018): 1) sharp contact and lateral extent, (2) fining upward trend, (3) rapid increase in grain size, (4) coarse clastic material and (5) change in sediment structure.

(1) *Sharp contact and lateral extent:* The abrupt change in sediment composition associated with tsunami deposits is often located across a sharp and erosional contact (Morton et al., 2007; Shanmugam, 2012; Szczuciński et al., 2012 a; Shennan et al., 2016). The lower contacts of Unit 2 and Unit 4 are very sharp and irregular in most cores. I infer from the irregularity that the contact is erosive, signifying that the surface of the units below were scoured when the anomalous deposits were laid down. These characteristics are compatible with sudden, high-

energy flow conditions. Furthermore, although not a sedimentary feature of the deposit itself, it is very significant that the sharp lower contacts of both deposits are traceable over such an extensive distance (>1.7 km) inland.

(2) *Fining upward sequence*: A fining upwards sequence is seen within the grain size distributions of Unit 2 and Unit 4. This trend is most prominent in Unit 2 (Figure 16 and Figure 17) in cores 22P and P1. A fining upward trend is commonly seen in modern and ancient tsunami sediments (Morton et al., 2007; Shanmugam, 2012) and is interpreted to signify decreasing velocities associated with successive waves, a decrease in the ability of individual waves to erode sediments and deposition from suspension rather than by currents (Dawson and Shi, 2000; Shennan et al., 2016).

(3) *Rapid increase in grain size*: Figure 16 shows that the densitometry and mean grain size increases abruptly across the lower contact of the anomalous units, with maximum grain size increasing from silt to sand. The coarser grain size (sand) deposits indicate a higher energy depositional process, and the abruptness of the change infers that the units were deposited suddenly (Shennan et al., 2016). While all of the units were classified as poorly sorted, the grain size distribution within Unit 2 and Unit 4 is very leptokurtic, compared to the platykurtic distribution of the other units, further distinguishing the deposits as anomalous. Samples were collected from a variety of modern sedimentary environments at Lake Grassmere (Figure 16), but neither the beach nor saltmarsh provided grain size distributions similar to samples from within the anomalous units (section 5.1.4). This means that I cannot attribute the sand to an analogous modern environment. However, the sand is likely to be from a marine location, given the abundance of marine shells.

(4) *Clastic material:* Unit 2 and Unit 4 both contain bioclastic coralline algae fragments, coarse clastic material, and in core 40P a (5 x 3 cm) greywacke clast. The coarse clastic material is more abundant in more landward cores (section 5.1.2, Figure 19) but is only found within Unit 2 and Unit 4, and not in surrounding sediment. The presence of clastic material is consistent with scouring and erosion of mixed environments that possibly extended to the hillside, before the anomalous deposits were laid down by the backwash of the waves. Wave inundation that scours the surrounding hills and transports sediment in the backwash is also compatible with the increased abundance of clastic material within more landward cores, as the heavy material would be deposited closer to its source as the wave retreats (Kortekaas and Dawson, 2007, Kitamura et al., 2018 a).

(5) *Change in sediment structure:* Although not a feature within the anomalous units themselves, there is a distinct change in sediment structure between Unit 1

and Unit 3. Unit 1 consists of fine laminated silts, whereas Unit 3 is almost homogenous (aside from a few sand lenses in coastal cores e.g. Figure 18). As both units accumulated subtidally (indicated by the foraminifera), and therefore do not require uplift to explain the change, it is likely that the difference reflects an increased disturbance of the sediment surface. Increased disturbance from wave and tidal currents would prevent the sediment from forming laminations and cause a more homogenous unit due to reworking. There are various possible causes for the alteration to the amount of surface sediment reworking such as shallowing of the water level and increased exposure to the ocean. Due to the position of this change across the emplacement of an anomalous unit, I infer that it may have been concurrent with the deposition of Unit 2.

7.1.2 Shell hash material

Shell material is not located anywhere else in the subtidal sediment that bounds both shell hashes, distinguishing Unit 2 and Unit 4 as anomalous because molluscs do not appear to have been living in situ at the depositional site. The shell assemblage is predominantly intertidal and not in life position. The juxtaposition of an intertidal shell assemblage within subtidal sediment strongly suggests the shells were transported from elsewhere. Accordingly, there must have been a habitat at or near Lake Grassmere capable of supporting a large assemblage of intertidal bivalves prior to both inundation events. The southern area of the lake, close to the smaller lagoon is suggested as the location of the former opening (Figure 35). The area of slightly higher elevation close to the tidal inlet provides a plausible candidate for an intertidal area that would be accumulating an assemblage of intertidal cockles, and therefore is possibly the source area of the displaced shells in Unit 2 and Unit 4. Section 2.2 describes how tsunamis have a large wave depth and therefore great potential to scour sediment and transport it in suspension before depositing it over a wide area (Donato et al., 2008). It is a reasonable suggestion that a tsunami wave entering Clifford Bay would scour sediment from the south side of the lake where the barrier is not as established and continue to travel across the water to deposit Unit 2 on the north side of the lake.

The overall preservation of the shells is excellent, including many articulated and fragile juvenile bivalves (Figure 25). This suggests that the shells were not reworked post-death and were rapidly buried by finer sediment (Reinhardt et al., 2006; Kitamura et al., 2018a, Kitamura et al., 2018b). Transport of articulated bivalves over large distances has been identified in palaeotsunami deposits at locations such as Israel and Oman, where the assemblage is preserved by the finer infilling sediment that accumulates after the main wave (Reinhardt et al., 2006; Donato et al., 2008; Kitamura et al., 2018 a).

7.1.3 Microfossils

Another useful indicator of palaeotsunami deposits is the presence of marine microfossils that have been washed in by tsunami waves from offshore sources (Goff et al., 2001; Pilarczyk et al., 2014; Dura et al., 2016 b). In general, foraminifera samples from the shell hashes are similar to the subtidal assemblages of the bounding units. One sample in Unit 4 contains 21% *Notorotalia* spp, which are commonly found at up to 20-30% within fully marine, inner shelf environments (Hayward et al., 1999). Despite it only being found in one sample, the assemblage from Unit 4 implies marine inundation. Szczuciński et al. (2013) demonstrates case studies in which globally derived tsunami features (such as abundant marine microfossils) are absent within deposits from modern tsunamis such as Tokoku-oki in 2011 (Szczuciński et al., 2012 a) and Vaigat Strait (Greenland) in AD 2000 (Szczuciński et al., 2012 b). In both cases, the sediment source was mainly derived from the beach, coastal dunes and soil, as may be the case at Lake Grassmere considering the foraminifera and grain size results. Although not evident in the anomalous units themselves, *Haynesina depressula* is introduced in Unit 3 directly after Unit 2 (Figure 21). I infer that this is associated with the change in subtidal sediment composition from laminated to homogenous silt as explained above.

It is significant that Unit 2 and Unit 4 are distinct in their abundance of foraminifera, which increases by a factor of ten compared to the bounding units (Figure 23). The higher abundance may reflect the preferential deposition of larger grain sizes in the anomalous deposits and, given that foraminifera make up a larger proportion of the coarser material than the finer, the anomalous deposit consequently has higher foraminifera abundance. The high velocity flow may also have winnowed away sediment finer than 63 µm, leaving behind coarser sediments that included a high abundance of >63 µm foraminifera. The test size distribution of Unit 2 and Unit 4 includes a higher abundance of larger test sizes (>250 µm) and a low abundance of small tests (63-125 µm) (Figure 23). This supports the concept that the foraminiferal assemblages are allochthonous, as the test size distribution of the bounding units consists of predominantly the 125-250 µm size range. Increased abundance and test size of foraminifera is not a common feature of tsunami deposits, however it is also difficult to explain by other mechanisms that mobilise microfossils, such as storm waves or floods.

7.1.4 Palaeogeography

The substantial coastal spit or barrier must have been present during the deposition of Units 1, 3 and 5, as indicated by the sheltered subtidal environment preferred by the foraminiferal association and orientation of the northern beach ridges (section 6.2). Pickrill (1977) outlines that the modern profile of the beach fronting Lake Grassmere is consistent with formation and erosion by storm waves of 1-3 m. Although I do not know the height of the palaeo-barrier, I infer that current wave dynamics would have been

comparable and so the short-period, steep-crested storm waves produced under northerly conditions (Pickrill, 1977) would have formed similar beach geomorphology to the modern barrier of 4-5 m. In addition, the coastline is likely to have been further seaward than at present, suggested by the current cliff erosion along the coast. Consequently, if it is assumed that the high energy wave(s) enters the lagoon from the seaward direction, it would have to negotiate the 4-5 m high barrier across the front of the lagoon with enough energy to deposit sand, shell and clastic material >1.7 km inland. It is reasonable to assume the only mechanism that would be capable of depositing the anomalous units with the characteristics outlined above would be tsunami. Barrier erosion caused by tsunami overtopping would also account for the palaeo-lagoon environment that is more exposed to disturbance from wave and currents and possibly increased salinity, inferred within Unit 3 immediately after deposition of Unit 2. Figure 36 demonstrates the proposed inundation process at the study site.

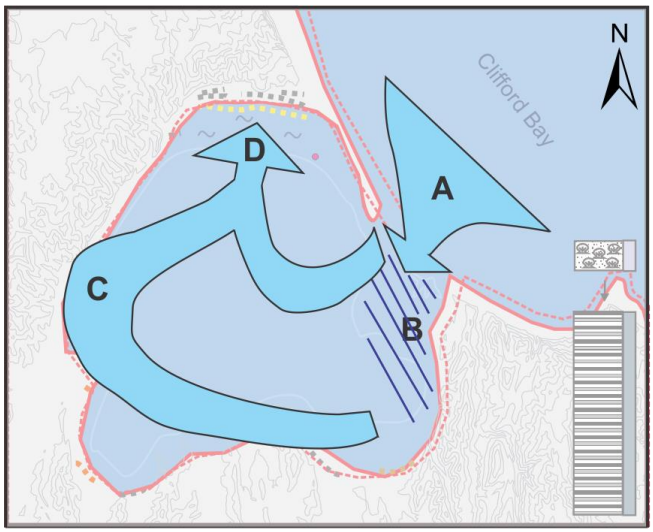

A) Tsunami wave(s) enters lake/lagoon to the south as well as overtopping and opening the barrier

B) The intertidal area that is accumulating intertidal molluscs at the mouth of the lake/lagoon is scoured by the wave

C) Tsunami wave(s) travels across the lagoon and surrounding land, entraining exotic sediment e.g. greywacke clasts, coralline algae and shells from mixed environments

D) Tsunami wave erodes the surface of Unit 1 and deposits the entrained material at the study site

Figure 36 – Proposed tsunami wave inundation of Lake Grassmere.

7.1.5 Incongruous characteristics

On the other hand it must be acknowledged that there are some features of palaeotsunami deposits that are not consistent with Unit 2 and Unit 4. Shanmugam (2012) summarises characteristics of palaeotsunami deposits from a suite of studies, outlined in section 2.3.1. Evidence of rip up clasts and internal mud drapes are not found in Unit 2 or Unit 4, however the detection of such features may be restricted by the size of the extruded piston core, compared to other studies that examine trenches for example (e.g. Matsumoto et al., 2008; Dura et al., 2015; Ishizawa et al., 2018). Although the landward extent of Unit 2 and Unit 4 is considerable at >1.7 km, there is no trend of thinning or fining landwards that is commonly associated with tsunami deposits (Abe et al., 2012; Szczuciński et al., 2012 a; Putra, 2018). Possibly the most distinctly absent feature is the lack of marine microfossils within the anomalous deposits, which is usually

a confident indicator if marine inundation during tsunami (Hemphill-Haley, 1995; Goff et al., 2012). Nevertheless, as Szczuciński et al (2013) explains, this assumes a microfossil rich sediment source and tsunami-laden water may be reflected from the onshore slope, as was the case for the 2011 Tohoku-oki tsunami deposits on the Sendai Plain (Szczuciński et al., 2012 a). While these observations do not rule out tsunami as a possible depositional mechanism they increase the importance of considering alternative mechanisms that may result in comparable deposits.

7.2 Alternative mechanisms for the deposition of anomalous units at Lake Grassmere

Evidence collated in section 7.1 suggests that the depositional mechanism for Unit 2 and Unit 4 must be able to satisfy the following features:

(A) Inland extent >1.7 km
(B) Accumulation of articulated bivalves
(C) Well preserved shell material
(D) Intertidal shell species
(E) Increased abundance of foraminifera
(F) Subtidal foraminifera
(G) Abrupt increase in grain size
(H) Sharp, erosional lower contact
(I) Change in subtidal sediment characteristics (laminated to homogenous) between Unit 1 and Unit 3
(J) Fining upwards sequence
(K) Clastic material and coralline algae fragments

Aside from the arguments presented that suggest tsunami satisfies these components, I recognise that the evidence is not unequivocal (section 7.1.5), and so it is important that alternative mechanisms for the deposition of these units are explored. This section evaluates several of the most plausible processes that could generate a deposit of similar characteristics. Some of the features outlined above are referred to throughout the discussion as Feature A, Feature B etc, to aid comparison between methods. It is noted that possibilities are not limited to the ones covered in this discussion. Alternative mechanisms are considered not only based on their potential to satisfy the deposit characteristics outlined above, but also to satisfy deposition within the proposed palaeoenvironmental setting at the study site.

7.2.1 *Sea-level change*

Sudden sea-level change could cause abrupt changes in sediment deposition (Feature I). Nevertheless, I establish in section 3.4.2 and section 6.2 that reconstructions by both

Clement et al (2016) and Hayward et al (2016), sea-level on the eastern South Island was gradually falling from the late Holocene highstand around ~4000 cal BP (Figure 11). There is no reasonable mechanism in which sea level could cause the deposition of the anomalous deposits at Lake Grassmere, and therefore it is rejected as a possible cause.

7.2.2 Barrier change

The barrier is a prominent feature of the geomorphology of Lake Grassmere and it has played an important role in the evolution of the lake and the palaeoenvironmental changes that ensued (section 6.2). Changing dynamics of the barrier impacts sediment deposition within the lake and so it should be considered that sudden barrier change could be a mechanism for the emplacement of anomalous units. In order for the sediment deposition in subtidal waters to be changed from laminated (Unit 1) to homogenous silt (Unit 3) (Feature I) with an accumulation of intertidal molluscs in sand between (Unit 2) (Feature D), the barrier must have been altered significantly, opening the lake/lagoon to substantially more influence from tidal currents and waves. If the lake/lagoon is suddenly more open to the mixing of sediment, it is possible that newly formed currents may have caused an accumulation of intertidal (dead) mollusc material transported from elsewhere in the lake. It is unlikely that such an alteration would be caused by non-extraordinary barrier modification alone, and more likely that a high-energy event caused the barrier to be altered. In this scenario, the high-energy event is the driving force of the abrupt changes in deposition and Unit 2 within the lagoon and not solely modification of the barrier morphology.

Overall it is more likely that modification of the barrier through variations in natural processes such as sea-level changes and sediment supply would manifest in incremental growth and erosion, which may be implied by the interbedded sand lenses that occur in Unit 3 and Unit 5 in coastal cores (Figure 18). If the depositional mechanism for the anomalous units is were to approach from a seward direction, then the barrier would probably damaged, meaning that periods of incremental re-growth after the two anomalous events supports the theory that the sand lenses are barrier-related.

7.2.3 Relict beach deposit

Since established beach ridge sequences are present at the study site at a similar time to the deposition of Unit 2 and Unit 4, the possibility that the anomalous intertidal shell hash units (Feature D) reflect relict beach deposits should be explored. A comparison between the shell assemblage of the anomalous deposits (Figure 24), and the assemblages retrieved from the modern beach deposits (Figure 26) shows that no common species are identified with the exception of *Ostrea chilensis* that is encountered in the shell hashes of cores 40P and P3. Similarly, the bivalves found within the northern beach ridge pit are not identified in any of the anomalous deposit units. While it is

recognised that the sampled beach and beach ridge environments may be different to the palaeoenvironment during the deposition of Unit 2 and Unit 4 in terms of exposure to the open coast, the lack of common species (Feature D), position of the unit within subtidal sediments (Feature F and I) and abruptness of the deposits (Features G and H) suggests that they are not characteristic of relict beaches.

7.2.4 Floods

High rainfall within the Lake Grassmere catchment may cause a flood capable of mobilising sediment and causing anomalous deposition within the inlet/lake sediment. Sakuna-Schwartz et al (2015) establish common features between tsunami and flash flood deposits within sediment cores in Thailand; yet distinguish units of monsoon deposition by their transitional boundaries and lack of sand compared to the tsunami deposits identified. Nevertheless, this scenario is unlikely for Lake Grassmere as there are no substantial rivers or streams that drain into the lake. Sudden high rainfall would mostly mobilise sediment from the surrounding hillsides, which are composed of Miocene-Pliocene mudstone (section 3.4.1). Figure 22 shows the foraminiferal composition of the hillside samples at Lake Grassmere and demonstrates that the bedrock assemblage dominated by *Bolivinita pliozea* is not present in Unit 2 or Unit 4 (Feature F). This infers that the material in the anomalous units was not mobilised from inland sources and is therefore unlikely to represent a flood deposit. Similarly, King et al (2017) delineate that while rapid run-off as a transport mechanism may be capable of depositing larger grain sizes (Feature G), it cannot account for the presence of intertidal shell material (Feature D).

7.2.5 Hiatus in clastic sedimentation

It is conceivable that Unit 2 and Unit 4 do not represent event deposits, but rather extended periods of time where shells accumulate (Feature B, C and D) due to a lack of, or significant decrease in clastic sedimentation, as discussed by Kidwell (1986). There is a span of ~300 years within the radiocarbon dates obtained from each shell hash. If the units were accruing naturally this would mean that no fine sediment was deposited for hundreds of years, or that an additional process was constantly winnowing fine silt and clays. There are multiple scenarios in which this could occur, producing different bioclastic shell deposits that are often differentiated by their taphonomic characteristics (Beckvar and Kidwell, 1988; Kumar et al., 2009). Kumar et al (2009) categorise shell beds within mixed early Miocene carbonate-siliciclastic systems. While this is dissimilar to the late Holocene soft sediment cores at Lake Grassmere, it is interesting to consider the differences between the deposit types described by Kumar et al (2009) and the shell hashes I describe from Lake Grassmere.

Kumar et al (2009) describes ‘shell lags’ and ‘hiatal/condensed shell concentrations’ that accumulate when fine material is winnowed by fluvial and tidal processes, condensing the coarse component of the deposit. Unit 2 and Unit 4 displays affinities with lag deposits that include a rich accumulation of randomly oriented bivalves of varied assemblage (including bivalves, annelid tubes, bryozoans, foraminifera and wood) (Feature D and K), sharp and erosional basal contact (Feature H) and wide lateral extent (Feature A). Most importantly, Kumar et al (2009) observe ‘hiatal shell concentrations’ to have an “exceptionally high concentration of well-preserved benthic foraminifera such as *Ammonia”* (Feature E). This component of the anomalous units, displayed in Figure 21 and Figure 23, is not found to be a common feature of any other depositional mechanism, suggesting that a hiatal shell concentration cannot be overlooked as a plausible explanation for Unit 2 and Unit 4.

Despite the similarity in foraminiferal concentration, the taphonomy of the shell assemblage is not compatible with shell lag formation. The predominantly intertidal shell assemblage within Unit 2 and Unit 4 is very well preserved with no encrustation or bioerosion (Feature C), and includes fragile, articulated bivalves (Feature B) that would be disarticulated and fragmented if exposed and re-worked into a slowly accumulating lag deposit (Kidwell, 1991; Brett, 1995). Further to this, there is no evidence of burrowing on the sharp lower contacts of the anomalous deposits in all cores. This feature would most likely be evident if the anomalous deposits were developing over hundreds of years, further signifying that the unit was rapidly preserved by infilling sediment and not continuously reworked and growing. While tidal-channel shell deposits may substantiate the concentration of coarse bioclastic material without fine sediments, Fleming et al (1992) state that substantial transportation of shells is primarily wave-based, and therefore restricted to elevations above mean low-tide in exposed settings, which is not compatible to the subtidal palaeoenvironment of the lake/lagoon. Furthermore, palaeo-channel deposition can be rejected due to the great lateral extent of the deposit (Feature A). Similarly, there is no reasonable explanation for a sudden hiatus in the deposition of fine sediment for a prolonged period across the whole subtidal lake/lagoon without external forcing from a process such as tectonics. As a result I summarise that this discussion has provided multiple inconsistencies that allow shell lags and hiatal shell concentrations to be discounted as plausible alternative justifications for Unit 2 and Unit 4 at Lake Grassmere.

7.2.6 Storms

Within palaeoseismology, one of the most highly debated topics surrounds whether it is possible to distinguish palaeotsunami deposits from prehistoric storm surge deposits (Goff et al., 2004, Tuttle et al., 2004, Kortekaas and Dawson, 2007). Both deposit types are generated by high-energy waves that rapidly inundate coastal areas, overtopping

coastal barriers and depositing sediment that contrasts the unit immediately below. It also plausible that both may entrain marine derived sediment that is detectable in microfossil analysis and grain size comparisons (Kortekaas and Dawson, 2007). Nanayama et al (2000) demonstrate this by comparing deposits from the 1993 Japan Sea tsunami and the 1959 Miyakojima typhoon, which both have a thickness of 50 cm that thins inland. The 1993 tsunami deposit is distinguishable by its poorly sorted grain size, bi-directional flow and shell material; characteristics that are shared with Unit 2 and Unit 4. There are no historically observed storm deposits identified within the piston cores at Lake Grassmere, which means that direct comparison is not possible.

The long wavelengths and periods of tsunami waves allow them to travel further before energy dissipates, with greater potential to scour than storm waves (Donato et al., 2008). Flow depth can be over 10 m, meaning that a large amount of material can be scoured and transported in suspension, and then distributed over a wide area when the load settles out of suspension as the flow decelerates (Morton et al., 2007). Both Unit 2 and Unit 4 have erosional lower contacts (Feature H, Figure 34) that are traceable inland over >1.7 km (Feature A). As in section 7.1.4, Pickrill (1977) explains that the beach fronting Lake Grassmere a product of short, steep storm waves of up to 3 m, and therefore typically only erode the foreshore and deposit close to the beach. Thus, storm waves are unlikely to have been able to entrain the dense shell hash material of Unit 2 and Unit 4, and are even less likely to have transported it in suspension over such a long distance. Lowe and de Lange (2000) support this in their suggestion that minimum wave height of 5 m is required in order to produce a visible deposit within coastal sediment.

Various features of the shell hash composition argue against a storm source (Features A and C). Kitamura et al (2018 a, b), explains how articulated bivalves within anomalous units signify a tsunami source when deposited over a large area, as opposed to localised areas such as lagoon mouths. Mass transport of live articulated bivalves is rare within modern storm deposits (Donato et al., 2008), as any entrained shells are reworked and taphonomically altered during multiple waves, rather than deposited and preserved by rapidly infilling sediment (Reinhardt et al., 2006). Although there are fragmented shells within Unit 2 and Unit 4, the presence of articulated individuals was prominent both on initial inspection of cores and in the three-dimensional CT output (Figure 34).

The barrier height is considered in section 7.1.4 in the case for attributing a tsunami source (Feature G), however here I consider whether it would be possible to achieve the deposition of Unit 2 and Unit 4 by storm waves. The barrier would be a significant obstacle to storm waves and they are unlikely to be large enough to overtop it (assuming the barrier was a similar elevation in the past), and I speculate there would be little energy remaining for the transport of sediment across the lake (>1.7 km inland from the coast). King et al (2017) considers this issue for tsunami deposits at Big Lagoon (which

has a barrier of similar elevation to Lake Grassmere, and similar climate and wave regime) and agrees that it is unlikely for storm waves to reach sufficient height to overtop the coastal spit and transport marine derived material 95-340 m inland. This is also supported by Goff et al (2004)'s comparison of storm and tsunami deposits in New Zealand, where they identify multiple common features but highlight that the substantial Easter storm of 2002 had an inland extent of 40 m and was not locally extensive, compared to the 15th century tsunami deposit that inundated to 200 m.

Inspection of the modern beach across the front of Lake Grassmere saw that while there was some evidence of storm deposition (large tree trunks and debris), this was placed 1-2 m lower than the crest of the barrier (Figure 37), implying that it was not breached or that material was deposited on the seaward side only. Further to this, the modern beach assemblages, shown in Figure 26 shows a clear disparity between the assemblages found on the seaward of the barrier and the assemblage located within Unit 2 and Unit 4, implying the shells were not entrained from the foreshore.

Figure 37– Left shows aerial view of the north beach, with storm debris circled in red at >12 m seaward of the barrier crest, and 1-2 m lower in elevation. Right shows a photograph of the southern beach where the barrier is slightly lower, but the storm debris is still below the crest.

It is also possible that the barrier was much lower at the time of deposition of Unit 2 and 4. This would make it more likely that a storm wave would be able to overtop the barrier, however this would also mean due to the higher frequency of storm events than tsunami, that we would see multiple deposits of this type throughout the core. Although there are some thin sand lenses within Unit 3 and Unit 5, they are not comparable to the composition of Unit 2 and Unit 4. Furthermore, there are no anomalous deposits within Unit 1, which extends at least ~3 m below Unit 2. Subsequently, it is more likely that Unit 2 and Unit 4 equate to less frequent, higher magnitude events than storms.

Overall, consideration of Unit 2 and Unit 4 alongside studies that compare storm and tsunami highlights multiple characteristics that suggest storm waves are not capable of depositing the shell hash units. Characteristics include; lateral continuity over a large area (Feature A), erosive basal contacts (Feature H), and a dense shell hash with articulated bivalves that are well preserved (Features B and C), as well as the restricted ability of storm waves to overtop the coastal barrier.

7.2.7 Summary

In summary, several alternative mechanisms for the deposition of Unit 2 and Unit 4 have been considered in the palaeoenvironmental context of Lake Grassmere. I believe that the discussion has shown that tsunami is the most likely origin for the anomalous deposits, based on the inadequacy of the alternative mechanisms that satisfy the criterion of features summarised Table 5. I suggest that the weight of evidence for the compatibility of Unit 2 and 4 with globally defined, multi-proxy features of palaeotsunami deposits outweighs the inconstancies reported in section 7.1.5. The next section considers whether there are any indications of coseismic vertical deformation within the sediment sequence, which may support the evidence outlined here in suggesting a tsunami source for Unit 2 and Unit 4.

Table 5 – Possible mechanisms for the deposition of palaeotsunami deposits at Lake Grassmere and the characteristics required to satisfy the deposit features. Not all of the features A-I are included in this summary.

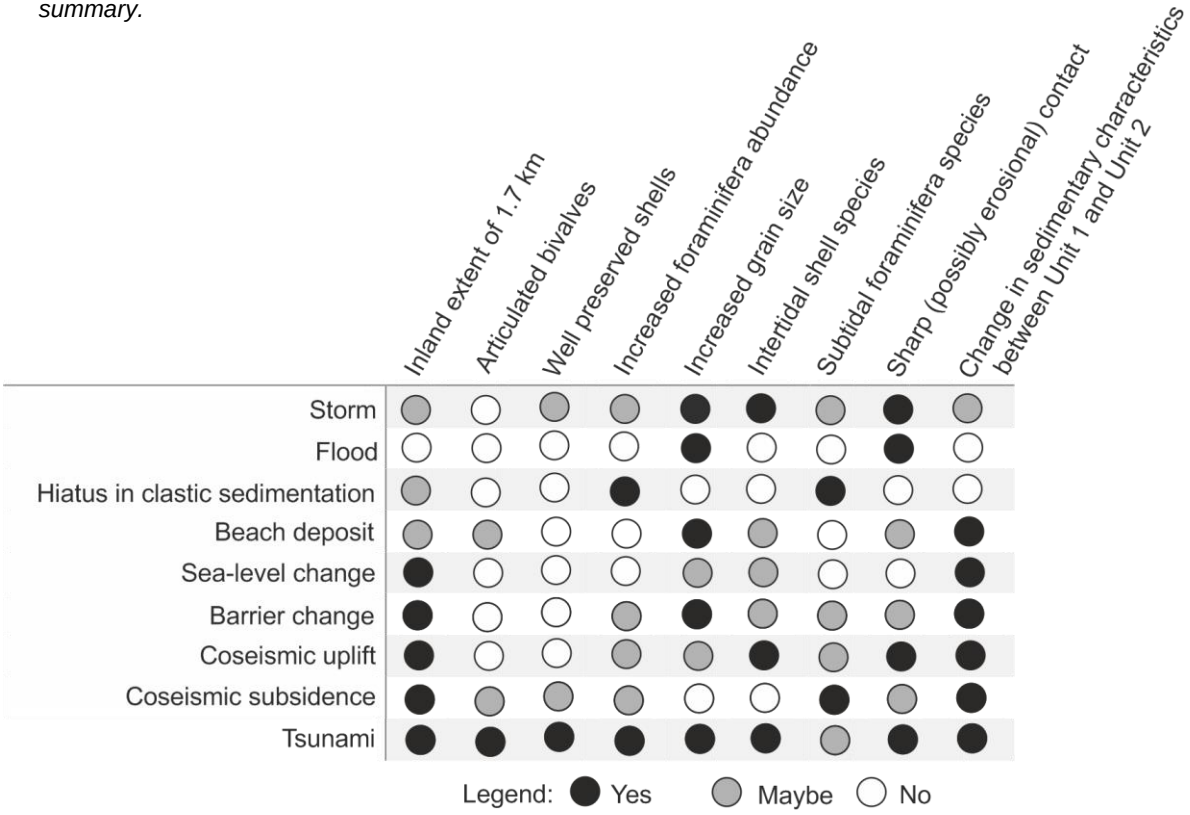

7.3 Assessing evidence for coseismic vertical deformation

Coseismic vertical deformation can accompany palaeotsunami deposition, and when the two occur together it is powerful evidence of a local source earthquake that caused crustal deformation and tsunamigenesis. The significant change in sediment character from laminated (Unit 1) to homogenous silt (Unit 3) (Feature I) could initially be interpreted as a change from subtidal to intertidal sediment based on the increased disturbance of surface sediments by tidal currents and waves. Nevertheless, the subtidal

foraminiferal associations identified in each sedimentary unit are not consistent with a change in water depth (although they are not sensitive enough to rule it out either). I attribute the change in sediment character to increased tidal influence from a widening of the inlet entrance associated with the scouring and rapid deposition of Unit 2. While this explanation does not require coseismic vertical deformation, it remains plausible.

Section 5.2.1 describes the broad environmental range of *Ammonia aoteana.* The monospecific assemblage is present in Unit 1 and Unit 2, and is unable to distinguish between intertidal and subtidal water depth to 3 m. From Unit 3 onwards, *H. depressula* occurs at 6%, which is suggestive of an association constrained to below low tide (Hayward et al., 2014 a). It is unclear whether there was a change in water depth associated with the introduction of *H. depressula*, as overall both assemblages are subtidal, and the abundance of foraminifera in Unit 1 is very low. Nevertheless, it is possible that coseismic land-level change could have occurred within the range of subtidal water in the lake/lagoon, and therefore may not be reflected in the microfossil assemblage.

If coseismic land-level change did occur, it is most likely to have been uplift that would result in a shallowing of the lake/lagoon, as this would support the suggestion of increased disturbance of the sediment surface by tides and waves. Long-term uplift is supported by the presence of subtidal sediment throughout the cores, which is now located up to 1.27 m AMSL (core P3). Lake Grassmere is situated just south of the boundary between uplift and subsidence for predicted vertical deformation in a full rupture of the Hikurangi subduction interface reported by Wallace et al (2014) indicating a possible uplift of ~0.5 m in such events (see section 8.3.7). In addition, Lake Grassmere responded to the 2016 Mw 7.8 Kaikoura earthquake with 0.4 m of uplift, inferring that this may be the trend of coseismic vertical land-level movements at the site in similar upper plate events. Taking this into account, the net amount of uplift that must have occurred at Lake Grassmere since the deposition of Unit 5 (post-1400 cal BP) and prior to 2016 is ≥1.47 m (below). Currently, I cannot allocate this uplift to any earthquakes or fault sources in particular, but it is evident that substantial uplift (interseismic and coseismic) must have occurred at Lake Grassmere in the late Holocene.

Height of the uplifted subtidal sediment		Minimum elevation of the subtidal sediment below mean sea level		2016 uplift		Net uplift since deposition of Unit 5
1.27 m	+	≥ 0.60 m	-	0.40 m	=	≥ 1.47 m

7.3.1 *Beach ridges as palaeoseismic indicators*

Uplift at the study site is also evident from the raised beach ridge sequence on the northern side of Lake Grassmere (Figure 35). The value of beach ridges as palaeoseismic indicators has been demonstrated in multiple locations (Nelson and

Manley, 1992; Kelsey et al., 2006; McSaveney et al., 2006; Sawai et al., 2009, Kelsey et al., 2015). The sequence at Lake Grassmere can be summarised by two main beach ridge sets (BR1 = lakeward, BR2 = landward) that are composed of successively prograding ridges that increase in height up to the main crests, with steep 1-1.5 m escarpments on the lakeward side (Figure 30). The crest of BR2 is currently at ~3.75 m (4.07 m AMSL), and the crest of BR 1 is ~3.25 m (3.57 m AMSL). The difference in elevation is laterally consistent across the northern plain (Figure 30). Figure 38 quantifies the height difference between the two main beach ridges using common features within the sequence. All three estimates of elevation change between the beach ridge sets are ~0.45 m, which is similar to the 0.4 m of uplift experienced in 2016 during the Kaikoura earthquake as well as the ~0.5 m uplift suggested for subduction earthquakes by Wallace et al (2014). If the mechanism for this offset is coseismic uplift, this agrees with evidence in the cores that suggests the overall vertical tectonic signature at Lake Grassmere is uplift.

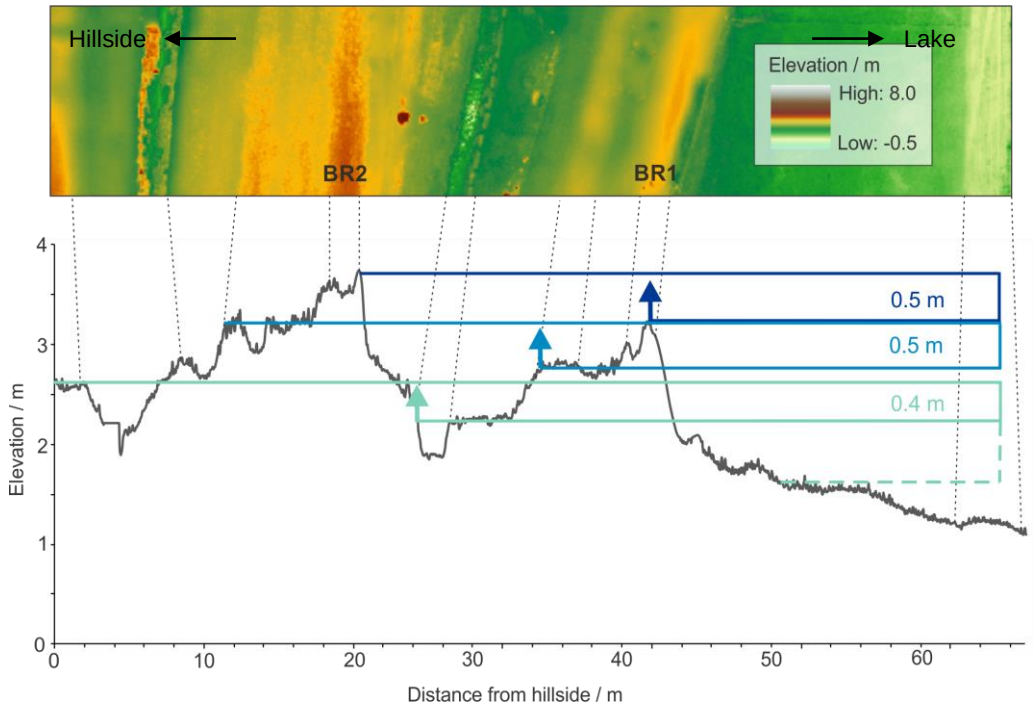

Figure 38 – Profile of northern beach ridge sequence and uplift between sets, derived from common features e.g.crest to crest, swale to swale and preceding ridge to preceding ridge.

The trend of dated beach ridges becoming younger towards modern lake extent supports the scenario in which they reflect falling sea-level (Clement et al., 2016; Hayward et al., 2016) (section 6.2 and Figure 11). Nevertheless, the step in beach ridge elevations is more consistent with sudden uplift, rather than gradual sea-level fall (Figure 38). Neither of the sea-level reconstructions by Clement et al (2016) and Hayward et al (2016) indicates sudden accelerations in the rate of sea-level fall that would be necessary to explain the abrupt change in beach ridge elevation. It is plausible to hypothesise that there is a tectonic signal within the beach ridges at Lake Grassmere.

The increasing height of the beach ridges that precede the main ridge in each beach ridge set is difficult to explain. It is assumed that the lake/seaward progradation of the beach ridges in general is driven by falling sea-level (Fraser et al., 2004; Tamura, 2012; Brooke et al., 2019), however this does not account for the increasing height seen in both sets. A similar sequence is described by Kelsey et al (2015) in Kenai, which shows prograding ridges increasing in height across the strandplain towards ocean, but the cause of this trend is not discussed. One possibility is that the height of the beach ridges reflects the length of time that the shoreline was maintained in that position, and so the longer is it stable, the higher the beach ridges (Carter, 1986). Although speculative, I hypothesize it is also possible that the increasing height of the prograding ridges indicates interseismic subsidence. Gradual interseismic subsidence of the lake/lagoon preceding the coseismic uplift events that are indicated by the offset between BR1 and BR2, would manifest in successively higher elevations of beach ridges building at the outskirts of the lake/lagoon. Nevertheless, this would also cause a landward transgression in beach ridge position which is not seen assuming a constant sediment supply, and would also contrast the long-term uplift signal that is indicated by the uplifted subtidal sediment in Unit 4 and by the 2016 earthquake. A schematic of possible beach ridge formation is shown in Figure 39, accounting for both sea-level fall, interseismic subsidence and coseismic uplift.

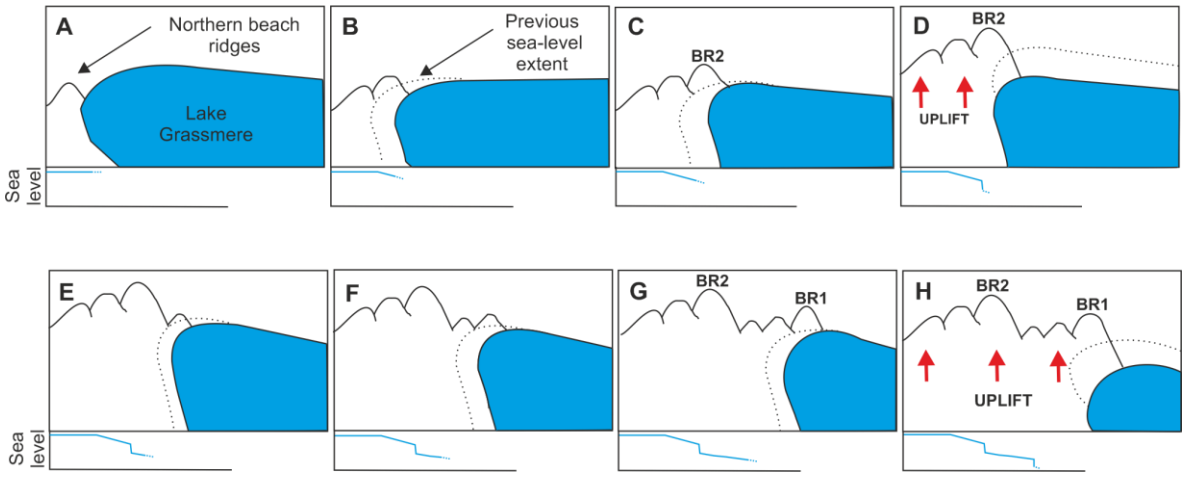

Figure 39 – Schematic of proposed beach ridge formation and uplift at Lake Grassmere. The schematic is oriented side-on to the lake. Sea-level curve to shows the response to eustatic sea-level trends and tectonic movement. A) Gravel beach ridges form at storm wave limit, at the edge of the lake/lagoon. B and C) As sea-level falls, beach ridges prograde towards the contracting lake extent in response. D) Coseismic uplift causes abandonment of the beach ridge set, E) The next beach ridge set begins to form at the new limit of the lake/lagoon. F and G) Sea-level continues to fall and the beach ridge set progrades lakewards. H) Coseismic uplift causes abandonment of the beach ridge set.

7.3.2 *Summary*

In summary, it is unclear whether vertical coseismic deformation occurred with the deposition of Unit 2 and Unit 4. Uplift is more likely to have occurred with deposition of Unit 2 given there appears to be increased disturbance of lake sediments between Unit 3

and Unit 1 (suggesting possible shallowing of the inlet). There is a step of ~0.45 m in elevation between the two main beach ridge sets that is not compatible with gradual sea-level fall, and therefore may indicate coseismic uplift. It is not currently possible to define whether the uplift and abandonment of beach ridges was concurrent with the deposition of either Unit 2 or Unit 4 due to insufficient dating of the beach ridges, however net tectonic uplift at the study site is indicated by both geomorphology and sedimentology. Regardless of whether coseismic vertical deformation was concurrent with the deposition of Unit 2 and Unit 4, I suggest that the evidence presented in section 7.1 provides a compelling argument in favour of a tsunami source for the anomalous units at Lake Grassmere. Consequently, the discussion from here assumes a tsunami source for the anomalous units at Lake Grassmere.

8.0 DISCUSSION OF RESEARCH QUESTION 3: HOW DOES THE TIMING OF PALAEOTSUNAMI EVENTS AT LAKE GRASSMERE FIT WITHIN THE REGIONAL PALAEOSEISMIC RECORD AND WHAT ARE THE IMPLICATIONS FOR POSSIBLE FAULT SOURCES?

I have shown in Section 7.0 that Unit 2 and Unit 4 were most likely deposited by a tsunami. To compare the tsunami age to regional palaeoseismic events, it is important to constrain the age of event deposits. Palaeotsunami studies often use radiocarbon age modelling to refine the age of event horizons within stratigraphic sequences.

8.1 Age Modelling

Age modelling of radiocarbon probability distributions using Bayesian statistical methods is often undertaken to provide a chronology of stratigraphic units and events within those units (Bronk Ramsey, 2017). Sequence models are used to place dates from units in stratigraphic order so that the age of event horizons can be estimated. Usually, this type of modelling relies on dates that bound the event unit or layer (e.g. Ishimura, 2017). Due to a lack of dateable material bounding the tsunami deposits, radiocarbon dating focused on molluscs from within the tsunami units themselves. While I cannot provide ages that reliably bound the tsunami deposits, I can suggest the youngest possible age of the event based on the molluscs within the deposit (cf. Ando et al., 2018).

I used the radiocarbon ages and stratigraphic information obtained in this study to construct a sequence model in Oxcal version 4.3.2 (Bronk Ramsey, 2017) with an aim of constraining the ages of the tsunami events of Unit 2 (Tsunami 1) and Unit 4 (Tsunami 2). Figure 40 shows the sequence model that gave the best fit to the data available. All three samples from Unit 3 have previously been identified as erroneous as they pre-date Unit 2 (section 6.2), and so they have been marked as outliers and excluded from the sequence model. It is clear from the error bars that my data is not suited to modelling in this format, as the only tangible constraints for the timing of Tsunami 1 are restricted to dates within Unit 2 itself and dates within Unit 4; these provide the boundaries for the event age. This is a result of most data points being obtained from within tsunami units rather than bounding the event (sections 2.4 and 4.4.2). The ages from Unit 3 provide the only constraint for the Tsunami 2, as there are no dates within Unit 5. This means that the lower boundary Tsunami 2 age is the upper limit of the phase, but the upper boundary is the boundary provided by the model. Consequently, it has to be considered that the event ages of Tsunami 1 and Tsunami 2 obtained from the model are derived

from different assumptions. Nevertheless, I have included the sequence model in Figure 40 to demonstrate the inadequacy of this method for my dataset.

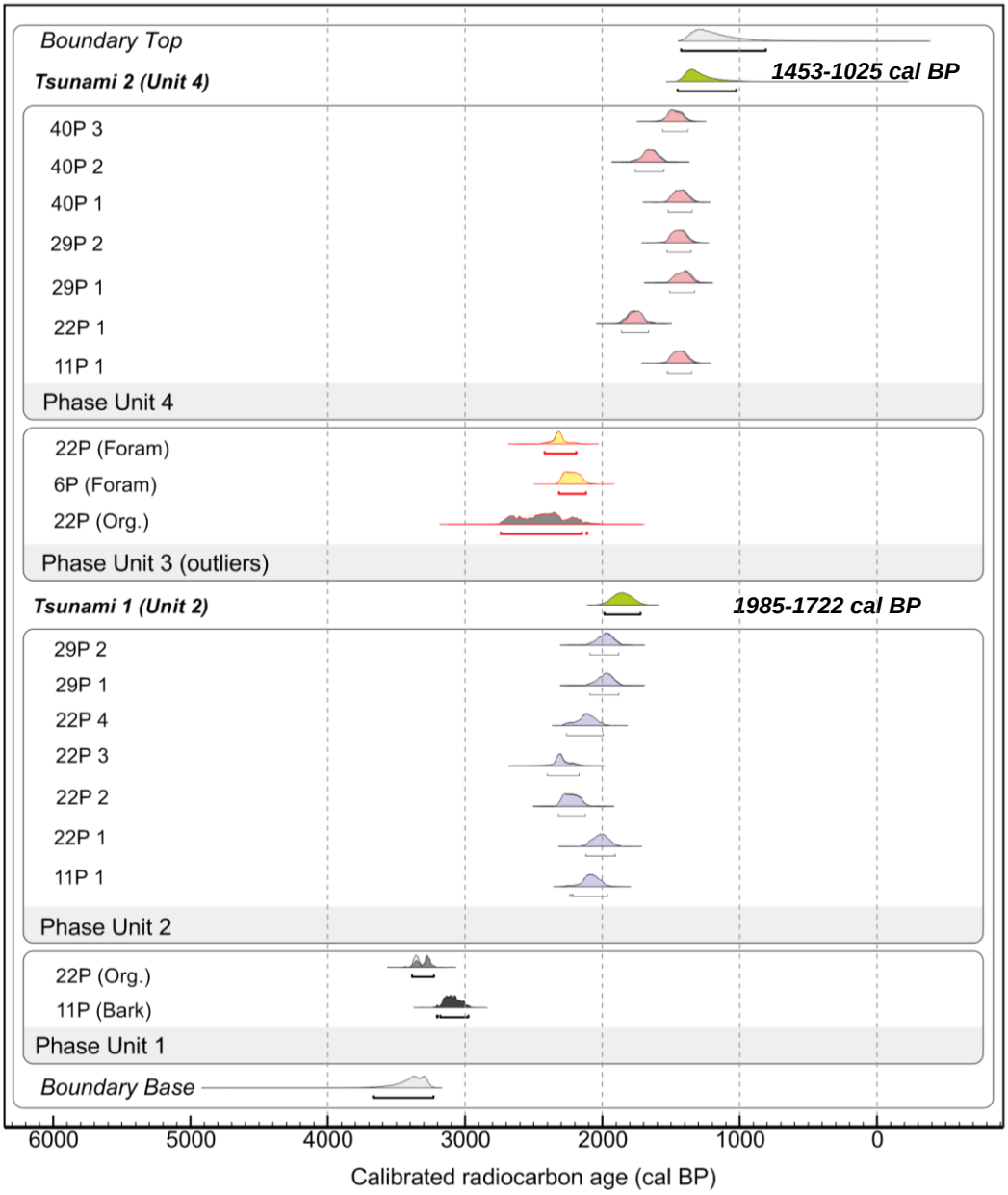

Figure 40 – Sequence model for constraining the ages of palaeotsunami deposits (Tsunami 1 and Tsunami 2) at Lake Grassmere. Tsunami ages are displayed in green, representing the 95% age range. Outliers are displayed by the red outlines. Each phase represents the sedimentary units, and the radiocarbon dates that were obtained from within them. Calibrated using SHCal13 atmospheric curve (Hogg et al., 2013) and Marine13 marine curve (Reimer et al., 2013).

In light of this, I explored alternative methods to estimate the timing of the tsunamis. The combine function in Oxcal 4.3.2 can be used to suggest the best fitting age for all of the dates obtained within each tsunami deposit (Figure 41 and Figure 42). In order to achieve the best fit, some samples with older ages were excluded if they caused the agreement index calculated by the model to be too low (<60%). Three samples from core 22P were excluded from the Unit 2 model. One sample from core 40P and one from core

22P were excluded from the Unit 4 model. This method gave dates of 2095-1932 and 1509-1370 cal BP for Unit 2 and Unit 4 respectively.

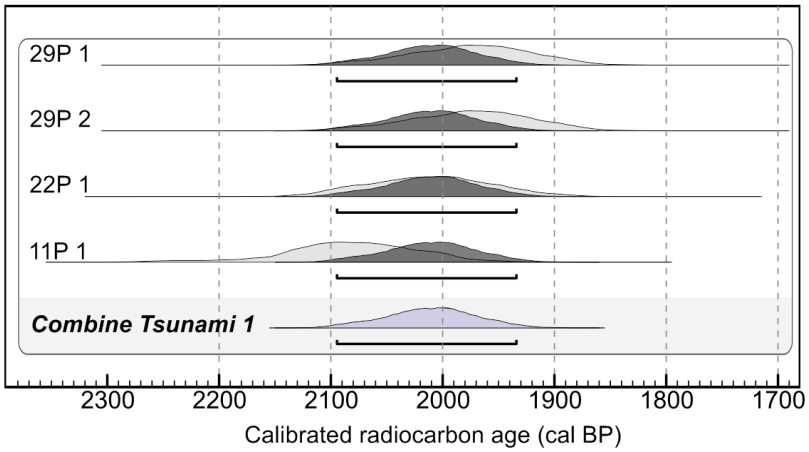

Figure 41 - Results of the combine function age model for dates in Unit 2, this yields an age of 2095-1932 cal BP for Tsunami 1.

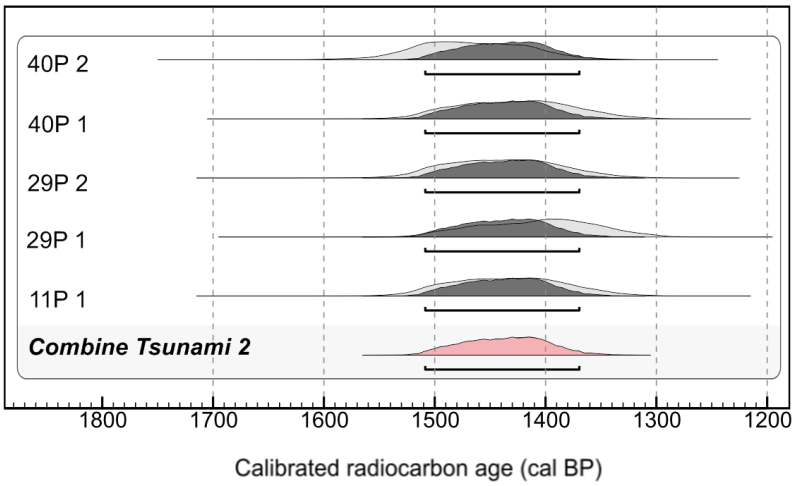

Figure 42 - Results of the combine function age model for dates in Unit 4, this model yields and age of 1509-1370 cal BP for Tsunami 2.

Alternatively, the youngest date obtained from each tsunami unit could be interpreted as the best estimation of the age of the event. Due to the nature of the tsunami deposit being reworked, it is anticipated that the shells within the hash have been scoured from a range of environments and possibly a range of depths. As explained in section 2.4, this means that as well as the fragile articulated bivalves that are assumed to have been transported alive and subsequently died as a result of the tsunami, the shell hash is likely to contain reworked molluscs that died previously and therefore do not represent the age of the event (Ando et al., 2018; Kitamura et al., 2018 b; Mannen et al., 2018). It is also worth noting here that the preservation and degree of encrustation of the shells is important for indicating whether the molluscs were subjected to reworking post-mortem, as explained in section 7.1.2. For this reason, a distribution of ages within the tsunami deposit is expected (as seen in Figure 41 and Figure 42), with a clustering of dates at the younger end of the distribution indicating the tsunami ‘death assemblage’ (Fujino et al.,

2014). When dates are only available from within tsunami deposits as opposed to the bounding units (as in this study), it is common practice to take the youngest age as an indication of the oldest possible age of the event (King et al., 2017, Ando et al., 2018). The youngest date within Unit 2 is 2089-1875 cal BP (median rounded to nearest 5, 1975 cal BP) and the youngest date in Unit 4 is 1509-1314 cal BP (median rounded to nearest 5, 1405 cal BP). Results of the alternative methods for the best age estimation of Tsunami 1 and 2 are compared in Figure 43, showing similar distributions for both the combined age and the youngest age. As a result of the similarity in estimates and the shell taphonomy that indicates shell death caused by the tsunami itself, I have chosen to use the youngest ages of each event to represent the maximum possible timing of each tsunami, now referred to as Tsunami 1 (1975 cal BP) and Tsunami 2 (1405 cal BP).

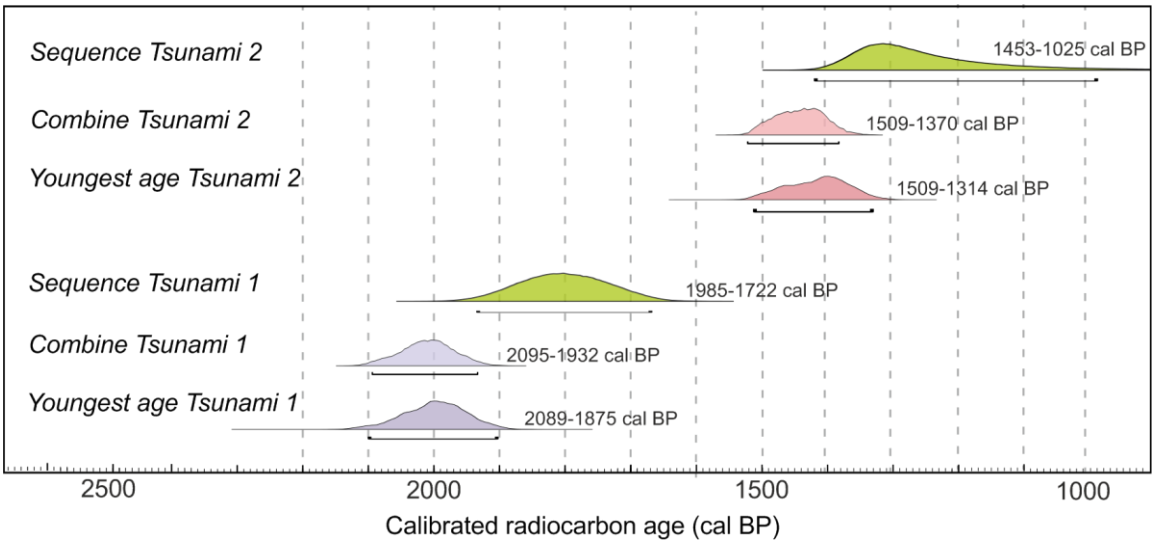

Figure 43 – Comparison of age estimates for Tsunami 1 and 2 from the sequence model (Figure 40), combine models (Figure 41 and Figure 42) and youngest age from each palaeotsunami deposit (Figure 27).

8.2 Regional Palaeoseismology

With the ages of Tsunami 1 and Tsunami 2 at Lake Grassmere taken to be 1975 cal BP and 1405 cal BP, we can consider how these events fit within the record of regional palaeoseismology. Investigating regional palaeoseismic correlations is important for delineating the source of the tsunami deposits (Power et al., 2016 b). Identification of synchronous earthquakes can infer possible fault sources and plausible scale of the tsunami (local, regional or distal). Determining other instances of prehistoric tsunamis triggered on nearby faults in the region can also indicate the tsunamigenic capability of these faults for the Lake Grassmere deposits. Evidence of palaeoearthquakes, palaeotsunami and coastal uplift have been collated in Figure 44 to summarise the palaeoseismology surrounding Lake Grassmere. Locations of studies included in Figure 44 are ordered by distance from Lake Grassmere, and are shown in Figure 44b.

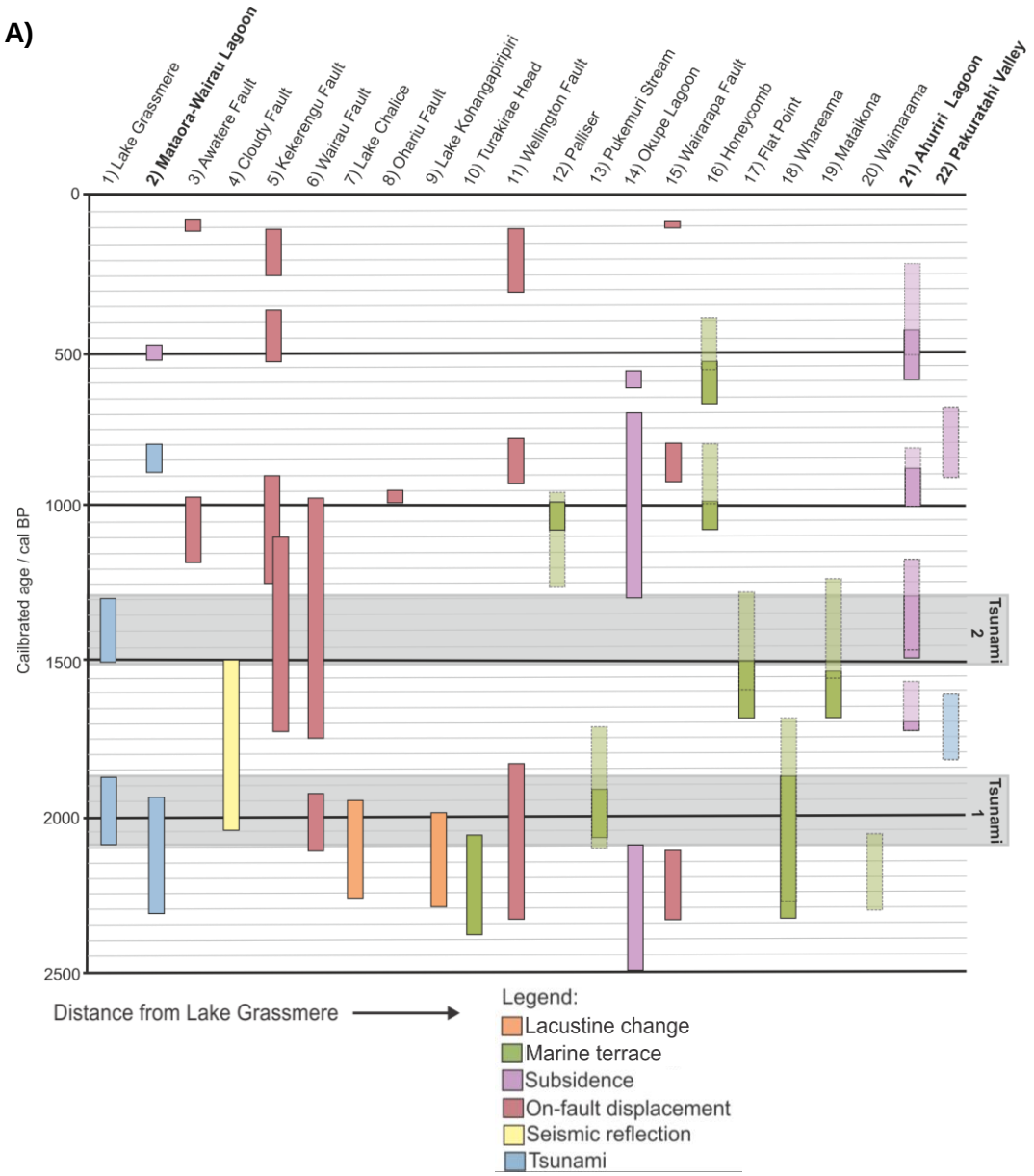

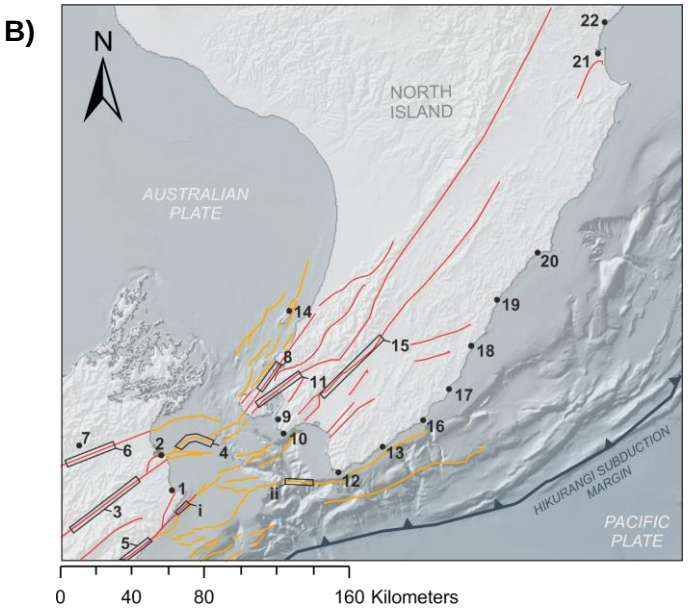

Figure 44 - A) Compilation of regional palaeoseismology surrounding Lake Grassmere (1). Evidence attributed to the subduction interface are shown in bold. Event age distributions are categorised by the type of evidence (see legend) and are ordered by distance from Lake Grassmere. Calibrated ages (95.4%) are taken from 2) Mataora-Wairau Lagoon (King et al., 2017), 3) Awatere Fault (Benson et al., 2001), 4) Cloudy Fault (Pondard and Barnes., 2010), 5) Kekerengu Fault (Little et al., 2018), 6) Wairau Fault (Nicol and van Dissen., 2018), 7) Lake chalice (Adams, 1981), 8) Ohariu Fault (Litchfield et al., 2010), 9) Lake Kohangapiripiri and 14) Okupe Lagoon (Cochran et al., 2007), 10) Turakirae Head (McSaveney et al., 2006), 11) Wellington fault (Langridge et al., 2011), 12) Palliser, 13) Pukemuri Stream, 16) Honeycomb, 17) Flat Point, 18) Whareama, 19) Mataikona, 20) Wairarama (Berryman et al., 2011; Clark et al., 2019), 15) Wairarapa Fault (Little at al., 2009) and 21) Ahuriri Lagoon (Hayward et al., 2016; Clark et al., 2019) and 22) Pakuratahi Valley (Clark et al., 2019). Transparent shaded events represent recalibrated ages from Clark et al., 2019. B) Locations of contributing studies. Yellow lines = offshore upper plate faults. Red lines = active upper plate faults. Also shown is i) Needles Fault and ii) Boo Boo Fault.

The evidence closest to Lake Grassmere comprises a palaeotsunami deposit identified at Mataora-Wairau Lagoon by King et al (2017). Piston cores from the location 15 km north of Lake Grassmere confirmed the two subduction earthquake deposits identified by Clark et al (2015) aged ~800 and ~500 cal BP, but also located a third tsunami deposit of 'medium sand embedded with a shell hash', which thins and fines with distance from the coast. King et al (2017) recognise that both dates that are obtained from wood within the third tsunami deposit may carry an in-built age and suggest that the minimum of age of 2028 cal BP is the best representation for the unit at this stage. The age and description of the laterally extensive deposit has many affinities with Tsunami 1 at Lake Grassmere, inferring a possible coeval event at Mataora-Wairau Lagoon. While no associated coseismic vertical deformation is confirmed at Mataora-Wairau Lagoon, the most likely direction of deformation is suggested to be subsidence.

Nicol and van Dissen (2018) describes a 6000-year record of palaeoseismology for the Wairau Fault. Geologic evidence of surface rupturing along 140 km of the fault is well constrained at multiple sites to 2110-1930 cal BP, with another poorly constrained event at 1750-970 cal BP. The older earthquake age is consistent with the stepped displacement of beach ridges on the Spring Creek section of the Wairau fault, with 7.7 ± 1.6m (1σ) of uplift dated to 2060–1800 cal BP within the same study (using peat and *Austrovenus stutchburyi* shells). This evidence has a very similar age range to Tsunami 1 at Lake Grassmere.

Lake Chalice is located 70 km east of Lake Grassmere in the Wairau Valley (see locations of Wairau Fault on Figure 44). Radiocarbon evidence for the formation of the lake is coincident with Tsunami 1. Dates obtained from drowned trees, 40 m below the surface, dated to 2315-1950 cal BP. Adams (1981) suggest that the lake became landslide-dammed in an earthquake dated to 2145–1885 cal BP, therefore it is likely this earthquake represents the coeval event on the Wairau Fault, and it also shares the same age range as Tsunami 1.

Pondard and Barnes (2010) use marine seismic reflection profiles to reveal faulted sediment sequences of the submarine Cloudy Fault in the Cook Strait (Figure 44b). The most recent earthquake identified is estimated to have occurred at 1800 ± 300 cal BP. This date overlaps with the timeframe for Tsunami 1 at Lake Grassmere, however the uncertainty is high and potentially spans both tsunamis identified at Lake Grassmere.

Trenches in multiple locations on the Wairarapa Fault show evidence for Holocene earthquakes, including the AD 1855 M_w 8.2 rupture and penultimate ruptures at 920-800 cal BP (Little et al., 2009). The trenches also reveal a rupture estimated to be of similar magnitude to the 1855 earthquake, dated to 2340-2110 (wood) and 2294-1991 cal BP

(charcoal). The preferred older age, derived from wood, puts the earthquake older than the age range for Tsunami 1. On-fault evidence of Wairarapa fault Figure 44b), where uplift of 9.1 m is well constrained by radiocarbon dating of bivalves to 2380-2060 cal BP (McSaveney et al., 2006).

Age ranges of marine terraces in other locations along the Wairarapa coast show similarities to the timing of Tsunami 1 and Tsunami 2. The timing of uplift of marine terraces at Palliser, Whareama and Waimarama/Cape Kidnappers overlaps with the age range of Tsunami 1 (Clark et al, 2019). Ages of terraces at Flat Point and Mataikona fit well with Tsunami 2 occurring ~1400 cal BP (Clark et al, 2019). Other marine terraces included in Figure 44 do not coincide with the Lake Grassmere events.

While Ahuriri Lagoon is 340 km north of Lake Grassmere and located on the central section of the Hikurangi subduction zone, it is included in Figure 44 because it is a key location for recording past subduction earthquakes on the central part of the Hikurangi margin and has an earthquake identified within the range of Tsunami 2. Coseismic subsidence of 0.7 m is dated to 1500-1300 cal BP (Hayward et al., 2016). Although the rupture is a significant distance from Lake Grassmere, it has been attributed to an earthquake on the subduction interface and therefore there is a possibility that the rupture could have extended onto the southern section of the margin, causing a tsunami to inundate Lake Grassmere.

A series of palaeoenvironmental changes associated with coseismic vertical deformation and tsunami are identified at Okupe Lagoon and Lake Kohangapiripiri by Cochran et al (2007; 2015). The lacustrine changes have been attributed to subduction earthquakes as well as rupture of upper plate faults such as the Ohariu and Wairarapa Faults (Clark et al., 2019), however none of the age ranges of earthquakes at these locations demonstrate significant temporal overlaps with Tsunami 1 and Tsunami 2 at Lake Grassmere.

Little et al (2018) describe the palaeoseismology for the Kekerengu Fault. While recent earthquakes (<500 yrs BP) are well constrained, an event that overlaps with the timeframe of Tsunami 2 has an age distribution of >600 years. A radiocarbon date obtained from a large fissure gave an age of 1726-1605 cal BP, however debate surrounds the origin and age of the infilling material, therefore the age of the fissuring event is 1673-1205 cal BP or >1605 cal BP. Consequently, it is possible that Tsunami 2 occurred within the same time frame as an earthquake on the Kekerengu Fault.

This section summarised the seismic events recorded within the regional palaeoseismology, that have overlapping age ranges with Tsunami 1 and Tsunami 2 at Lake Grassmere. Ultimately, Figure 44 shows that there are multiple candidates for

coeval events within the vicinity of the study site that may offer insights into the earthquake origin of the tsunami deposits. The next section considers these fault sources and their likelihood of being responsible for tsunamis inundating Lake Grassmere in the late Holocene.

8.3 Possible Fault Sources

This section discusses the various faults that may have been capable of generating tsunamis that inundated Lake Grassmere, evidenced by the Tsunami 1 deposit at 1975 cal BP, and then by the Tsunami 2 deposit at 1405 cal BP. Each fault is considered separately however attention is also given to the likelihood that multiple faults may have ruptured together in light of historic earthquakes such as the 1855 Wairarapa earthquake and 2016 Kaikoura earthquake as evidence that the southern Hikurangi margin is prone to multi-fault rupture (Clark et al., 2017; Hamling et al., 2017). It is recognised that this discussion is speculative without the aid of tsunami modelling to systematically constrain the possible scenarios, however a candidate for the most likely earthquake source is put forward.

8.3.1 Distant source

When assessing all of the possible earthquake sources for Tsunami 1 and Tsunami 2, distant source tsunamis must be considered. Evidence from historic tsunamis and hazard models highlight the largest threat from distant sources are trans-pacific tsunamis originating in South America (Power et al., 2007). The highest magnitude earthquake ever recorded was M_w 9.5 located in southern Chile in AD 1960. No tsunami was recorded at Cape Campbell for this event (GNS Science, 2019) or for the previous 2 high-magnitude earthquakes in northern Chile (section 3.2.3), suggesting that it is unlikely that Tsunami 1 and Tsunami 2 originated from trans-Pacific sources.

8.3.2 Submarine landslides

Lake Grassmere is adjacent to Cook Strait in which submarine landslide slide scars have been identified within the canyons (Mountjoy et al., 2014). While this suggests that submarine landslides have occurred within the Cook Strait canyons, it does not indicate their tsunamigenic capability (Lane et al., 2016). It is unknown how large tsunamis caused by submarine landslides within Cook Strait would be, however it is unlikely that this source alone would able to displace a substantial amount of water in order to create a tsunami large enough to satisfy the palaeotsunami deposits at Lake Grassmere (Power et al., 2016). Submarine landslides were considered as a source for the tsunami generated by the 2016 Kaikoura earthquake; however, models showed that the entire

tsunami budget was satisfied by the tectonic seafloor deformation and did not require submarine landslides to justify the wave heights (Gusman et al., 2018). Although this does not preclude the possibility that other earthquakes (either similar or dissimilar sources) have caused significant submarine landsliding in the past, the 2016 earthquake may suggest that high-magnitude earthquakes that terminate near the Cook Strait do not trigger submarine landslides capable of generating tsunamis large enough to inundate Lake Grassmere. It is still possible that submarine landslides contributed to the palaeotsunami deposits at Lake Grassmere, however, only as a secondary feature of tectonic ruptures.

8.3.3 Cook Strait faults

The Cook Strait contains many identified faults and possible fault connections that facilitate the transfer of plate boundary deformation from the southern North Island to the northern South Island (Barnes, 2005; Pondard and Barnes, 2010; Grapes and Holdgate, 2014). The Cloudy Fault is highlighted as a possible fault source for tsunamis at Lake Grassmere due to its proximity and orientation that would direct a wave towards Clifford Bay, and its tsunamigenic normal fault type (Pondard and Barnes, 2010). Despite the work of Pondard and Barnes (2010) identifying an event ~1800 cal BP that is within the age range of Tsunami 1, the tsunami potential of the Cloudy Fault is limited by its short length. According to conventional scaling relationships (Abe, 1975), short faults are less capable of causing large earthquakes than long faults, and therefore their size also limits the amount of seafloor displacement that occurs meaning that only small tsunamis are generated. Consequently, the Cloudy Fault probably only hosts small earthquakes proportionate to its length and, as a result, is unlikely to be the primary source of the Lake Grassmere tsunamis. Nevertheless, the Cloudy Fault maintains the ability to contribute towards tsunami size if rupture occurred synchronously with other larger tsunamigenic faults such as the Hikurangi subduction margin.

Another Cook Strait fault of interest due to its proximity to Lake Grassmere is the Needles Fault. The Needles Fault is the closest active, offshore fault to Lake Grassmere and it responsible (along with some minor faults on the Cape Campbell block) for the 0.4 m of coseismic uplift experienced at the study site during the 2016 M_w 7.8 Kaikoura earthquake (Clark et al., 2017). Nevertheless, the fault is strike-slip and therefore probably does not generate sufficient vertical displacements to cause large tsunamis, even in large multi-fault ruptures such as the Kaikoura earthquake (Kearse et al., 2018). Likewise, the majority of other Cook Strait faults are dominantly strike-slip and have low tsunamigenic potential e.g. Boo Boo (Barnes, 2005; Pondard and Barnes, 2010). As a result, it is unlikely that a combination of exclusively Cook Strait faults are the source for

the extensive Lake Grassmere tsunami deposits, and that a scenario with some contribution of upper plate and subduction interface faulting is necessary.

8.3.4 Awatere Fault

Proximity to the study site means that the Awatere fault should be explored as a possible fault source. Palaeoseismology of the Awatere Fault does not reveal any palaeoearthquakes of similar age to Tsunami 1 or Tsunami 2 (Benson et al., 2001). A M_w 7.4-7.7 historic earthquake occurred on the Awatere Fault in 1848, however due to the strike-slip nature of the fault, no tsunami was generated by the offshore portion of the fault (Grapes et al., 1998). Consequently, it is unlikely that the Awatere Fault is the origin of the tsunami deposits at Lake Grassmere.

8.3.5 *Wairau Fault*

The Wairau Fault must be considered as a potential source for tsunami deposits at Lake Grassmere, due to its proximity to the study site (35 km north), lengthy offshore segment and history of earthquakes with similar timing to Tsunami. The penultimate rupture on the Wairau Fault is dated to 2110-1930 cal BP (Nicol and van Dissen, 2018) and it is estimated that a full rupture of the fault would cause high-magnitude earthquake of M_w 7.5-8.0 (Barnes and Pondard, 2010). Although the fault is strike-slip and therefore has low tsunamigenic potential despite its significant offshore portion, it is plausible that an earthquake of this magnitude may trigger the nearby upper plate faults in the Marlborough Fault System (MFS), as well as thrust faults within Cook Strait (e.g. Cloudy Fault). Nicol and van Dissen (2018) suggest the preferred timing of the well-constrained event to be 2020 ± 90 cal BP, which is coincident with: (i) rupture in the Wairau Valley reported by Zachariasen et al (2006), (ii) within the timeframe estimated for the most recent rupture on the Cloudy Fault (Barnes and Pondard, 2010) (iii) and the formation of Lake Chalice ~2100 cal BP. The weight of evidence for a large earthquake on the Wairau Fault ~2000 cal BP presents it as a possible coeval event with the deposition of Tsunami 1 at Lake Grassmere. Despite this, it is unlikely that any of the onshore, strike-slip, upper plate faults would be capable of generating a substantial tsunami. As a result, the Wairau Fault is discarded as a fault source for the Lake Grassmere tsunamis, but it remains possible that the fault rupture was triggered by the same event.

8.3.6 Wairarapa Fault

The dated beach ridge sequence at Turakirae Head is thought to represent rupture on the Wairarapa Fault and offshore extensions such as Wharekahau Thrust and Nicholson Bank Fault (McSaveney et al., 2006; Little et al., 2009). Palaeoearthquake evidence from Little et al (2009) places an event at 2340-2110 cal BP, which is just outside the age

distribution of the youngest date obtained for Tsunami 1. Nevertheless, previous estimates of the same event by McSaveney et al (2006) do allow a slight overlap in age distributions and therefore the Wairarapa fault is considered here.

The penultimate rupture of the Wairarapa Fault and previous events documented at Turakirae Head demonstrate similar amounts of uplift to the most recent AD 1855 M_w 8.2 earthquake (Grapes and Downes, 1997; Little et al. 2009). This suggests that prehistoric earthquakes may have been of a similar magnitude and therefore had a similar tsunami response. In AD 1855, the maximum tsunami run up of 10 m was observed 40 km east of Wellington, with run ups of 4-5 m reported in the southern North Island and northern South Island, including Marlborough (Grapes and Downes, 1997). The historic accounts (Eiby, 1980, Grapes and Downes, 1997) and modelled simulation shown in Figure 8b (Power et al., 2008 within Clark et al., 2015) confirm that tsunamis generated on the Wharekahau Fault in ruptures similar to the events of 1855, do propogate towards Lake Grassmere. As a result, King et al (2017) infer that the poorly constrained palaeotsunami deposit dated to ~2000 cal BP at Mataora-Wairau Lagoon is most likely attributable to the similarly timed rupture on the Wairarapa Fault, and tsunamigenic Wharekahau Fault.

Despite the similar inundation of Mataora-Wairau Lagoon and Lake Grassmere shown in Figure 8b, there is no geological evidence of the 1855 tsunami was apparent at the study site. Thus, I infer that although there is comprehensive evidence for a coincident rupture of the Wairarapa (and Wharekahau) Fault, the earthquake source for the Lake Grassmere palaeotsunami deposits requires either a) a higher magnitude rupture than the 1855 earthquake or b) an additional/alternative source of submarine vertical displacement in order to generate large enough tsunami waves. Darby and Beanland (1992), and Beavan and Darby (2005) consider the contribution of the Hikurangi subduction interface to the 1855 earthquake, and imply deep subduction interface rupture is necessary to account for the historically observed coseismic subsidence within the Wairau Valley. The Hikurangi subduction margin as an earthquake source for the Lake Grassmere palaeotsunami deposits is discussed further in section 8.3.7. Overall, I suggest that the ~2000 cal BP rupture of the Wairarapa Fault may have contributed to the generation of Tsunami 1 that inundated Lake Grassmere. It is likely that the source of Tsunami 1 may also require synchronous rupture of the deep portion Hikurangi subduction interface below the southern North Island to substantiate the large wave height necessary to breach the barrier and satisfy the deposit characteristics, as suggested by King et al (2017). There is no record of rupture on the Wairarapa Fault synchronous with Tsunami 2 and therefore I discount the Wairarapa Fault as an earthquake source for the younger palaeotsunami deposit.

8.3.7 The Hikurangi Subduction Margin

In this discussion, I have highlighted numerous upper plate structures on which paleoearthquakes coincide with the age ranges obtained for palaeotsunami deposits at Lake Grassmere. Nevertheless, it is recognised that even large magnitude earthquakes on nearby faults such as the Wairau and Awatere Faults probably do not generate substantial tsunamis due to their predominantly strike-slip motion and limited vertical seafloor deformation. The Wharekahau Fault that ruptures with the Wairarapa Fault is shown to have been tsunamigenic in historic earthquakes and displays a palaeoearthquake that coincides with Tsunami 1, however no evidence of the M_w 8.2 1855 tsunami has been identified within the Lake Grassmere sediment sequence, indicating that tsunamis generated by this fault are not significant at the study site. In addition to this, rupture of the Wairarapa Fault is incapable of causing the suggested uplift of Lake Grassmere with Tsunami 1 (and possibly 2). In the absence of a sizeable reverse faulted, upper plate structures, the subduction interface is considered to be a probable cause for tsunami inundation at Lake Grassmere.

As stated in section 3.3, the palaeoseismology of the southern Hikurangi subduction margin is very poorly constrained with the only evidence of subduction earthquakes limited to the findings at Mataora-Wairau Lagoon (Clark et al., 2015; King et al., 2017), hence the significance of this study. Evidence of the younger two subduction earthquakes at Mataora-Wairau Lagoon (~800 and 500 cal BP) was not located at Lake Grassmere (Figure 44). It is most likely that these events impacted Lake Grassmere to some degree and that the absence of evidence is a function of poor preservation and post-depositional erosional processes. As discussed in section 7.3, the amount of coseismic uplift estimated would elevate the site out of the tidal range and therefore increase its exposure to erosion, in addition to the wide scale anthropogenic manipulation that has occurred more recently. Nevertheless, the oldest palaeotsunami deposit at Mataora-Wairau Lagoon is dated to a similar age to Tsunami 1 at Lake Grassmere, and King et al (2017) speculate the source to be rupture on the Wairarapa and Wharekahau Faults with likely contribution from the subduction interface. Tsunami 2 does in fact coincide with the age range of a subduction earthquake on the central section of the Hikurangi margin at Ahuriri lagoon (Hayward et al., 2016; Clark et al., 2019). In addition to this, the dates of multiple uplifted marine terraces along the Wairarapa coast also coincide with both Tsunami 1 and Tsunami 2 (Figure 44). Tsunami 1 is coincident with uplifted coastal geomorphology identified at Turakirae, Pukemuri Stream, Whareama and Waimarama (Clark et al., 2019) (Figure 44). Tsunami 2 is concurrent with marine terraces at Flat Point and Mataikona (Clark et al., 2019) (Figure 44). This is of particular significance because, while Berryman et al (2011) attributed the

uplift of Wairarapa marine terraces to rupture of the Wairarapa Fault, Clark et al (2019) consider the alternative possibility that they could represent subduction earthquakes. If this is the case, it would present evidence for subduction earthquakes occurring within the same timeframe as Tsunami 1 and Tsunami 2 at Lake Grassmere. The different locations of marine terrace uplift could be explained by differing locations of the rupture patch along the Hikurangi margin. For example, the clustering of coeval palaeoseismicity around the southern North Island and MFS around 2000 cal BP may indicate a rupture with slip concentrated on the most southern section of the interface, whereas the uplifted terraces and coincident tsunami deposit at Ahuriri around 1400 cal BP is likely to indicate a more northern rupture.

The scenario in which the Lake Grassmere palaeotsunamis represent subduction earthquakes is supported by a recent report by Power et al (2018). Power et al (2018) produce several tsunami models for a M_w 8.9 earthquake on the Hikurangi subduction zone, with variations in slip distributions and rupture patch parameters. The scenario displayed in Figure 45 accounts for slip that is weighted towards the southern-most section of the subduction interface, resulting in 1) large vertical displacements within the Cook Strait, 2) 3-4 m uplift along the Wairarapa coast, and 3) a tsunami with an average run up at the coast of 7-10 m for the Wellington and Marlborough regions. This model represents one of an infinite number of possibilities for the specific slip distribution of a large subduction earthquake, but it is clear that rupture of the southern section of the interface is capable of generating a tsunami with wave heights capable of overtopping the modern barrier at Lake Grassmere. Further to this, Figure 46 shows the likely direction of upper plate, coseismic vertical deformation for subduction earthquakes on the southern Hikurangi margin (Clark et al., 2015). Although Lake Grassmere is close to the axis of vertical movement, it lies within the contours that suggest 0-0.5 m of uplift, which agrees with both the direction of coseismic vertical deformation indicated with Tsunami 1 and the amount of uplift indicated between the beach ridge sets. The position of the contours along the Wairarapa coast also suggest uplift (1-3.5 m) (Figure 46), which further supports the inference that subduction earthquakes on the southern Hikurangi margin may be responsible for the uplifted marine terraces (Clark et al., 2019).

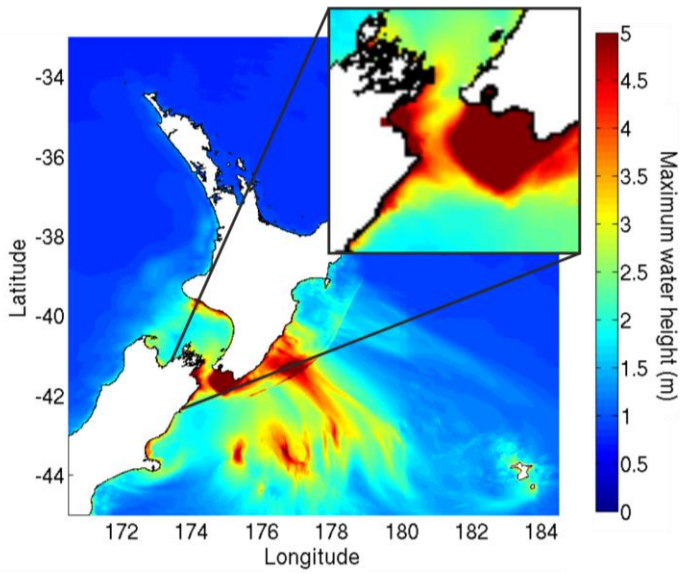

Figure 45 - Maximum water surface elevation for the M_w 8.9 Hikurangi plate-interface earthquake (Power et al., 2018). Slip distributions are calculated based on a 'weighting-factor', which causes the slip distribution to be greater in the region that is strongly coupled under the southern North Island based on Wallace and Beavan (2010). The colour scale is limited so that water heights above 5m appear as 5m.

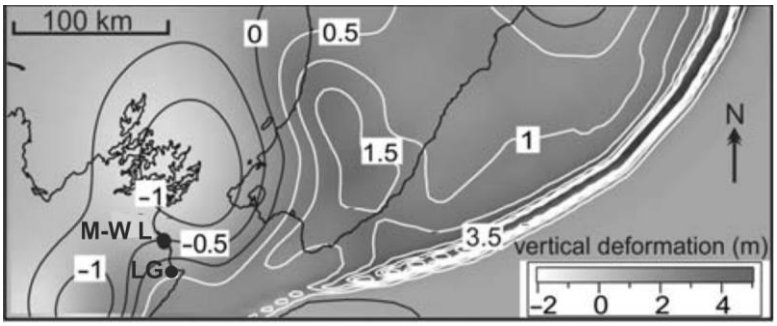

Figure 46– Upper plate deformation produced by plausible southern Hikurangi subduction interface earthquake scenario. Elastic dislocation, half-space modelling was used to replicate a subduction earthquake with 500 years of accumulated slip based on present day interseismic locking patterns show areas of uplift and black contours show areas of subsidence. Intervals are 0.5 m. Lake Grassmere is located close to the +0.5 m contour. Adapted from Clark et al., 2015.

8.4 Summary

In summary I have constrained the age of the Lake Grassmere tsunamis to 2090-1875 and 1510-1315 cal BP, based on the youngest date obtained from each deposit. Using these ages I have collated the regional palaeoseismology to search for evidence of earthquakes that occur within the age range of Tsunami 1 and Tsunami 2. These events have informed the discussion of potential fault sources for the Lake Grassmere tsunamis. I suggest that the most likely source of the earthquakes responsible for the palaeotsunami deposits at Lake Grassmere is rupture on the southern Hikurangi subduction interface. Although the deposits are slightly different in their probability of associated coseismic vertical uplift based on the sediment stratigraphy, I suggest a

similar rupture scenario for both events because 1) there are no other fault sources with large enough tsunamigenic potential to satisfy the deposit characteristics in both cases and 2) the regional palaeoseismology does not offer any temporal correlations for Tsunami 2. Coincident earthquake ages suggest the possibility that the Wairarapa Fault also ruptured synchronously with the proposed subduction earthquakes related to Tsunami 1 at 1975 cal BP (McSaveney et al., 2006). A subduction earthquake source for both paleotsunamis is supported by a recent model of tsunamis generated by subduction earthquakes on the southern section of the Hikurangi margin that predicts tsunami waves of >5 m at the coast. The implications of identifying two more instances of subduction earthquakes on the southern Hikurangi margin are important for better constraining the recurrence interval of these probably high magnitude earthquakes, and therefore more confidence is required in assigning this tsunami source in order to potential hazard to be properly assessed. The following section considers the next steps that should be taken to improve the certainty of assigning the subduction earthquake source of the Lake Grassmere tsunami deposits.

9.0 CONCLUSIONS

9.1 Summary and Implications

Lake Grassmere is situated at the southern end of the Hikurangi subduction zone; approximately 25 km above the plate interface (Williams et al., 2013). There have been no significant earthquakes on the Hikurangi margin in historic time and geologic evidence of subduction earthquakes on the southern section of the interface is limited to two dates at one site (Clark et al., 2015; King et al., 2017; Clark et al., 2019). The shallow coastal embayment of Lake Grassmere is located at an ideal site to record earthquakes at the southern end of the Hikurangi subduction zone and has potential to help determine a critical question of how far south ruptures propagate and whether they are highly tsunamigenic (Power et al., 2016).

In this study I have inferred the palaeoenvironmental evolution of Lake Grassmere from multiproxy analysis of sediment cores and geomorphic features. Lake Grassmere evolved from an open embayment at the sea-level maximum at 7000 cal BP; growth of the barrier across the front of the lagoon created a subtidal environment with a fine-grained, sheltered sedimentary regime that is interjected by two instances of anomalous deposition of coarse-grained shell hashes. A series of beach ridges present at the north of the lake indicates progradation under falling sea level, and steps in elevation between beach ridge sets indicate a possible signature of repeated coseismic uplift in the late Holocene, which has raised the mid-late Holocene subtidal sequence to near and above present mean sea level.

The anomalous deposits within the fine-grained subtidal sequence are characterised by a broad lateral extent (>1.7 km), sharp lower contact, abrupt increase in grain size from silt to sand and a densely packed shell hash including well-preserved articulated bivalves of dominantly intertidal molluscs. I attribute the anomalous deposits to tsunamis, based on the similarity of the deposits to many globally-derived characteristics of modern and ancient tsunami deposits. Alternative depositional mechanisms such as storm surges and hiatus in fine sediment are considered but are less compatible with the deposit's characteristics than tsunami. Coseismic vertical deformation associated with the tsunami deposits is plausible and the likely sense of movement would be uplift; however, there is no high confidence evidence of uplift within the sediment stratigraphy. Coseismic uplift concurrent with Tsunami 1 is very likely given the change in sediment characteristics from below to above the shell hash (Unit 2), although microfossil evidence suggests both environments were subtidal.

In light of identifying palaeotsunamis at Lake Grassmere, I aimed to constrain the age of the tsunamis with age modelling of the radiocarbon dates. I used the youngest age

from *Austrovenus stutchuryi* bivalves in each tsunami deposit, to constrain the timing of each tsunami. This gives an age of 2090-1875 cal BP for Tsunami 1 and 1510-1315 cal BP for Tsunami 2. In order to constrain possible sources for the tsunamis I compiled a catalogue of regional paleoseismic histories of nearby active faults relevant for Lake Grassmere (Figure 44). Multiple prehistoric fault ruptures offered compatible age ranges with the palaeotsunami deposits at Lake Grassmere. Tsunami 1 is synchronous with the ~2000 cal BP rupture of the Wairarapa Fault and several uplifted marine terraces on the Wairarapa coast, as well as of the Wairau Fault. Although Wairarapa Fault earthquakes have been tsunamigenic within the historic record, I suggest that an additional source of submarine seafloor displacement would be required to generate wave heights large enough to overtop the coastal barrier at Lake Grassmere and deposit the coarse bioclastic sediment so far inland. Tsunami 2 is not coeval with any known upper plate earthquakes, but is within the timeframe of a subduction earthquake on the central section of the margin at Ahuriri Lagoon. Taking into account the palaeoseismology and properties of the tsunami deposits, I suggest the most probable explanation for Tsunami 1 and Tsunami 2 at Lake Grassmere is rupture of the southern section of the Hikurangi subduction interface.

Assigning a subduction interface source to the Lake Grassmere tsunami deposits has important implications for improving the understanding of rupture history of the southern Hikurangi subduction margin. There are two subduction earthquakes at ~800 and ~500 yrs BP recorded by subsided saltmarsh soils and a tsunami deposit at Mataora-Wairau Lagoon, located 20 km north of Lake Grassmere (Clark et al., 2015). An older tsunami deposit recorded at Mataora-Wairau Lagoon was dated by King et al (2017) at ~2000 cal BP, and this may be correlative to Tsunami 1 recorded at Lake Grassmere. If, as I interpret them, both Tsunami 1 and Tsunami 2 represent subduction earthquakes, the earthquakes at ~1400 cal BP and ~2000 cal BP provide a record of 4 events in total for subduction earthquakes on the southern Hikurangi margin. Event timing of 2000, 1400, 800 and 500 cal BP, although variable, support the suggestion by Clark et al (2015) that the recurrence interval between southern subduction earthquakes is rather short (~600-300 years). Overall, the potential contribution of the Lake Grassmere tsunamis to the understanding of the dynamics of the southern section of the subduction interface is great, and therefore I recommend the further steps that should be taken in order to increase to confidence of assigning the subduction earthquake source.

9.2 Future work

Within the scope of this study I am unable to definitively identify a source for palaeotsunami deposits at Lake Grassmere; however, the most likely scenario has been

put forward. To improve the confidence of attributing the Lake Grassmere tsunamis to subduction earthquakes, the following further work could be undertaken: (1) reanalysis of cores from Mataora-Wairau Lagoon taken by King et al (2017) and (2) using tsunami models to explore scenarios of tsunami inundation that fit the parameters deduced from the palaeotsunami deposits at Lake Grassmere. Undertaking this work should allow the earthquake sources for Tsunami 1 and Tsunami 2 to be better constrained, although there is likely to always be some inherent degree of uncertainty.

9.2.1 (1) Reanalysis of cores taken by King et al (2017) at Mataora-Wairau Lagoon.

The radiocarbon dates obtained from Unit 2, places Tsunami 1 at Lake Grassmere at a similar age to the oldest palaeotsunami deposit at Mataora-Wairau Lagoon, where two younger instances of subduction earthquakes on the southern Hikurangi margin have been identified (Clark et al., 2015; King et al., 2017). The study by King et al (2017) recognise that the age of the 'disturbance unit' identified is poorly constrained due to their reliance on two dates on unidentified wood fragments from within the deposit itself. As section 8.1 outlines, dating from within the deposit has a high risk of returning reworked ages, and therefore only the youngest date (2093-1994 cal BP) can be taken as a maximum age of the event (King et al., 2017). Descriptions of the sedimentary characteristics of the ~2000 cal BP palaeotsunami deposit at Mataora-Wairau Lagoon are very similar to the Lake Grassmere deposits, with sharp lower contacts, increased grain size from silt to sand, wide lateral extent and the presence of shell hash material. For this reason I suggest that the Mataora-Wairau Lagoon deposit is worthy of further radiocarbon dating in order to better constrain its age. I suspect that dateable material bounding the deposit is scarce, hence the reason for not utilising the traditional method of dating palaeotsunami deposits originally (section 2.4), and so the target material for further work should focus on the *Austrovenus stutchburyi* shell material that is present (based on descriptions). This will allow direct comparison of ages of the two deposits so that the inference of synchronous deposition can be made with more confidence. Identifying multiple sites containing evidence for the same palaeotsunami event adds weight to the suggestion that the magnitude of the event must have been large, and therefore more likely to be generated by rupture on the southern Hikurangi subduction margin rather than an offshore, upper plate fault.

9.2.2 (2) Constraining the tsunami model parameters to satisfy the deposit characteristics.

The outcome of this work can be used to compare to tsunami models that can help constrain the source of the tsunami deposits. This is demonstrated by Satake et al (2008), by testing different fault scenarios including tsunami earthquakes and inter-plate

earthquakes to satisfy tsunami deposits on the Pacific coast of eastern Hokkaido. Other examples of similar modelling techniques include delineation of earthquakes sources by Koshimura et al (2002) for an 1100 cal BP palaeotsunami deposit in Washington, as well as by Butler et al (2014) for a large palaeotsunami deposit in Hawaii, among others (Shaw et al., 2008; Nakamura, 2009; Witter et al., 2012; Priest et al., 2017). Power et al (2016) reviewed the geophysical and geological information that can be used to better inform models of tsunami generated by earthquakes on the southern section of the Hikurangi interface, including geodesy, active and passive source seismology and prehistoric and historic tsunamis. Tsunami wave heights and inundation distances of realistic earthquake scenarios can be estimated by numerical simulation models such as COMCOT (Cornell multi-grid coupled tsunami) (Wang and Power, 2011). Future work could use tsunami models to test different earthquake scenarios and see how the tsunami wave heights and inundation distances match the characteristics of the palaeotsunami deposits identified in this study at Lake Grassmere. This information alone can help rule out fault sources for the generation of tsunamis that are incompatible with the parameters suggested by the tsunami deposits. Table 6 summarises the information gathered from each tsunami deposit that may be useful in constraining tsunami models and narrowing the range of possible fault sources.

Table 6 – Features of the Lake Grassmere tsunami deposits that can be used to inform tsunami models

Parameter	**Tsunami 1 (2090-1875 cal BP)**	**Tsunami 2 (1510-1315 cal BP)**
Minimum inland extent (west)	1.7 km	1.7 km
Height of the barrier	Assumed to be 4-5 m, seaward of current position	Assumed to be 4-5 m unless damaged by Tsunami 1, and seaward of current position
Thickness of the deposit	3.0-6.5 cm	2.0-6.0 cm
Landward trends	No thickening or thinning	No thickening or thinning, bioclastic sediment more abundant in landward cores
Sediment type	Coarse silt to fine sand	
Sediment source	Unknown, no modern equivalents found	
Entrained material	Intertidal shells, coralline algae, greywacke clasts	
Nearby faults with palaeoearthquakes of similar ages	Cloudy, Wellington, Wairarapa, Wairau, uplifted marine terraces on Wairarapa coast	Central subduction interface (Hawkes Bay), Wairau, Kekerengu, uplifted marine terraces on Wairarapa coast

Direction of possible coseismic vertical deformation	Uplift	Unknown
Amount of coseismic vertical deformation	Unknown but within the range of subtidal water depths	

This study is a significant step towards the more spatially and temporally extensive collection of evidence of the palaeoseismicity of the southern Hikurangi subduction interface that is called for by papers such as Power et al (2016) and Clark et al (2019). With the support from the next steps that I propose, future work and the outcome of models should provide insights into realistic rupture patches for future events. This is important for the southern section of the Hikurangi margin, as tsunami wave height is sensitive to the extent of rupture into the Cook Strait, as well as to the undip limit of the slip towards the trench (Power et al., 2016). Earthquakes of the same magnitude demonstrate vastly different tsunami heights that in turn have differing associated risk for the Wellington and Marlborough population. As a result, defining the most likely rupture patches and properties of prehistoric earthquakes will better inform models that delineate the hazard planning for future earthquakes.

APPENDIX 1

Table of gouge core descriptions. See also Appendix 3 for gouge core locations from the handheld GPS and core top elevations.

Core	Location	Depth	Description
LG18 1	At the site of the depression, seaward of confluence	0-0.49	Grey silt
		0.49-0.5	Coarse dark sand
		0.5-0.7	Very coarse sand with rounded pebbles and shell fragments, dark beach sand = barrier sand
		0.7-0.9	Fine dark sand w/ one articulated shell (1cm)
LG18 2	Depression, landward site of confluence	0-0.4	Light grey silt
		0.4-0.45	Coarse sand as above, pebbles fining upwards, sharp upper ocntact with silt
		0.45-0.9	Gravel, not as coarse, max 5mm gravel
		0.9-1.0	Quite sharp upper contact with fine silt, unsure if the gravel layer is thicker or thinner but at least 50cm of gravel/coarse sand above. Smaller shell fragments, no whole shells found
LG18 3	Depression, 10 m W of 2 away from the beach, nearer to the tall grasses and transition to salacornia	0-0.3	Grey silt with sharp lower contact with coarse unit
		0.3-0.65	Gravel unit 35 cm thick - in pit 40x40cm, thickest seen = 50cm
LG18 4	Depression, 100 m S of car, W of stream	0-0.4	Grey silt then sharp contact with sand unit That the sand/gravel unit is extensive - unsure whether fines or thins landward but definitely thicker closer to the barrier
LG18 5	Depression, close to the deflation of the current barrier, E of stream	0-0.2	Silty soil
		0.2-0.7	Coarse sand/gravel, very dark grey, rounded gravel of 0.5 cm, shell fragments very small, looks like barrier deposit, no whole or fresh shells

			Inferred that this unit is old barrier extent
LG18 6	Depression, 10 m W of 5, checking with gauge	0-0.4	Grey silt Suggested that the silt layers thickens away from the barrier?
LG18 7	Crossroad with beach road and lake outer road, E of LG6 location	0-0.5	Silt with thin sand layers within, oxidised, air pockets
		0.5-0.7	Sharp upper contact, medium fine sand, grey
		0.7-0.8	^ with very small shell fragments Assumed LG6 shell hash layer
		0.8-1.0	Sharp upper contact with laminations Laminations beneath - confirm similar location
LG18 8	In a transect with the car at the crossroad, cored in mud ditch	0.75	Shell hash layer directly above laminations LG6 shell hash
LG18 9	10 m in seaward (?) of 8, along ditch at side of lake (just above water level)	0.7	Shell hash layer directly above laminations LG6 shell hash
LG18 10	10 m round from 9, in ditch (towards the barrier)	0.35	Shell hash layer directly above laminations LG6 shell hash Orange grey couplet within the laminations is ubiquitous - lateral continuity
LG18 11	30 m along from 10, in ditch 10 cm above the water level,	0-0.55	Thin sand layers that are in overlying silt get thicker First piston tried here but only retrieved 60 cm of 1 m drive from the surface (LG18 11p s1), second drive - no core retrieved. Went back to same location following day to retrieve top 70 cm with wide gauge auger (LG18 11G), then piston down to 3.7 m (LG18 11 S2/S3)
		0.5-0.55	Shell hash with decent size fragments This shell hash changes in height above the laminations - sometimes not found
		0.55-0.95	Silty sand
		0.95-1.0	LG6 shell hash right above the contact with laminations Different to LG6 location at 7 - good place for a core

		1.0-1.4	Laminated beneath with couplet
LG18 12	Further towards barrier than 11, coring at the water level	0-0.5	Sandier - thin sand layers in silt are thickening
		0.5-1.0	Upper shell layer is questionable, not as obvious within the sands and above the sandier silt. Shell hash on boundary with laminated sequence. Couplet located. Upper shell layer not continuous but cores get sandier in top unit getting closer to the barrier
		1.0.1.25	Still laminated
LG18 13a	60 m along ditch towards sea/barrier	0-0.5	Silty fine sand
		0.5-1.0	Silty (no hash)
		1.0-1.5	Laminated beneath with couplet
b	^	0-1	Silty with some questionable sand layers
		1-1.05	Less densely packed shell layer in sand, right on top of laminations (?) Unsure which shell layer
LG18 14	Carrying on along ditch from 13, towards barrier, just before the culvert linking under the road to the sea, really horrible black anoxic sludge	0-0.5	Black anoxic sludge
		0.5-1.0	Reworked - abondoned - Locations near culverts are heavily reworked
LG18 15	1 pylon away from 11 landwards (50 m), coring at water level in ditch, past the corner	0-0.75	Grey wilt with colour changes, sand layers within quite thick
		0.75-0.77	Shell hash 2 cm thick, not articulated, small fragile shells LG6 shell hash
		0.77-1.0	Laminated
LG18 16	1 pylon along landwards	0-0.49	Silt top, sand layer up to 4cm thick (pic) with sharp upper and lower, sandier silt below

		0.49-0.5	Slight shell hash right at the bottom of the barrell
		0.5-0.70	Silty sand - homogenous
		0.7-0.75	Big shell hash woth very varied species LG6 shell hash
		0.75-1.0	Laminated silt with some sand layers. 0.8 m = wood chunk (pic) (didnt save)
LG18 17	1 pylon along landwards	0-0.45	Silt with some thin sand layers
		0.45-0.47	Dispersed shell fragments in fine sand
		0.47-0.75	Fine silty sand with silty clay unit of 3cm directly above shell hash LG6 shell hash
		0.75-0.8	Shell hash in very fine sand silt. sharp lower contact
		0.8-1.0	Laminated sequence
LG18 18	1 pylon along landwards, 5 m seawards (E) of culvert	0-0.45	Silt with some thin sand layers
		0.45-0.47	A more dense shell layer/ larger fragments
		0.47-0.7	Homogenous silt
		0.7-0.75	Shell hash in sand layer thats 5 cm thick, shells at the base, sharp lower contact - maybe erosive Possible erosive base of the shell hash - could trace couplets in laminations to try and work out
		0.75-1.0	Laminated sequence
LG18 19	1 pylon along landwards	0-0.48	Silt with thin sand layers, layer of micromolluscs (mm size) at 0.25, within anoxic sediment
		0.48-0.5	Upper shell layer
		0.5-0.7	Homogenous silt
		0.7-0.75	Sand, fines upwards with shells at the base, large fragments
		0.75-1.0	Laminations Traceable couplets in laminations
LG18 20	Assumed 1 pylon landwards	0-0.5	Silt with think sand layers taht look chaotically bedded, likely reworked
		0.5-0.7	Homogenous silt
		0.7-0.75	Sandy shell hash, sand fines upwards

			LG6 shell hash
		0.75-1.0	Laminated but couplet seems lower in sequence Maybe the shell hash layers is erosive and has removed some of the laminations elsewhere
LG18 21a	Assumed 1 pylon landwards	0-0.5	Reworked to 0.45 then sand where shell fragments but not many, fragile, sand to 0.5
		0.5-1.0	Homogenous grey silt with shell fragments at 0.8 but not a layer and no sand Think reworked
b	^	0-0.5	Reworked to 0.45 then sand where shell fragments but not many, fragile, sand to 0.5
		0.5-0.7	Homogenous silt
		0.7-0.72	Shell hash layer directly above laminations LG6 shell hash
		0.72-1.0	Laminated sequence
LG18 22	Assumed 1 pylon landwards	0-0.5	Reworked to 0.45 then sand where shell fragments but not many, fragile, sand to 0.5
		0.5-0.7	Homogenous silt
		0.7-0.715	Shell hash layer directly above laminations LG6 shell hash
		0.715-1.0	Laminated sequence Same as previous core but thinner shell hash
LG18 23	2 pylons, 100 m from 22	0-0.5	Reworked to 0.45 then sand where shell fragments but not many, fragile, sand to 0.5
		0.5-0.53	Homogenous silt
		0.53-0.55	Shell hash layers, still sandy but thinner than previously seen, large wood chunk within LG6 shell hash
		0.55-1.0	Laminated sequence Same as previous core but thinner shell hash
LG18 24	2 pylons, 100 m from 23	0-0.6	Reworked silts and sands
		0.6-0.62	Shell hash but no homogenous silt above, sharp contact with laminations below No homogenous layer above - pinched out here
		0.62-1.0	Laminated sequence with fewer sandy and more light coloured laminations
LG18 25	1 pylon from 24	0-0.45	Reworked silts and sands

		0.45-0.58	Laminated dark grey silts
		0.58-0.62	Light grey fine silty sand laminations
		0.62-0.69	Medium sand with shell hash, sharper lower contact Hash within laminations
		0.69-0.71	Grey laminated silts
		0.71-0.72	Shell hash in sand LG6 shell hash
		0.72-0.95	Laminated sequence
LG18 26	At the corner	0-0.5	Reworked silts and sands
		0.5-0.75	Reworked black sludge
		0.75-0.85	Light grey orange laminations
		0.85	Some shells, no sand, grey silt
		0.85-1.0	Grey silt, no lams?
LG18 27	Past corner, level with house	0-0.5	Reworked
		0.5-0.7	One silt layer, shell sample taken, no sand
		0.7-0.85	Clay with silt, not sharp transition, much more clayey, maybe in rafted shells
LG18 32	50 m seaward of 31, 20 m into paddock (in the shallow N-S ditch in the paddock)	0.-1.5	Reworked sequence then silts, thinner shell hash layer within this sequence above homogenous silt (similar depth to LG18 30) Additional upper shell layer
		1.5-1.52	Shell hash layer LG6 shell hash
		1.52-2.0	Laminations, wood chunk at 1.75 within the laminations, sample taken LG18 A sample of wood
LG18 33	5 m landwards (E) of 32 in paddock), augered 1 m then gauge	0-1.5	Reworked sequence then silts with the upper shell hash layer at 1.5
		1.5-1.6	Homogenous grey silt

		1.6-1.62	Shell hash layer LG6 shell hash
		1.62-2.0	Laminated sequence
		2-2.5	Laminated sequence
		2.5-3.3	All laminated sequence, more lighter layers that look like clasty, layered rock/limestone, accretion/dessication, there are fewer sand layers Deeper than previously been
		3.3-3.4	Period of non-lamination
		3.4-3.5	Laminated sequence (doesn't go as far as the shell layers within the laminations thats seen elsewhere (40)
LG18 34	Northwards along the fence of paddock, at the corner/cross with the treeline (the one before the barn treeline)	0-1.5	Oxidised reworked sediment
		1.5-1.6	Grey silt
		1.6-1.62	Upper shell layer in fine sand (finer than previous)
		1.62-1.8	Homogenous grey silt
		1.8-1.81	Shell hash layer, directly on top of laminations LG6 shell hash, thinner here
LG18 35	Half way between 34 and treeline against the barn, so in the middle of the next paddock north, before the beach ridge that runs through the next seaward paddock	0-1.3	Oxidised reworked sediment
		1.3-1.5	20 cm thick gravel layer, fining upwards, rounded grains like current ridge deposit, shell fragments sampled Shell fragments from beach ridge material LG18 B
		1.5-1.8	Oxidised grey silt, layer of orange oxidised v v fine sand between, some shells just above this
		1.8-2	V v fine sand, only top oxidised, grey beneath
		2-2.2	Sand fines downwards into homogenous silt with very fine sand thin layers, some shells within this but look in situ Possible LG6 hash
		2.2	Laminated sequence begins Significance: only one beach ridge deposit within this so must be the youngest beach ridge as quite near the top

too. Means that the beach ridge closest to the lake is the youngest.

Transect 22 - Core 1	Aimed for transect landward from location of 22P, first in paddock (mid way)	0.05-0.30	Topsoil grading into grey brown silt
		0.30-0.65	Grey clayey silt with orange mottles
		0.65-0.92	Grey clayey silt with orange mottles, couple of sandy pods
		0.92-1.15	Interbedded fine grey sand and grey silt (slightly oxidised)
		1.15-1.34	Grey silt (darker) with few interbedded fine sands
		1.34-1.38	Darker grey fine sand with silt
	Repeat hole	1.38-1.53	Interbedded silts and fine sands, grey
		1.53-1.59	Fine sand with some silt, shell fragments (hash) - cockle, sharp upper and lower contacts
		1.59-1.96	Homogenous grey silt
		1.96-2.00	Fine grey sand with few shell fragments (not hash)
		2.00-2.14	Laminated sequence

Transect 22 - Core 2	Same transect across paddock from 22P, between previous and the tree line	0.0-0.90	Grey oxidised silts
		0.9-1.3	Fine grey sand, contact not too sharp, massive, bit brown
		1.3-1.44	Fine sand with brown colouring in places, shells at 1.33-1.35
		1.44-1.68	Grey silt wih some interbedded fine sands
		1.68-1.7	Fine silty sand
		1.70-2.15	Fining downwards from silty fine sand to homogenous grey silt, contact not defined, somewhere 1.9-2.0
		2.15-2.18	Fine grey sand with some silt and shell fragments - cockle, not a hash, sharp lower contact
		2.18-2.65	Laminated silts, very in colour, couple of very fine sand laminae but not many
		2.65-3.15	Laminated silts, very in colour, couple of very fine sand laminae

Transect 22 - Pit 1	Same transect, pit right on top of most lakeward beach ridge (youngest)	0-0.05	Topsoil
		0.05-0.20	Fine gravel
		0.20-0.70	Coarse gravel up to 5cm, shell fragments very well weathered (ID'd)
Transect 28 - Core 1	Aimed for transect landward from location of 22P, first in paddock (mid way)	0.0-0.60	Grey silt with orange mottles
		0.6-0.9	Grey silts, few fine sand laminations
		0.9-1.22	Grey silts, few fine sand laminations
		1.22-1.32	Fining upwards from fine sand to silt, very sharp lower, sharp upper
		1.32-1.4	Homogenous grey silt (darker)
		1.4-1.43	Homogenous grey silt (darker)
		1.43-1.47	Fine grey silty sand
		1.47-1.63	Fine grey silty sand with large shell fragments at base (wetter)
		1.63-1.84	Homogenous grey silt , sharp upper and lower contact
		1.84-1.91	Fine grey sand with large cockle shell hash, dense hash with sharp lower contact
		1.91-1.97	Fine grey sand with large cockle shell hash, whole preserved shells, articulated Nucula and juvenile cockles
		1.97-2.43	Laminated silts with fine sand laminae
Transect 28 - Core 2	Same transect, between previous and tree line	0-1.3	Grey oxidised silts
		1.3-1.32	Fine grey sand, sharp upper contact
		1.32-1.56	Fine grey sand
		1.56-1.72	Grey silts interbedded with fine sand layers, sharp upper
		1.72-1.85	Really hard fine sand with cockles, dark grey colour
		1.85-2.13	Homogenous grey silt. Lower boundary distorted between 2.05 and 2.13. Wood chunk at boundry.
		2.13-2.23	Fine grey sand with large shell fragment

Ditch 1	Ditch along road to marfells beach	0-0.14	Clayey silty medium brown grey topsoil, few clasts and shels within it, possibly bioturbated/ploughed
		0.14-0.31	Sandy, very poorly sorted, crumbly, shell hash with silty fine sandy matrix, shell composition very varied but deffinitely cockles, Zeacumantus, topshells like the other one, fragments to whole articulated not abraded - shells up to 6cm to articulated juveniles, abudant cobbles encrusted in coralline algae up to 20cm within the layer, lots of coralline algae fragments very abundant throughout varying in size,
		0.31-71	Clayey silty medium brown grey topsoil, few clasts and shels within it, possibly bioturbated/ploughed
Ditch 2	Ditch along road to marfells beach, further W on road, away from beach	0-0.15	Brown grey topsoil
		0.15-0.40	Medium brown/grey silty fine sand, slightly mottled
		0.40-0.46	Fine sandy matrix, abundant shells, whole fragment, lots of coraline algae and encrusted bolders
		0.46-->	Clayey silty medium brown grey topsoil, few clasts and shels within it, possibly bioturbated/ploughed
Ditch 3	Ditch along road to marfells beach, further W on road, away from beach	0.-0.1	Top soily brown silt
		0.1-0.3	Light brown homogenous silt, bioturbated - few scattered shells that don't look in situ
		0.3-0.34	Dark grey fine sandy silt with abudant shells, mostly cockles and smaller gastropods, fragments of coralline algae, still some cobbles but becoming less common here than they are further seaward
		0.34-->	Clayey silty medium brown grey topsoil, few clasts and shels within it, possibly bioturbated/ploughed
Lagoon Pit 1 -	Saltmarsh near central lake (transect B)	0-0.05	Topsoil and roots
		0.05-0.15	Grey oxidised silt
		0.15-0.24	Chunky gravel similar to previous core but nly in a layer, 7 cm thick, sharp upper contact with silt, coarse sand, rounded clasts up to 2-3 mm to 15-30 mm, sharp lower contact with sand unit below
		0.24-->	Fine sand, roots through, well sorted, possible tiny shell fragments or limestone
Lagoon core 1	Vegetated marsh south side	0-0.17	Topsoil and reworked silts

		0.17-0.33	Grey homogenous silt
		0.33-0.50	Grey sand, medium, some brown sections that are finer
Lagoon core 2	Into marsh mud	0-0.05	Grey silt
		0.05-0.17	Coarsening downwards from fine sand to coarse sand with gravel and cockle shells, sharp upper and lower contact
		0.17-0.45	Grey silt

APPENDIX 2

Stratigraphic logs of piston cores

Legend

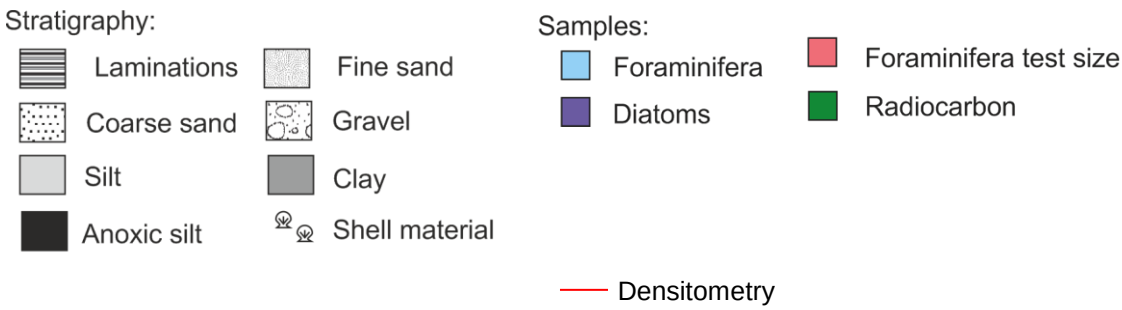

Core 11G

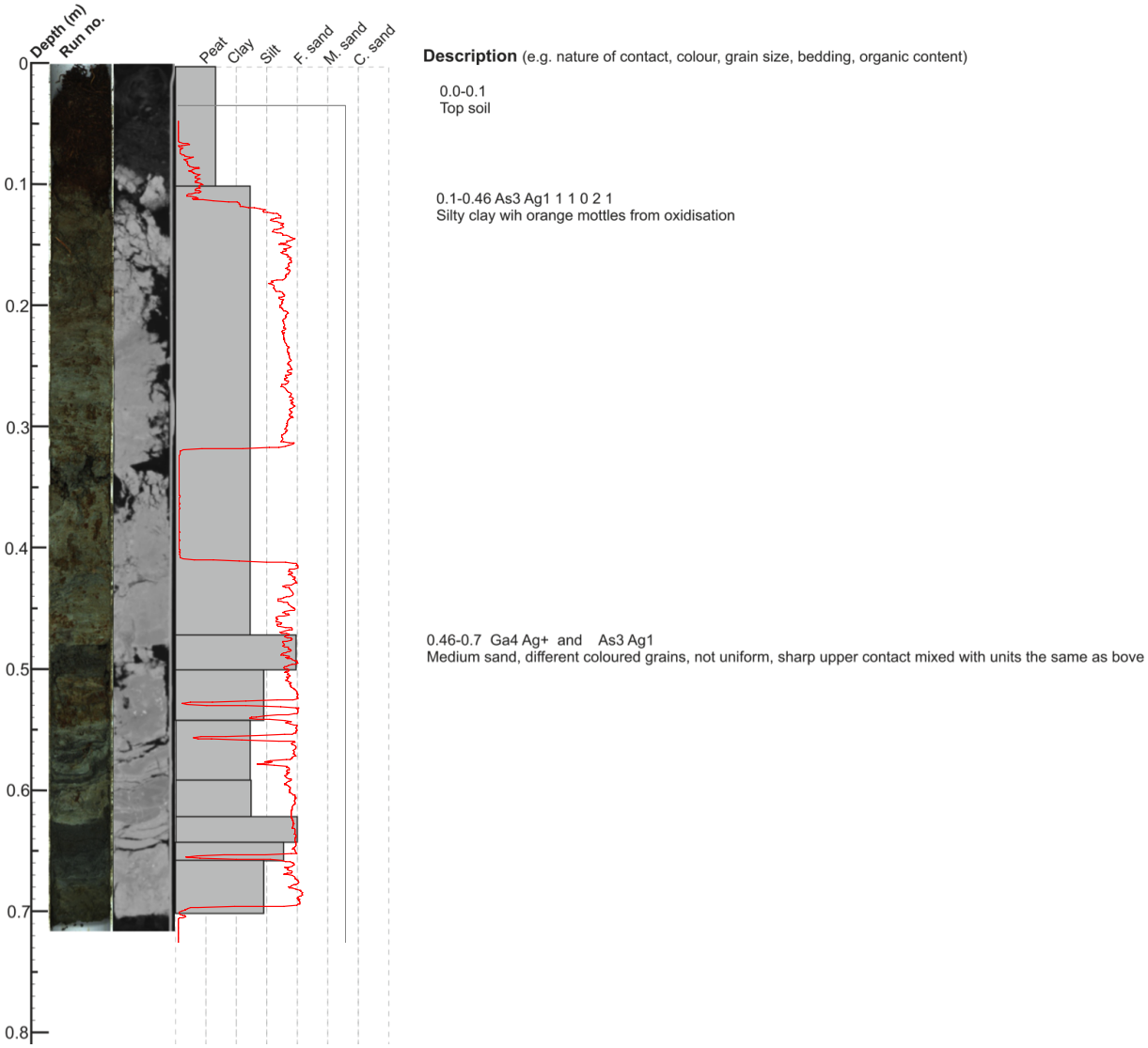

Core 11P S2

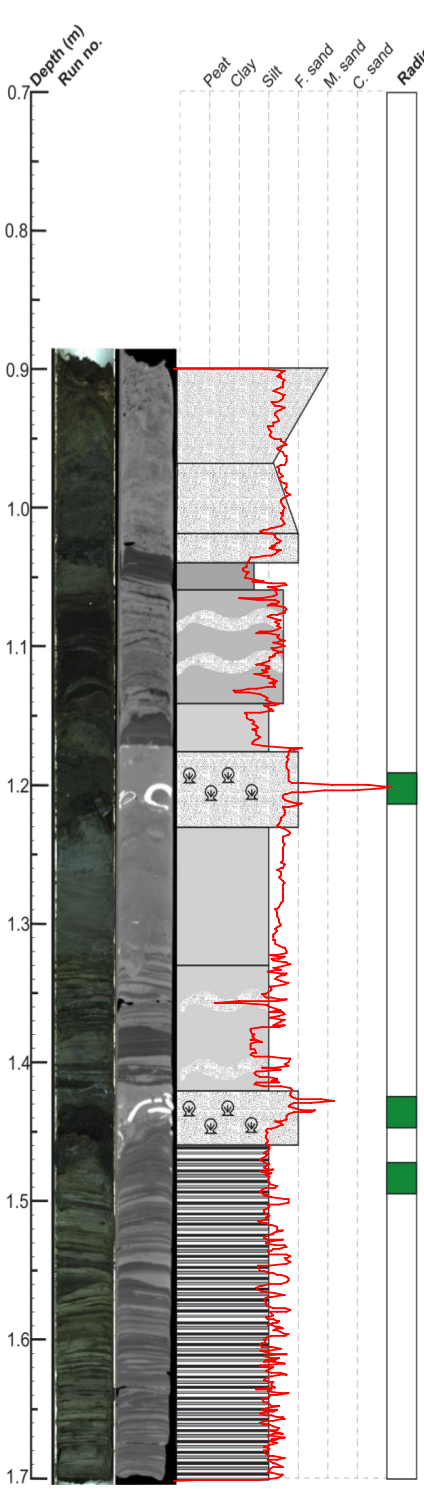

Description (e.g. nature of contact, colour, grain size, bedding, organic content)

Compression 0.7-0.9

0.9-0.97 Ag2 Ga2 2 1 0 2 -
Medium sand and silt, brown sand with grey silt, more silty higher up

0.97-1.02 Ag3 Ga1 1 0 0 2 0
Siltier with finer sand, medium/ dark grey silts, not mottling, gradual boundary

1.02-1.04 Ga4 Ag+ 1 0 0 2 2
Medium grey sand with tiny shell frag (white) and some silt to hold, 0.5 cm boundary upper, very sharp lower

1.04-1.06 Ag3 As1 1 0 1 2 4
Homogenous grey silt with some clay, very sharp upper boundaryr

1.06-1.14 Ga3 Ag1 0 4 0 2 4
Medium sand with fine silt laminations, very very small shell fragments, sharp upper and lower

1.14-1.18 Ag3 As1 Ga+ 2 3 1 2 3
Lighter silt and some clay, fewer laminations with depth, sand laminations stop, continue with different colours of silt, very wavy upper laminations, fines downwards

1.18-1.22 Ag2 Ga2 Ptm+ 1 0 0 1 4
Very very fine sand and silt, quite dark grey, homogenous sediment, shell hash dense a bottom, fragments mainly, no visible whole shells, cockles, large pieces

1.22-1.33 Ag2 As2 2 0 0 2 4
Homogenous medium grey silty clay, no laminations, sharp upper irregular - shells probably disrupted

1.33-1.43 Ag2 As1 Ga1 2 4 1 2 2
Laminated sequence of clayey silts, silts and thin fine/medium sands, sand layers of up to 0.5 cm, non uniform in distribution and thickness, darkness and grey/brown varies

1.43-1.46 Ga3 Ag1 Ptm+ 1 0 0 1 3
Shell hash with very very large frgments within very very fine sand, quite dark, cockle looking

1.8-2.7 Ag2 As1 Ga1 2 4 1 2 2
Laminated sequence of clayey silts, silts and thin fine/medium sands, sand layers of up to 0.5 cm, non-uniform in distribution and thickness, colours very variable.

Core 11P S3

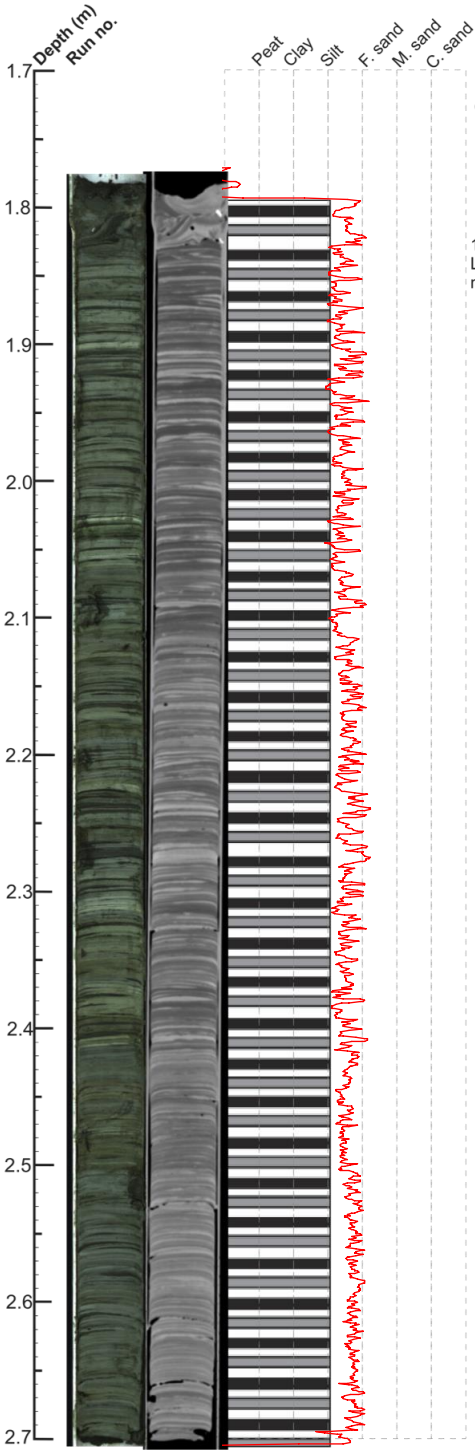

Description (e.g. nature of contact, colour, grain size, bedding, organic content)

Compression 1.7-1.8

1.8-2.7 Ag2 As1 Ga1 2 4 1 2 2
Laminated sequence of clayey silts, silts and thin fine/medium sands, sand layers of up to 0.5 cm, non-uniform in distribution and thickness, colours very variable.

Core 11P S4

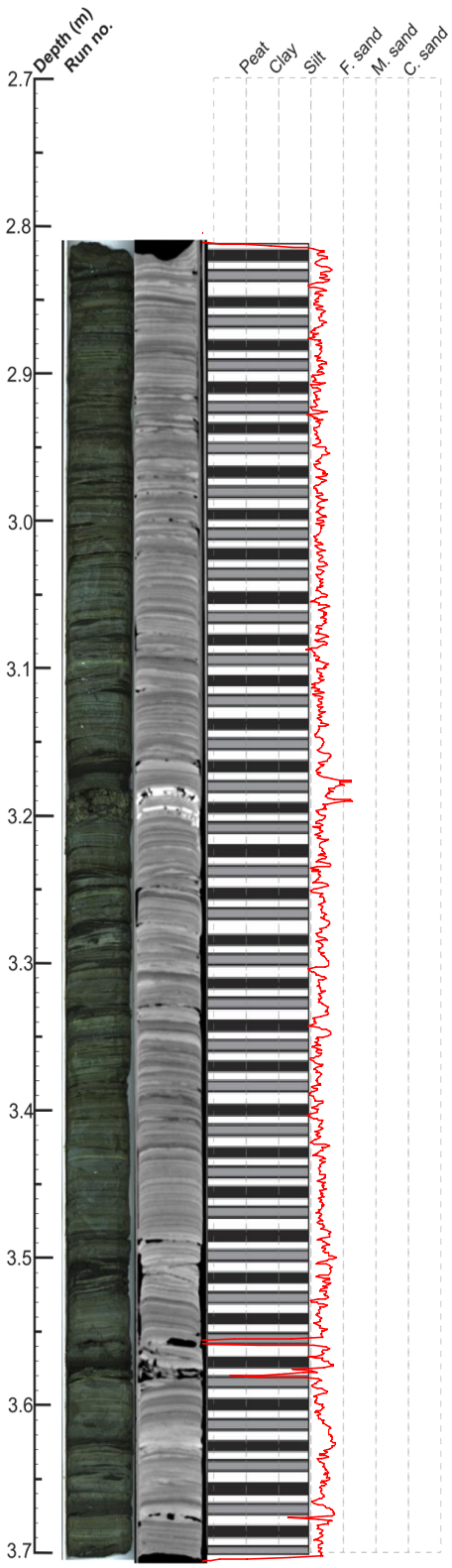

Description (e.g. nature of contact, colour, grain size, bedding, organic content)

Compression 2.7-2.88

2.88-3.22 Ag2 As1 Ga1 2 4 1 2 2
Laminated sequence of clayey silts, silts and thin fine/medium sands, sand layers of up to 0.5 cm, non-uniform in distribution and thickness, colours very variable.

3.22-3.24 Ag2 As2 0 4 0 4 3
Yellow coloured, hard laminated chunk, crumbly, maybe precipitate, sharp upper and lower

3.24-3.7 Ag2 As1 Ga1 2 4 1 2 2
Laminated sequence of clayey silts, silts and thin fine/medium sands, sand layers of up to 0.5 cm, non-uniform in distribution and thickness, colours very variable.

Core 22P

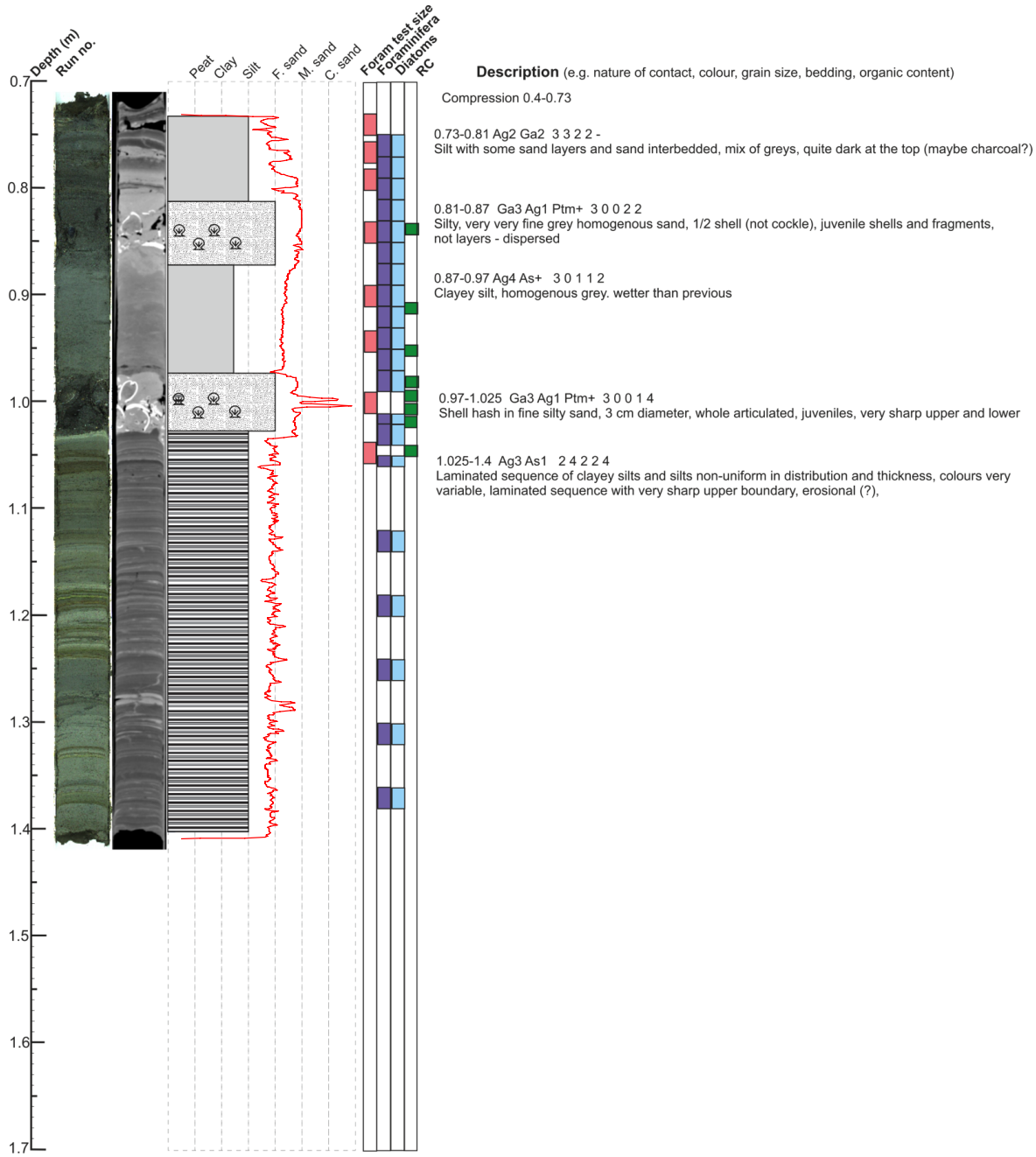

Description (e.g. nature of contact, colour, grain size, bedding, organic content)

Compression 0.4-0.73

0.73-0.81 Ag2 Ga2 3 3 2 2 -
Silt with some sand layers and sand interbedded, mix of greys, quite dark at the top (maybe charcoal?)

0.81-0.87 Ga3 Ag1 Ptm+ 3 0 0 2 2
Silty, very very fine grey homogenous sand, 1/2 shell (not cockle), juvenile shells and fragments, not layers - dispersed

0.87-0.97 Ag4 As+ 3 0 1 1 2
Clayey silt, homogenous grey. wetter than previous

0.97-1.025 Ga3 Ag1 Ptm+ 3 0 0 1 4
Shell hash in fine silty sand, 3 cm diameter, whole articulated, juveniles, very sharp upper and lower

1.025-1.4 Ag3 As1 2 4 2 2 4
Laminated sequence of clayey silts and silts non-uniform in distribution and thickness, colours very variable, laminated sequence with very sharp upper boundary, erosional (?),

Core 28P

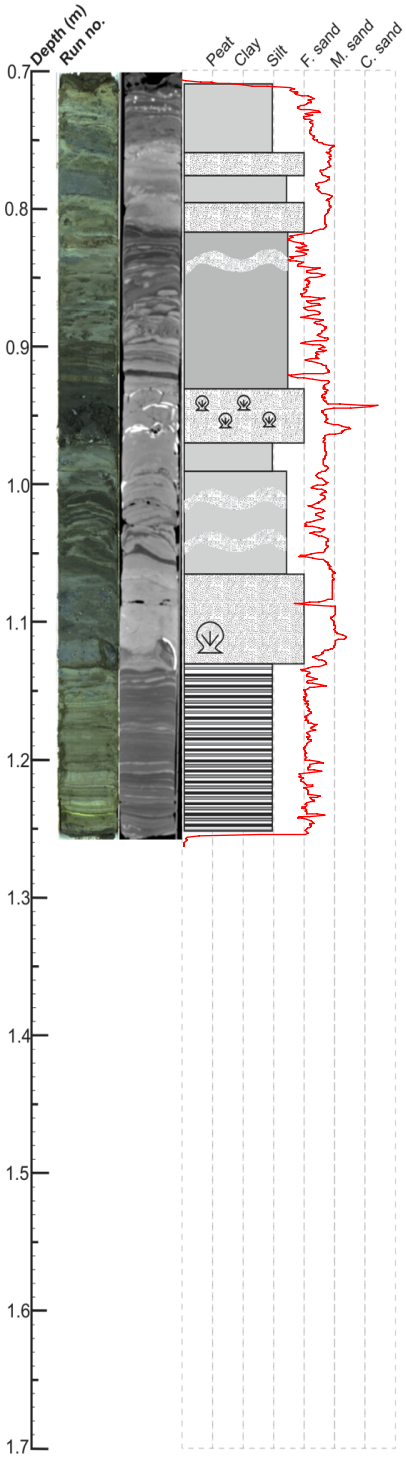

Description (e.g. nature of contact, colour, grain size, bedding, organic content)

Compression 0.25-0.71

0.71-0.76 Ag4 2 3 2 2 -
Interbedded light and dark silts

0.76-0.775 Ga2 Ag2 2 0 2 2 3
Fine sand and silt that is browner than previous, larger particles of sand (multi-coloured), slightly gritty

0.775-0.795 As3 Ag1 1 0 3 2 4
Homogenous grey silty clay

0.795-0.82 Ga2 Ag2 2 2 1 1 4
Brown fine sands and grey silts

0.82-0.93 Ag3 Ga1 2 3 1 3 1
Dark grey silts with interbedded sands, possible charcoal at 0.825, more sandy laminations towards the bottom, possible flow structures

0.93-0.97 Ga4 Ptm+ 1 0 0 3 4
Fine dark grey sand with shell hash at bottom, very small shell fragments

0.97-0.99 As3 Ag1 2 0 1 3 4
Homogenous grey clay, silty

0.99-1.065 Ag3 Ga1 1 3 1 3 1
Interbedded silt and fine dark grey sands, flow patterns similar to 0.82-0.93

1.065-1.13 Ag2 Ga2 Ptm+ 2 0 2 2 0
Silt with some sand, shell fragments quite small, 1 1/2 shell at the base, not that sandy - siltier and stickier than previous hashes

1.13-1.25 Ag3 Ga1 2 4 2 2 4
Laminated sequence similar to other cores, only very very thin sand layers, very light yellow layer here, very sharp upper boundary

Core 29P

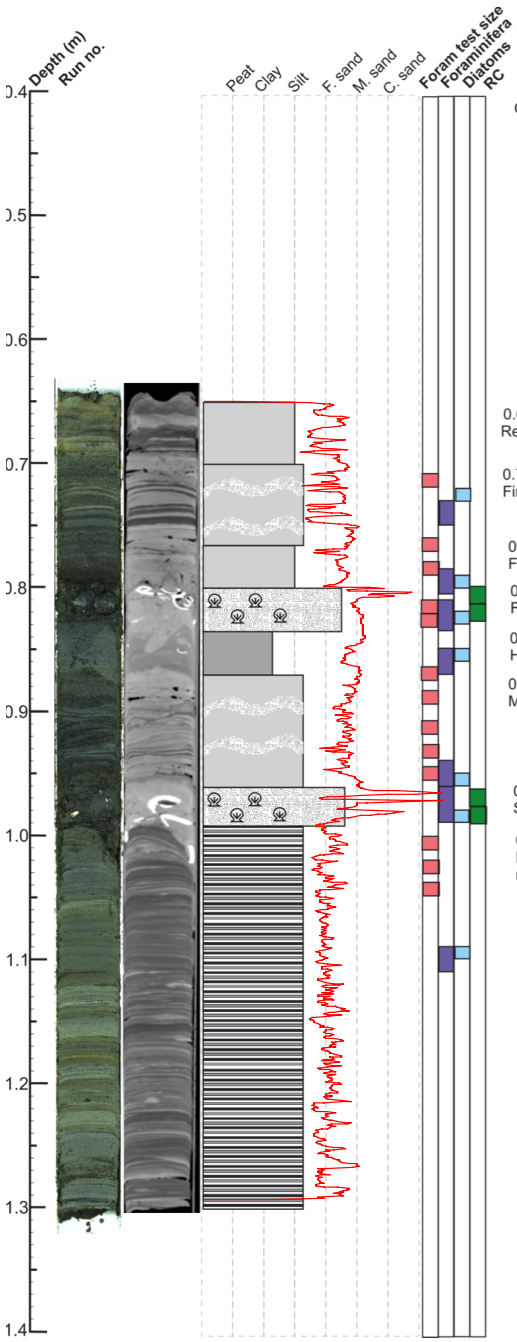

Description (e.g. nature of contact, colour, grain size, bedding, organic content)

Compression 0.3-0.65

0.65-0.7 Ag3 Ga1 2 2 2 -
Reworked-looking browny grey/orange oxidised silt with some interbedded sand

0.7-0.765 Ga3 Ag1 2 3 1 2 3
Fine medium grey sand with interbdded light and dark grey silts, clear laminations, less reworked

0.765-0.8 Ga3 Ag1 2 3 1 2 3
Fine grey sand with some silt - no laminations

0.8-0.835 Ga3 Ag1 ptm+ 1 0 1 3 1
Fine grey sand with little silt, shell hash with weird species, large specimen not cockle

0.835-0.87 Ag2 As2 2 0 2 2 2
Homogenous grey silt

0.87-0.96 Ga3 Ag1 1 3 1 3 1
Medium grey fine silty sand with very thin clayey silt light grey laminations, very wavy - flow structures

0.96-0.99 Ga2 Ag2 Ptm+ 1 0 1 2 4
Silty fine sand, quite sharp upper, shell fragments - quite large

0.99-1.3 Ag2 As1 Ga1 2 4 2 2 4
Laminated sequence of multicoloured silts, some very very thin sand layers, more towards the bottom, not as thick as other cores e.g. LG11, max 0.3 cm

Core 30P

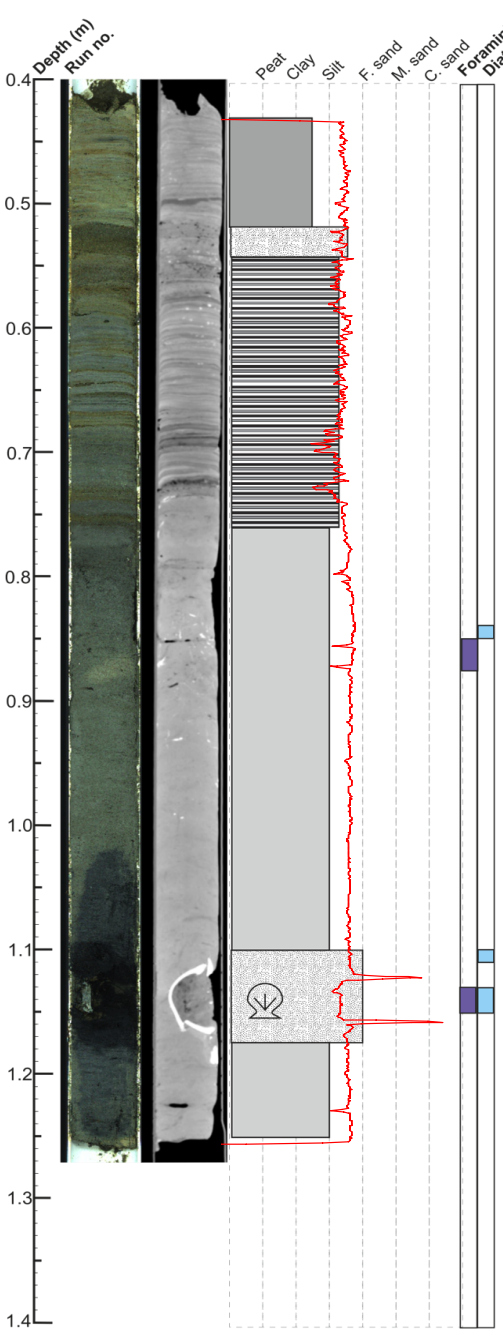

Description (e.g. nature of contact, colour, grain size, bedding, organic content)

Compression 0.35-0.43

0.43-0.52 Ag3 As1 1 4 1 1 -
Clayey silt laminations of grey and browns, some fine sands in very thin layers, interbedded and quite wet

0.52- 0.54 Ga3 Ag1 1 2 0 0 4
Very wet fine sand and silt, brown to grey at the top, sharp upper contact

0.54-0.76 Ag2 Ga2 1 4 1 0 3
Wet fine sand and silt laminations, fines downwards, still some layers of very very fine sand within a mix of blue grey silts and browner oxidised silts

0.76-1.1 Ag3 Ga12 0 1 2 3
Fine sandy grey silt, fines downwards to just silt at the npttom, no laminations, strange lighter section at 0.9

1.1-1.18 Ag4 Ptm+ 4 0 0 3 4
Black anoxic silt (looks like charcoal), very sharp upper and lower contacts, huge 4 cm articulated shell (not cockle) with others

1.18-1.25 Ag3 As1 2 0 1 2 3
Grey clayey silts with darker grey mottling

Core 31P

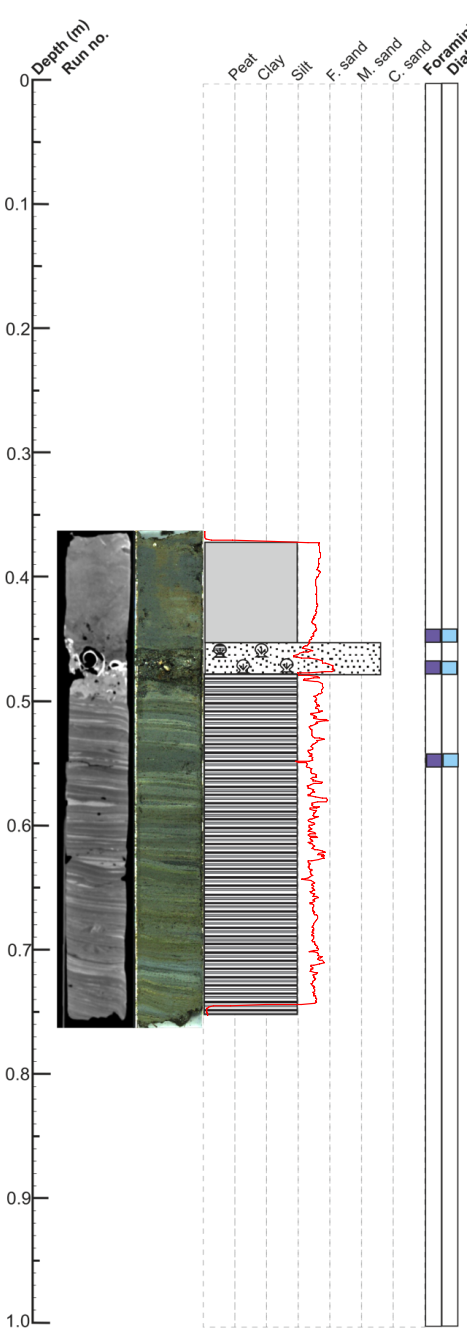

Description (e.g. nature of contact, colour, grain size, bedding, organic content)

Compression 0.35-0.37, top section removed by gauge

0.37-0.45 As2 Ag2 2 0 1 2 -
Grey clayey silts with orange mottles from oxidisation, looks bioturbated (path) into shell layer below, pretty sticky and homogenous

0.45-0.475 Ga4 Ptm+ 2 0 0 2 4
Shell hash, dense, in medium/coarse sand with articulated juveniles

0.475-0.75 As2 Ag2 2 4 2 2 4
Laminate sequence of brown and grey silts with fine sand laminations of up to 0.3-0.4 cm, weird light organic pieces at 0.53, wood chunk for dating around 0.5 on back of labelled half, fewer sand layers at the top

Core 40P

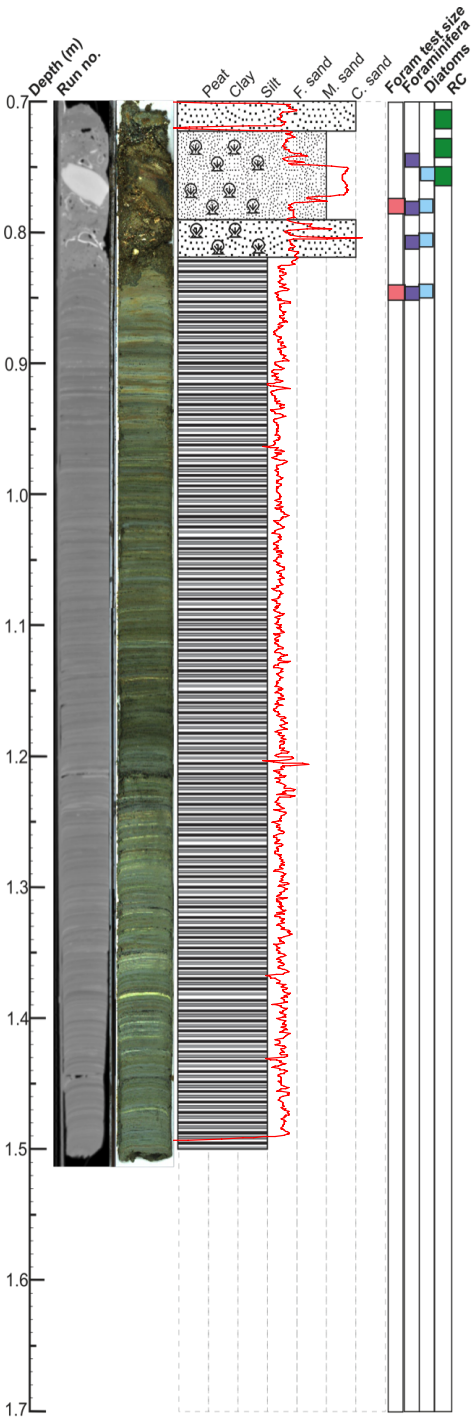

Description (e.g. nature of contact, colour, grain size, bedding, organic content)

Compression 0.5-0.69

0.69-0.72 Ga4 Ag+ Ptm+ 3 0 0 3 0
Coarse sand layer with shell fragments, organic material, silt blob suspected from the homogenous above

0.72-0.79 Ag2 Ga2 Ptm+ 3 0 0 3 3
Siltier unit of medium sand, dense shell hash with large and whole pieces as well as tiny fragments within the sand, more brown in colour. Shells at the base are aligned horizontaly at the sharp boundary. Huge clast that almost fills the core barrell, hard grey and red rock 2cm thick

0.79-0.82 Ga3 Ag1 3 0 0 3 1
Coarse sand and shell fragments- maybe fines downwards, brown colour and 2 units previously, a little silt, very sharp wavy (erosional(?)) lower contact

0.82-1.5 As2 Ag2 2 4 2 2 4
Laminated sequence of brown/grey/yellow/orange clays and silts, some fine sands in thinnest layers so far, some brown layers may contain OM, sand layers at 1.21 has shell in it

Core P1

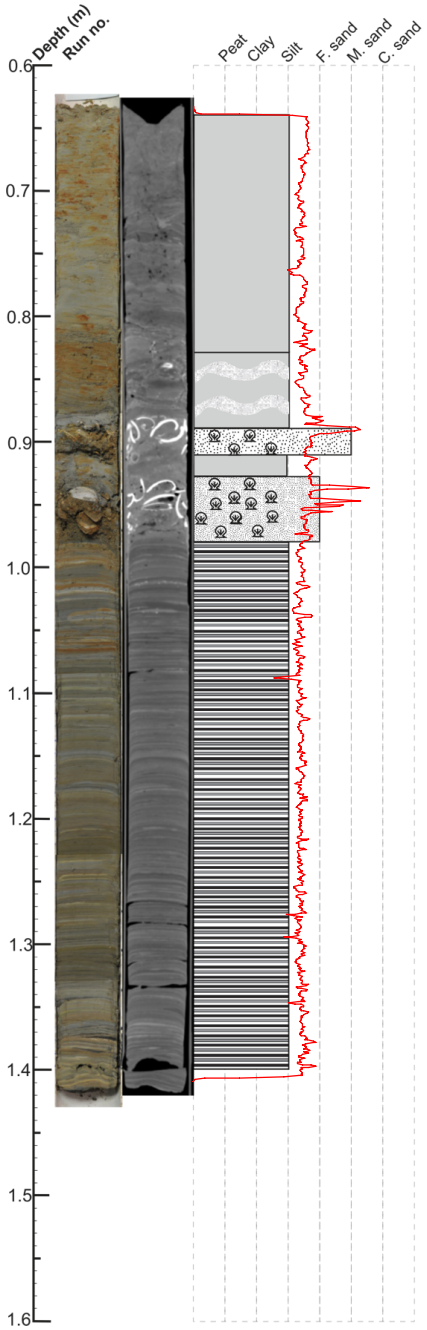

Description (e.g. nature of contact, colour, grain size, bedding, organic content)

Compression = 0.40-0.64

0.64-0.83 Ag3 As1 2 1 2 2 -
Light grey clayey silt with brown/orange mottles, few interbedded fine sands, tiny frags - possibly charcoal or seeds, white fragments that are large forams are visible 0.66-0.68

0.83-0.89 Ag3 Ga1 2 2 2 1 0
Gradational upper into more orange mottled clayey silt, more sands interbedded - these seem to have white frags in and are organic

0.89-0.91 Ga4 Ptm+ 2 0 1 4 0
Densely packed cockle hash with Nucula in medium sand with some silt, v v sharp upper

0.91-0.93 Ag3 Ga1 2 2 2 1 0
Grey silt with orange mottles, non uniform U and L, maybe a lens, shells packed either side of boundary

0.93-0.98 Ga4 Ptm+ 2 0 1 4 0
Densely packed shell hash, v v v sharp lower contact, medium sand at base for 1cm then coarser with shells above to 0.94 above which sand and non-uniform boundary, finer silty sand at top, species = cockle, nucula (arctic), cyclomactra maybe - well preserved

0.98-0.1.4 As2 Ag2 2 4 2 2 4
Laminated sequence of brown/grey/yellow/orange clays and silts, some fine sands in thinnest layers , some brown layers may contain OM

Core P2

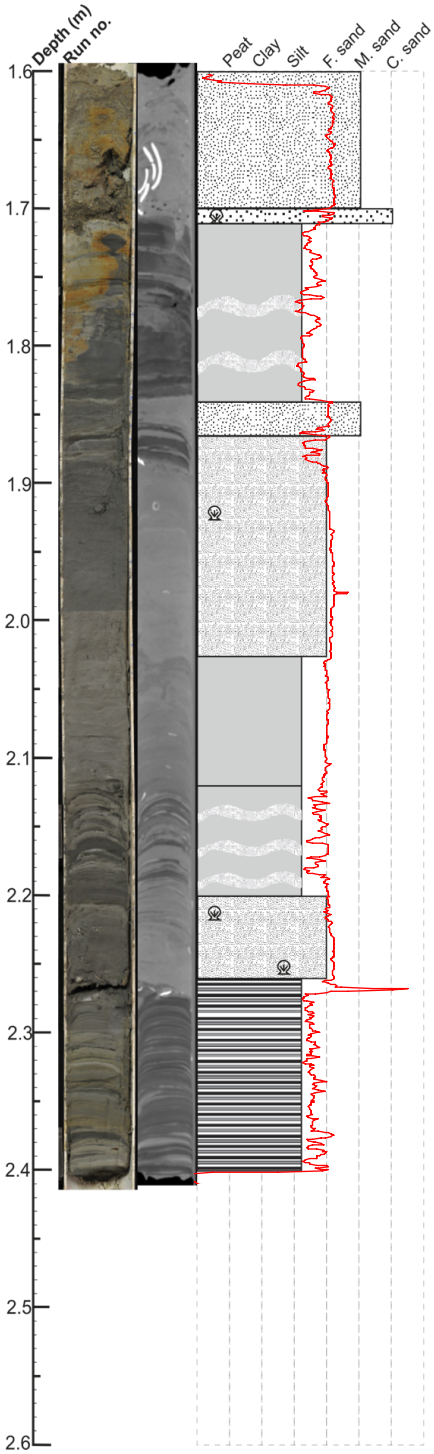

Description (e.g. nature of contact, colour, grain size, bedding, organic content)
Compression = 1.4-1.6
1.6-1.7 Ga4 2 0 1 4 -
Medium grey sand with white flecks (forams?) interbedded with sand and oxidised orange silt, hole where something was - shell - must be in other half - check ID

1.7-1.71 Ga4 3 0 0 4 2
Coarser grey wet sand (beach?) with tiny shell frags, no large ones, darker colour, unclear U, v v sharp L - erosional and non-uniform

1.71-1.84 Ag2 As2 2 1 1 2 4
Sticky clayey silt interbedded with fine sands, very strange colour variation - looks like burrowed upwards but same matrix, ranges from light grey - orange - anoxic black

1.84-1.865 Ga3 Ag1 2 0 1 4 4
Medium, mid grey sand with some silt - maybe charcoal?, v sharp U + L, some layering within

1.865-2.025 Ga3 Ag1 Ptm+ 2 2 1 4 4
ery hard dark grey fine sand with some silt, silt coarsens out from sand upwards to 0.89 where fine wet sand with some shell frags and exposed articulated nucula at 0.92, 0.865-0.89 = interbedded fine sand and silts, shells could be in situ, sharp U, v v sharp L but difficult to see - erosional

2.025-2.12 Ag4 3 0 2 2 4
Homogenous grey silt, sharp U, sharp L

2.12-2.20 Ag3 Ga1 2 3 2 2 3
Interbedded light grey silt with dark grey medium sands, looks finely laminated, very sharp boundaries, some are irregular

2.20-2.26 Ga4 Ptm+ 3 0 1 4 4
Hard dry medium grey fine sand with shells frags dispersed and whole nucula exposed, not hash, might be if dig around to see cockles, L disturbed but can see sharp in places - check CT

2.26-2.40 Ag3 Ga1 2 4 2 2 4
Laminated sequence of brown/grey/yellow/orange clays and silts, some fine sands in thinnest layers so far, some brown layers may contain OM

Core P3

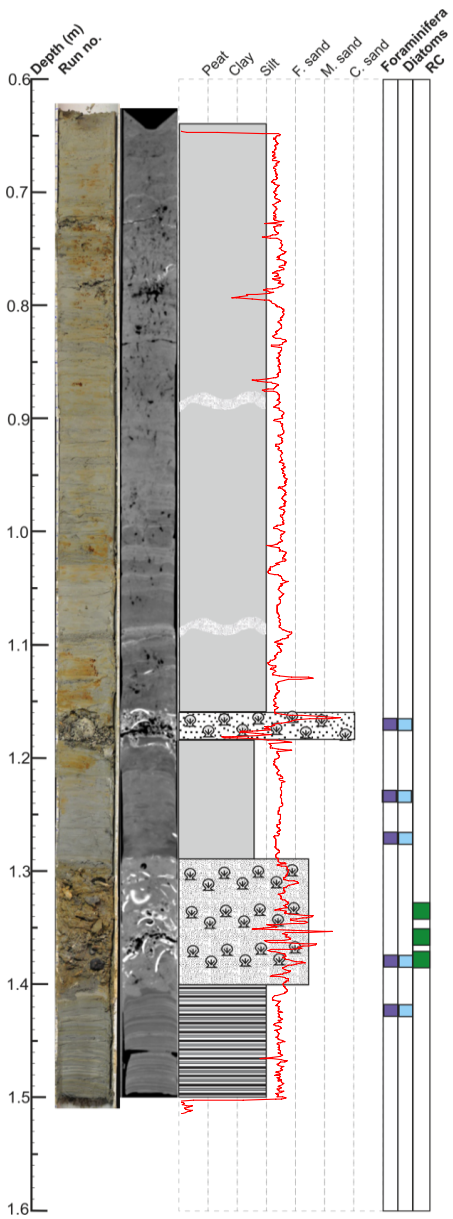

Description (e.g. nature of contact, colour, grain size, bedding, organic content)
Compression = 0.5-0.64

0.64-1.16 Ag3 As1 2 1 2 2 -
Light grey clayey silt with brown/orange mottles in places, orange areas look organic, interbedded with sand in some places - prominent at 0.725-0.73 with some tiny shell frags,

0.64-0.71 = packed with black seeds,

0.89-0.90 sand layer but may just be lens, ,

1.04-1.08 = homogenous grey section

1.09-1.095 = fine sand layer with sharp U + L, irregular L, tiny shell frags, oxidised below

1.11-1.14 = packed with seeds

1.16-1.185 Ga4 Ptm+ 2 0 1 4 0
(diagonal) Dense shell hash with variety of species inc potamopyrgus, cockle, amphibola, zeacumantus, some fine gravel - not really sandy, v v sharp U + L

1.185-1.29 Ag3 As1 2 1 2 2 0
Homogenous grey clayey silt as above but less oxidised

1.29-1.4 Ga4 Ptm+ 2 0 1 4 0
V v v sharp U + L, L= erosional and irregular, fine grey sand at base and tp of unit between hash (dense) of varied species including all above plus oyster and topshells, might be bit silty in middle, shells well preserved, weird black clast (washed and replaced)

1.4-1.5 As2 Ag2 2 4 2 2 4
Laminated sequence of brown/grey/yellow/orange clays and silts, some fine sands in thinnest layers so far, some brown layers may contain OM

Core 6P S1

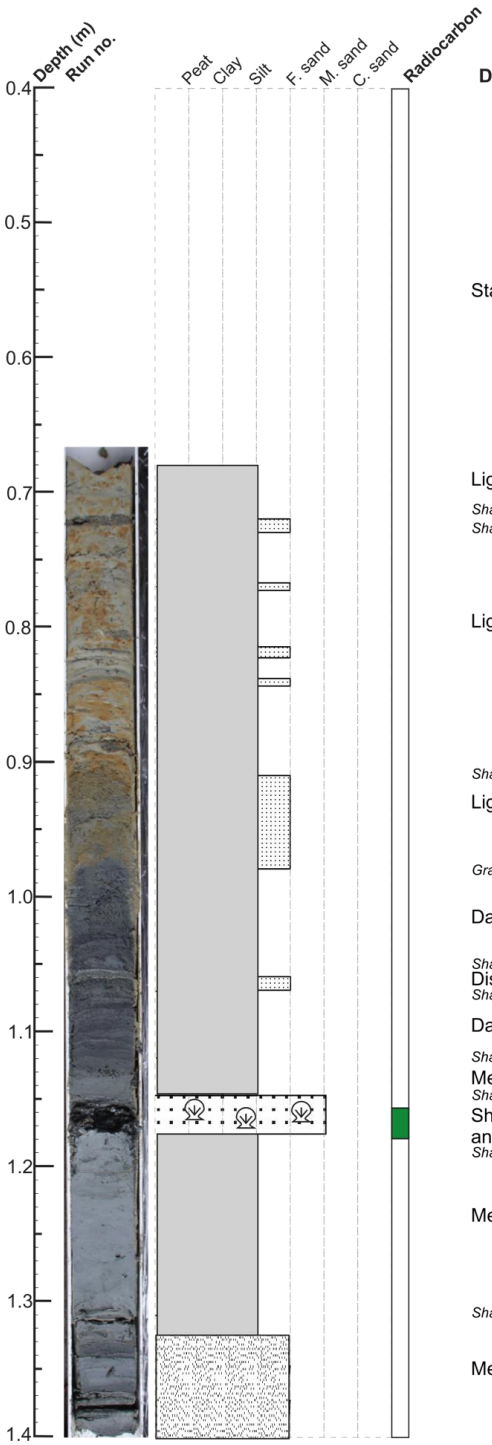

Description (e.g. nature of contact, colour, grain size, bedding, organic content)

Started coring at 0.4 m, 0.4 - 0.67 m: core compression.

Light brown-grey fine sandy silt with orange mottles.

Sharp contact
Sharp contact
Medium grey fine sand, very sharp upper and lower contacts.

Light grey silt, orange mottles, occasional mm-scale laminae of fine sand.

Sharp contact

Light orange-grey silty fine sand, faint bedding of siltier units.

Gradational contact

Dark grey fine sandy silt.

Sharp contact
Distinct layer of light grey fine sand.
Sharp contact

Dark grey laminated fine sandy silt, fine sand & silt.

Sharp contact
Medium grey clay, massive.
Sharp contact
Shell hash in dark grey medium-fine sand; unit composed mostly of shell and shell fragments, one large 30 mm diam *Austrovenus,* whole 3 mm gastropods.
Sharp contact

Medium grey clay, massive.

Sharp contact

Medium grey clay with frequent laminae of medium dark grey silty fine sand.

Core 6P S2

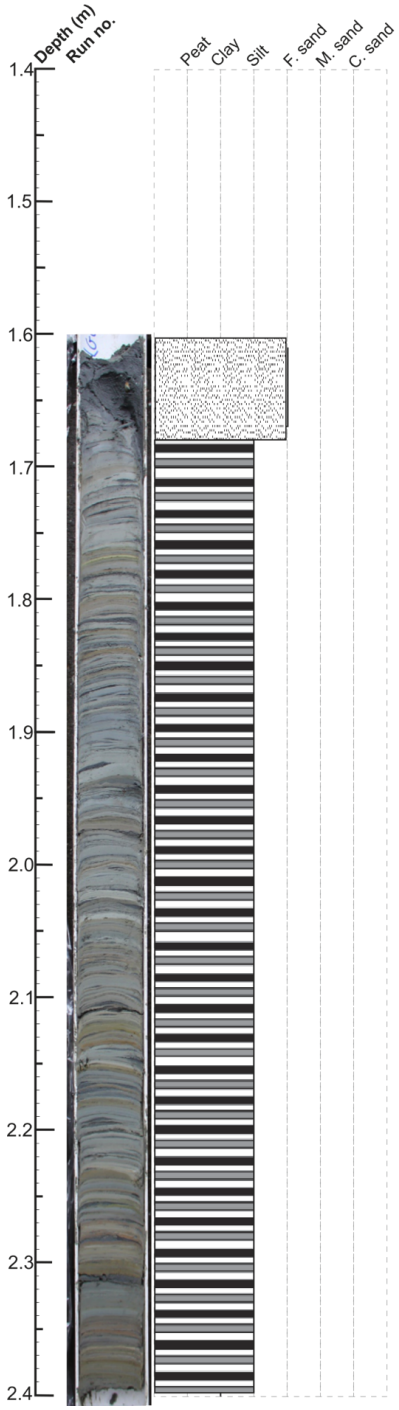

Description (e.g. nature of contact, colour, grain size, bedding, organic content)

Core compression 1.4 - 1.61 m.

Medium grey silty fine sand - ***core fall back.***

Sharp, irregular contact

<mm-scale finely laminated clay with frequent fine sand and silt laminae, mostly medium grey but alternating light grey, brown-grey and dark grey laminae.

APPENDIX 3

Coordinates and elevation of sample points, gouge and piston core tops

Type	ID code	X	Y	Elevation NZVD	Elevation AMSL
Gouge	LG18-1	5382412.687	1696201.014	0.31	0.68
	LG18-2	5382415.753	1696117.571	0.31	0.68
	LG18-3	5382381.678	1695888.334	0.31	0.68
	LG18-4	5382365.821	1697170.165	0.31	0.68
	LG18-5	5382418.18	1696022.728	0.31	0.68
	LG18-6	5382473.462	1696386.299	0.31	0.68
	LG18-G7	5382190.074	1697780.815	0.31	0.68
	LG18-G8	5382260.699	1697594.691	0.31	0.68
	LG18-G9	5382226.035	1697650.123	0.31	0.68
	LG18-G10	5382177.891	1697724.137	0.31	0.68
	LG18-G11	5382202.362	1697688.671	0.31	0.68
	LG18-G12	5382133.77	1697787.958	0.31	0.68
	LG18-G13a	5382080.853	1697874.212	0.31	0.68
	LG18-G14	5382022.115	1697966.287	0.31	0.68
	LG18-G15	5382371.307	1697142.494	0.31	0.68
	LG18-G16	5382380.039	1697078.543	0.31	0.68
	LG18-G17	5382391.705	1696996.491	0.31	0.68
	LG18-G18	5382401.651	1696908.107	0.31	0.68
	LG18-G19	5382404.764	1696808.545	0.31	0.68
	LG18-G20	5382404.422	1696727.795	0.31	0.68
	LG18-G21	5382411.411	1696637.548	0.31	0.68
	LG18-22	5382401.651	1696908.107	0.31	0.68
	LG18-G23	5382413.743	1696375.269	0.31	0.68
	LG18 24	5382617.947	1697527.918	0.31	0.68
	LG18-G25	5382412.687	1696201.014	0.31	0.68
	LG18-G26	5382415.753	1696117.571	0.31	0.68
	LG18-G27	5382381.678	1695888.334	0.31	0.68
	LG18 29	5382413.743	1696375.269	0.31	0.68
	LG18 30	5382613.022	1697502.061	0.31	0.68
	LG18 31	5382566.726	1697576.521	1.00	1.37
	LG18-G32	5382473.462	1696386.299	1.00	1.37
	LG18-G33	5382474.232	1696375.441	1.00	1.37
	LG18-G34	5382640.684	1696321.339	1.80	2.17
	LG18-G35	5382723.283	1696278.866	2.70	3.07
	LG18 29	5382413.743	1696375.269	0.31	0.68
	LG18 30	5382613.022	1697502.061	0.31	0.68
	LG18 31	5382566.726	1697576.521	1.00	1.37
	LG18-G32	5382473.462	1696386.299	1.00	1.37
	LG18-G33	5382474.232	1696375.441	1.00	1.37
	LG18-G34	5382640.684	1696321.339	1.80	2.17
	LG18-G35	5382723.283	1696278.866	2.70	3.07
	LG18-G34	5382640.684	1696321.339	1.80	2.17
Gouge	GRAVEL PIT TOP	5380023.58	1698975.343	2.61	0.38
	GRAVEL PIT BASE	5380019.259	1698976.674	1.44	0.38
	BEACHRIDGE1	5380321.059	1698392.156	1.77	0.38
	LAGOONPIT 1	5380329.962	1698338.788	1.24	0.38
	LAGOONCORE 1	5380344.387	1698281.107	1.22	0.38
	LAGOONCORE 2	5380358.058	1698255.194	0.94	0.38
	T22 CORE1	5382478.669	1696589.044	1.64	0.37
	T22 CORE2	5382603.085	1696575.817	1.85	0.37
	T22 PIT1 (br)	5382685.116	1696635.871	3.56	0.37

	T28 CORE1	5382456.845	1696963.557	1.63	0.37
	T28 CORE2	5382527.328	1696969.235	1.93	0.37
	STREAM1 SHELL LR	5379005.383	1694284.79	1.44	0.38
	DITCH1	5380057.094	1699476.536	2.28	0.38
	DITCH2	5379965.825	1699450.488	2.17	0.38
	DITCH3	5379793.375	1699400.904	2.13	0.38
Piston	11P	5382207.557	1697682.986	1.12	0.37
	22P	5382407.334	1696549.89	0.68	0.37
	28P	5382398.664	1696945.557	0.74	0.37
	29P	5382365.895	1697168.866	0.64	0.37
	30P	5382415.116	1696023.257	0.66	0.37
	31P	5382415.176	1696296.672	0.68	0.37
	40P	5382448.156	1696205.402	1.32	0.37
	LGP1 18	5382438.049	1696233.124	1.23	0.37
	LGP2 18	5382460.576	1697271.546	1.92	0.37
	LGP3 18	5382572.447	1696116.134	1.91	0.37
Point samples	TA 1 INTERTIDAL	5380400.553	1699587.161	1.23	0.37
	TA 2 HIGH TIDE	5380392.227	1699581.83	0.39	0.38
	TA 3 STORMBEACH	5380385.699	1699574.299	1.00	0.38
	TA 4 DUNE	5380375.028	1699564.45	1.84	0.38
	COBBLE BEACH	5380192.206	1700019.088	3.81	0.38
	HT SHELLHASH	5380180.615	1700016.637	0.53	0.38
	TB 1	5380344.201	1698281.417	1.12	0.38
	TB 2	5380357.575	1698242.693	1.23	0.38
	TB 3	5380393.929	1698171.995	0.96	0.38
	TB 4	5380427.875	1698129.896	0.92	0.38
	TC INTERTIDAL	5382656.898	1697814.756	0.78	0.38
	TC HIGH TIDE	5382647.944	1697797.84	0.74	0.37
	TC STORM BEACH	5382645.087	1697791.244	2.69	0.37
	TC TOP OF DUNE	5382636.643	1697782.839	3.75	0.37
	TC DUNE SWALE	5382637.024	1697752.804	6.25	0.37
	TC SELLIARIA	5382611.713	1697622.263	2.63	0.37
	TC SARCOCORNIA	5382607.049	1697595.815	1.84	0.37
	TD SEDIMENT1	5378600.8	1699101.177	1.79	0.37
	TD SEDIMENT2	5378617.511	1699051.825	1.00	0.38
	TD SEDIMENT3	5378631.473	1699034.812	1.31	0.38

APPENDIX 4

Percentage distribution of grain sizes in cores

	Percentage distribution of grain sizes/ %									Grain size statistics (Geometric Method of Moments)			
Depth below surface / m	Medium Sand	Fine Sand	V Fine Sand	V Coarse Silt	Coarse Silt	Medium Silt	Fine Silt	V Fine Silt	Clay	Mean	Sorting	Skewness	Kurtosis
Core 22P													
0.74	0.01	0.03	0.13	0.17	0.16	0.16	0.14	0.14	0.07	14.62	3.85	-0.01	1.99
0.75	0.00	0.02	0.27	0.22	0.13	0.12	0.10	0.10	0.04	23.12	3.65	-0.58	2.13
0.76	0.00	0.02	0.10	0.13	0.17	0.19	0.16	0.15	0.07	12.24	3.45	0.08	2.07
0.77	0.00	0.00	0.11	0.19	0.18	0.17	0.14	0.14	0.06	13.41	3.34	-0.16	1.91
0.78	0.01	0.05	0.27	0.33	0.12	0.08	0.06	0.06	0.02	32.95	3.19	-0.96	3.27
0.79	0.00	0.00	0.08	0.25	0.19	0.16	0.13	0.13	0.06	14.20	3.23	-0.33	1.93
0.80	0.00	0.00	0.18	0.44	0.18	0.09	0.06	0.05	0.02	28.64	2.62	-1.31	4.05
0.81	0.00	0.04	0.30	0.37	0.11	0.06	0.05	0.05	0.02	36.02	2.92	-1.31	4.12
0.82	0.00	0.03	0.22	0.50	0.12	0.05	0.04	0.03	0.01	37.44	2.48	-1.58	5.74
0.83	0.00	0.01	0.14	0.47	0.16	0.08	0.06	0.05	0.03	27.80	2.78	-1.27	3.99
0.84	0.00	0.00	0.10	0.50	0.19	0.08	0.05	0.05	0.02	27.14	2.52	-1.43	4.45
0.85	0.00	0.00	0.08	0.50	0.20	0.08	0.06	0.06	0.03	25.17	2.62	-1.38	4.09
0.86	0.00	0.02	0.08	0.36	0.21	0.13	0.09	0.08	0.03	20.57	2.99	-0.69	2.74
0.87	0.00	0.00	0.02	0.43	0.24	0.12	0.08	0.07	0.03	19.88	2.66	-1.06	3.15
0.88	0.00	0.00	0.03	0.36	0.24	0.14	0.10	0.09	0.04	17.54	2.82	-0.81	2.59
0.89	0.00	0.00	0.00	0.10	0.23	0.26	0.19	0.16	0.06	9.19	2.57	-0.20	2.14
0.91	0.00	0.01	0.03	0.10	0.22	0.23	0.18	0.16	0.07	9.98	2.88	0.06	2.43
0.92	0.00	0.03	0.04	0.09	0.17	0.21	0.19	0.18	0.08	9.66	3.26	0.45	2.69
0.93	0.00	0.00	0.04	0.11	0.20	0.24	0.18	0.16	0.07	9.74	2.83	-0.01	2.20
0.94	0.00	0.00	0.03	0.11	0.20	0.24	0.19	0.17	0.07	9.27	2.82	0.02	2.13

0.95	0.00	0.01	0.06	0.11	0.19	0.22	0.18	0.16	0.07	10.73	3.14	0.15	2.31
0.96	0.00	0.00	0.04	0.17	0.24	0.22	0.15	0.13	0.05	12.19	2.86	-0.27	2.16
0.97	0.00	0.00	0.03	0.16	0.24	0.21	0.15	0.14	0.06	11.45	2.88	-0.24	2.10
0.98	0.00	0.02	0.12	0.23	0.18	0.15	0.12	0.12	0.05	16.71	3.40	-0.30	2.07
0.99	0.00	0.00	0.15	0.40	0.22	0.09	0.06	0.05	0.02	26.34	2.69	-1.14	3.77
1.00	0.00	0.01	0.20	0.44	0.18	0.07	0.04	0.04	0.02	31.41	2.58	-1.36	4.56
1.01	0.00	0.02	0.23	0.43	0.17	0.06	0.04	0.04	0.02	33.62	2.60	-1.42	4.83
1.02	0.00	0.03	0.24	0.41	0.15	0.06	0.04	0.04	0.02	34.56	2.71	-1.32	4.49
1.03	0.00	0.01	0.25	0.38	0.16	0.08	0.06	0.05	0.02	30.28	2.84	-1.17	3.66
1.04	0.00	0.00	0.01	0.09	0.16	0.24	0.23	0.21	0.08	7.65	2.65	0.19	2.18
1.05	0.00	0.00	0.04	0.16	0.21	0.22	0.17	0.15	0.06	10.98	2.91	-0.13	2.06
1.06	0.00	0.03	0.05	0.12	0.19	0.20	0.17	0.17	0.07	10.72	3.28	0.22	2.34
1.07	0.00	0.00	0.01	0.08	0.16	0.22	0.22	0.22	0.09	7.33	2.69	0.21	2.17
1.08	0.00	0.00	0.01	0.10	0.18	0.22	0.20	0.20	0.08	8.18	2.77	0.11	2.05
Core P1													
0.83	0.00	0.00	0.00	0.00	0.06	0.11	0.11	0.15	0.58	1.64	3.81	0.23	2.02
0.84	0.00	0.00	0.00	0.00	0.05	0.14	0.10	0.13	0.59	1.55	3.98	0.20	1.91
0.85	0.00	0.00	0.00	0.00	0.01	0.09	0.07	0.13	0.69	1.16	3.37	0.42	2.34
0.86	0.00	0.00	0.00	0.00	0.02	0.08	0.07	0.11	0.73	0.98	3.59	0.56	2.39
0.87	0.00	0.00	0.00	0.00	0.04	0.14	0.11	0.14	0.57	1.62	3.84	0.17	1.93
0.88	0.00	0.00	0.00	0.00	0.03	0.08	0.17	0.20	0.53	1.61	3.54	-0.07	2.07
0.89	0.00	0.00	0.00	0.00	0.01	0.08	0.26	0.26	0.39	2.15	3.04	-0.58	2.53
0.9	0.00	0.00	0.00	0.00	0.03	0.16	0.33	0.20	0.28	2.99	3.26	-0.84	2.91
0.91	0.00	0.00	0.00	0.00	0.02	0.11	0.24	0.20	0.44	2.02	3.42	-0.37	2.11
0.92	0.00	0.00	0.00	0.00	0.03	0.14	0.22	0.18	0.43	2.14	3.57	-0.30	2.07
0.93	0.00	0.00	0.00	0.00	0.00	0.07	0.14	0.17	0.62	1.25	3.26	0.04	1.95
0.94	0.00	0.00	0.00	0.00	0.05	0.14	0.18	0.15	0.49	1.88	4.00	-0.09	1.87
0.95	0.00	0.00	0.00	0.00	0.05	0.33	0.34	0.12	0.16	4.81	2.88	-1.32	4.29

0.96	0.00	0.00	0.00	0.00	0.08	0.42	0.31	0.09	0.11	6.02	2.65	-1.70	5.92
0.97	0.00	0.00	0.00	0.00	0.04	0.40	0.24	0.08	0.24	4.22	3.43	-1.09	3.04
0.98	0.00	0.00	0.00	0.00	0.00	0.05	0.08	0.15	0.72	1.02	3.00	0.32	2.39
0.99	0.00	0.00	0.00	0.00	0.00	0.04	0.10	0.17	0.70	1.05	2.98	0.17	2.18
1	0.00	0.00	0.00	0.00	0.01	0.06	0.11	0.17	0.65	1.22	3.26	0.19	2.17
1.01	0.00	0.00	0.00	0.00	0.01	0.03	0.09	0.18	0.69	1.07	2.99	0.17	2.29
Core P3													
1.15	0.00	0.00	0.00	0.00	0.00	0.03	0.09	0.14	0.74	0.90	3.03	0.54	2.72
1.16	0.00	0.03	0.24	0.19	0.14	0.00	0.00	0.00	0.41	1.41	4.39	0.50	2.19
1.17	0.00	0.00	0.00	0.00	0.03	0.09	0.10	0.09	0.69	0.76	2.78	-0.13	1.60
1.18	0.00	0.00	0.00	0.00	0.00	0.00	0.00	0.28	0.72	1.15	3.67	0.51	2.24
1.19	0.00	0.00	0.00	0.02	0.07	0.09	0.09	0.11	0.63	8.11	10.40	-0.35	1.33
1.2	0.00	0.00	0.00	0.00	0.01	0.04	0.06	0.13	0.77	0.92	2.98	0.28	2.15
1.28	0.00	0.00	0.00	0.00	0.03	0.29	0.40	0.18	0.10	2.05	3.51	-0.35	1.94
1.29	0.00	0.00	0.00	0.00	0.04	0.36	0.44	0.08	0.08	3.28	2.87	-1.05	3.42
1.3	0.00	0.00	0.00	0.00	0.07	0.34	0.34	0.12	0.12	3.20	3.04	-1.03	3.26
1.31	0.00	0.00	0.00	0.00	0.02	0.19	0.26	0.17	0.37	3.22	2.85	-0.97	3.40
1.32	0.00	0.00	0.00	0.00	0.01	0.19	0.31	0.25	0.25	2.93	3.03	-0.80	2.91
1.33	0.00	0.00	0.00	0.00	0.01	0.14	0.28	0.26	0.31	2.66	3.04	-0.72	2.81
1.34	0.00	0.00	0.00	0.00	0.01	0.17	0.30	0.23	0.29	3.18	2.85	-0.96	3.41
1.35	0.00	0.00	0.00	0.00	0.01	0.18	0.33	0.24	0.24	2.55	3.41	-0.54	2.22
1.36	0.00	0.00	0.00	0.00	0.01	0.18	0.37	0.19	0.25	5.34	2.75	-1.56	5.49
1.37	0.00	0.00	0.00	0.00	0.01	0.17	0.38	0.20	0.24	5.79	2.34	-2.07	7.96
1.38	0.00	0.00	0.00	0.00	0.01	0.13	0.26	0.16	0.44	5.07	2.28	-1.54	6.30

Percentage distribution of grain sizes in modern and point samples

	Percentage distribution of grain sizes/ %												
	Clay	Very fine silt	Fine silt	Medium silt	Coarse silt	V fine sand	Fine sand	Medium sand	Coarse sand	V. coarse sand	V coarse sand	Gravel (granule)	Gravel (pebble)
TA 1 Int	0.00	0.00	0.00	0.00	0.00	9.32	15.92	1.13	11.99	14.25	29.45	11.32	6.60
TA 2 HT	0.00	0.00	0.00	0.00	0.01	32.33	62.25	0.07	0.00	0.00	0.00	0.00	5.33
TA 3 SB	0.00	0.00	0.00	0.00	0.00	9.68	45.03	8.80	23.18	9.35	1.74	2.22	0.00
TA 4 D	0.00	0.00	0.00	0.00	0.00	20.85	77.05	2.10	0.00	0.00	0.00	0.00	0.00
TB 1	7.74	3.99	5.03	11.56	33.95	33.55	4.18	0.00	0.00	0.00	0.00	0.00	0.00
TB 2	21.39	11.37	12.27	13.67	15.15	18.62	7.54	0.00	0.00	0.00	0.00	0.00	0.00
TB 3	12.41	7.86	11.66	21.74	25.90	17.68	2.75	0.00	0.00	0.00	0.00	0.00	0.00
TB 4	12.72	6.46	6.84	9.12	16.39	30.85	17.62	0.01	0.00	0.00	0.00	0.00	0.00
TC 1 Int.	0.00	0.00	0.00	0.00	0.00	0.20	0.52	5.02	55.35	32.66	6.26	0.00	0.00
TC 2 HT	0.00	0.00	0.00	0.00	0.08	0.10	0.59	4.75	8.38	2.85	10.51	46.59	26.16
TC 3 SB	0.00	0.00	0.00	0.00	0.13	0.34	1.14	7.40	36.32	15.72	23.08	11.29	4.68
TC 4 DT	0.19	0.14	0.20	0.29	0.28	0.56	2.23	19.98	71.59	4.53	0.00	0.00	0.00
TC 5 DS	0.27	0.20	0.25	0.40	0.42	0.65	1.54	4.28	17.39	5.86	5.69	16.30	46.74
TC 6 M	35.10	15.35	15.25	15.47	10.97	6.90	0.96	0.00	0.00	0.00	0.00	0.00	0.00
TC 7 M	19.34	13.72	15.89	19.43	16.89	10.42	4.20	0.11	0.00	0.00	0.00	0.00	0.00
TD 1	18.69	9.75	9.66	9.40	7.58	16.22	27.91	0.78	0.00	0.00	0.00	0.00	0.00
TD 2	24.47	12.30	10.80	8.90	7.05	17.12	19.08	0.29	0.00	0.00	0.00	0.00	0.00
TD 3	18.82	10.40	10.04	9.06	6.57	16.16	27.40	1.55	0.00	0.00	0.00	0.00	0.00
T22 Pit 1 G	0.00	0.00	0.00	0.00	0.06	0.00	0.00	0.08	3.73	5.44	8.74	27.05	54.92
Lagoon Pit 1 G	3.78	1.99	1.94	2.16	2.39	9.65	10.18	2.08	11.88	7.03	12.39	11.52	23.03
Hillside #2	25.77	17.02	21.31	24.47	10.62	0.81	0.00	0.00	0.00	0.00	0.00	0.00	0.00

APPENDIX 5

Raw foraminifera counts

Raw counts of foraminifera from the piston cores at Lake Grasmere. Note 'A' in the unit column signifies the anoxic unit 5.1 in core 30P. Purple = Unit 2, Pink = Unit 4.

Core	Unit	Sample mid-depth (cm)	Dry sample weight (g)	Fraction counted	Weight counted	Forams per 1g sediment	Total benthics counted	Ammonia aoteana	Ammonia pustulosa	Bolivina cocazela	Bolivina spp	Bolivinita pliozea	Bulimina spp.	Cibicides corticalus	Cibicides lobatulus	Cibicides marlboroughensis	Discorbinella bertheloti	Elphidium advenum	Elphidium charlottense	Elphidium excavatum	Elphidium novozealandicum	Elphidium spp.	Globocassidulina canalisuturata	Globocassidulina minuta	Haynesina depressula	Laevidentalina inflexa	Laevidentalina subemaciata	Lagena hispeda	Lagena spiratoformis	Lagena striata	Lenticulina australis	Mucronina spp.	Nonionellina flemingi	Notorotalia aucklandica	Notorotalia depressa	Notorotalia inornata	Notorotalia spp	Oridorsalis spp.	Quinqueloculina spp.	Rosalina bradyi	Siphogenerina raphana	Siphotextularia spp.	Spiropectinella proxispera	Trifarina pacifica	Uvigerina bradyi	Zeafloris parri
22	5	0.76	0.89	1/2	0.45	252	112	103					2												3	1					1										1			
22	5	0.78	0.68	1/4	0.17	676	115	85					3			2	2	1							8		1	1					3	2		2						1	4		
22	5	0.80	1.50	1/2	0.75	161	121	91	11					2		1				1				1	6	1									1			1				1	3	1	
22	4	0.82	1.00	1/4	0.25	504	126	96															2									25			3									
22	4	0.84	0.74	1/8	0.09	2000	185	173			1														9												2							
22	4	0.86	0.32	1/8	0.04	3600	144	131																	11												2							
22	3	0.88	0.11	1/2	0.06	3782	208	193						1								2			10												2							
22	3	0.90	0.26	1	0.26	115	30	28			1														1																			
22	3	0.92	0.31	1	0.31	187	58	52			1			1											2											1			1					
22	3	0.94	0.95	3/4	0.71	152	108	99		1												1		1	1	1											1					1	1	
22	3	0.96	0.46	1/2	0.23	457	105	84					2			4							1		7									1	1		4							
22	2	0.98	1.29	1/32	0.04	3522	142	135					2												1								2				1							
22	2	1.01	2.92	1/16	0.18	1748	319	308																													11							
22	1	1.03	0.13	1/2	0.13	292	38	37					1																																
22	1	1.06	0.31	1	0.31	113	35	34										1																											
22	1	1.13	0.12	1	0.12	58	7	7																																				
22	1	1.19	0.20	1	0.20	30	6	4																1								1											
22	1	1.25	0.09	1	0.09	0	0	0																																				

22	1	1.31	0.15	1	0.15	0	0	0																																				
22	1	1.37	0.07	1	0.07	0	0	0																																				
29	5	0.74	0.33	1/2	0.17	0	0																																					
29	5	0.80	1.25	1/8	0.16	186	29	29																																				
29	4	0.82	1.45	1/8	0.18	1137	206	203														3																						
29	3	0.86	0.84	1/2	0.42	193	81	75	1		1						1	1					2																					
29	3	0.95	0.50	1/4	0.13	24	3	3																																				
29	2	0.98	1.76	1/16	0.11	1382	152	148				1											3																					
29	1	1.10	0.10	1	0.10	170	17	16															1																					
30	5	0.86	2.85	1/8	0.36	202	72	50			1						1		3		1		15				1																	
30	A	1.14	5.19	1/8	0.65	99	64	38							1	13				1			10																					
31	3	0.45	0.45	3/8	0.17	599	101	97			1								2																			1						
31	2	0.47			0		0																																					
31	1	0.55	0.59	1/4	0.15	20	3	3																																				
40	4	0.71	1.78	1/16	0.11	1771	197	176			3										1		3						2						3	1	3	1		1			3	
40	4	0.74	0.65	1/8	0.08	2437	198	187										1					6																	1			3	
40	2	0.82	0.85	1/16	0.05	2033	108	103																													4						1	
40	1	0.86	0.20	1/2	0.10	280	28	28																																				
6	5	0.94		1/16			119	102			2						1						14																					
6	4	1.16		1/16			108	105									1						2																					
6	3	1.22		1/2			95	86			1						3						5																					
6	1	1.76	2.13	1	2.13	0	0																																					
P3	5	1.14	0.16	3/4	0.12	1000	120	112			2								1		1		1							1		1											1	
P3	4	1.17	1.64	1/4	0.41	285	117	113																											1								3	
P3	3	1.20	0.06	1	1.64	21	34	34																																				
P3	3	1.28	0.11	1	0.06	3133	188	161		1	4							1				1	12						1						1				2				3	
P3	2	1.35	1.88	1/32	0.07	2587	152	138					1				2						3						1					1			2						3	
P3	1	1.43	0.07	1	1.88	10	19	18					1																															
Hillside #1			0.37	1/2	0.19	686	127				25				14						9		16						16		1				8	14				2			20	1
Hillside #2			1.07	1/16	0.07	1869	125			41	20	8								1	2		34			2		1	2		4				3					4			3	

APPENDIX 6

Oxcal Codes For Age Models

Sequence model

```
Plot()
 {
  Sequence("Grassmere1")
  {
   Boundary("Base");
   Phase("Below LSH")
   {
    Curve("SHCal13","SHCal13.14c");
    R_Date("LG18 11P Below LSH", 2982, 23);
    R_Date("Org - Below LSH 22P", 3160, 22);
   };
   Phase("LSH")
   {
    Curve("Marine13","Marine13.14c");
    Delta_R("LocalMarine",4,25);
    R_Date("LG18 11 LSH", 2444, 27);
    R_Date("LG18 22 LSH 1", 2387, 26);
    R_Date("LG18 22 LSH 2", 2555, 26);
    R_Date("LG18 22 LSH 3", 2620, 27);
    R_Date("LG18 22 LSH 4", 2468, 27);
    R_Date("LG18 29 LSH 1", 2357, 26);
    R_Date("LG18 29 LSH 2", 2357, 26);
   };
   Date("Tsunami (LSH)");
   Phase("Between (outliers)")
   {
    Curve("SHCal13","SHCal13.14c");
    R_Date("Terrestrial", 2395, 115)
    {
     Outlier("Terrestrial")
     {
      color="Red";
     };
    };
    Curve("Marine13","Marine13.14c");
    Delta_R("LocalMarine",4,25);
    R_Date("Foram 1", 2553, 25)
    {
     Outlier("Foram 1");
{
      color="Red";
     };
    };
    R_Date("Foram 2", 2637, 25)
    {
     Outlier("Foram 2");
     {
      color="Red";
     };
    };
   };
   Phase("USH")
```

```
  {
   Curve("Marine13","Marine13.14c");
   Delta_R("LocalMarine",4,25);
   R_Date(" LG18 11 USH", 1891, 27);
   R_Date("LG18 22 USH", 2174, 26);
   R_Date("LG18 29 USH 1", 1865, 26);
   R_Date("LG18 29 USH 2", 1896, 26);
   R_Date("LG18 40 USH 1", 1885, 26);
   R_Date("LG18 40 USH 2", 2082, 26);
   R_Date("LG18 40 USH 3", 1926, 26);
  };
  Date("Tsunami (USH)");
  Boundary("Top");
 };
};
```

Combine model, Unit 2 (Tsunami 1)

```
Plot()
 {
  Curve("Marine13","Marine13.14c");
  Delta_R("LocalMarine",4,25);
  Combine("LSH")
  {
   R_Date("LG18 11 LSH", 2444, 27);
   R_Date("LG18 22 LSH 1", 2387, 26);
   R_Date("LG18 29 LSH 2", 2357, 26);
   R_Date("LG18 29 LSH 1", 2357, 26);
  };
 };
```

Combine model, Unit 4 (Tsunami 2)

```
Plot()
 {
  Curve("Marine13","Marine13.14c");
  Delta_R("LocalMarine",4,25);
  Combine("USH")
  {
   R_Date(" LG18 11 USH", 1891, 27);
   R_Date("LG18 29 USH 1", 1865, 26);
   R_Date("LG18 29 USH 2", 1896, 26);
   R_Date("LG18 40 USH 1", 1885, 26);
   R_Date("LG18 40 USH 2", 1926, 26);
  };
 };
```

REFERENCES

Abe, K. (1975). Reliable estimation of the seismic moment of large earthquakes. *Journal of Physics of the Earth*, 23(4), pp.381-390.

Abe, T., Goto, K. and Sugawara, D. (2012). Relationship between the maximum extent of tsunami sand and the inundation limit of the 2011 Tohoku-oki tsunami on the Sendai Plain, Japan. *Sedimentary Geology*, 282, pp.142-150.

Adams J 1981. Earthquake-dammed lakes in New Zealand. Geology 9: 215-219.

Ando, M., Kitamura, A., Tu, Y., Ohashi, Y., Imai, T., Nakamura, M., Ikuta, R., Miyairi, Y., Yokoyama, Y. and Shishikura, M. (2018). Source of high tsunamis along the southernmost Ryukyu trench inferred from tsunami stratigraphy. *Tectonophysics*, 722, pp.265-276.

Ascough, P., Cook, G. and Dugmore, A. (2005). Methodological approaches to determining the marine radiocarbon reservoir effect. *Progress in Physical Geography*, 29(4), pp.532-547.

Ashi, J. (1997). Computed tomography scan image analysis of sediments. *Proceedings of the Ocean Drilling Program, 156 Scientific Results*, 156.

Atwater, B. (1987). Evidence for Great Holocene Earthquakes Along the Outer Coast of Washington State. *Science*, 236(4804), pp.942-944.

Axelsson, V. (2001). Monitoring sedimentation by radiographic core-to-core correlation. *Geo-Marine Letters*, 21(4), pp.236-244.

Baisden, W., Prior, C., Chambers, D., Canessa, S., Phillips, A., Bertrand, C., Zondervan, A., Turnbull, J., Kaiser, J. and Bruhn, F. (2013). Rafter radiocarbon sample preparation and data flow: Accommodating enhanced throughput and precision. *Nuclear Instruments and Methods in Physics Research Section B: Beam Interactions with Materials and Atoms*, 294, pp.194-198.

Barlow, N., Shennan, I., Long, A., Gehrels, W., Saher, M., Woodroffe, S. and Hillier, C. (2013). Salt marshes as late Holocene tide gauges. *Global and Planetary Change*, 106, pp.90-110.

Barnes, P. (2005). The southern end of the Wairarapa Fault, and surrounding structures in Cook Strait. In: *The 1855 Wairarapa Earthquake Symposium - Proceedings Volume*. [online] Wellington: Greater Wellington Regional Council, pp.66-71. Available at: http://www.gw.govt.nz/assets/council-publications/the_1855_wairarapa_earthquake_symposium_proceedings_volume_web_version.pdf#page=59 [Accessed 7 Jan. 2019].

Barnes, P. and Pondard, N. (2010). Derivation of direct on-fault submarine paleoearthquake records from high-resolution seismic reflection profiles: Wairau Fault, New Zealand. *Geochemistry, Geophysics, Geosystems*, 11(11), p.n/a-n/a.

Beavan, J. and Darby, D. (2005). Fault motion in the 1855 Wairarapa earthquake based on new and reassessed vertical motion observations: did slip occur on the subduction interface?. In: *The 1855 Wairarapa Earthquake Symposium - Proceedings Volume*. [online]

Wellington: Greater Wellington Regional Council, pp.31-41. Available at: http://www.gw.govt.nz/assets/council-publications/the_1855_wairarapa_earthquake_symposium_proceedings_volume_web_version.pdf#page=59 [Accessed 7 Jan. 2019].

Beckvar, N. and Kidwell, S. (1988). Hiatal shell concentrations, sequence analysis, and sealevel history of a Pleistocene coastal alluvial fan, Punta Chueca, Sonora. *Lethaia*, 21(3), pp.257-270.

Bell, R., Holden, C., Power, W., Wang, X. and Downes, G. (2014). Hikurangi margin tsunami earthquake generated by slow seismic rupture over a subducted seamount. *Earth and Planetary Science Letters*, 397, pp.1-9.

Benson, A., Little, T., Van Dissen, R., Hill, N. and Townsend, D. (2001). Late Quaternary paleoseismic history and surface rupture characteristics of the eastern Awatere strike-slip fault, New Zealand. *Geological Society of America Bulletin*, 113(8), pp.1079-1091.

Berryman, K. (2005). *Review of tsunami hazard and risk in New Zealand.*. MCDEM Report No. 2005/104. Wellington, p.139.

Berryman, K., Ota, Y., Miyauchi, T., Hull, A., Clark, K., Ishibashi, K., Iso, N. and Litchfield, N. (2011). Holocene Paleoseismic History of Upper-Plate Faults in the Southern Hikurangi Subduction Margin, New Zealand, Deduced from Marine Terrace Records. *Bulletin of the Seismological Society of America*, 101(5), pp.2064-2087.

Beta Analytic (2019). *AMS Dating Forams and Ostracods, C14 Lab - Beta Analytic*. [online] Carbon Dating Service - Beta Analytic. Available at: https://www.radiocarbon.com/ams-dating-forams.htm [Accessed 6 Feb. 2019].

Beu, A., Maxwell, P., Raine, J. and Beu, A. (1990). *Cenozoic mollusca of New Zealand*. Lower Hutt, N.Z.: Institute of Geological and Nuclear Sciences Limited.

Blott, S. and Pye, K. (2001). GRADISTAT: a grain size distribution and statistics package for the analysis of unconsolidated sediments. *Earth Surface Processes and Landforms*, 26(11), pp.1237-1248.

Boffa Miskell (2015). *Marlborough Landscape Study*. [online] Available at: http://www.boffamiskell.co.nz/downloads/publications/Marlborough_Landscape_Study_2015_AllVolumes.PDF [Accessed 12 Sep. 2018].

Bourne, S., Árnadóttir, T., Beavan, J., Darby, D., England, P., Parsons, B., Walcott, R. and Wood, P. (1998). Crustal deformation of the Marlborough Fault Zone in the South Island of New Zealand: Geodetic constraints over the interval 1982-1994. *Journal of Geophysical Research: Solid Earth*, 103(B12), pp.30147-30165.

Brett, C. (1995). Sequence Stratigraphy, Biostratigraphy, and Taphonomy in Shallow Marine Environments. *PALAIOS*, 10(6), p.597.

Bronk Ramsey, C. (2017) . Methods for Summarizing Radiocarbon Datasets. Radiocarbon, 59(2), 1809-1833.

Brooke, B., Huang, Z., Nicholas, W., Oliver, T., Tamura, T., Woodroffe, C. and Nichol, S. (2019). Relative sea-level records preserved in Holocene beach-ridge strandplains – An example from tropical northeastern Australia. *Marine Geology*, 411, pp.107-118.

Butler, R., Burney, D. and Walsh, D. (2014). Paleotsunami evidence on Kaua'i and numerical modeling of a great Aleutian tsunami. *Geophysical Research Letters*, 41(19), pp.6795-6802.

Callard, L., Long, A., Plets, R., Cooper, A., Belknap, D., Edwards, R., Jackson, D., Kelley, J., Long, D., Milne, G., Monteys, X. and Quinn, T. (2013). Radiocarbon dating of marine material: mollusc versus foraminifera ages (Abstract id. PP53B-2006). In: *American Geophysical Union, Fall Meeting*. [online] American Geophysical Union. Available at: http://adsabs.harvard.edu/abs/2013AGUFMPP53B2006C [Accessed 7 Mar. 2019].

Carter, R. (1986). The morphodynamics of beach-ridge formation: Magilligan, Northern Ireland. *Marine Geology*, 73(3-4), pp.191-214.

Chagué-Goff, C., Schneider, J., Goff, J., Dominey-Howes, D. and Strotz, L. (2011). Expanding the proxy toolkit to help identify past events — Lessons from the 2004 Indian Ocean Tsunami and the 2009 South Pacific Tsunami. *Earth-Science Reviews*, 107(1-2), pp.107-122.

Cisternas, M., Atwater, B., Torrejón, F., Sawai, Y., Machuca, G., Lagos, M., Eipert, A., Youlton, C., Salgado, I., Kamataki, T., Shishikura, M., Rajendran, C., Malik, J., Rizal, Y. and Husni, M. (2005). Predecessors of the giant 1960 Chile earthquake. *Nature*, 437(7057), pp.404-407.

Clague, J., Bobrowsky, P. and Hutchinson, I. (2000). A review of geological records of large tsunamis at Vancouver Island, British Columbia, and implications for hazard. *Quaternary Science Reviews*, 19(9), pp.849-863.

Clark, K., Hayward, B., Cochran, U., Wallace, L., Power, W. and Sabaa, A. (2015). Evidence for Past Subduction Earthquakes at a Plate Boundary with Widespread Upper Plate Faulting: Southern Hikurangi Margin, New Zealand. *Bulletin of the Seismological Society of America*, 105(3), pp.1661-1690.

Clark, K., Howarth, J., Litchfield, N., Cochran, U., Turnbull, J., Dowling, L., Howell, A., Berryman, K. and Wolfe, F. (2019). Geological evidence for past large earthquakes and tsunamis along the Hikurangi subduction margin, New Zealand. *Marine Geology*, 412, pp.139-172.

Clark, K., Nissen, E., Howarth, J., Hamling, I., Mountjoy, J., Ries, W., Jones, K., Goldstien, S., Cochran, U., Villamor, P., Hreinsdóttir, S., Litchfield, N., Mueller, C., Berryman, K. and Strong, D. (2017). Highly variable coastal deformation in the 2016 MW7.8 Kaikōura earthquake reflects rupture complexity along a transpressional plate boundary. *Earth and Planetary Science Letters*, 474, pp.334-344.

Clement, A., Whitehouse, P. and Sloss, C. (2016). An examination of spatial variability in the timing and magnitude of Holocene relative sea-level changes in the New Zealand archipelago. *Quaternary Science Reviews*, 131, pp.73-101.

Cochran, U., Berryman, K., Zachariasen, J., Mildenhall, D., Hayward, B., Southall, K., Hollis, C., Barker, P., Wallace, L., Alloway, B. and Wilson, K. (2006). Paleoecological insights into subduction zone earthquake occurrence, eastern North Island, New Zealand. *Geological Society of America Bulletin*, 118(9-10), pp.1051-1074.

Cochran, U., Hannah, M., Harper, M., Van Dissen, R., Berryman, K. and Begg, J. (2007). Detection of large, Holocene earthquakes using diatom analysis of coastal sedimentary sequences, Wellington, New Zealand. *Quaternary Science Reviews*, 26(7-8), pp.1129-1147.

Cochran, U., Litchfield, N., Clark, K., Reis, W., Villamor, P., Howarth, J., Watson, C. and Strong, D. (2015). *Improved Age Control for a Fourteenth Century Earthquake and Tsunami From Okupe Lagoon, Kapiti Island*. GNS Science Report 2015/28. Lower Hutt (NZ): GNS Science, p.37.

Cotton, C. (1914). Preliminary note on the uplifted east coast of Marlborough. *Transactions and proceedings of the New Zealand Institute*, 46, pp.286–294.

Cowan, H. and McGlone, M. (1991). Late Holocene displacements and characteristic earthquakes on the Hope River segment of the Hope Fault, New Zealand. *Journal of the Royal Society of New Zealand*, 21(4), pp.373-384.

Darby, D. and Beanland, S. (1992). Possible source models for the 1855 Wairarapa Earthquake, New Zealand. *Journal of Geophysical Research*, 97(B9), p.12375.

De Lange, W. and Healy, T. (1986). New Zealand tsunamis 1840–1982. *New Zealand Journal of Geology and Geophysics*, 29(1), pp.115-134.

DeMets, C., Gordon, R., Argus, D. and Stein, S. (1994). Effect of recent revisions to the geomagnetic reversal time scale on estimates of current plate motions. *Geophysical Research Letters*, 21(20), pp.2191-2194.

Dominion Salt Ltd (2019). *About Dominion Salt | Leaders in the World's Most Essential Mineral*. [online] Dominion Salt Limited. Available at: https://www.dominionsalt.co.nz/about-us/ [Accessed 15 Jan. 2019].

Donato, S., Reinhardt, E., Boyce, J., Rothaus, R. and Vosmer, T. (2008). Identifying tsunami deposits using bivalve shell taphonomy. *Geology*, 36(3), p.199.

Doser, D. and Webb, T. (2003). Source parameters of large historical (1917-1961) earthquakes, North Island, New Zealand. *Geophysical Journal International*, 152(3), pp.795-832.

Downes, G., Barberopoulou, A., Cochran, U., Clark, K. and Scheele, F. (2017). The New Zealand Tsunami Database: Historical and Modern Records. *Seismological Research Letters*, 88(2A), pp.342-353.

Dura, T., Engelhart, S., Vacchi, M., Horton, B., Kopp, R., Peltier, W. and Bradley, S. (2016 a). The Role of Holocene Relative Sea-Level Change in Preserving Records of Subduction Zone Earthquakes. *Current Climate Change Reports*, 2(3), pp.86-100.

Dura, T., Hemphill-Haley, E., Sawai, Y. and Horton, B. (2016 b). The application of diatoms to reconstruct the history of subduction zone earthquakes and tsunamis. *Earth-Science Reviews*, 152, pp.181-197.

Eiby, G. (1980). The Marlborough earthquake of 1848. New Zealand Department of Scientific and Industrial Research bulletin 225.

Elvy, W. (1949). *Kaikoura coast: the history, traditions and Māori place-names of Kaikoura*. Christchurch, New Zealand: Hundalee Scenic Board.

Engel, M., Oetjen, J., May, S. and Brückner, H. (2016). Tsunami deposits of the Caribbean – Towards an improved coastal hazard assessment. *Earth-Science Reviews*, 163, pp.260-296.

Fine, I., Rabinovich, A., Bornhold, B., Thomson, R. and Kulikov, E. (2005). The Grand Banks landslide-generated tsunami of November 18, 1929: preliminary analysis and numerical modeling. *Marine Geology*, 215(1-2), pp.45-57.

Fleming, B., Schubert, H., Hertweck, G. and Müller, K. (1992). Bioclastic tidal-channel lag deposits: a genetic model. *Senckenbergiana marit*, [online] 22(3/6), pp.109-129. Available at: https://www.researchgate.net/publication/234842079_Bioclastic_tidal-channel_lag_deposits_a_genetic_model [Accessed 7 Apr. 2019].

Folk, R. (1966). A Review of Grain Size Parameters. *Sedimentology*, 6(2), pp.73-93.

Forman, S. and Polyak, L. (1997). Radiocarbon content of pre-bomb marine mollusks and variations in the14C Reservoir age for coastal areas of the Barents and Kara Seas, Russia. *Geophysical Research Letters*, 24(8), pp.885-888.

Fortin, D., Francus, P., Gebhardt, A., Hahn, A., Kliem, P., Lisé-Pronovost, A., Roychowdhury, R., Labrie, J. and St-Onge, G. (2013). Destructive and non-destructive density determination: method comparison and evaluation from the Laguna Potrok Aike sedimentary record. *Quaternary Science Reviews*, 71, pp.147-153.

Fraser, C., Hill, P. and Allard, M. (2004). Morphology and facies architecture of a falling sea level strandplain, Umiujaq, Hudson Bay, Canada. *Sedimentology*, 52(1), pp.141-160.

Fujii, Y. and Satake, K. (2007). Tsunami Source of the 2004 Sumatra-Andaman Earthquake Inferred from Tide Gauge and Satellite Data. *Bulletin of the Seismological Society of America*, 97(1A), pp.S192-S207.

Fujino, S., Sieh, K., Meltzner, A., Yulianto, E. and Chiang, H. (2014). Ambiguous correlation of precisely dated coral detritus with the tsunamis of 1861 and 1907 at Simeulue Island, Aceh Province, Indonesia. *Marine Geology*, 357, pp.384-391.

Garrett, E., Shennan, I., Woodroffe, S., Cisternas, M., Hocking, E. and Gulliver, P. (2015). Reconstructing paleoseismic deformation, 2: 1000 years of great earthquakes at Chucalén, south central Chile. *Quaternary Science Reviews*, 113, pp.112-122.

GeoNet (2019). *GeoNet Earthquake Stories*. [online] Geonet.org.nz. Available at: https://www.geonet.org.nz/earthquake/story [Accessed 8 Jan. 2019].

Gibb, J.G., 1986. A New Zealand regional Holocene eustatic sea level curve and its application for determination of vertical tectonic movements. Bull. R. Soc. N.Z., 24: 377- 395.

GNS Science (2019). *New Zealand Tsunami Database*. [online] Data.gns.cri.nz. Available at: https://data.gns.cri.nz/tsunami/dataDetails.html?id=466 [Accessed 17 Apr. 2019].

Goff, J., Chagué-Goff, C., Nichol, S., Jaffe, B. and Dominey-Howes, D. (2012). Progress in palaeotsunami research. *Sedimentary Geology*, 243-244, pp.70-88.

Goff, J., McFadgen, B. and Chagué-Goff, C. (2004). Sedimentary differences between the 2002 Easter storm and the 15th-century Okoropunga tsunami, southeastern North Island, New Zealand. *Marine Geology*, 204(1-2), pp.235-250.

Goff, J., Nichol, S. and Kennedy, D. (2009). Development of a palaeotsunami database for New Zealand. *Natural Hazards*, 54(2), pp.193-208.

Google Earth (2019). *Google Earth*. [online] Earth.google.com. Available at: https://earth.google.com/web/ [Accessed 29 Apr. 2019].

Grapes, R. and Downes, G. (1997). The 1855 Wairarapa, New Zealand, earthquake—analysis of historical data. *Bulletin of the New Zealand Society for Earthquake Engineering*, 30, pp.271–368.

Grapes, R. and Holdgate, G. (2014). Earthquake clustering and possible fault interactions across Cook Strait, New Zealand, during the 1848 and 1855 earthquakes. *New Zealand Journal of Geology and Geophysics*, 57(3), pp.312-330.

Grapes, R., Little, T. and Downes, G. (1998). Rupturing of the Awatere Fault during the 1848 October 16 Marlborough earthquake, New Zealand: Historical and present day evidence. *New Zealand Journal of Geology and Geophysics*, 41(4), pp.387-399.

Guilbault, J., Clague, J. and Lapointe, M. (1995). Amount of subsidence during a late Holocene earthquake—evidence from fossil tidal marsh foraminifera at Vancouver Island, west coast of Canada. *Palaeogeography, Palaeoclimatology, Palaeoecology*, 118(1-2), pp.49-71.

Gusman, A., Satake, K. and Harada, T. (2017). Rupture process of the 2016 Wharton Basin strike-slip faulting earthquake estimated from joint inversion of teleseismic and tsunami waveforms. *Geophysical Research Letters*, 44(9), pp.4082-4089.

Gusman, A., Satake, K., Gunawan, E., Hamling, I. and Power, W. (2018). Contribution from Multiple Fault Ruptures to Tsunami Generation During the 2016 Kaikoura Earthquake. *Pure and Applied Geophysics*, 175(8), pp.2557-2574.

Hamling, I., D'Anastasio, E., Wallace, L., Ellis, S., Motagh, M., Samsonov, S., Palmer, N. and Hreinsdóttir, S. (2014). Crustal deformation and stress transfer during a propagating earthquake sequence: The 2013 Cook Strait sequence, central New Zealand. *Journal of Geophysical Research: Solid Earth*, 119(7), pp.6080-6092.

Hamling, I., Hreinsdóttir, S., Clark, K., Elliott, J., Liang, C., Fielding, E., Litchfield, N., Villamor, P., Wallace, L., Wright, T., D'Anastasio, E., Bannister, S., Burbidge, D., Denys, P., Gentle, P., Howarth, J., Mueller, C., Palmer, N., Pearson, C., Power, W., Barnes, P., Barrell, D., Van

Dissen, R., Langridge, R., Little, T., Nicol, A., Pettinga, J., Rowland, J. and Stirling, M. (2017). Complex multifault rupture during the 2016 M w 7.8 Kaikōura earthquake, New Zealand. *Science*, 356(6334), p.eaam7194.

Harbitz, C., Løvholt, F. and Bungum, H. (2014). Submarine landslide tsunamis: how extreme and how likely?. *Natural Hazards*, 72(3), pp.1341-1374.

Hawkes, A., Horton, B., Nelson, A. and Hill, D. (2010). The application of intertidal foraminifera to reconstruct coastal subsidence during the giant Cascadia earthquake of AD 1700 in Oregon, USA. Quaternary International, 221(1-2), pp.116-140.

Hayward, B. (2014 a). "Monospecific" And Near-Monospecific Benthic Foraminiferal Faunas, New Zealand. *The Journal of Foraminiferal Research*, 44(3), pp.300-315.

Hayward, B., Clark, K., Sabaa, A. and Cochran, U. (2015 a). Taphonomically- and infaunally-adjusted salt marsh foraminiferal record of late Holocene earthquake displacements and a tsunami sand, New Zealand. The Journal of Foraminiferal Research, 45(4), pp.354-368.

Hayward, B., Figueira, B., Sabaa, A. and Buzas, M. (2014 b). Multi-year life spans of high salt marsh agglutinated foraminifera from New Zealand. *Marine Micropaleontology*, 109, pp.54-65.

Hayward, B., Grenfell, H., Reid, C. and Hayward, K. (1999). *Recent New Zealand shallow water benthic foraminifera : taxonomy, ecologic distribution, biogeography, and use in paleoenvironmental assessment*. Institute of Geological & Nuclear Sciences monograph 21; New Zealand Geological Survey paleontological bulletin 75. Lower Hutt, Wellington, NZ: Institute of Geological & Nuclear Sciences, p.258.

Hayward, B., Grenfell, H., Sabaa, A., Cochran, U., Clark, K., Wallace, L. and Palmer, A. (2016). Salt-marsh foraminiferal record of 10 large Holocene (last 7500 yr) earthquakes on a subducting plate margin, Hawkes Bay, New Zealand. *Geological Society of America Bulletin*, 128(5-6), pp.896-915.

Hayward, B., Sabaa, A. and Triggs, C. (2019). Using foraminiferal test-size distribution and other methods to recognise Quaternary bathyal turbidites and taphonomically-modified faunas. *Marine Micropaleontology*, 148, pp.65-77.

Hayward, B., Sabaa, A., Grenfell, H., Cochran, U., Clark, K., Litchfield, N., Wallace, L., Marden, M. and Palmer, A. (2015 b). Foraminiferal record of Holocene paleo-earthquakes on the subsiding south-western Poverty Bay coastline, New Zealand. *New Zealand Journal of Geology and Geophysics*, 58(2), pp.104-122.

Heier-Nielsen, S., Conradsen, K., Heinemeier, J., Knudsen, K., Nielsen, H., Rud, N. and Sveinbjörnsdóttir, Á. (1995). Radiocarbon Dating of Shells and Foraminifera from the Skagen Core, Denmark: Evidence of Reworking. *Radiocarbon*, 37(02), pp.119-130.

Hemphill-Haley, E. (1995). *Geological Society of America Bulletin*, 107(3), p.0367.

Hemphill-Haley, E. (1996). Diatoms as an aid in identifying late-Holocene tsunami deposits. *The Holocene*, 6(4), pp.439-448.

Hewitt, J., Thrush, S., Cummings, V. and Pridmore, R. (1996). Matching patterns with processes:predicting the effect of size and mobility on the spatial distributions of the bivalves Macomona liliana and Austrovenus stutchburyi. *Marine Ecology Progress Series*, 135, pp.57-67.

Higham, T. and Hogg, A. (1997). Evidence for Late Polynesian Colonization of New Zealand: University of Waikato Radiocarbon Measurements. *Radiocarbon*, 39(02), pp.149-192.

Higham, T., Anderson, A. and Jacomb, C. (1999). Dating the first New Zealanders: the chronology of Wairau Bar. *Antiquity*, 73(280), pp.420-427.

Higman, B. and Bourgeois, J. (2008). Deposits of The 1992 Nicaragua Tsunami. *Tsunamiites*, pp.81-103.

Hill, E., Yue, H., Barbot, S., Lay, T., Tapponnier, P., Hermawan, I., Hubbard, J., Banerjee, P., Feng, L., Natawidjaja, D. and Sieh, K. (2015). The 2012 M w 8.6 Wharton Basin sequence: A cascade of great earthquakes generated by near-orthogonal, young, oceanic mantle faults. *Journal of Geophysical Research: Solid Earth*, 120(5), pp.3723-3747.

Hogg, A., Fifield, L., Turney, C., Palmer, J., Galbraith, R. and Baille, M. (2006). Dating ancient wood by high-sensitivity liquid scintillation counting and accelerator mass spectrometry—Pushing the boundaries. *Quaternary Geochronology*, 1(4), pp.241-248.

Hogg, A., Higham, T. and Dahm, J. (1997). 14C Dating of Modern Marine and Estuarine Shellfish. *Radiocarbon*, 40(02), pp.975-984.

Hogg, A., Hua, Q., Blackwell, P., Niu, M., Buck, C., Guilderson, T., Heaton, T., Palmer, J., Reimer, P., Reimer, R., Turney, C. and Zimmerman, S. (2013). SHCal13 Southern Hemisphere Calibration, 0–50,000 Years cal BP. *Radiocarbon*, 55(04), pp.1889-1903.

Holden, C., Kaiser, A., Van Dissen, R. and Jury, R. (2013). Sources, ground motion and structural response characteristics in wellington of the 2013 cook strait earthquakes. *Bulletin of the New Zealand Society for Earthquake Engineering*, 46, pp.188-195.

Holden, C., Kaneko, Y., D'Anastasio, E., Benites, R., Fry, B. and Hamling, I. (2017). The 2016 Kaikōura Earthquake Revealed by Kinematic Source Inversion and Seismic Wavefield Simulations: Slow Rupture Propagation on a Geometrically Complex Crustal Fault Network. *Geophysical Research Letters*, 44(22), pp.11,320-11,328.

Horton, B. (1999). The distribution of contemporary intertidal foraminifera at Cowpen Marsh, Tees Estuary, UK: implications for studies of Holocene sea-level changes. Palaeogeography, Palaeoclimatology, Palaeoecology, 149(1-4), pp.127-149.

Hull, A. (1990). Tectonics of the 1931 Hawke's Bay earthquake. *New Zealand Journal of Geology and Geophysics*, 33(2), pp.309-320.

Ishimura, D. (2017). Re-examination of the age of historical and paleo-tsunami deposits at Koyadori on the Sanriku Coast, Northeast Japan. *Geoscience Letters*, 4(1).

Ishizawa, T., Goto, K., Yokoyama, Y., Miyairi, Y., Sawada, C. and Takada, K. (2018). Reducing the age range of tsunami deposits by 14C dating of rip-up clasts. *Sedimentary Geology*, 364, pp.334-341.

Juggins, S. (2010). *C2 Software for Ecological and Palaeoecological Analysis and Visualisation*. Newcastle-upon-Tyne: Department of Geography, University of Newcastle.

Kanamori, H. (1977). The energy release in great earthquakes. *Journal of Geophysical Research*, 82(20), pp.2981-2987.

Kaneko, Y., Hamling, I., Van Dissen, R., Motagh, M. and Samsonov, S. (2015). InSAR imaging of displacement on flexural-slip faults triggered by the 2013Mw6.6 Lake Grassmere earthquake, central New Zealand. *Geophysical Research Letters*, 42(3), pp.781-788.

Kearse, J., Little, T., Van Dissen, R., Barnes, P., Langridge, R., Mountjoy, J., Ries, W., Villamor, P., Clark, K., Benson, A., Lamarche, G., Hill, M. and Hemphill- Haley, M. (2018). Onshore to Offshore Ground- Surface and Seabed Rupture of the Jordan–Kekerengu–Needles Fault Network during the 2016 Mw 7.8 Kaikōura Earthquake, New Zealand. *Bulletin of the Seismological Society of America*, 108(3B), pp.1573-1595.

Kelsey, H., Engelhart, S., Pilarczyk, J., Horton, B., Rubin, C., Daryono, M., Ismail, N., Hawkes, A., Bernhardt, C. and Cahill, N. (2015). Accommodation space, relative sea level, and the archiving of paleo-earthquakes along subduction zones. *Geology*, 43(8), pp.675-678.

Kelsey, H., Witter, R., Engelhart, S., Briggs, R., Nelson, A., Haeussler, P. and Corbett, D. (2015). Beach ridges as paleoseismic indicators of abrupt coastal subsidence during subduction zone earthquakes, and implications for Alaska-Aleutian subduction zone paleoseismology, southeast coast of the Kenai Peninsula, Alaska. *Quaternary Science Reviews*, 113, pp.147-158.

Kidwell, S. (1986). Models for fossil concentrations: paleobiologic implications. *Paleobiology*, 12(01), pp.6-24.

Kidwell, S. (1991). The stratigraphy of shell concentrations. In: P. Allison and D. Briggs, ed., *Taphonomy: Releasing the Data Locked in the Fossil Record*. Plenum Press: New York, pp.211-290.

King, D. (2015). Tsunami hazard, assessment and risk in Aotearoa–New Zealand: A systematic review AD 1868–2012. *Earth-Science Reviews*, 145, pp.25-42.

King, D. and Goff, J. (2010). Benefitting from differences in knowledge, practice and belief: Māori oral traditions and natural hazards science. *Natural Hazards and Earth System Science*, 10(9), pp.1927-1940.

King, D., Goff, J., Chagué-Goff, C., McFadgen, B., Jacobsen, G., Gadd, P. and Horrocks, M. (2017). Reciting the layers: Evidence for past tsunamis at Mataora-Wairau Lagoon, Aotearoa-New Zealand. *Marine Geology*, 389, pp.1-16.

Kitamura, A., Ito, M., Ikuta, R. and Ikeda, M. (2018 a). Using molluscan assemblages from paleotsunami deposits to evaluate the influence of topography on the magnitude of late

Holocene mega-tsunamis on Ishigaki Island, Japan. *Progress in Earth and Planetary Science*, 5(1).

Kitamura, A., Ito, M., Sakai, S., Yokoyama, Y. and Miyairi, Y. (2018 b). Identification of tsunami deposits using a combination of radiometric dating and oxygen-isotope profiles of articulated bivalves. *Marine Geology*, 403, pp.57-61.

Kluyver, T., Ragan-Kelley, B., Pérez, F., Granger, B., Bussonnier, M., Frederic, J., Kelley, K., Hamrick, J., Grout, J., Corlay, S., Ivanov, P., Avila, D., Abdalla, A. and Willing, C. (2016). Jupyter Notebooks – a publishing format for reproducible computational workflows. In: *Positioning and Power in Academic Publishing: Players, Agents and Agendas*. [online] IOS Press, pp.87-90. Available at: http://ebooks.iospress.nl/publication/42900 [Accessed 6 Jan. 2019].

Kortekaas, S. and Dawson, A. (2007). Distinguishing tsunami and storm deposits: An example from Martinhal, SW Portugal. *Sedimentary Geology*, 200(3-4), pp.208-221.

Koshimura, S., Mofjeld, H., González, F. and Moore, A. (2002). Modeling the 1100 bp paleotsunami in Puget Sound, Washington. *Geophysical Research Letters*, 29(20), pp.9-1-9-4.

Kumar, P., Saraswati, P. and Banerjee, S. (2009). Early Miocene shell concentration in the mixed carbonate-siliciclastic system of Kutch and their distribution in sequence stratigraphic framework. *Journal of the Geological Society of India*, 74(4), pp.432-444.

Lane, E., Mountjoy, J., Power, W. and Mueller, C. (2016). Probabilistic Hazard of Tsunamis Generated by Submarine Landslides in the Cook Strait Canyon (New Zealand). *Pageoph Topical Volumes*, pp.3757-3774.

Langridge, R., Van Dissen, R., Cochran, U., Litchfield, N., Berryman, K., Begg, J., Villamor, P., Nicol, A., Townsend, D. and Heron, D. (2005). Active Faulting And Paleoearthquakes In The Wairarapa And Wellington Regions. In: *The 1855 Wairarapa Earthquake Symposium - Proceedings Volume*. [online] Wellington: Greater Wellington Regional Council, pp.49-59. Available at: http://www.gw.govt.nz/assets/council-publications/the_1855_wairarapa_earthquake_symposium_proceedings_volume_web_version.pdf#page=59 [Accessed 7 Jan. 2019].

Langridge, R., Van Dissen, R., Rhoades, D., Villamor, P., Little, T., Litchfield, N., Clark, K. and Clark, D. (2011). Five Thousand Years of Surface Ruptures on the Wellington Fault, New Zealand: Implications for Recurrence and Fault Segmentation. *Bulletin of the Seismological Society of America*, 101(5), pp.2088-2107.

Leapfrog (2018). *Leapfrog Geo 3D software*. Seequent Limited.

Linick, T., Damon, P., Donahue, D. and Jull, A. (1989). Accelerator mass spectrometry: The new revolution in radiocarbon dating. *Quaternary International*, 1, pp.1-6.

LINZ (2019). *Tide predictions - Cape Campbell*. [online] Land Information New Zealand (LINZ). Available at: https://www.linz.govt.nz/docs/hydro/tidal-info/tide-tables/sec-ports/lyttelton.pdf [Accessed 10 Jan. 2019].

Litchfield, N., van Dissen, R., Hemphill-Haley, M., Townsend, D. and Heron, D. (2010). Post c. 300 year rupture of the Ohariu Fault in Ohariu Valley, New Zealand. *New Zealand Journal of Geology and Geophysics*, 53(1), pp.43-56.

Litchfield, N., Van Dissen, R., Sutherland, R., Barnes, P., Cox, S., Norris, R., Beavan, R., Langridge, R., Villamor, P., Berryman, K., Stirling, M., Nicol, A., Nodder, S., Lamarche, G., Barrell, D., Pettinga, J., Little, T., Pondard, N., Mountjoy, J. and Clark, K. (2013). A model of active faulting in New Zealand. *New Zealand Journal of Geology and Geophysics*, 57(1), pp.32-56.

Little, T., Grapes, R. and Berger, G. (1998). *Geological Society of America Bulletin*, 110(2), p.0127.

Little, T., Van Dissen, R., Kearse, J., Norton, K., Benson, A. and Wang, N. (2018). Kekerengu Fault, New Zealand: Timing and Size of Late Holocene Surface Ruptures. *Bulletin of the Seismological Society of America*, 108(3B), pp.1556-1572.

Little, T., Van Dissen, R., Schermer, E. and Carne, R. (2009). Late Holocene surface ruptures on the southern Wairarapa fault, New Zealand: Link between earthquakes and the uplifting of beach ridges on a rocky coast. *Lithosphere*, 1(1), pp.4-28.

Lowe, D. and de Lange, W. (2000). Volcano-meteorological tsunamis, thec. AD 200 Taupo eruption (New Zealand) and the possibility of a global tsunami. *The Holocene*, 10(3), pp.401-407.

Mannen, K., Yoong, K., Suzuki, S., Matsushima, Y., Ota, Y., Kain, C. and Goff, J. (2018). History of ancient megathrust earthquakes beneath metropolitan Tokyo inferred from coastal lowland deposits. *Sedimentary Geology*, 364, pp.258-272.

Marsden, I. (2004). Effects of reduced salinity and seston availability on growth of the New Zealand little-neck clam Austrovenus stutchburyi. *Marine Ecology Progress Series*, 266, pp.157-171.

Mason, D. and Little, T. (2006). Refined slip distribution and moment magnitude of the 1848 Marlborough earthquake, Awatere Fault, New Zealand. *New Zealand Journal of Geology and Geophysics*, 49(3), pp.375-382.

McCaffrey, R. (2008). Global frequency of magnitude 9 earthquakes. *Geology*, 36(3), p.263.

McFadgen, B. G. (1982). Dating New Zealand archaeology by radiocarbon. New Zealand Journal of Science 25, 379–392.

McFadgen, B., Bagley, S. and Mosen, J. (1996). *Late Holocene geology and archaeology of a small dune system on the eastern shore of Lake Grassmere*. A report to the Department of Conservation on the significance of archaeological remains and subfossil bird bone deposits found in the dunes. Department of Conservation.

McGranahan, G., Balk, D. and Anderson, B. (2007). The rising tide: assessing the risks of climate change and human settlements in low elevation coastal zones. *Environment and Urbanization*, 19(1), pp.17-37.

McSaveney, M., Graham, I., Begg, J., Beu, A., Hull, A., Kim, K. and Zondervan, A. (2006). Late Holocene uplift of beach ridges at Turakirae Head, south Wellington coast, New Zealand. *New Zealand Journal of Geology and Geophysics*, 49(3), pp.337-358.

Morales, J., Borrego, J., San Miguel, E., López-González, N. and Carro, B. (2008). Sedimentary record of recent tsunamis in the Huelva Estuary (southwestern Spain). *Quaternary Science Reviews*, 27(7-8), pp.734-746.

Mori, N., Takahashi, T., Yasuda, T. and Yanagisawa, H. (2011). Survey of 2011 Tohoku earthquake tsunami inundation and run-up. *Geophysical Research Letters*, 38(7), p.n/a-n/a.

Morton, R., Gelfenbaum, G. and Jaffe, B. (2007). Physical criteria for distinguishing sandy tsunami and storm deposits using modern examples. *Sedimentary Geology*, 200(3-4), pp.184-207.

Mountjoy, J., Howarth, J., Orpin, A., Barnes, P., Bowden, D., Rowden, A., Schimel, A., Holden, C., Horgan, H., Nodder, S., Patton, J., Lamarche, G., Gerstenberger, M., Micallef, A., Pallentin, A. and Kane, T. (2018). Earthquakes drive large-scale submarine canyon development and sediment supply to deep-ocean basins. *Science Advances*, 4(3), p.eaar3748.

Mountjoy, J., Micallef, A., Stevens, C. and Stirling, M. (2014). Holocene sedimentary activity in a non-terrestrially coupled submarine canyon: Cook Strait Canyon system, New Zealand. *Deep Sea Research Part II: Topical Studies in Oceanography*, 104, pp.120-133.

Mueller, C., Mountjoy, J., Power, W., Lane, E. and Wang, X. (2016). Towards a Spatial Probabilistic Submarine Landslide Hazard Model for Submarine Canyons. *Submarine Mass Movements and their Consequences*, pp.589-597.

Murray, J. (2006). *Ecology and applications of benthic foraminifera*. Cambridge: Cambridge University Press.

Murray, J. (2011). *Ecology and palaeoecology of benthic foraminifera*. Harlow, Essex: Longman.

Nakamura, M. (2009). Fault model of the 1771 Yaeyama earthquake along the Ryukyu Trench estimated from the devastating tsunami. *Geophysical Research Letters*, 36(19).

Nanayama, F., Shigeno, K., Satake, K., Shimokawa, K., Koitabashi, S., Miyasaka, S. and Ishii, M. (2000). Sedimentary differences between the 1993 Hokkaido-nansei-oki tsunami and the 1959 Miyakojima typhoon at Taisei, southwestern Hokkaido, northern Japan. *Sedimentary Geology*, 135(1-4), pp.255-264.

Nelson, A. (1992). Discordant 14C Ages from Buried Tidal-Marsh Soils in the Cascadia Subduction Zone, Southern Oregon Coast. *Quaternary Research*, 38(01), pp.74-90.

Nelson, A. and Manley, W. (1992). Holocene coseismic and aseismic uplift of Isla Mocha, south-central Chile. *Quaternary International*, 15-16, pp.61-76.

Nelson, A., Shennan, I. and Long, A. (1996). Identifying coseismic subsidence in tidal-wetland stratigraphic sequences at the Cascadia subduction zone of western North America. *Journal of Geophysical Research: Solid Earth*, 101(B3), pp.6115-6135.

Neumann, B., Vafeidis, A., Zimmermann, J. and Nicholls, R. (2015). Future Coastal Population Growth and Exposure to Sea-Level Rise and Coastal Flooding - A Global Assessment. *PLOS ONE*, 10(3), p.e0118571.

New Zealand Palaeotsunami Database. (2017). *New Zealand Palaeotsunami Database*. [online] Available at: https://ptdb.niwa.co.nz/#!/db/270?out=map&map=control&colorby=validity&view=-42.0483|173.9671|10||1180|824 [Accessed 9 May 2018].

Nicol, A. and Beavan, J. (2003). Shortening of an overriding plate and its implications for slip on a subduction thrust, central Hikurangi Margin, New Zealand. *Tectonics*, 22(6), p.n/a-n/a.

Nicol, A. and Dissen, R. (2018). A 6000-year record of surface-rupturing paleoearthquakes on the Wairau Fault, New Zealand. *New Zealand Journal of Geology and Geophysics*, 61(3), pp.341-358.

Nicol, A., van Dissen, R., Robinson, R. and Harvison, A. (2012). *Variability in single event slip and recurrence intervals for large paleoeartquakes on New Zealands active faults*. GNS Science Report 2012/41. [online] GNS Science, p.17. Available at: https://www.eqc.govt.nz/sites/public_files/3774-single-event-slip-recurrence-intervals-nz-faults.pdf [Accessed 24 Feb. 2019].

Orsi, T., Edwards, C. and Anderson, A. (1994). X-ray computed tomography; a nondestructive method for quantitative analysis of sediment cores. *Journal of Sedimentary Research*, 64(3a), pp.690-693.

Ota, Y., Berryman, K., Hull, A., Miyauchi, T. and Iso, N. (1988). Age and height distribution of holocene transgressive deposits in eastern North Island, New Zealand. *Palaeogeography, Palaeoclimatology, Palaeoecology*, 68(2-4), pp.135-151.

Ota, Y., Brown, L., Berryman, K., Fujimori, T., Miyauchi, T., Beu, A., Kashima, K. and Taguchi, K. (1995). Vertical tectonic movement in northeastern Marlborough: Stratigraphic, radiocarbon, and paleoecological data from Holocene estuaries. *New Zealand Journal of Geology and Geophysics*, 38(3), pp.269-282.

Peters, R. and Jaffe, B. (2010). Identification of tsunami deposits in the geologic record; developing criteria using recent tsunami deposits. *U.S. Geological Survey - Open-File Report*, 2010-1239.

Peterson, C., Carver, G., Cruikshank, K., Abramson, H., Garrison-Laney, C. and Dengler, L. (2011). Evaluation of the use of paleotsunami deposits to reconstruct inundation distance and runup heights associated with prehistoric inundation events, Crescent City, southern Cascadia margin. *Earth Surface Processes and Landforms*, 36(7), pp.967-980.

Pickrill, R. (1977). Coastal processes, beach morphology, and sediments along the north-east coast of the South Island, New Zealand. *New Zealand Journal of Geology and Geophysics*, 20(1), pp.1-15.

Pilarczyk, J. and Reinhardt, E. (2012). Homotrema rubrum (Lamarck) taphonomy as an overwash indicator in Marine Ponds on Anegada, British Virgin Islands. Natural Hazards, 63(1), pp.85-100.

Pilarczyk, J., Dura, T., Horton, B., Engelhart, S., Kemp, A. and Sawai, Y. (2014). Microfossils from coastal environments as indicators of paleo-earthquakes, tsunamis and storms. Palaeogeography, Palaeoclimatology, Palaeoecology, 413, pp.144-157.

Plater, A. and Shennan, I. (1992). Evidence of Holocene sea-level change from the Northumberland coast, eastern England. *Proceedings of the Geologists' Association*, 103, pp.201-216.

Polet, J. and Kanamori, H. (2000). Shallow subduction zone earthquakes and their tsunamigenic potential. *Geophysical Journal International*, 142(3), pp.684-702.

Pondard, N. and Barnes, P. (2010). Structure and paleoearthquake records of active submarine faults, Cook Strait, New Zealand: Implications for fault interactions, stress loading, and seismic hazard. *Journal of Geophysical Research*, 115(B12).

Power, W. (2013). *Review of Tsunami Hazard in New Zealand (2013 Update)*. GNS Science Consultancy Report 2013/131.

Power, W., Clark, K., King, D., Borrero, J., Howarth, J., Lane, E., Goring, D., Goff, J., Chagué-Goff, C., Williams, J., Reid, C., Whittaker, C., Mueller, C., Williams, S., Hughes, M., Hoyle, J., Bind, J., Strong, D., Litchfield, N. and Benson, A. (2017). Tsunami runup and tide-gauge observations from the 14 November 2016 M7.8 Kaikōura earthquake, New Zealand. *Pure and Applied Geophysics*, 174(7), pp.2457-2473.

Power, W., Downes, G. and Stirling, M. (2007). Estimation of Tsunami Hazard in New Zealand due to South American Earthquakes. *Pure and Applied Geophysics*, 164, pp.547-564.

Power, W., Kaneko, Y., Becker, J., Yin, S., Holden, C. and Mueller, C. (2018). *Hikurangi Response Plan - Developing a scenario for an Mw 8.9 Hikurangi earthquake, including tsunami modelling and preliminary description of impacts*. GNS Science consultancy report; 2018/168. Lower Hutt (NZ): GNS Science, p.39.

Power, W., Mountjoy, J., Lane, E., Popinet, S. and Wang, X. (2016 a). Assessing landslide-tsunami hazard in submarine canyons, using the Cook strait canyon system as an example. *Journal of Tsunami Society International*, 35(3), p.145.

Power, W., Reyners, M. and Wallace, L. (2008). Tsunami hazard posed by earthquakes on the Hikurangi subduction zone interface. *GNS Science Consultancy Report 2008/40, EQC Project 06/521*.

Power, W., Wallace, L., Mueller, C., Henrys, S., Clark, K., Fry, B., Wang, X. and Williams, C. (2016 b). Understanding the potential for tsunami generated by earthquakes on the

southern Hikurangi subduction interface. *New Zealand Journal of Geology and Geophysics*, 59(1), pp.70-85.

Priest, G., Witter, R., Zhang, Y., Goldfinger, C., Wang, K. and Allan, J. (2017). New constraints on coseismic slip during southern Cascadia subduction zone earthquakes over the past 4600 years implied by tsunami deposits and marine turbidites. *Natural Hazards*, 88(1), pp.285-313.

Purchase, N. and Fergusson, J. (1986). Chione (austrovenus) stutchburyi, a New Zealand cockle, as a Bio-indicator for lead pollution. *Environmental Pollution Series B, Chemical and Physical*, 11(2), pp.137-151.

Putra, P. (2018). Tsunami sediments and their grain size characteristics. *IOP Conference Series: Earth and Environmental Science*, 118(12035).

Rattenbury, M.S., Townsend, D.B., Johnston, M.R. (compilers) 2006: Geology of the Kaikoura area. Institute of Geological & Nuclear Sciences 1:250 000 geological map 13. 1 sheet + 70p. Lower Hutt, New Zealand. GNS Science

Reed, D. (1995). The response of coastal marshes to sea-level rise: Survival or submergence?. *Earth Surface Processes and Landforms*, 20(1), pp.39-48.

Reid, J. (2019). *Lake Grassmere before 1940*. [online] Teara.govt.nz. Available at: https://teara.govt.nz/en/photograph/4329/lake-grassmere-before-1940 [Accessed 29 Apr. 2019].

Reimer, P., Bard, E., Bayliss, A., Beck, J., Blackwell, P., Ramsey, C., Buck, C., Cheng, H., Edwards, R., Friedrich, M., Grootes, P., Guilderson, T., Haflidason, H., Hajdas, I., Hatté, C., Heaton, T., Hoffmann, D., Hogg, A., Hughen, K., Kaiser, K., Kromer, B., Manning, S., Niu, M., Reimer, R., Richards, D., Scott, E., Southon, J., Staff, R., Turney, C. and van der Plicht, J. (2013). IntCal13 and Marine13 Radiocarbon Age Calibration Curves 0–50,000 Years cal BP. *Radiocarbon*, 55(04), pp.1869-1887.

Reinhardt, E., Goodman, B., Boyce, J., Lopez, G., van Hengstum, P., Rink, W., Mart, Y. and Raban, A. (2006). The tsunami of 13 December A.D. 115 and the destruction of Herod the Great's harbor at Caesarea Maritima, Israel. *Geology*, 34(12), p.1061.

Reinhardt, E., Pilarczyk, J. and Brown, A. (2012). Probable tsunami origin for a Shell and Sand Sheet from marine ponds on Anegada, British Virgin Islands. *Natural Hazards*, 63(1), pp.101-117.

Renter, J. (1989). Applications of computerized tomography in sedimentology. *Marine Geotechnology*, 8(3), pp.201-211.

Reyners, M. (1998). Plate coupling and the hazard of large subduction thrust earthquakes at the Hikurangi subduction zone, New Zealand. *New Zealand Journal of Geology and Geophysics*, 41(4), pp.343-354.

Rozanski, K., Stichler, W., Gonfiantini, R., Scott, E., Beukens, R., Kromer, B. and Van Der Plicht, J. (1992). The IAEA 14C Intercomparison Exercise 1990. *Radiocarbon*, 34(03), pp.506-519.

Sakuna-Schwartz, D., Feldens, P., Schwarzer, K., Khokiattiwong, S. and Stattegger, K. (2015). Internal structure of event layers preserved on the Andaman Sea continental shelf, Thailand: tsunami vs. storm and flash-flood deposits. *Natural Hazards and Earth System Sciences*, 15(6), pp.1181-1199.

Satake, K., Nanayama, F. and Yamaki, S. (2008). Fault models of unusual tsunami in the 17th century along the Kuril trench. *Earth, Planets and Space*, 60(9), pp.925-935.

Sawai, Y., Kamataki, T., Shishikura, M., Nasu, H., Okamura, Y., Satake, K., Thomson, K., Matsumoto, D., Fujii, Y., Komatsubara, J. and Aung, T. (2009). Aperiodic recurrence of geologically recorded tsunamis during the past 5500 years in eastern Hokkaido, Japan. *Journal of Geophysical Research: Solid Earth*, 114(B1).

Schallenberg, M., Goff, J. and Harper, M. (2012). Gradual, catastrophic and human induced environmental changes from a coastal lake, southern New Zealand. *Sedimentary Geology*, 273-274, pp.48-57.

Schellart, W. (2008). Overriding plate shortening and extension above subduction zones: A parametric study to explain formation of the Andes Mountains. *Geological Society of America Bulletin*, 120(11-12), pp.1441-1454.

Schellart, W. and Rawlinson, N. (2013). Global correlations between maximum magnitudes of subduction zone interface thrust earthquakes and physical parameters of subduction zones. *Physics of the Earth and Planetary Interiors*, 225, pp.41-67.

Schermer, E., Little, T. and Rieser, U. (2009). Quaternary deformation along the Wharekauhau fault system, North Island, New Zealand: Implications for an unstable linkage between active strike-slip and thrust faults. *Tectonics*, 28(6), p.n/a-n/a.

Scott, D. and Medioli, F. (1980). *Quantitative studies of marsh foraminiferal distributions in Nova Scotia*. 1st ed. Washington, D.C.: Cushman Foundation for Foraminiferal Research, p.58.

Scott, G. (1961). Foraminifera from an alternating sequence, Eketahuna, New Zealand. *New Zealand Journal of Geology and Geophysics*, 4(1), pp.73-88.

Senatorski, P. (2017). Effect of slip-area scaling on the earthquake frequency-magnitude relationship. *Physics of the Earth and Planetary Interiors*, 267, pp.41-52.

Shanmugam, G. (2011). Process-sedimentological challenges in distinguishing paleo-tsunami deposits. *Natural Hazards*, 63(1), pp.5-30.

Shaw, B., Ambraseys, N., England, P., Floyd, M., Gorman, G., Higham, T., Jackson, J., Nocquet, J., Pain, C. and Piggott, M. (2008). Eastern Mediterranean tectonics and tsunami hazard inferred from the AD 365 earthquake. *Nature Geoscience*, 1(4), pp.268-276.

Shennan, I. and Hamilton, S. (2006). Coseismic and pre-seismic subsidence associated with great earthquakes in Alaska. *Quaternary Science Reviews*, 25(1-2), pp.1-8.

Shennan, I., Bruhn, R. and Plafker, G. (2009). Multi-segment earthquakes and tsunami potential of the Aleutian megathrust. *Quaternary Science Reviews*, 28(1-2), pp.7-13.

Shennan, I., Garrett, E. and Barlow, N. (2016). Detection limits of tidal-wetland sequences to identify variable rupture modes of megathrust earthquakes. *Quaternary Science Reviews*, 150, pp.1-30.

Shennan, I., Long, A., Rutherford, M., Green, F., Innes, J., Lloyd, J., Zong, Y. and Walker, K. (1996). Tidal marsh stratigraphy, sea-level change and large earthquakes, i: a 5000 year record in washington, U.S.A. *Quaternary Science Reviews*, 15(10), pp.1023-1059.

Shennan, I., Long, A., Rutherford, M., Green, F., Innes, J., Lloyd, J., Zong, Y. and Walker, K. (1996). Tidal marsh stratigraphy, sea-level change and large earthquakes, i: a 5000 year record in Washington, U.S.A. *Quaternary Science Reviews*, 15(10), pp.1023-1059.

Shennan, I., Scott, D., Rutherford, M. and Zong, Y. (1999). Microfossil analysis of sediments representing the 1964 earthquake, exposed at Girdwood Flats, Alaska, USA. *Quaternary International*, 60(1), pp.55-73.

Sieh, K., Natawidjaja, D., Meltzner, A., Shen, C., Cheng, H., Li, K., Suwargadi, B., Galetzka, J., Philibosian, B. and Edwards, R. (2008). Earthquake Supercycles Inferred from Sea-Level Changes Recorded in the Corals of West Sumatra. *Science*, 322(5908), pp.1674-1678.

Stanley, D. and Blanchard, L. (1967). Scanning of long unsplit cores by X-radiography. *Deep Sea Research and Oceanographic Abstracts*, 14(3), pp.379-IN12.

Stuiver, M. and Polach, H. (1977). Discussion Reporting of 14C Data. *Radiocarbon*, 19(03), pp.355-363.

Szczuciński, W. (2013). Limitations of tsunami deposits identification - problem of sediment sources, sedimentary environments and processes, and post-depositional changes. In: *4th International INQUA Meeting on Paleoseismology, Active Tectonics and Archeoseismology (PATA), 9-14 October 2013*. Paleoseismicity.org.

Szczuciński, W., Kokociński, M., Rzeszewski, M., Chagué-Goff, C., Cachão, M., Goto, K. and Sugawara, D. (2012 a). Sediment sources and sedimentation processes of 2011 Tohoku-oki tsunami deposits on the Sendai Plain, Japan — Insights from diatoms, nannoliths and grain size distribution. *Sedimentary Geology*, 282, pp.40-56.

Szczuciński, W., Rosser, N., Strzelecki, M., Long, A., Lawrence, T., Buchwal, A., Chague-Goff, C. and Woodroffe, S. (2012 b). Sedimentary Record and Morphological Effects of a Landslide-Generated Tsunami in a Polar Region: The 2000 AD Tsunami in Vaigat Strait, West Greenland. *American Geophysical Union (AGU) Fall Meeting, San Francisco*, ID: 1479941.

Tamura, T. (2012). Beach ridges and prograded beach deposits as palaeoenvironment records. *Earth-Science Reviews*, 114(3-4), pp.279-297.

Tamura, T., Nicholas, W., Oliver, T. and Brooke, B. (2018). Coarse-sand beach ridges at Cowley Beach, north-eastern Australia: Their formative processes and potential as records of tropical cyclone history. *Sedimentology*, 65(3), pp.721-744.

Tappin, D., Watts, P. and Grilli, S. (2008). The Papua New Guinea tsunami of 17 July 1998: anatomy of a catastrophic event. *Natural Hazards and Earth System Sciences*, 8(2), pp.243-266.

Thatcher, W. (1984). The earthquake deformation cycle at the Nankai Trough, southwest Japan. *Journal of Geophysical Research: Solid Earth*, 89(B5), pp.3087-3101.

Thompson, T. and Baedke, S. (1995). Beach-ridge development in Lake Michigan: shoreline behavior in response to quasi-periodic lake-level events. *Marine Geology*, 129(1-2), pp.163-174.

Titov, V., Mofjeld, H., Thomson, R. and Gonzalez, F. (2005). The Global Reach of the 26 December 2004 Sumatra Tsunami. *Science*, 309(5743), pp.2045-2048.

Townsend, D. and Little, T. (1998). Pliocene- Quaternary deformation and mechanisms of near-surface strain close to the eastern tip of the Clarence Fault, northeast Marlborough, New Zealand. *New Zealand Journal of Geology and Geophysics*, 41(4), pp.401-417.

Troels-Smith, J. (1955). Karakterisering af lose jordarter. Characterization of unconsolidated sediments. *Geological Survey of Denmark*, 3(10).

Turnbull, J. (10 Decemeber 2018). Personal Communication.

Tuttle, M., Ruffman, A., Anderson, T. and Jeter, H. (2004). Distinguishing Tsunami from Storm Deposits in Eastern North America: The 1929 Grand Banks Tsunami versus the 1991 Halloween Storm. *Seismological Research Letters*, 75(1), pp.117-131.

van Dissen, R. and Nicol, A. (2009). Mid- late Holocene paleoseismicity of the eastern Clarence Fault, Marlborough, New Zealand. *New Zealand Journal of Geology and Geophysics*, 52(3), pp.195-208.

van Dissen, R. and Yeats, R. (1991). Hope fault, Jordan thrust, and uplift of the Seaward Kaikoura Range, New Zealand. *Geology*, 19(4), p.393.

van Dissen, R., McSaveney, M., Townsend, D., Hancox, G., Little, T., Reis, W., Perrin, N., Archibald, G., Dellow, G., Massey, C. and Misra, S. (2014). Landslides and liquefaction generated by the Cook Strait and Lake Grassmere earthquakes: A reconnaissance report. *Bulletin of the New Zealand Society for Earthquake Engineering*, 64, pp.196-200.

Wacker, L., Lippold, J., Molnár, M. and Schulz, H. (2013). Towards radiocarbon dating of single foraminifera with a gas ion source. *Nuclear Instruments and Methods in Physics Research Section B: Beam Interactions with Materials and Atoms*, 294, pp.307-310.

Wallace, L. and Beavan, J. (2010). Diverse slow slip behavior at the Hikurangi subduction margin, New Zealand. *Journal of Geophysical Research*, 115(B12).

Wallace, L., Barnes, P., Beavan, J., Van Dissen, R., Litchfield, N., Mountjoy, J., Langridge, R., Lamarche, G. and Pondard, N. (2012 a). (A) The kinematics of a transition from subduction

to strike-slip: An example from the central New Zealand plate boundary. *Journal of Geophysical Research: Solid Earth*, 117(B2), p.n/a-n/a.

Wallace, L., Beavan, J., Bannister, S. and Williams, C. (2012 b). Simultaneous long-term and short-term slow slip events at the Hikurangi subduction margin, New Zealand: Implications for processes that control slow slip event occurrence, duration, and migration. *Journal of Geophysical Research: Solid Earth*, 117(B11), p.n/a-n/a.

Wallace, L., Beavan, J., McCaffrey, R. and Darby, D. (2004). Subduction zone coupling and tectonic block rotations in the North Island, New Zealand. *Journal of Geophysical Research*, 109(B12).

Wallace, L., Cochran, U., Power, W. and Clark, K. (2014). Earthquake and Tsunami Potential of the Hikurangi Subduction Thrust, New Zealand: Insights from Paleoseismology, GPS, and Tsunami Modeling. *Oceanography*, 27(2), pp.104-117.

Wallace, L., Hreinsdóttir, S., Ellis, S., Hamling, I., D'Anastasio, E. and Denys, P. (2018). Triggered Slow Slip and Afterslip on the Southern Hikurangi Subduction Zone Following the Kaikōura Earthquake. *Geophysical Research Letters*, 45(10), pp.4710-4718.

Wallace, L., Reyners, M., Cochran, U., Bannister, S., Barnes, P., Berryman, K., Downes, G., Eberhart-Phillips, D., Fagereng, A., Ellis, S., Nicol, A., McCaffrey, R., Beavan, R., Henrys, S., Sutherland, R., Barker, D., Litchfield, N., Townend, J., Robinson, R., Bell, R., Wilson, K. and Power, W. (2009). Characterizing the seismogenic zone of a major plate boundary subduction thrust: Hikurangi Margin, New Zealand. *Geochemistry, Geophysics, Geosystems*, 10(10).

Walrond, C. (2006). *Salt - Early industry at Lake Grassmere*. [online] Te Ara - the Encyclopedia of New Zealand. Available at: https://teara.govt.nz/en/photograph/4329/lake-grassmere-before-1940 [Accessed 11 Dec. 2018].

Wang, T., Wei, S., Shi, X., Qiu, Q., Li, L., Peng, D., Weldon, R. and Barbot, S. (2018). The 2016 Kaikōura earthquake: Simultaneous rupture of the subduction interface and overlying faults. *Earth and Planetary Science Letters*, 482, pp.44-51.

Wang, X. and Liu, P. (2006). An analysis of 2004 Sumatra earthquake fault plane mechanisms and Indian Ocean tsunami. *Journal of Hydraulic Research*, 44(2), pp.147-154.

Wang, X. and Power, W. (2011). *COMCOT : a tsunami generation, propagation and run-up model*. GNS Science Report 2011/43. [online] Lower Hutt, NZ: GNS Science, p.121. Available at: https://shop.gns.cri.nz/sr_2011-043-pdf/ [Accessed 7 May 2018].

Williams, C., Eberhart-Phillips, D., Bannister, S., Barker, D., Henrys, S., Reyners, M. and Sutherland, R. (2013). Revised Interface Geometry for the Hikurangi Subduction Zone, New Zealand. *Seismological Research Letters*, 84(6), pp.1066-1073.

Witter, R., Kelsey, H. and Hemphill-Haley, E. (2003). Great Cascadia earthquakes and tsunamis of the past 6700 years, Coquille River estuary, southern coastal Oregon. *Geological Society of America Bulletin*, 115(10), p.1289.

Witter, R., Zhang, Y., Wang, K., Goldfinger, C., Priest, G. and Allan, J. (2012). Coseismic slip on the southern Cascadia megathrust implied by tsunami deposits in an Oregon lake and earthquake-triggered marine turbidites. *Journal of Geophysical Research: Solid Earth*, 117(B10).

Worthy, T. (1998). A remarkable fossil and archaeological avifauna from Marfells Beach, Lake Grassmere, South Island, New Zealand. *Records of the Canterbury Museum*, 12(1), pp.79-176.

Yeats, R., Sieh, K. and Allen, C. (1997). *The geology of earthquakes*. New York: Oxford University Press, p.568.

Zachariasen, J., Berryman, K., Langridge, R., Prentice, C., Rymer, M., Stirling, M. and Villamor, P. (2006). Timing of late Holocene surface rupture of the Wairau Fault, Marlborough, New Zealand. *New Zealand Journal of Geology and Geophysics*, 49(1), pp.159-174.

Zong, Y., Shennan, I., Combellick, R., Hamilton, S. and Rutherford, M. (2003). Microfossil evidence for land movements associated with the AD 1964 Alaska earthquake. The Holocene, 13(1), pp.7-20.